


11-3-2021

Ligands for Complexation, Extraction, and Sensing of Mercury(II) for Application to High-Level Waste (HLW) at the Savannah River Site (SRS)

Adenike O. Fasiku
nikefasiku@gmail.com

Follow this and additional works at: <https://digitalcommons.fiu.edu/etd>

 Part of the [Analytical Chemistry Commons](#), [Environmental Chemistry Commons](#), [Inorganic Chemistry Commons](#), [Oil, Gas, and Energy Commons](#), [Organic Chemistry Commons](#), [Radiochemistry Commons](#), and the [Water Resource Management Commons](#)

Recommended Citation

Fasiku, Adenike O., "Ligands for Complexation, Extraction, and Sensing of Mercury(II) for Application to High-Level Waste (HLW) at the Savannah River Site (SRS)" (2021). *FIU Electronic Theses and Dissertations*. 4865.
<https://digitalcommons.fiu.edu/etd/4865>

This work is brought to you for free and open access by the University Graduate School at FIU Digital Commons. It has been accepted for inclusion in FIU Electronic Theses and Dissertations by an authorized administrator of FIU Digital Commons. For more information, please contact dcc@fiu.edu.

FLORIDA INTERNATIONAL UNIVERSITY

Miami, Florida

LIGANDS FOR COMPLEXATION, EXTRACTION, AND SENSING OF
MERCURY(II) FOR APPLICATION TO HIGH-LEVEL WASTE (HLW) AT THE
SAVANNAH RIVER SITE (SRS)

A dissertation submitted in partial fulfillment of the

requirements for the degree of

DOCTOR IN PHILOSOPHY

in

CHEMISTRY

by

Adenike Fasiku

2021

To: Dean Michael R. Heithaus
College of Arts, Sciences, and Education

This dissertation, written by Adenike Fasiku and entitled Ligands for Complexation, Extraction, and Sensing of Mercury(II) for Application to High-Level Waste (HLW) at the Savannah River Site (SRS) having been approved in respect to style and intellectual content, is referred to you for judgment.

We have read this dissertation and recommend that it be approved.

Jose Almirall

Yong Cai

Yelena Katsenovich

Raphael Raptis

Konstantinos Kavallieratos, Major Professor

Date of Defense: November 3, 2021

The dissertation of Adenike Fasiku is approved.

Dean Michael R. Heithaus
College of Arts, Sciences and Education

Andrés G. Gil
Vice President of Research and Economic Development
and Dean of the University Graduate School

Florida International University, 2021

© Copyright 2021 by Adenike Fasiku

All rights reserved.

DEDICATION

This dissertation is dedicated to God Almighty and to my family and friends; thank you for being my source of inspiration, direction, and strength. Without your support, it could not have been achieved.

ACKNOWLEDGMENTS

I express my profound gratitude to my amazing major supervisor, Dr. Konstantinos Kavallieratos, for his incredible support, guidance, and encouragement. To my dissertation committee members: Dr. Jose Almirall, Dr. Yong Cai, Dr. Yelena Katsenovich, and Dr. Raphael Raptis, thank you for sharing your expertise with dependable feedback and valuable corrections during this process.

I acknowledge this research project's support by the US Department of Energy Minority Serving Institution Partnership Program (MSIPP) managed by the Savannah River National Laboratory under SRNS contract BOA No: 541, TOA No. 0000332972 and 0000403067 to FIU. Also, the support of the Florida International University Dissertation Year Fellowship (DYF) awarded to me for the 2021 Spring and Summer terms.

Special thanks to Ms. Magalie Autie, our graduate program assistant, for her selfless love and genuine service. Also, to Dr. Indranil Chakraborty for his help with X-ray crystallography. To my present and former lab mates and colleagues who made this process easier with their help: Oluwaseun Adedoyin, Dr. Rene Panzer, Dr. Ingrid Lehman-Andino, Dr. Tosin M. Jonah, Gabriel A. Flores, Dr. Xinrui Zhang, Dr. Joshua Silverman, Dr. Setareh Sakhdari, David Ayodele, Matthew T. Fortunato, Carlos Aguilera, Valentina Caminos, and Laura Garcia, thank you all for the supports and kind attitudes which kept me strong all through the years shared in the lab with you. I also acknowledge the help of Clement Olanrewaju, Peter Oladoye, and Olutobi Ogunbiyi with this work, thank you guys.

To Adedotun, thank you for all your sacrifice and your steadfast love. To my three children, Damola, Doyin, and Tomi, you may be too young now to know how great of an inspiration you are to me; thank you for your hugs, kisses, and most significantly, your patience while I was writing this dissertation. To my parents, Mr. and Mrs. Sam Aribatise and Mr. and Mrs. Joshua Fasiku, thank you for your prayers and supports toward me during this time; you are true inspirations to my life.

Finally, I am lucky enough to have amazing siblings and friends (the Aribatises, Popoolas, Olanrewajus, and Adedoyins), that support me at my lows and would do anything for me. Words are not enough to express my deepest gratitude to you all and every other individual who has helped make this dissertation possible. Gracias!

ABSTRACT OF THE DISSERTATION

LIGANDS FOR COMPLEXATION, EXTRACTION, AND SENSING OF
MERCURY(II) FOR APPLICATION TO HIGH-LEVEL WASTE (HLW) AT THE
SAVANNAH RIVER SITE (SRS)

by

Adenike Fasiku

Florida International University, 2021

Miami, Florida

Professor Konstantinos Kavallieratos, Major Professor

Mercury (Hg) separation and sensing is of high significance due to Hg^(II) environmental mobility and toxicity. Furthermore, the use of Hg in nuclear applications has resulted in its accumulation in several DOE sites, such as in Oak Ridge and Savannah River reservations. Organic mercury species have been found in low activity waste (LAW) streams resulting from high-level waste (HLW) processing at the Savannah River Site (SRS), therefore posing a threat to humans and the environment. Mercury, being a soft Lewis acid, has a strong affinity for softer Lewis bases, such as S- or N-donor ligands. Therefore, we focus on synthesizing and studying soft-donor organic ligands, such as thioamides and sulfonamides, as effective complexants, extractants or chemosensors for inorganic mercury.

We studied the interaction of Hg^(II) with bis-arylsulfonamide ligand derivatives derived from substituted *o*-phenylenediamine and several sulfonyl chlorides. Successful extraction of Hg^(II) from alkaline aqueous phases into dichloroethane was observed, with

extraction efficiency and recovery as high as 97.4 % and 81.5 %, respectively, at pH 12.0 by the disulfonamide ligand L4. The influence of pH, ligand concentration, and the presence of the organic base (triethylamine) was studied in detail. The crystal structure of the isolated Hg^(II) complex with the disulfonamide analog L2 shows a 1:2 Hg^(II):L2 stoichiometry with two triethylammonium counteranions (Et₃NH⁺) coordinating in the outer sphere. The bis-dansylsulfonamide (L_D) derivative was shown to be an effective Hg^(II) sensor, as fluorescence quenching was observed upon gradual addition of HgCl₂ solution with complete quenching occurring at Hg^(II):L_D molar ratio of 1:1.

Thioamide ligands derived from 2,6-diaminopyridine were also studied. The pyridine N atom and the thiocarbonyl moiety on these ligands result in strong Hg^(II) binding (log K = 7.43). The lipophilic derivative of this thioamide ligand (PDT) is a potential extractant for industrial solvent extraction processes. PDT extracts Hg^(II) with an extraction efficiency of 99.7% and discriminates the presence of mercury over various competing metal ions, which are present in higher concentrations at HLW. We also carried out a spectroscopic and structural study on a Hg^(II)-mediated cyclization reaction of a dithioamide ligand derived from *o*-phenylenediamine to a benzimidazole derivative, which has led to a potentially new paradigm for Hg^(II) sensing.

Overall, with high observed recovery for extracted Hg^(II), strong binding, and high selectivity for several of our studied ligands, this research has demonstrated new pathways for application of Hg^(II) sensing, complexation, and recovery from alkaline high-level tank waste.

TABLE OF CONTENTS

CHAPTER	PAGE
CHAPTER I: Introduction: Mercury and its Separation and Sensing Applications.....	1
1.1 Biogeochemical and environmental importance of mercury	1
1.1.1. General properties of mercury	1
1.1.2. Sources of mercury emissions to the environment.....	2
1.1.3. The chemistry and the biogeochemical cycle of mercury	4
1.1.4. Mercury bioaccumulation and toxicity	7
1.2 Mercury coordination chemistry.....	8
1.3 Mercury (II) removal methods from aqueous solutions.....	11
1.3.1 Overview.....	11
1.3.2 Adsorption.....	12
1.3.3 Precipitation.....	12
1.3.4 Filtration.....	13
1.3.5 Electrochemical treatment	13
1.3.6 Solvent extraction	13
1.4. Mercury sensing.....	17
1.4.1 Overview.....	17
1.4.3 Colorimetric chemical sensing of mercury	18
1.4.2 Fluorescent chemical sensing of mercury.....	18
1.5. The mercury problem in high-level waste at the Savannah River Site (SRS)	21
1.5.1 Overview.....	21
1.5.2 Nuclear waste management at the SRS	21
1.5.3. Mercury in the liquid waste streams at SRS.....	23
1.5.4. Choice of ligands for mercury remediation at SRS	26
1.6 Principles for ligand design for mercury complexation.....	27
1.7 Sulfonamide ligands for toxic metal complexation.....	28
1.8 Thioamide ligands for toxic metal complexation	31
1.9 Analytical methods: Instrumentation, methodology, and data analysis	34
1.9.1 Overview.....	34
1.9.2 Determination of complexation equilibria by titration.....	35
1.9.3 Determination of stoichiometry by Job plot	35

1.9.4	Determination of complexation affinity and stoichiometry by non-linear regression analysis	36
1.9.5	Hg ^(II) quantification by the dithizone method	38
1.9.6	Validation of analytical methods	38
1.10	References	40

CHAPTER II: Complexation and Efficient Extraction of Mercury(II) in Alkaline Conditions by a Family of Bis-Arylsulfonamide Ligands		49
2.1	Abstract	49
2.2	Introduction.....	50
2.3	Experimental section	53
2.3.1	Materials and methods	53
2.3.2	Synthesis of Hg ^(II) complexes of bis-arylsulfonamide ligands	53
2.3.3	UV-Vis titrations.....	55
2.3.4	Extraction studies.....	56
2.3.5	¹ H-NMR titration - Determination of complexation equilibria	58
2.3.6	Determination of stoichiometry by the continuous variation method (Job Plot).....	58
2.3.7	X-ray crystallography for C2	59
2.4.	Results and discussion.....	59
2.4.1	Isolation and characterization of Hg ^(II) complexes.....	59
2.4.1.1	Synthesis	59
2.4.1.2	FT-IR studies.....	61
2.4.1.3	NMR studies.....	62
2.4.2	Extraction studies.....	67
2.4.2.1	General remarks.....	67
2.4.2.2	Extraction dependence on pH	68
2.4.2.3	Extraction dependence on ligand concentration.....	71
2.4.3	UV-Vis binding studies.....	74
2.4.4	Single-crystal X-ray crystallography	78
2.5	Conclusions.....	96
2.6	Acknowledgments.....	96
2.7	References	97

CHAPTER III: A bis-Dansylamide Derivative of <i>o</i> -Phenylenediamine as a Fluorescent Chemosensor for the Detection of Hg(II) in Alkaline Solutions	102
3.1 Abstract	102
3.2 Introduction.....	103
3.3 Experimental section	105
3.3.1 Materials and methods	105
3.3.2 Synthesis of N,N'-(4,5-dimethyl-1,2-phenylene)bis(5-(dimethylamino)naphthalene-1-sulfonamide) (L _D).....	105
3.3.3 Synthesis of Hg-L _D complex	106
3.3.4 UV-Visible titrations.....	107
3.3.5 Fluorescence titrations	107
3.3.6 Determination of stoichiometry by the continuous variation method (Job Plot).....	108
3.3.7 Comparative experiments	108
3.3.8 Extraction studies.....	109
3.3.9 X-ray crystallography for L _D	110
3.4 Results and discussion.....	110
3.4.1 Synthesis	110
3.4.2 FT-IR studies	111
3.4.3 ¹ H and ¹³ C NMR studies.....	112
3.4.4 UV-Vis spectroscopy.....	115
3.4.5 Fluorescence spectroscopy.....	116
3.4.6 Extraction studies.....	120
3.4.7 X-Ray crystallography of L _D	122
3.4 Conclusions.....	132
3.5 Acknowledgments.....	132
3.6 References	132

CHAPTER IV: Mercury (II) Sensing via Cyclization of a Dithioamide into a Benzimidazole Derivative: A Structural and Spectroscopic Study.	136
4.1 Abstract	137
4.2 Introduction.....	137
4.3 Experimental.....	140
4.3.1 Materials and methods	140

4.3.2.	Synthesis of N,N'-(1,2-phenylene)dibenzothioamide (L).....	140
4.3.3.	Synthesis of phenyl(2-phenyl-1H-benzimidazol-1-yl)methanethione (L')	141
4.3.4.	X-ray crystallography	142
4.4	Results and discussion.....	142
4.4.1.	Synthesis.....	142
4.4.2.	FT-IR studies	145
4.4.3.	UV-Visible sensing studies - titrations.....	146
4.4.4.	NMR spectroscopy	150
4.4.5.	Single crystal X-ray crystallography	152
4.5	Conclusions.....	162
4.6	Acknowledgements.....	163
4.7	References	163

CHAPTER V: Pyridine-thioamide Ligands as Extractants and Sensors for Hg^(II) in Alkaline Solutions.....

	Alkaline Solutions.....	167
5.1	Abstract	167
5.2	Introduction.....	168
5.3	Experimental section	170
5.3.1	Materials and methods	170
5.3.3	Synthesis of N,N'-(pyridine-2,6-diyl)dithioacetamide (PDAT)	171
5.3.4	Synthesis of N,N'-(pyridine-2,6-diyl)didodecanethioamide (PDT).....	171
5.3.5	Synthesis of Hg ^(II) complex of PDAT [HgCl(HPDAT)].....	172
5.3.6	Synthesis of the Hg ^(II) complex of PDT [HgCl(HPDT)]	173
5.3.7	UV-Vis titration of PDAT or PDT with HgCl ₂	174
5.3.8	Competitive UV-Vis titration of PDAT with HgCl ₂ in the presence of other metals.	174
5.3.9	UV-Vis spectroscopic experiments (Hg ^(II) vs other metals)	175
5.3.10	Determination of complexation stoichiometry by the continuous variation method (Job Plot).....	175
5.3.11	Extraction studies.....	176
5.3.12	X-ray crystallography	177
5.4	Results and discussion.....	177
5.4.1	Synthesis	177
5.4.2	FT-IR studies	179

5.4.3	NMR spectroscopy.....	180
5.4.4	UV-Vis binding and sensing studies.....	182
5.4.4.1	UV-Vis titrations	182
5.4.4.2	Determination of binding stoichiometry for Hg ^(II) complexation (Job Plots)	185
5.4.4.3	Optical sensing of Hg ^(II) with PDT and PDAT: comparison with other metals	186
5.4.5	Extraction studies.....	189
5.4.5.1	pH dependent extraction of Hg ^(II) by PDT	189
5.4.5.2	Effects of PDT concentration on the extraction of Hg ^(II)	190
5.4.6	X-ray Crystallography	190
5.5	Conclusions.....	192
5.6	Acknowledgments.....	193
5.7	References	193
CHAPTER VI: Summary and General Conclusions		197
APPENDICES		201
VITA.....		224

LIST OF TABLES

TABLES	PAGE
Table 1.1: Mercury(II) coordination with several ligands	10
Table 1.2: Some colorimetric/fluorescent Hg(II) chemosensors.	19
Table 1.3: HSAB classification of Acids and Bases	28
Table 2.1: Selected IR bands of the bis-arylsulfonamide ligands and their corresponding Hg ^(II) complexes	61
Table 2.2: Association constants of the complexes obtained from titrating the corresponding ligands with HgCl ₂ in methanol.	78
Table 2.3. Crystal data and structure refinement parameters for the complex	79
Table 2.4. Selected geometrical parameters to assess the distortion of the geometry of C2 from idealized tetrahedral and square planar	80
Table 2.5: Fractional atomic coordinates and isotropic or equivalent isotropic displacement parameters (Å ²)	83
Table 2.6: Atomic displacement parameters (Å ²)	87
Table 2.7: Geometric parameters (Å, °)	89
Table 3.1: Crystal data and structure refinement parameters for the complex	123
Table 3.2: Fractional atomic coordinates and isotropic or equivalent isotropic displacement parameters (Å ²)	123
Table 3.3: Atomic displacement parameters (Å ²)	126
Table 3.4: Geometric parameters (Å, °)	127
Table 4.1: Experimental details for X-ray structure determination.	153
Table 4.2: Fractional atomic coordinates and isotropic or equivalent isotropic displacement parameters (Å ²) for L	156
Table 4.3: Atomic displacement parameters (Å ²) for L	158
Table 4.4: Geometric parameters (Å, °) for L	158
Table 4.5: Fractional atomic coordinates and isotropic or equivalent isotropic displacement parameters (Å ²) for L'	160
Table 4.6: Atomic displacement parameters (Å ²) for L'	161
Table 4.7: Geometric parameters (Å, °) for L'	161
Table 5.1: Crystal data of PDAT	191
Table B.1: Crystal data of tris-thiocarboxamide ligand, L _{4a}	222

LIST OF FIGURES

FIGURES	PAGE
Figure 1.1 Global sources of mercury. Source: Technical Background Report of the Global Mercury Assessment, 2018.	4
Figure 1.2: The mercury cycling pathways in the environment	7
Figure 1.3: Structures of chelating agents used for mercury detoxification.	10
Figure 1.4: Principles of solvent extraction separation showing the two steps: i) Extraction and ii) Stripping (recovery).....	14
Figure 1.5: Structures of calix(4)arenes used for Hg ^(II) extraction	16
Figure 1.6: Structures of thiacrown ethers used for Hg ^(II) extraction.	16
Figure 1.7: Jablonski diagram	19
Figure 1.8: The three physical forms of waste at the SRS.....	22
Figure 1.9: Savannah River Remediation (SRR) liquid waste program.....	23
Figure 1.9: Mercury in the liquid waste stream at the Savannah River Site.....	25
Figure 1.11: Structures of the triple sulfa drugs (TSD)	29
Figure 1.12: (a) Deprotonated sulfa drug (b) Sulfadiazine-mercury complex with DMF co-ligands	30
Figure 1.13: Lead and cadmium complexes of o-phenylenediamine-derived sulfonamide ligands	31
Figure 1.14: Some fluorescent sulfonamide ligands used for metal ion detection and complexation. Metal ions detected are; (a) Pb ^(II) (b) Cu ^(II) , Cd ^(II) , Zn ^(II) , and Co(II) (c) Zn ^(II)	31
Figure 1.15: Secondary thioamide and its resonance structures	34
Figure 1.16: Pd ^(II) pincer complexes of dithiopicolinamide.....	34
Figure 1.17: Schematic of a calibration curve plot showing the LOD and linear dynamic range.....	39
Figure 2.1. Structures of bis-arylsulfonamide ligands.....	60
Figure 2.2: FT-IR Spectra of (a) C1 (b) C2 (c) C3 (d) C4.....	62
Figure 2.3. ¹ H-NMR of L2H ₂ and isolated (Et ₃ NH) ₂ [Hg(L2) ₂] in CDCl ₃	63
Figure 2.4: ¹ H-NMR of (a) L1 and (Et ₃ NH) ₂ [Hg(L1) ₂] (b) L3 and (Et ₃ NH) ₂ [Hg(L3) ₂] (c) L4 and (Et ₃ NH) ₂ [Hg(L4) ₂] in CDCl ₃	64
Figure 2.5: ¹³ C-NMR of (a) L1 and (Et ₃ NH) ₂ [Hg(L1) ₂] (b) L2 and (Et ₃ NH) ₂ [Hg(L2) ₂] (c) L3 and (Et ₃ NH) ₂ [Hg(L3) ₂] (d) L4 and (Et ₃ NH) ₂ [Hg(L4) ₂] in CDCl ₃	65
Figure 2.6: ¹ H-NMR titration of HgCl ₂ (4.0 x 10 ⁻² M stock solution) into a solution of L2H ₂ (4.0 x 10 ⁻³ M) and Et ₃ N (2.2 equiv.) in MeOD (various equiv. of Hg ^(II) are labelled on each spectrum). The effect of Hg ^(II) addition is shown	

in (a) the aromatic proton region of L2H ₂ and (b) the aliphatic proton region of L2H ₂	67
Figure 2.7: Calibration curve for the quantification of Hg ^(II) using the dithizone-Hg complex absorbance at 490 nm.....	68
Figure 2.8. pH-dependent extraction of Hg ^(II) by (a) L2H ₂ and (b) L4H ₂ into DCE both in the absence (black) and presence (red) of triethylamine. ([Hg ^(II)] = 1.0 mM, [L2H ₂] or [L4H ₂] = 2.0 mM, [Et ₃ N] = 4.0 mM).....	70
Figure 2.11. Distribution experiments (% recovery after stripping) showing: (a) Influence of L2H ₂ or L4H ₂ concentration on Hg ^(II) extraction efficiency in the absence of triethylamine. Conditions: pH = 12.0, [Hg ^(II)] = 1.0 mM, [L2H ₂] or [L4H ₂] = 0.30 – 2.0 mM, [Et ₃ N] = 5.0 mM (b) Relationship between log D _{Hg} and log [L2H ₂] or [L4H ₂] showing the stoichiometry of the Hg ^(II) :L complexes that are formed at various Hg ^(II) :L ratios. (c) Influence of L2H ₂ or L4H ₂ concentration on Hg ^(II) extraction efficiency in the presence of triethylamine. Conditions: pH = 12, [Hg(II)] = 1.0 mM, [L2H ₂] or [L4H ₂] = 0.30 – 2.0 mM, [Et ₃ N] = 5.0 mM (d) Relationship between log D _{Hg} and log [L2H ₂] or [L4H ₂] showing the stoichiometry of the Hg ^(II) /L complexes that are formed at various Hg ^(II) :L ratios.....	73
Figure 2.12. Amount of Hg ^(II) found in the aqueous phases after L2 extraction and stripping experiments in the (a) absence of triethylamine and (b) presence of triethylamine (5.0 mM) ([Hg ^(II)] = 1.0 mM, [L2] = 0.30 – 2.0 mM, pH = 12.0).....	74
Figure 2.13. Amount of Hg ^(II) found in the aqueous phases after L4 extraction and stripping experiments in the (a) absence of triethylamine and (b) presence of triethylamine (5.0 mM) ([Hg ^(II)] = 1.0 mM, [L4] = 0.30 – 2.0 mM, pH = 12.0).....	74
Figure 2.14. UV-Vis titration of ligand L2H ₂ (4.0 x 10 ⁻⁵ M) and Et ₃ N (2.2 eq) in CH ₃ OH upon gradual addition of HgCl ₂ (4.0 x 10 ⁻⁴ M). The concentration of the ligand was constant during the titration. Inset: UV-Vis titration binding curve of L2 with Hg ^(II) at 304 nm.	76
Figure 2.15. UV-Vis titration curves for bis-arylsulfonamide ligands (L1H ₂ - L4H ₂) (4.0 x 10 ⁻⁵ M) and Et ₃ N (2.2 eq.) with Hg ^(II) at 304 nm (4.0 x 10 ⁻⁴ M). Titration in the absence of ligand (purple diamond) indicates no complexation between triethylamine and mercury.....	77
Figure 2.16. Job plot of L2 (2.0 x 10 ⁻⁴ M) and Et ₃ N (4.8 x 10 ⁻⁴ M) with Hg ^(II) (2.0 x 10 ⁻⁴ M) in methanol.	77
Figure 2.18. Packing pattern of complex C2 along c axis (top) and H-bonding interactions involving the N atoms of Et ₃ NH ⁺ ions and O atoms of sulfonamide moieties (bottom).	82

Figure 2.19. Polyhedral representation of the packing pattern revealing the site of 3-fold axis	83
Figure 3.1: FT-IR spectra of L _D vs its Hg ^(II) complex.	112
Figure 3.2: ¹ H-NMR titration of L _D (4.0 mM) and 2.2 eq. of DIPEA with HgCl ₂ in MeOD. Concurrent decrease in ligand signals and the appearance of new complex signals indicates initial 1-2 Hg:L _D complex formation, followed by 1-1 Hg:L _D complex formation.	113
Figure 3.3: Aliphatic region of the ¹ H-NMR spectra from the titration of L _D (4.0 mM) and 2.2 eq. of DIPEA with HgCl ₂ in MeOD.....	114
Figure 3.4: ¹³ C- ¹ H-NMR of L _D vs Hg-L _D complex in MeOD at 298 K	115
Figure 3.5: UV-Vis spectra of L _D (2.0 × 10 ⁻⁵ M) in the presence of DIPEA (5.0 × 10 ⁻⁵ M) with gradual addition of HgCl ₂ (0 - 950 μL of 4.0 × 10 ⁻⁴ M) in methanol.....	116
Figure 3.6: Results showing (a) Fluorescence titration spectra of L _D (2.0 × 10 ⁻⁵ M) and 2.5 eq. DIPEA with HgCl ₂ in methanol. λ _{exc} = 334 nm. (b) Plot of ΔI at 533 nm vs. Hg ^(II) concentration (c) Stern-Volmer plot for fluorescence quenching of L _D by Hg ^(II) in methanol, K _{SV} = 2.8 × 10 ⁵ M ⁻¹ (d) Linear curve of the fluorescence intensity at 533 nm vs Hg ^(II) concentration (0 – 13.4 μM)	118
Figure 3.7: Fluorescence spectra of L _D (0.10 mM) and 2.5 eq. DIPEA before and after addition of various metals (0.20 mM, added as chloride salts) in methanol. λ _{exc} = 334 nm.....	119
Figure 3.8: Job plot of L _D -Hg ^(II) complex in methanol. L _D = 2.0 × 10 ⁻³ M; 2.5 eq. DIPEA; [Hg ^(II)] _t = 2.0 × 10 ⁻³ M; λ _{exc} = 334 nm.....	120
Figure 3.9: Results showing (a) the pH dependent extraction of Hg ^(II) by L _D into DCE Conditions; [Hg ^(II)] = 1.0 mM, [L _D] _t = 2.0 mM (b) % recovery of Hg ^(II) after extraction into DCE and subsequent stripping at various concentrations of L _D . Conditions; [Hg ^(II)] _t = 1.0 mM, [L _D] _t = 0.20 – 4.0 mM, pH = 11.0....	121
Figure 3.10: Extraction results showing (a) Influence of L _D concentration on Hg ^(II) extraction efficiency. Conditions; [Hg ^(II)] _t = 1.0 mM, [L _D] _t = 0.30 – 2.0 mM, [DIPEA] _t = 5.0 mM (b) Relationship between log D _{Hg} and log [L _D] _t showing the stoichiometry of the Hg ^(II) -L _D complexes that are formed at various Hg ^(II) :L _D ratios.....	122
Figure 3.11: ORTEP representation of the X-ray Structure of L _D (50 % probability ellipsoids).....	122
Figure 4.1. FT-IR spectra of the dithioamide ligand (L) and the cyclized benzimidazole (L').....	146

Figure 4.2. FT-IR spectra of the transient Hg ^(II) -L complex.....	146
Figure 4.3. UV-Vis spectra of i) L (0.1 mM) in MeOH, ii) isolated L' (0.1 mM) in MeOH and iii) reaction mixture after addition of HgCl ₂ (1 eq., 0.1 mM) to L in MeOH, after standing for 24 h.	148
Figure 4.4. UV-Vis spectra of L (0.02 mM) in CH ₃ OH vs L + Hg(OAc) ₂ (2 eq.). No organic base was added.....	148
Figure 4.5. UV-Vis titration of L (0.02 mM) and DIPEA (2.2 eq.) in CH ₃ OH after gradual addition of HgCl ₂ (0.5 mM) at constant L and DIPEA concentration.....	149
Figure 4.6. UV-Vis spectra of L (0.1 mM) before and after addition of chloride salts of Zn ^(II) , Pb ^(II) , Cd ^(II) , or Hg ^(II) (1 eq.) in MeOH after standing for 24 h.	149
Figure 4.7. UV-Vis spectra of L (0.1 mM) before and after addition of chloride salts of Ca(II), Ag ^(I) , Cr ^(III) , and Hg ^(II) (1 eq.) in MeOH, after standing for 24 h. .	150
Figure 4.8. ¹ H-NMR spectra of di-thioamide (L) and the cyclized benzimidazole product (L') in CDCl ₃	151
Figure 4.9. ¹ H-NMR spectra of L (3.2 mM) (top) in comparison with L + DIPEA (2.2 eq.) (middle) and the reaction mixture after addition of HgCl ₂ (1.2 eq.) showing the transient Hg ^(II) -L complex formation at 8.06, 7.45, and 28 ppm (bottom).	151
Figure 4.10. ORTEP representation (50% probability ellipsoids) for the X-ray crystal structure of dithioamide L, with atom labeling scheme, showing an N-H...S intramolecular hydrogen bonding interaction.....	154
Figure 4.11. Packing pattern of L along a axis. The dotted lines indicate both intra- and inter-molecular H-bonding interactions	155
Figure 4.12. ORTEP representation (50% probability ellipsoids) for the X-ray crystal structure of benzimidazole L', with atom labeling scheme.	155
Figure 4.13. Packing pattern of L' along b axis. The dotted lines indicate intermolecular H-bonding interactions.	156
Figure 5.1: (a) FT-IR spectrum of PDT vs. the PDT-Hg ^(II) complex (b) FT-IR spectrum of PDAT vs. the PDAT-Hg ^(II) complex.....	180
Figure 5.2: ¹ H-NMR spectra of PDT vs. the PDT-Hg ^(II) complex in CDCl ₃ , 298K.....	181
Fig. 5.3: Aromatic region of the ¹ H-NMR titration spectra of PDAT with HgCl ₂ . ([PDAT]: 4.0 x 10 ⁻³ M, [Hg(II)]: 4.0 x 10 ⁻² M, DIPEA: 2.2 eq., Solvent: MeOD, temp: 298 K)	182
Figure 5.4: (a) UV-Vis titration spectra of PDAT (2 x 10 ⁻⁵ M) and DIPEA (4.4 x 10 ⁻⁴ M) with HgCl ₂ (2.0 x 10 ⁻⁴ M) in methanol. (b) Absorption as a function of Hg ^(II) concentration at 319 nm.....	183

Figure 5.5: (a) UV-Vis titration spectra of PDAT (2.0×10^{-5} M) and DIPEA (4.4×10^{-4} M) with HgCl_2 (2×10^{-4} M) in methanol. (b) Absorption as a function of $\text{Hg}^{(\text{II})}$ concentration at 319 nm.....	184
Figure 5.6: (a) UV-Vis titration spectra of PDAT with HgCl_2 in the absence of organic base ([PDAT]: 2.0×10^{-5} M, $[\text{Hg}^{(\text{II})}]_t$: 2.0×10^{-4} M, Solvent: Methanol) (b) absorption as a function of $\text{Hg}^{(\text{II})}$ -PDAT molar ratio at 278, 319, 335 and 365 nm. Dash lines indicate $\text{Hg}^{(\text{II})}$ -PDAT complex stoichiometries.....	185
Figure 5.7: Job plot of PDT and $\text{Hg}^{(\text{II})}$ in methanol. ([PDT]: 1.0×10^{-4} M, DIPEA: 2.2×10^{-4} M, $[\text{Hg}^{(\text{II})}]_t$: 1.0×10^{-4} M)	186
Figure 5.8: UV-Vis spectra of PDT and PDT-metal methanolic solutions ([PDT] _t : 1.0×10^{-4} M, DIPEA: 2.2 eq., $[\text{M}^{2+}]_t$ or $[\text{M}^+]_t$: 1.0×10^{-4} M (prepared as chloride or fluoride salts), solvent: methanol)	187
Figure 5.9: (a) UV-Vis titration spectra of PDAT with HgCl_2 in the presence of competitive cations([PDAT]: 2.0×10^{-5} M, DIPEA: 2.2 eq., $[\text{Hg}^{(\text{II})}]_t$: 2.0×10^{-4} M, Solvent: Methanol, $[\text{Sr}^{(\text{II})}]_t$, $[\text{Ca}^{(\text{II})}]_t$, $[\text{K}^{(\text{I})}]_t$, $[\text{Cs}^{(\text{I})}]_t$: 1.0×10^{-3} M, $[\text{Na}^{(\text{I})}]_t$: 1.0×10^{-2} M (b) absorption as a function of $\text{Hg}^{(\text{II})}$ concentrations at 319 nm comparing titration with $\text{Hg}^{(\text{II})}$ alone and titration with $\text{Hg}^{(\text{II})}$ in the presence of other cations. : (c) UV-Vis titration spectra of PDAT with HgCl_2 in the presence of competitive cations ([PDAT]: 2×10^{-5} M, DIPEA: 2.2 eq., $[\text{Hg}^{(\text{II})}]_t$: 2.0×10^{-4} M, Solvent: Methanol, $[\text{Sr}^{(\text{II})}]_t$, $[\text{Ca}^{(\text{II})}]_t$, $[\text{K}^{(\text{I})}]_t$, $[\text{Cs}^{(\text{I})}]_t$: 1.0×10^{-3} M, $[\text{Zn}^{(\text{II})}]_t$, $[\text{Pb}^{(\text{II})}]_t$, $[\text{Cd}^{(\text{II})}]_t$: 1.0×10^{-4} M, $[\text{Na}^+]_t$: 1.0×10^{-2} M (d) absorption as a function of $\text{Hg}^{(\text{II})}$ concentrations at 319 nm comparing titration with $\text{Hg}^{(\text{II})}$ alone and titration with $\text{Hg}^{(\text{II})}$ in the presence of other metals including Zn, Pb and Cd.	188
Figure 5.10: Effect of pH on the extraction of $\text{Hg}^{(\text{II})}$ by PDT. ([PDT] _t : 5.0×10^{-3} M, $[\text{Hg}^{(\text{II})}]_t$: 1.0×10^{-3} M, Organic phase: 1:9 Octanol:Dodecane)	189
Figure 5.11: Extraction behavior of Hg^{2+} with PDT at pH 13.0. ($[\text{Hg}^{(\text{II})}]_t$: 1.0×10^{-3} M, organic phase: 1:9 Octanol:Dodecane, pH: 13.0)	190
Figure 5.12: (a) X-ray crystal structure of PDAT (b) ORTEP representation (50% probability ellipsoids) for the X-ray crystal structure of PDAT, with atom labeling scheme, showing three 3 crystallographically independent molecules within the asymmetric unit	192
Figure A.1. ^1H -NMR spectra comparison of L and isolated C_1	207
Figure A.2. ^1H -NMR spectra comparison of L and isolated C_2	207
Figure A.3. (a) UV/Visible spectra for the titration of L (2.0×10^{-5} M) and 2.2 eq. of triethylamine with HgCl_2 (2.0×10^{-4} M) in acetonitrile. (b) absorption as a function of $\text{Hg}^{(\text{II})}$ concentrations at 415 nm.	208

Figure A.4. (a) UV-Visible spectra for the titration of L (2.0×10^{-5} M) with Hg(OAc) ₂ (2.0×10^{-4} M) in acetonitrile. (b) absorption as a function of Hg ^(II) concentrations at 415 nm.....	209
Figure B.1: X-ray structure of dinuclear mercury complex formed from the complexation of N ² ,N ⁶ -diphenylpyridine-2,6-bis(carbothioamide) with Hg ^(II)	213
Figure B.2. FT-IR spectra of ligand L _{4a} vs. its Hg ^(II) complex.	218
Figure B.3. (a) ¹ H-NMR and (b) ¹³ C-NMR of new tripodal thioamide ligand, L _{4a}	219
Figure B.4. UV-Vis study of ligand L _{4a} (a) Titration spectra taken after gradual addition of HgCl ₂ to ligand and DIPEA (3.3 equiv.) in CH ₃ CN solution (0.020 mM). (b) UV-Vis responses of L _{4a} (0.10 mM, 3.3 Et ₃ N) to addition of various metals added as chloride salts (1 equiv.) in MeOH after standing for 24 h.....	221
Figure B.5. X-ray crystal structure of tris-thioacarboxamide ligand, L _{4a}	221

LIST OF SCHEMES

SCHEMES	PAGE
Scheme 1.1: Synthetic pathway for a secondary sulfonamide by reacting a primary amine with a sulfonyl halide or sulfonic acid.	29
Scheme 1.2: Mechanism of Lawesson's reaction	33
Scheme 1.3: Formation of the trimer by-product, p-methoxyphenylmetathiophosphonate	33
 Scheme 2.1: Synthesis of Hg ^(II) -bis-arylsulfonamide complexes	 60
 Scheme 3.1: Synthesis of N,N'-(4,5-dimethyl-1,2-phenylene)bis(5-(dimethylamino)naphthalene-1-sulfonamide) (L _D).....	 111
 Scheme 4.1: Synthesis of N,N'-(1,2-phenylene)dibenzothioamide (L) and Phenyl(2-phenyl-1H-benzo[d]imidazol-1-yl)methanethione (L').....	 144
Scheme 4.2: Proposed mechanism of Hg ^(II) -catalyzed cyclization reaction transforming L into L'	145
 Scheme 5.1: Synthetic route to the short-chain thioamide ligand PDAT	 178
Scheme 5.2: Synthetic route to the long-chain thioamide ligand PDT	178
Scheme 5.3: Proposed structure of Hg ^(II) pincer complexes.	178
 Scheme A.1: Synthesis of N,N'-(4-nitro-1,2-phenylene)bis(4-(tert-butyl)benzenesulfonamide), L	 205
Scheme A.2: Possible structure of isolated mercury complex.....	205
 Scheme B.1: Synthesis of trithioamide ligand L _{4a}	 217
Scheme B.2: Synthesis of the Hg ^(II) complex of trithioamide ligand L _{4a}	218

LIST OF ABBREVIATIONS

AAS	Atomic Absorption Spectroscopy
CSSX	Caustic-Side Solvent Extraction
DCM	Dichloromethane
DCE	1,2-dichloroethane
DIPEA	Diisopropylethylamine
D _M	Distribution ratio
DMF	Dimethylformamide
DWPF	Defense Waste Processing Facility
DOE	Department of Energy
DOM	Dissolved Organic Matter
EDTA	Ethylenediaminetetraacetic acid
ETP	Effluent Treatment Project
FT-IR	Fourier Transform Infrared Spectroscopy
HLW	High Level Waste
HPLC	High-Performance Liquid Chromatography
ICP-OES	Inductively-Coupled Plasma Optical Emission Spectrometry
LAW	Low Activity Waste
LMCT	Ligand to Metal Charge Transfer
LOD	Limit of Detection
MCU	Modular CSSX unit
MLCT	Metal to Ligand Charge Transfer
MS	Mass Spectroscopy
NMR	Nuclear Magnetic Resonance

PUREX	Plutonium Uranium Redox Extraction
SF	Separation Factor
SNF	Spent Nuclear Fuel
SRAT	Sludge Receipt and Adjustment Tank
SRS	Savannah River Site
UNEP	United Nations Environment Program
UV-Vis	Ultraviolet-Visible Spectroscopy
WHO	World Health Organization

CHAPTER I: Introduction: Mercury and its Separation and Sensing Applications

1.1 Biogeochemical and environmental importance of mercury

1.1.1. General properties of mercury

Mercury (Hg), a naturally occurring metal, is known as liquid silver or quicksilver due to its shiny silver appearance. It has an atomic number of 80 and a standard atomic weight of 200.59 g/mol. It is 13.5 times heavier than water, with a density of 13.534 g/cm³. It has a boiling point of 356.7 °C and a melting point of -38.8 °C, making it the only metallic element that remains a liquid at ambient temperatures.¹ At room temperature, it has a solubility of 5-50 mg/L in lipids and 60 mg/L in water, while its vapor is insoluble in water. Mercury has a fair conductivity of electricity but a poor conductivity of heat compared to other metals. As it is relatively volatile in the metallic state, it is known to have the highest volatility of any metal. It vaporizes to become a colorless, odorless gas with a high vapor pressure of 0.170 pa.¹ Because of its ability to dissolve some metals such as tin, silver, and gold by easily forming amalgams with them, it has found application in extracting these metals from their ores.²

Mercury transport, distribution, and migration are very different from other metals because of its volatile metallic state, promoting its transformation to other oxidation states through redox and microbial activities. In the atmosphere, mercury is emitted as gaseous elemental mercury (Hg⁰), which travels long distances to be deposited as either oxidized (Hg^{II}) or particulate-bound mercury species (Hg^P) to the aquatic and terrestrial ecosystems through dry and wet deposition.³

1.1.2. Sources of mercury emissions to the environment

Mercury naturally exists in many mineral forms, including cinnabar (HgS), calomel (Hg₂Cl₂), corderoite (Hg₃S₂Cl₂), and livingstonite (HgSb₄S₈). Cinnabar is the most prevalent mercury ore, which is often found in large deposits as a reddish mineral in Spain and some other countries such as Mexico, Italy, the former USSR, China, North Africa, and the USA (California).⁴ It is often associated with many volcanic activities and alkaline hot springs. During the roasting of cinnabar, elemental mercury is isolated from the ores by condensation in water-sprayed towers.¹

Mercury emission to the atmosphere is primarily from natural, re-emission, or anthropogenic sources. Mercury is transported across the global environment after its release from different geological reservoirs with an atmospheric lifetime of over a year. Natural and re-emitting sources of mercury emissions include volcanic eruptions, geothermal activities, forest fires, and degassing from mercury mineral deposits.⁵ Its natural emissions to the atmosphere are low compared with the total global mercury emissions. It has been estimated that biomass burning such as forest fires constitutes up to 560 – 930 metric tons of annual mercury emissions worldwide.⁵ Photochemical and photobiological processes and the sources of the emission play essential roles in the re-emission of elemental mercury from the aquatic systems.⁶

Anthropogenic activities, including fossil fuel combustion, metal smelting, solid waste incineration (municipal and medical), pyrometallurgical processes, and cement production, are some of the most common human activities contributing to the

atmospheric emission of mercury. Fossil fuel combustion and solid waste incineration account for more than half of the total global mercury emissions.⁷

According to the 2018 United Nations Environment Program (UNEP) global mercury assessment, the significant anthropogenic sources of mercury emissions to the environment are shown in Figure 1.1. These anthropogenic sources belong to two categories: i) Byproducts or unintentional emissions, where the release of mercury is due to its presence in fuels and raw materials as an impurity. These sources include coal-burning (33%) and mining and smelting activities (22%), with minor contributions from the combustion of fossil fuel (1%) and oil refining (1%). ii) Releases of mercury from processes involving the intentional use of mercury. The primary source of mercury to the atmosphere in this category is artisanal and small-scale gold mining (37 %), followed by consumer product waste disposal or processing (6.7 %). Other sources include emissions from its use in the Chlor-alkali manufacturing plants (1 %) and dental filling release during human cremation (<1 %).⁸

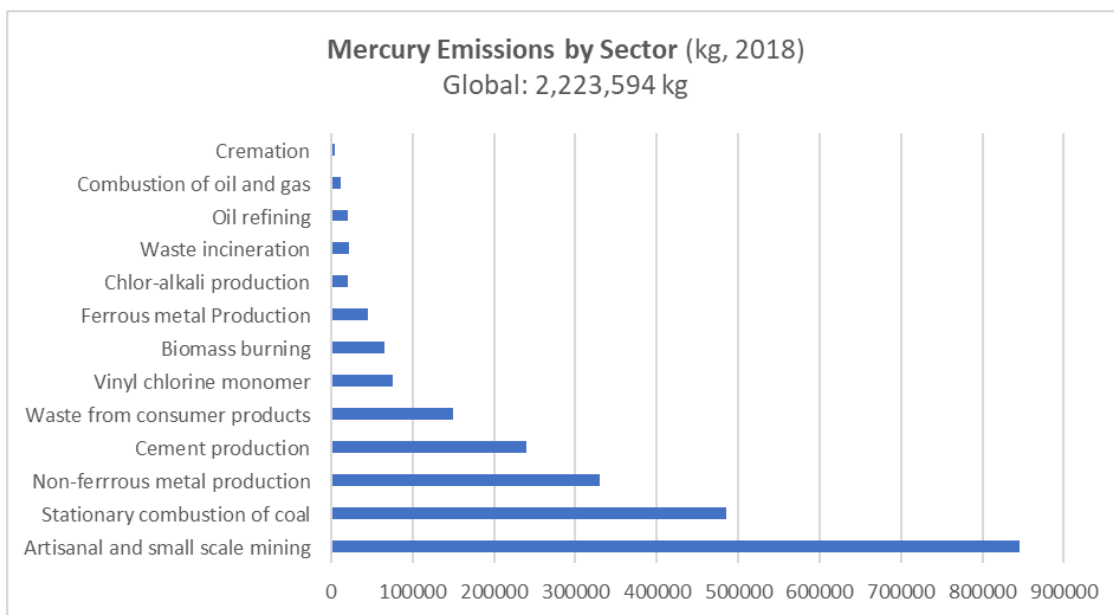


Figure 1.1 Global sources of mercury. Source: *Technical Background Report of the Global Mercury Assessment, 2018*.⁸

Industrial waste discharges are an important source of mercury in the environment. These include the Chlor-alkali industries, where it is used as a catalyst during the electrolysis of brine to produce sodium hydroxide and chlorine. Mercury is also commonly used in consumer products such as batteries, thermometers, barometers, felt production, electrical switches, fluorescent lights, and pesticides. At present, mercury is used in scientific research, and its amalgam materials are still being used for dental fillings. Because of mercury's toxicity, its use is being phased out from many mining, industrial, medical, and agricultural applications.⁹

1.1.3. The chemistry and the biogeochemical cycle of mercury

Mercury has a ground-state electronic configuration of $[\text{Xe}]4f^{14}5d^{10}6s^2$. It exists as monoatomic in its vapor phase at low temperatures due to weak intermolecular forces.

Due to its filled 4f and 5d sublevels, it experiences electron shielding, making it different in its chemistry from the other group 12 metals, cadmium, and zinc.¹⁰ It has greater electronegativity due to high relativistic effects, which cause the contraction of the s and p orbitals. These relativistic effects are responsible for mercury's unique physical, chemical, and spectroscopic properties.¹¹ Inorganic mercury exists in both the +1 (Hg^{I}) and +2 (Hg^{II}) oxidation states. Higher oxidation states than +2 are not typically encountered due to its high ionization potential.¹⁰

Mercury exists in three primary forms in the environment; these include elemental mercury (Hg^0), inorganic mercury (Hg^{2+} or Hg^+), and organic mercury (R-Hg^+ or R_2Hg). Elemental mercury is very volatile and partially soluble in water. It is transformed into other forms of mercury through redox reactions. The inorganic forms are the mercurous +1 state (Hg^+) and the mercuric +2 state (Hg^{2+}). The mercurous state exhibits covalent metal-metal bonding (Hg-Hg), making it the most common metal polycation. An example is the mercury mineral calomel (Hg_2Cl_2). Hg^{2+} is very soluble and environmentally mobile. It could either bind to particulate matters in the atmosphere or be deposited into the land and water, forming complexes with sulfur-containing ligands. Organic mercury compounds are organometallic mercury forms, which are covalently bound to carbon. These include methyl mercury (MeHg^+ or CH_3Hg^+), ethyl mercury ($\text{C}_2\text{H}_5\text{Hg}^+$), phenylmercury ($\text{C}_6\text{H}_5\text{Hg}^+$), and dimethylmercury ($\text{CH}_3\text{-Hg-CH}_3$).¹⁰ Of all these organic mercury species, MeHg^+ is the most toxic. It is popularly known for its potent neurotoxicity in humans.

Elemental mercury (Hg^0) is released into the atmosphere as vapor from both natural and anthropogenic activities. Hg vapor in the atmosphere is widely dispersed and can last up to a year, during which it undergoes long-range transport.¹² Hg^0 undergoes several transformation processes in the atmosphere; the most common is its photochemical oxidation to mercuric ion (Hg^{2+}).¹³ Hg^{2+} then combines with particulate matter or water vapor in the atmosphere and is released back to the earth's surface through dry or wet depositions.¹³ Hg^{2+} accumulates in the soil and can be washed by erosions to the water bodies or re-emitted as Hg^0 to the atmosphere through forest fires. While in the water bodies, such as oceans or lakes, Hg^{2+} may bind to reduced sulfides, particulate matters, or dissolved organic matter (DOM). These mercury-bound materials then settle out of the water into the sediments through sedimentation processes.¹⁴ Aside from the sedimentation of mercury in the aquatic systems, Hg^{2+} can also be methylated. Methylation of mercury to methylmercury (MeHg^+) occurs mainly in anaerobic conditions under the influence of methanogenic or sulfate-reducing bacteria present in these systems.¹⁵ MeHg^+ bioaccumulates in living organisms tissues and then increases in concentration through biomagnification up the food chain (planktons \rightarrow small fish \rightarrow big fish \rightarrow humans). The methylated mercury may also undergo biotic- or photo-demethylation to Hg^{2+} . The Hg^{2+} is then reduced by sulfites to Hg^0 for further re-emission into the atmosphere (Figure 1.2). These continuous biogeochemical cycles promote the exchange of mercury between the atmosphere and the aquatic and terrestrial ecosystems.¹⁴

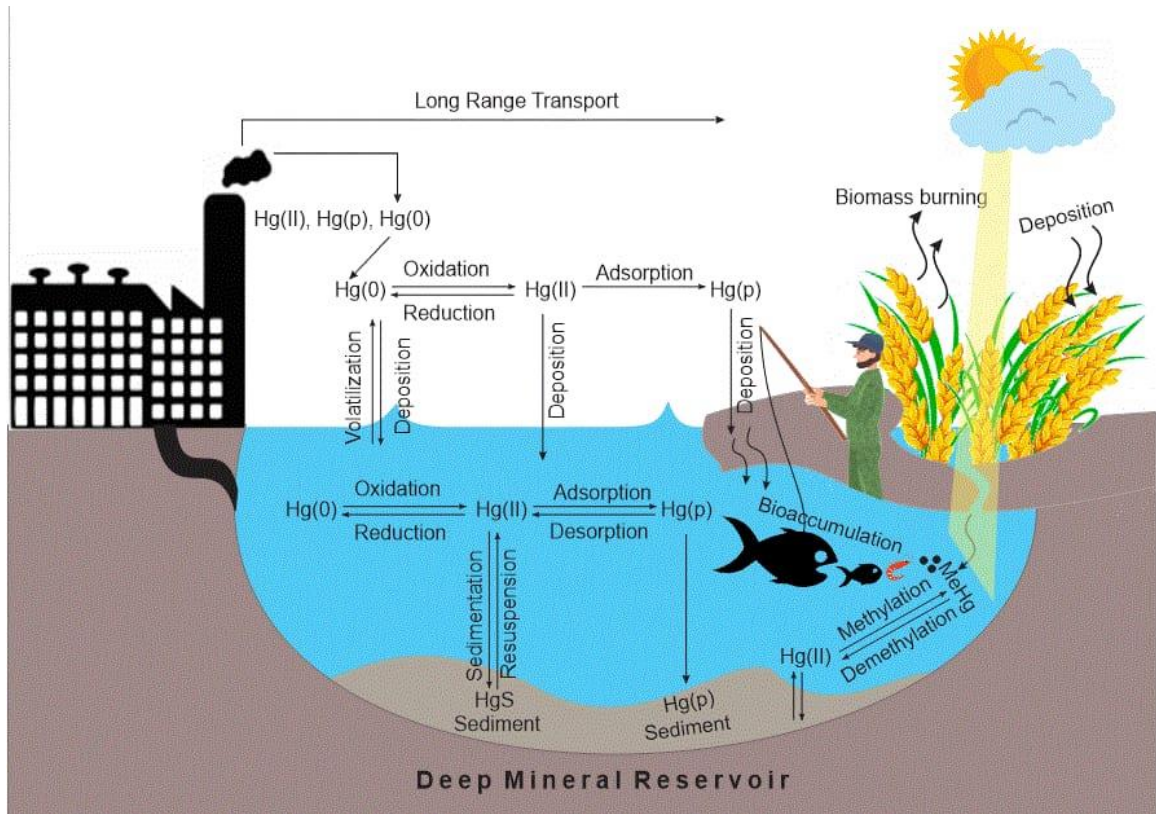


Figure 1.2: The mercury cycling pathways in the environment¹³

1.1.4 Mercury bioaccumulation and toxicity

The biological effects and the degree of mercury toxicity depend on the form of mercury (elemental, inorganic, or organic). Mercury exposure is usually through ingestion, inhalation, and dermal absorption. When inhaled, elemental mercury vapor is absorbed into the bloodstream and is converted to $\text{Hg}^{\text{(II)}}$ through oxidation processes. Exposure to inorganic mercury such as $\text{Hg}^{\text{(I)}}$ and $\text{Hg}^{\text{(II)}}$ can be through the inhalation of aerosols, ingestion of their salts, or dermal contact. $\text{Hg}^{\text{(I)}}$ converts to $\text{Hg}^{\text{(II)}}$ upon absorption. At the same time, $\text{Hg}^{\text{(II)}}$ binds to sulfur-containing amino acids of proteins, such as cysteine, which enhances their solubility in lipids, promoting its transport

through biological membranes. Microbial actions on $\text{Hg}^{\text{(II)}}$ in the gastrointestinal tract lead to its conversion to more toxic organic mercury forms, such as methyl mercury. Methylmercury is lipid-soluble; it binds to cysteine residues and passes through biological membranes, therefore inhibiting the functions of these proteins. Its strong interaction with sulfur-containing biological compounds interferes with enzyme functions, cellular structure, and protein synthesis. Because of its high lipophilicity, methylmercury bioaccumulates in living tissues and biomagnifies through the aquatic food chain. Therefore, ingestion of contaminated fish is a significant source of mercury exposure to humans, such as the infamous public health disaster case at Minamata Bay, Japan.¹⁶ Severe exposure to mercury may lead to neurological disorders, brain, kidney, or liver damage, congenital disabilities, and in some cases, death.

1.2 Mercury coordination chemistry

The coordination chemistry of mercury describes the bonding behavior between mercury in its two common oxidation states, +1 and +2, and electron donors such as neutral or negatively charged ligands. The monovalent state (+1 state) acts as a polycation that forms a metal-metal bond (Hg_2^{2+}). The divalent state (+2 state), on the other hand, has a filled d^{10} orbital which lacks strong coordination geometry preferences. Hg^{2+} binds strongly to electron donors containing S, N, or P due to its soft properties,¹⁷ however, these complexes commonly undergo rapid ligand exchange while polydentate ligands have shown slow-exchange interactions.¹⁸ Several factors, such as ligand donor atom type, ligand chelation mode, metal center coordination geometry, coordination number, and the Hg mode of polymerization, are important in the formation of the

complexes' crystal units. Mercury is quite different in its chemistry when compared to other main group elements. It has a flexible coordination environment due to its spherical d^{10} configuration. For d^{10} metals, coordination geometry varies from two-coordinate (linear) to six-coordinate (octahedral) or even eight-coordinate (hexagonal bipyramidal) with severe distortions.¹⁹ $Hg^{(II)}$, because of its spherical d^{10} configuration, tends to form low-coordinate structures with either linear or tetrahedral geometries. Therefore, the most common coordination numbers of $Hg^{(II)}$ are two (linear) and four (mostly distorted tetrahedral). Sometimes, $Hg^{(II)}$ forms 3-coordinate structures; however, these are rare cases.²⁰

Mercury chelation occurs when it forms coordinate bonds with polydentate ligands. A chelating agent (or chelator) tends to have more than one coordination site for metal complexation. Biological ligands in organisms, such as proteins, contain groups with sulfur donor atoms (cysteine or glutathione) that promote strong covalent mercury-ligand bonding during mercury poisoning and prevent the natural heavy metal excretion after intake. However, artificial chelating agents can be used to displace the biological ligands and form stronger complexes with mercury, which can then be excreted out of the living organism (chelation therapy). A good chelator should have good solubility in both lipids and water, should not be bio-transformed, should have the ability to reach the target mercury accumulation sites, should form stable complexes at the body pH level, and its complexes should not be toxic.²¹ Chelating agents used for mercury detoxification (Figure 1.3) include 2,3-dimercaptopropan-1-ol (BAL), 2,3-dimercaptopropane-1-sulfonic acid (DMPS), *meso*-dimercaptosuccinic acid (DMSA), and α -lipoic acid ((*R*)-5-(1,2-dithiolan-3-yl)pentanoic acid, LA).^{22,23}

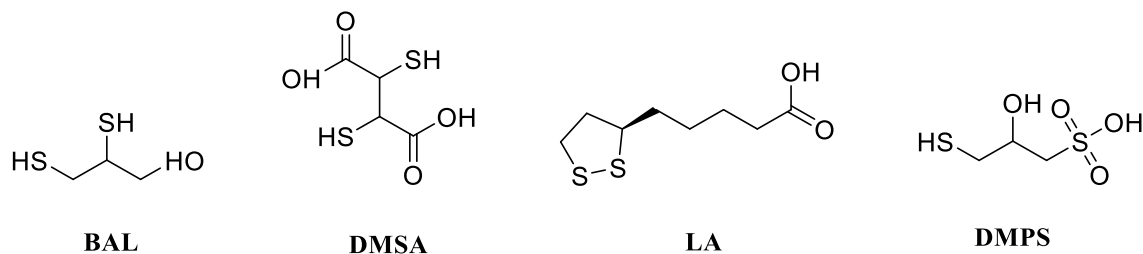
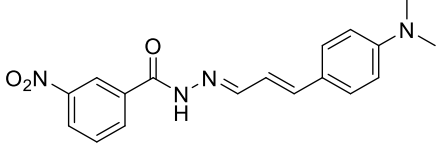
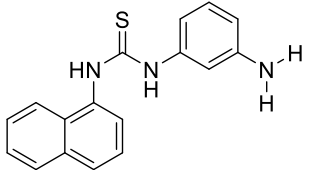
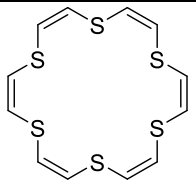


Figure 1.3: Structures of chelating agents used for mercury detoxification.

The strength of interaction and stability of a metal-ligand complex is quantified by the stability constant, often termed as binding constant or just binding affinity. Several natural or synthetic organic molecules have been reported to form mercury complexes with high stability constants. For instance, Dissolved Organic Matter (DOM), a complex heterogeneous mixture of molecules with multiple functional groups, binds to mercury strongly through thiol groups under natural conditions.²⁴ Other ligands, such as ethylenediaminetetraacetic acid (EDTA), form strong complexes with many metal ions due to multidentate moieties. EDTA has been reported to form a 1:1 complex with Hg^{2+} with a $\log K_a$ of 22.07.²⁵ Table 1.1 shows studies of $\text{Hg}^{(II)}$ complexation, including the ligand structures and the respective stability constants for $\text{Hg}^{(II)}$ complexation.

Table 1.1: Mercury(II) coordination with several ligands

Ligand Type	Structures	Stability (or dissociation) Constant	References
Thiophene		$K_a = 9.76 \times 10^{10} \text{ M}^{-2}$	Shigemoto et al. ²⁶

Schiff bases		$K_a = 2.0 \times 10^9 \text{ M}^{-2}$	Kim et al. ²⁷
Thiourea		$K_d = 1.659 \text{ M}$	Ngah et al. ²⁸
Thiacrown ether		$\text{p}K_d = 1.4$	Tsuchiya et al. ²⁹

K_d = Dissociation Constants

K_a = Association Constants

1.3 Mercury (II) removal methods from aqueous solutions

1.3.1 Overview

The primary form of mercury in the atmosphere is Hg^0 , while CH_3Hg^+ is dominant mainly in the biota. Since the most prevalent form of mercury in soil, water, and sediment is $\text{Hg}^{(\text{II})}$, most of our studies will be on the remediation or sensing of $\text{Hg}^{(\text{II})}$ from aqueous solutions. Often, $\text{Hg}^{(\text{II})}$ degradation does not occur chemically or biologically. However, $\text{Hg}^{(\text{II})}$ may be transformed into other toxic compounds in the environment.³⁰ $\text{Hg}^{(\text{II})}$ should be removed from wastewater before its discharge into aquatic environments. Researchers have reported various techniques such as adsorption, precipitation, filtration, solvent extraction, reverse osmosis, and electrochemical methods of $\text{Hg}^{(\text{II})}$ removal from aqueous solutions.³¹

1.3.2. Adsorption

Several adsorption processes involving the use of bio-adsorbents or ion exchange resins for $\text{Hg}^{(\text{II})}$ removal from wastewater have been studied. Biomaterials, such as dried dead algae, fungi, or bacteria, have been used due to their chemical composition that favors mercury biosorption. In a study by Martinez-Juarez et al., biomasses of different fungi were used for $\text{Hg}^{(\text{II})}$ adsorption. The removal efficiency of 95.3 % at pH 5.5 was reported for one of the fungi.³² Ion exchange resins functionalized with thiol groups have also been widely studied. The commercially available resin TP-214, for instance, removed mercury from aqueous solutions with an adsorption capacity of 456 mg/g.³³ Other commonly used resins for $\text{Hg}^{(\text{II})}$ adsorption from wastewater are Duolite GT-73,³⁴ Purolite S-920,³⁵ and Amberlite GT-73A.³⁶ Other $\text{Hg}^{(\text{II})}$ adsorbents include clay,³⁷ activated carbon (either commercially available³⁸ or derived from carbonaceous waste materials³⁹), and nanoparticles.⁴⁰

1.3.3. Precipitation

A precipitation process in wastewater treatment involves the conversion of soluble or suspended pollutants to solid precipitates, after which the precipitates are separated. Chemical precipitation of soluble mercury is typically carried out using sulfide salts. $\text{Hg}^{(\text{II})}$ is commonly precipitated out as insoluble mercury sulfide (HgS) using sodium sulfide (Na_2S).⁴¹ Often, the resulting metal sulfide sludge poses a secondary waste problem. Softening, another form of precipitation method involves using excess $\text{Ca}(\text{OH})_2$ to precipitate soluble mercury as insoluble $\text{Hg}(\text{OH})_2$. The high pH and the concentration of soluble mercury in the solution play a crucial role in this case.

Coagulants, such as $\text{Al}_2(\text{SO}_4)_3$, are also employed for precipitation and removal of mercury from wastewater.⁴²

1.3.4. Filtration

The membrane filtration method for mercury removal is known for its high efficiency and simple design. However, it is also considered expensive due to high purchase and running costs. Ultrafiltration,⁴³ nanofiltrations,⁴⁴ and reverse osmosis⁴⁵ are other membrane filtration processes used for mercury removal.

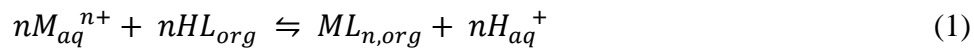
1.3.5. Electrochemical treatment

Wastewater treatment for mercury removal can also be carried out by applying a direct electric current to the solution. This mechanism encourages the migration and cathodic deposition of mercury in these solutions. Applications of electrochemical techniques, such as electrodialysis,⁴⁶ electrocoagulation,⁴⁷ and electrochemical alloy formation,⁴⁸ have been widely studied.

1.3.6. Solvent extraction

Solvent extraction is used in extractive metallurgy to recover soluble metals from aqueous solutions. Typically, two immiscible liquid phases; the aqueous phase that contains the soluble metal forms (solute A) or possible interferent (solute B) and the organic phase (containing the organic solvent and the organic extractant), are contacted in a separator. The bound metals (by organophilic ligands) migrate to the organic phase, followed by phase separation.⁴⁹

The stoichiometry of the chemical reaction occurring during the extraction process both in the aqueous or organic phases is represented as;



where M^{n+} is the metal species, HL is the extractant, and ML_n is the extractant-metal complex. Figure 1.4 describes the principle of solvent extraction. During the phase contact, the metal species (solute A) distribute in both phases until equilibrium is reached.

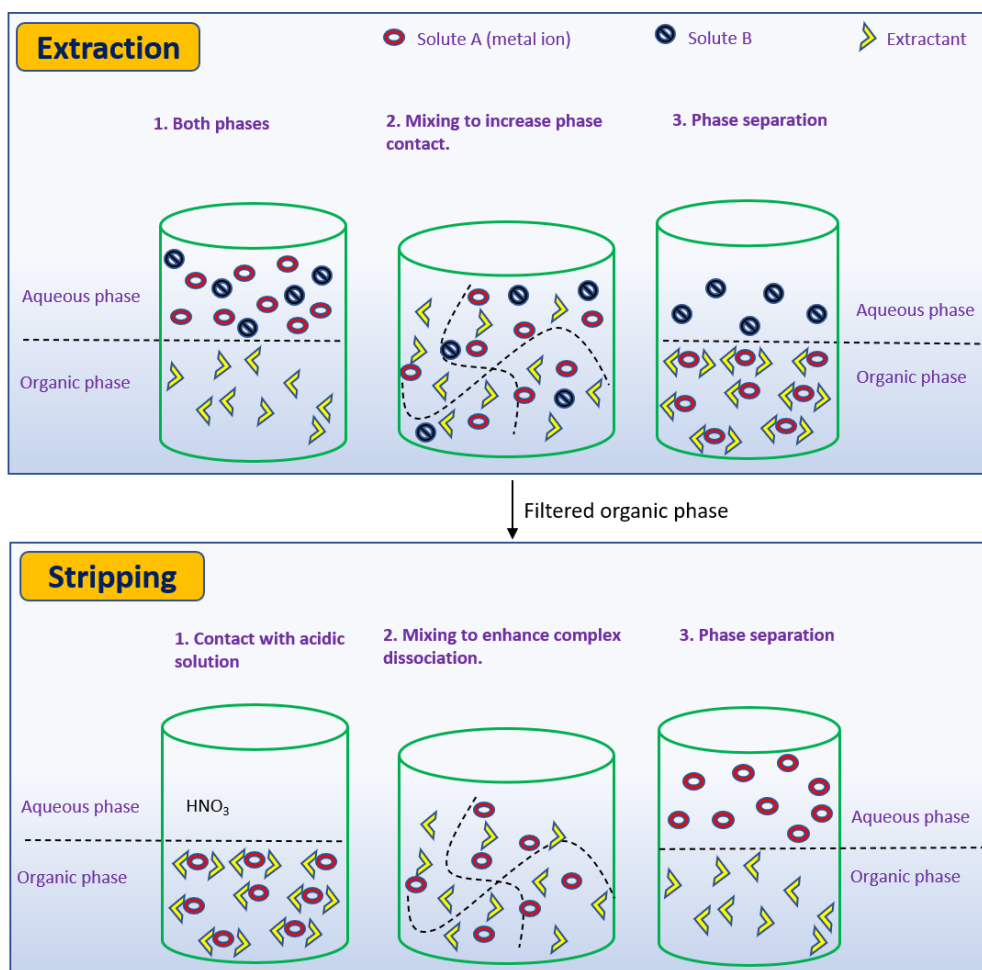


Figure 1.4: Principles of solvent extraction separation showing the two steps: i) Extraction and ii) Stripping (recovery)

The distribution ratio (D_A) of solute A between both phases at equilibrium is given as;

$$D_A = \frac{[A^{n+}]_{org}}{[A^{n+}]_{aq}} = \frac{[A^{n+}]_{aq,initial} - [A^{n+}]_{aq,final}}{[A^{n+}]_{aq,final}} \quad (2)$$

$[A]_{org}$ and $[A]_{aq}$ are the concentrations at the equilibrium of solute A in the organic and aqueous phases, respectively.⁴⁹

The separation factor, $SF_{A/B}$ of solute A from solute B, indicates the ligand (extractant) extraction selectivity. It is derived from the distribution ratios of both solutes as;

$$SF_{A/B} = \frac{D_A}{D_B} \quad (3)$$

After extraction, a subsequent process is carried out to recover the organically bound metal from the organic extractant by contacting the organic phase with an acidic aqueous phase. This process is known as stripping. A stripping agent, such as dilute acid, is added to the aqueous phase to facilitate the complex dissociation. Afterward, the metal migrates back to the aqueous phase while the extractant remains in the organic phase. This process leads to the recovery of both the metal (in a new aqueous phase) and the extractant (in the organic phase), which may be reused for further extraction. The pH variation and the metal oxidation state typically influence extraction efficiency and selectivity.

Several extractants have been studied for $Hg^{(II)}$ removal. Reddy et al. reviewed the use of calix(4)arenes as extractants for mercury extraction.⁵⁰ Yordanov et al. used calix(4)arenes with sulfur-containing lower rim functionalities (Figure 1.5) for heavy

metal extraction into chloroform. They reported extraction efficiencies of 86 % for $\text{Hg}^{(\text{II})}$ and 100 % for $\text{Au}^{(\text{III})}$.⁵¹ Other calixarenes have also been investigated.⁵²⁻⁵⁴

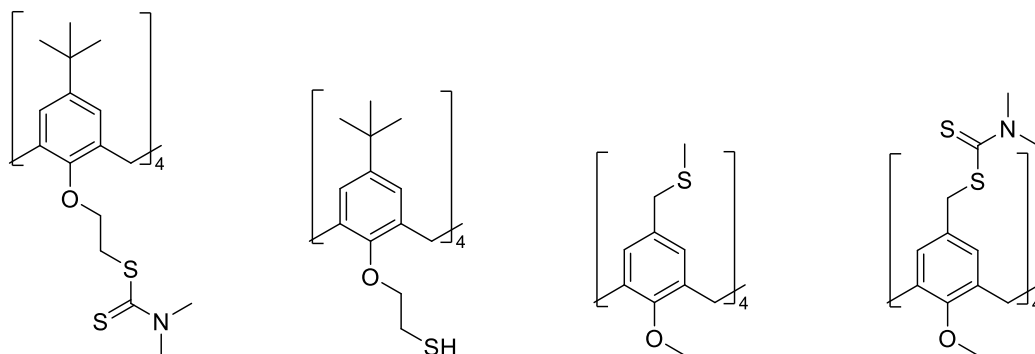


Figure 1.5: Structures of calix(4)arenes used for $\text{Hg}^{(\text{II})}$ extraction

Crown thioethers (Figure 1.6) are also popular for $\text{Hg}^{(\text{II})}$ extraction due to their strong $\text{Hg}^{(\text{II})}$ affinity and stability in acidic media.⁵⁵⁻⁶⁰ Other reagents, such as high molecular weight amines (primene, aliquat 336, alamine 336, and amberlite LA-1),⁶¹⁻⁶³ thiourea,⁶⁴ tributylphosphate-TBP,⁶⁵ and dithizone,⁶⁶ have been widely used for $\text{Hg}^{(\text{II})}$ extraction.

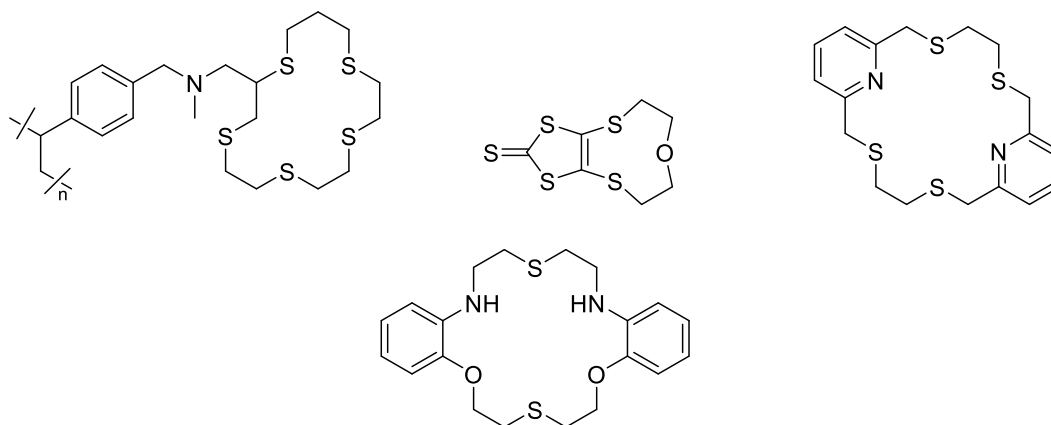


Figure 1.6: Structures of thiacrown ethers used for $\text{Hg}^{(\text{II})}$ extraction.

Factors such as the pH effect, ionic strength, extractant concentration, and the extraction contact time play major roles in observed Hg^(II) extraction efficiency.

1.4. Mercury sensing

1.4.1 Overview

An important goal in the sensing of mercury is the development of highly selective and sensitive (low detection limit) detectors. Various conventional sensing methods, such as spectrophotometry, high-performance liquid chromatography (HPLC), atomic absorption spectroscopy (AAS), inductively-coupled plasma optical emission spectrometry (ICP-OES), voltammetry, and electrochemical stripping analysis, have been developed to selectively detect and quantify toxic metals, including Hg. Although these methods have good accuracy, the instrumentation is bulky, tedious to maintain, and has a high cost of purchase and maintenance. UV-Visible and fluorescence spectrophotometry are often preferred methods because they are simple, portable, easy to maintain, and require small concentrations of samples for analysis. Binding-induced mechanisms for metal detection typically use various photophysical processes, such as photoinduced electron transfer (PET), electronic energy transfer (EET), charge transfer (CT), and fluorescence resonance energy transfer (FRET).⁶⁷

Chemosensors are analyte detectors that convert chemical stimuli into specific responses that are mainly detected by a change in optical (color), fluorescence, or electronic signals. They are developed for use in the analysis of biological, environmental, and industrial samples. They are also used in medicine as biosensors.

During analyte detection by chemosensors, signal transduction and molecular recognition occur through some sensor components. These include a receptor and a spacer.

1.4.3 Colorimetric chemical sensing of mercury

Colorimetry is an analytical method that monitors the color change of an optical sensor by the influence of a physical or chemical stimulus on its sensing ability. Chromophoric-bearing organic molecules undergo complexation reactions with metal species, resulting in color change. The altering of the electron density on the chromophore leads to the visual color change (“naked eye” observations) or change in the UV-Visible absorbance. The color change observed is usually a result of chemical interactions, such as charge transfer (CT), involving the transfer of electrons from the metal to the ligand (MLCT) or from the ligand to the metal (LMCT). In MLCT, there is usually a shift of the absorption band(s) to shorter wavelengths (blue or hypochromic shift), while LMCT typically leads to a shift in the absorption band(s) to a longer wavelength (red or bathochromic shift).⁶⁸ Colorimetric sensing involves the use of ligands that can form organic-soluble metal complexes with variable optical spectroscopic properties that can be used for toxic metal optical sensing. Table 1.2 shows some of the colorimetric chemosensors that have been used for mercury sensing.

1.4.2 Fluorescent chemical sensing of mercury

In fluorescence, certain compounds are irradiated by photons, leading to their excitation. Photon absorption leads to electron excitation from the singlet ground state to the singlet excited state. The excited state return to the ground state gives emission of a lower energy photon (longer wavelength) than the absorbed photon. The transitions of

electrons from these different states are shown in the Jablonski energy diagram below (Figure 1.7). A fluorescent chemosensor is a compound that possesses a binding site, a fluorophore, and a spacer. Table 1.3 shows some fluorescent chemosensors that have been used for Hg^(II) sensing.

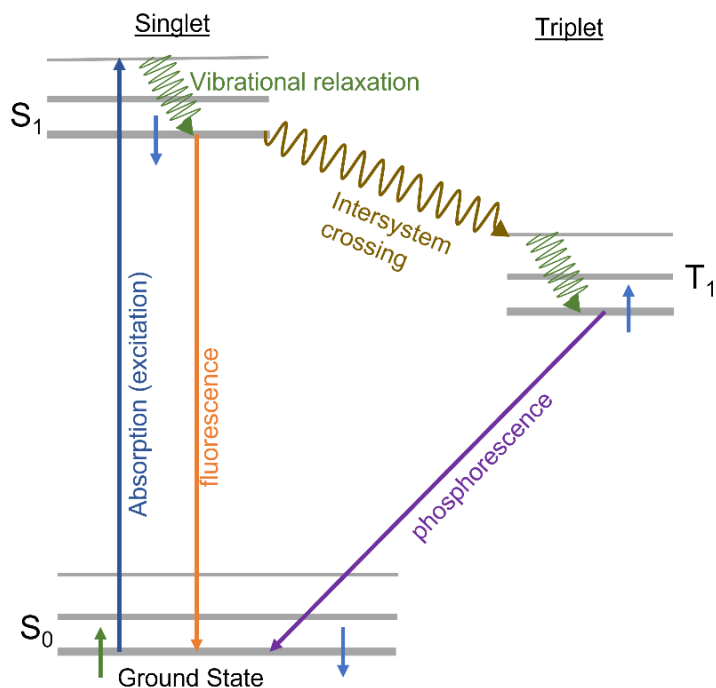
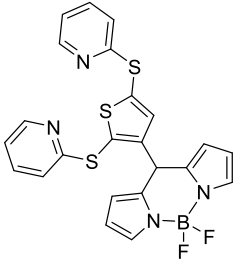
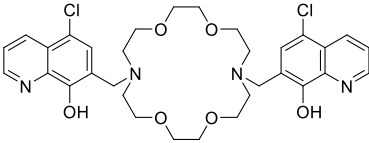
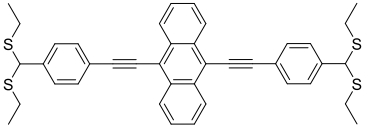
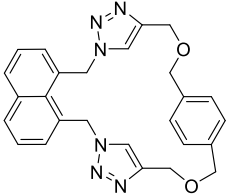
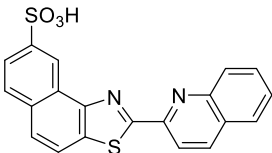
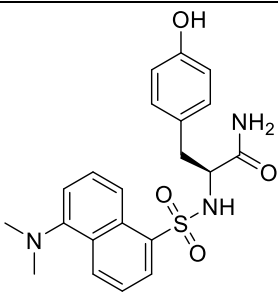
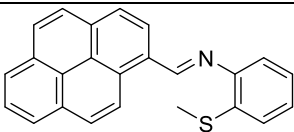


Figure 1.7: Jablonski diagram⁶⁹

Table 1.2: Some colorimetric/fluorescent Hg(II) chemosensors.

Chemosensor	Structure	Color change/ emission color	Detection limit	References
Schiff base- diazazole		Yellow to colorless	5.47 x 10 ⁻¹¹ M	Saleem et al. ⁷⁰

BODIPY (boron dipyrromethene)		Yellow-orange red	10^{-6} M	Singh et al. ⁷¹
Quinolines			-	Prodi et al. ⁷²
Anthracenes		Green emission	5.94×10^{-8} M	Swamy et al. ⁷³
Naphthalene			1.55×10^{-7} M	Dai et al. ⁷⁴
Naphthothiazole		Colorless to yellow/ Green emission	3.42×10^{-8} M	Jonaghani et al. ⁷⁵
Dansyl		Green emission	2.35×10^{-8} M	Wang et al. ⁷⁶
Pyrene		Yellow to colorless/ Blue emission	2.2×10^{-8} M	Sivaraman et al. ⁷⁷

1.5. The mercury problem in high-level waste at the Savannah River Site (SRS)

1.5.1 Overview

The Savannah River Site (SRS), located in Aiken, SC, United States, has a mercury concern due to traces of organomercury forms in the saltstone low activity deposits that are produced after processing of high-level alkaline radioactive waste (HLW), which has been accumulated over years of PUREX processing for plutonium production used for nuclear weapons.⁷⁸ Mercury in HLW originates mainly from its use as an acidic dissolution catalyst for aluminum cladding from target fuels within the uranium and plutonium processing operations. It is present to about 60 metric tons in HLW tanks. Organic mercury species have also been found in low activity waste (LAW). Therefore, there is a need to convert organic mercury to other less toxic forms and complex and remove Hg prior to disposal of LAW in saltstone.

1.5.2 Nuclear waste management at the SRS

During the cold war era, alkaline high-level radioactive waste (HLW) has been accumulated due to nuclear weapons production and has been stored in carbon steel tanks at the Savannah River Site (SRS), South Carolina. The original aim of SRS was to support the U.S. nuclear weapons program by separating uranium and plutonium from irradiated targets and spent nuclear fuel from on-site reactors.⁷⁹ Both canyons F and H at SRS piped highly radioactive liquid waste from the chemical processing operations to a set of tanks located in its area.⁷⁹ The waste from these canyons contains radionuclides, including fission products (¹³⁷Cs) and actinides, such as ²³⁷Np, which are not separated

during plutonium recovery. It also contains several salts and neutralizing and alkalinizing chemicals, as well as several trace metals and even some organics. The tank mixtures were alkalinized intentionally in order to avoid corrosion of the carbon steel tanks.⁷⁹

The HLW tanks contain three separate phases (Figure 1.8): Supernatant liquid which contains soluble salts; salt cake in which much of the salts initially in solution crystallize to form a solid cake after evaporation; and sludge which is mainly insoluble hydroxides of transition metals generated when NaOH was added to acidic waste to neutralize it and make it alkaline before it was pumped to the tanks.

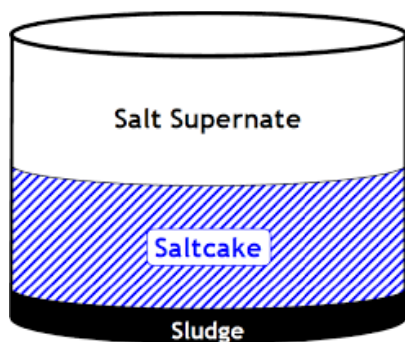


Figure 1.8: *The three physical forms of waste at the SRS*

The current processing of HLW at SRS involves the separation of radioactive species from the waste in order to produce a highly radioactive solid for vitrification and geological deposition and a low activity stream for long-term saltstone storage (Figure 1.9). These processes involve a front-end Actinide Removal Process (ARP) in which radioactive components such as ^{14}C , ^{79}Se , ^{99}Tc , ^{129}I , ^{126}Sn , ^{237}Np , and various isotopes of U (234, 235, and 238) are removed alongside ^{90}Sr .⁷⁹ This is followed by Cs separation by the Caustic Side Solvent Extraction (CSSX) process in the Modular CSSX Unit (MCU). ^{137}Cs and ^{90}Sr contribute to 95% of the radioactivity in the waste stream. After the extraction/scrub/strip cycle sequence, the highly concentrated Cs stream is vitrified at the

Defense Waste Processing Facility (DWPF), together with the An and Sr components. The Low Activity Waste (LAW) is accumulated in Tank 50-H for saltstone disposal.

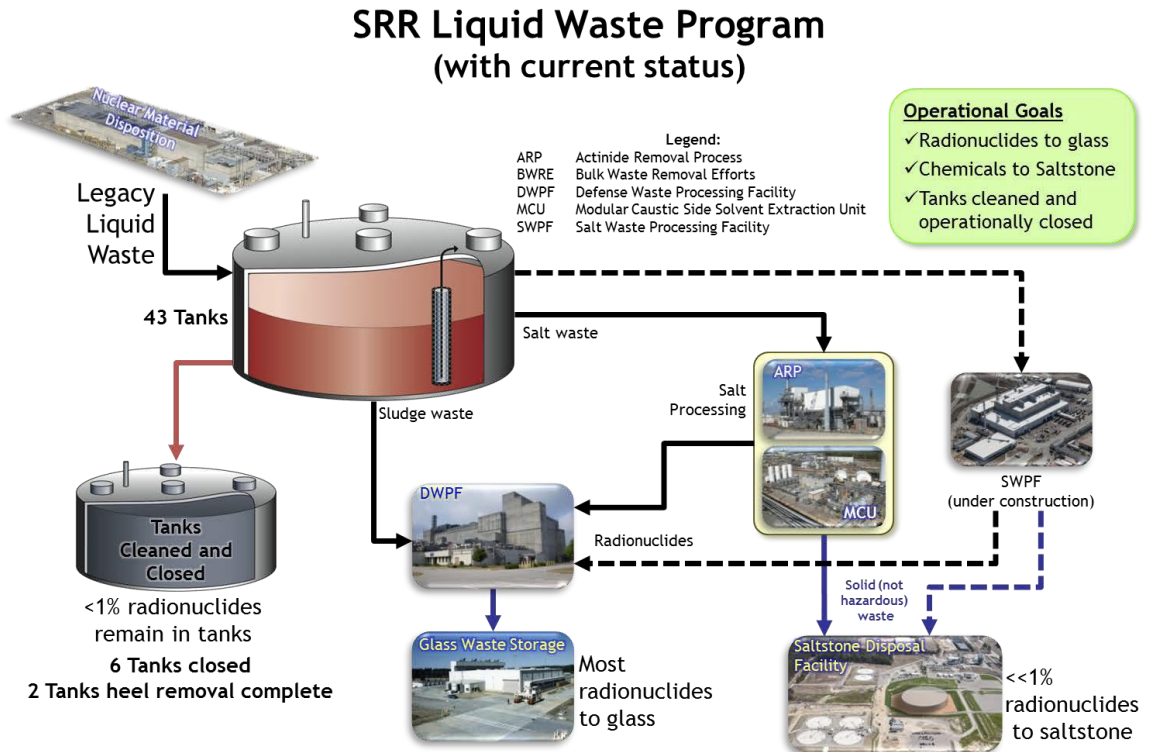


Figure 1.9: Savannah River Remediation (SRR) liquid waste program⁸⁰

1.5.3. Mercury in the liquid waste streams at SRS.

Mercury at SRS originated from its use as a catalyst for the acidic dissolution of aluminum cladding from targets and fuels, aluminum alloy fuels, and aluminum–uranium cermet within the uranium and plutonium processing operations in the liquid waste stream.⁸¹ To dissolve the aluminum cladding and the U-Al fuel, mercury in the form of soluble Hg^(II) nitrate was added to accelerate the process.⁷⁸ It is present to about 60,000 to 70,000 kg in the waste stream, and it occurs in various forms in solid and solution phases with concentrations ranging from 100 mg/kg to 3,600 mg/kg in the processed sludge batches.⁸² It is present in the sludge as elemental mercury (Hg⁰), whose vapors

constitute the principal chemical hazard, and insoluble mercuric oxide, HgO. The liquid waste solution contains inorganic mercuric salts, Hg^(II), and organomercury as RHgX and R₂Hg compounds, where R = Me, Et, and other alkyls and X = NO₃⁻, Cl⁻, and other anions. The organomercury tank content (> 55 mg/L) is approximately two to three times higher than the total mercury in all other forms (~20 mg/L). Quarterly monitoring of Tank 50 shows that the ratio of organomercury to total mercury has been continuously increasing.⁸² This high organomercury content of the saltstone renders the current HLW processing unsustainable long-term. Furthermore, immediate major concerns arise from elevated levels of soluble mercury: The mercury levels within the Liquid Waste System (LWS) are being encountered at higher than previously predicted (Figure 1.10). This may be attributed to ineffective removal of mercury from the processed waste streams. DWPF, which was designed initially with a mercury purge point, is no longer functional. In order to reduce the overall mercury levels, a method of removing mercury from the DWPF process stream must be re-established.⁸⁰

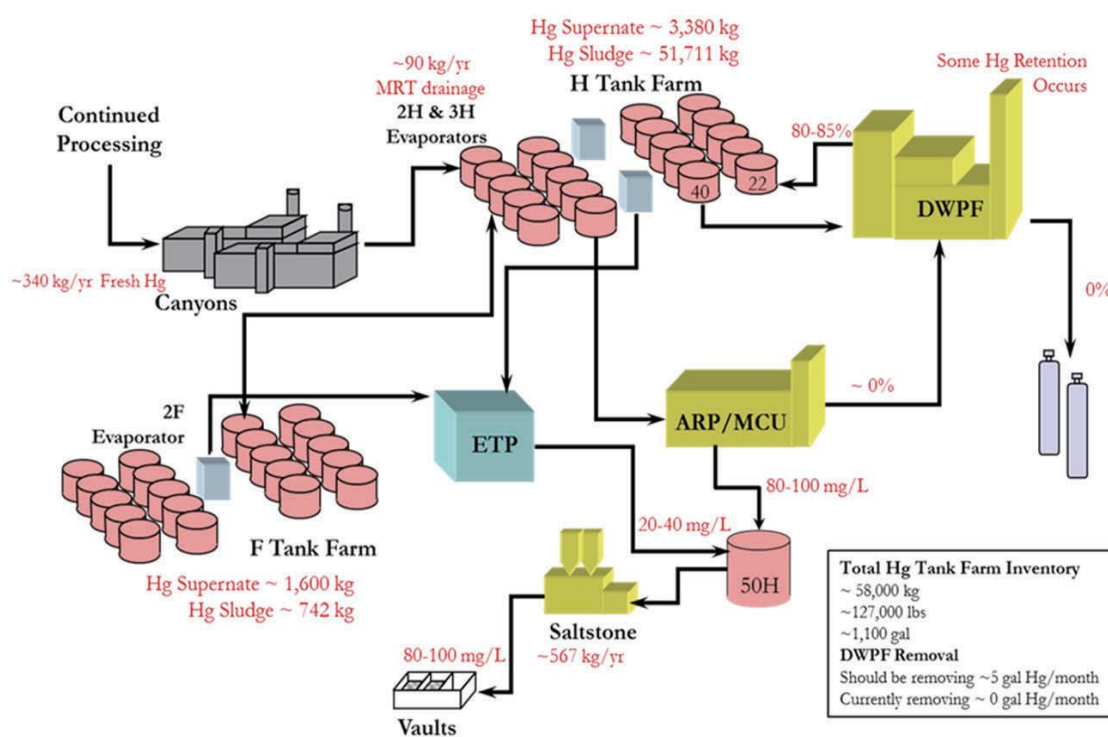


Figure 1.9: Mercury in the liquid waste stream at the Savannah River Site⁸²

The primary processing points for mercury removal under examination at SRS include the DWPF, which was designed to be the primary purge point for mercury; the evaporators, which currently collect elemental Hg; Tank 50, the saltstone feed tank; and finally, the saltstone formulation itself.⁸² Initially, the bulk of mercury removal was done prior to vitrification via steam stripping in the sludge receipt and adjustment tank (SRAT) by reducing mercury in its oxide or nitrate forms to Hg⁰ with formic acid (HCOOH). At elevated temperatures, the metallic mercury vaporized and then collected, washed, and purified in the mercury purification cell and removed from the system.⁸⁴ However, this method is only 33% efficient.⁸⁵ Cation exchange resins were also used for mercury treatment at the effluent treatment plant (ETP).³¹ Columns packed with resins

functionalized with thio groups were arranged in parallel so that the effluent passes through the columns for ion exchange to occur. The columns being buried on site after exhaustion could lead to the leaching of mercury and groundwater contamination over time. Other methods of aqueous mercury treatment, such as precipitation with sulfides, coagulation with alum, and membrane separations, also present the disadvantage of secondary waste accumulation.³¹

Applications of improved mercury separation and removal technologies could be the key to addressing these challenges. Several improved removal and remediation techniques have been proposed for mercury removal from the liquid waste system, which includes conversion of inorganic mercury to elemental Hg prior to evaporator processing, application of mercury sorbents to remove organomercury from highly alkaline waste solutions, conversion of organomercury to inorganic mercury at Tank 50, immobilization of mercury by ligand complexants and precipitating it out in tank 50 (LAW), and the extraction of mercury from HLW into organic solvents by modifying CSSX and subsequent removal together with cesium, strontium, and actinides.⁸¹

1.5.4. Choice of ligands for mercury remediation at SRS

Ligands that can be used for mercury precipitation in the low activity waste stream (Tank 50) must be available in large quantities from inexpensive starting materials. In contrast, ligands for use as organic extractants from the high-level waste stream (MCU) should be highly lipophilic, stable under radiolytic conditions, and fully recoverable post-extraction for available reuse. Luminescent derivatives of these ligand

frameworks that can complex $\text{Hg}^{(\text{II})}$ can act as sensors for quantifying $\text{Hg}^{(\text{II})}$ in the complicated matrices of liquid waste streams.

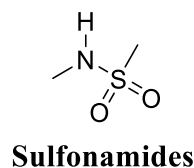
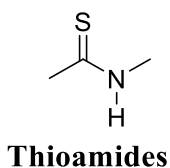
1.6 Principles for ligand design for mercury complexation

The most important characteristic of these ligands to be considered is their ability to bind strongly and selectively to $\text{Hg}^{(\text{II})}$. For this reason, we are considering the hard-soft acids and bases theory (HSAB theory)¹⁷ in choosing our ligands. According to Lewis,⁸⁶ $\text{Hg}^{(\text{II})}$ is classified as an acid (Lewis acid). Thus, it acts as an electron acceptor while electron donors, such as water and other ligands that form complexes with metals, are classified as Lewis bases. Pearson in 1963 classified Lewis acids and bases as either hard or soft. He defined a hard metal ion as one that has a high charge and small size and can strongly retain its valence electrons. While a soft metal ion does not strongly retain its valence electrons, it has a relatively large size and low positive charge.¹⁷ The hardness or softness properties of the electron donor (coordinating group - ligand) and the electron acceptor (metal ion) play a role in determining the stability of the formed complexes. Typically, stable complexes are formed from either interaction of hard acids with hard bases or of soft acids with soft bases. The classification of metals, and the coordinating groups, according to their hard, intermediate (borderline), and soft character, is provided in Table 1.3.

Table 1.3: HSAB classification of Acids and Bases

	Soft	Borderline	Hard
Bases	H ₂ S, C ₂ H ₄ , RSH, R ₂ S, C.N. ⁻ , RCN, H ²⁻ , R ₃ P, R-S ⁻ , I ⁻	C ₆ H ₅ NH ₂ , C ₅ H ₅ N, C ₃ H ₄ N, N ₂ , Br ⁻ , N ₃ ⁻	RCOO ⁻ , O.H. ⁻ , R ₂ O, N ₂ H ₄ , RNH ₂ , NH ₃ , H ₂ O, CO ₃ ²⁻ , F ⁻ , Cl ⁻
Acids	Cd ²⁺ , Cu ⁺ , Ag ⁺ , Hg ²⁺ , Pd ²⁺ , Pt ²⁺ , Hg ⁺ , CH ₃ Hg ⁺ , Pt ⁴⁺	Sn ²⁺ , Bi ³⁺ , Ni ²⁺ , Zn ²⁺ , Pb ²⁺ , Cu ²⁺ , Sb ³⁺ , Fe ²⁺	H ⁺ , Li ⁺ , Mg ²⁺ , Al ³⁺ , Ga ³⁺ , Ti ⁴⁺ , La ³⁺ , In ³⁺ , Zr ⁴⁺ , Sn ⁴⁺ , Na ⁺ , Sr ²⁺ , Ca ²⁺ , Be ²⁺ , Cr ³⁺ , Fe ³⁺ , UO ₂ ²⁺ , VO ²⁺

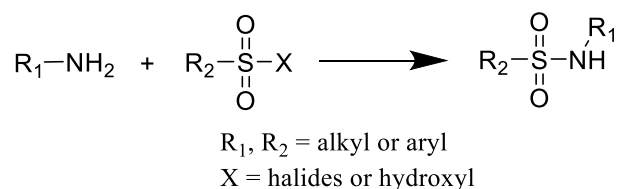
Mercuric ion (Hg²⁺) is classified as a soft metal ion. This makes it ideal for binding strongly to sulfur and nitrogen-containing molecules. It would prefer coordination by ligands classified as soft bases such as thiols (R₂S, RSH, and R-S⁻) and borderline coordinating groups, such as amines (RNH₂). Therefore, for ligand design considerations, compounds bearing S or N donor atoms would be favorable, and thus we chose ligands, such as thioamides and sulfonamides, for mercury sensing, complexation, and extraction for our studies.



1.7 Sulfonamide ligands for toxic metal complexation

Sulfonamides are common organic compounds that are widely used in clinical and pharmacological applications. The primary sulfonamides are of the type RSO₂NH₂,

where R is an aromatic, aliphatic, or heterocyclic moiety. They have pharmacological applications due to their antifungal, antibacterial, and cytotoxic properties.⁸⁷ They are easily synthesized in one step from commercially available starting materials by reacting a sulfonyl halide or sulfonic acid with an amine (Scheme 1.1).



Scheme 1.1: Synthetic pathway for a secondary sulfonamide by reacting a primary amine with a sulfonyl halide or sulfonic acid.

Metal complexes of sulfonamides have specific antimicrobial properties, promoting their applications in topical medicines (antiseptics). Certain sulfonamide family types called triple sulfa drugs (TSD), which include sulfadiazine, sulfamerazine, and sulfamethazine (Figure 1.11), are versatile metal complexing agents. This is due to their multiple active sites, such as amino, sulfonamidic, and pyrimido nitrogens, and sulfonyl oxygens.⁸⁸

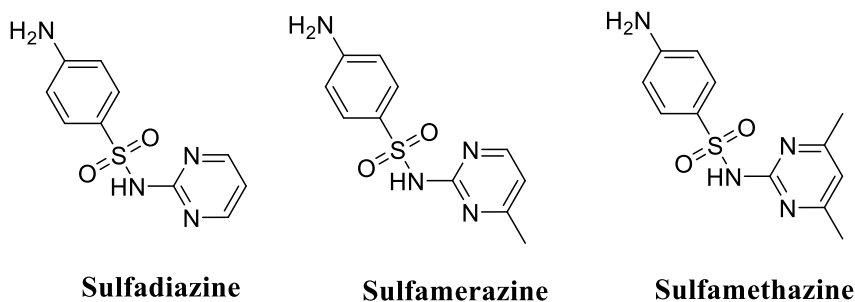


Figure 1.11: Structures of the triple sulfa drugs (TSD)

Deprotonation of the acidic hydrogen in TSDs leads to negatively-charged nitrogen that is available for coordination with metals (Figure 1.12a). Several metal complexes of sulfa drugs and their spectroscopic characterization have been reported.^{89,90} For instance, a mercury complex of sulfadiazine having DMF as co-ligands was reported by Hossain et al. in 2007 (Figure 1.12b).⁸⁸

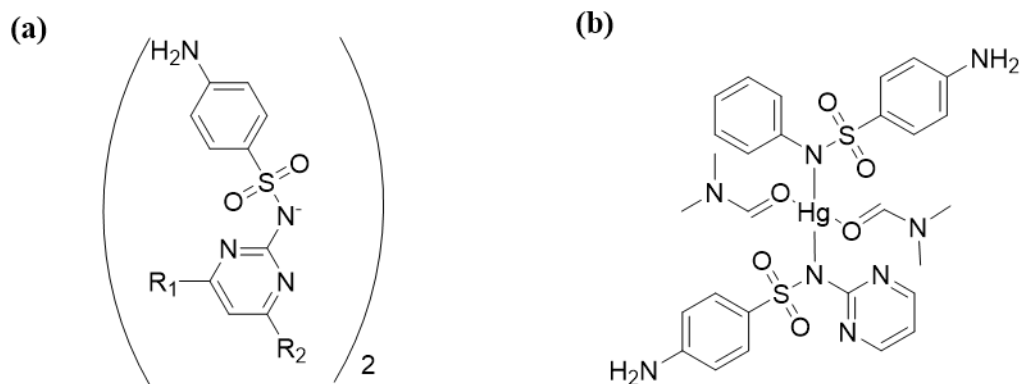


Figure 1.12: (a) Deprotonated sulfa drug (b) Sulfadiazine-mercury complex with DMF co-ligands.⁸⁸

Our research group has reported sulfonamide ligands derived from *o*-phenylenediamine and various sulfonyl chlorides as effective extractants and sensors for Pb^(II) and other toxic metals, such as Cd^(II). Pb^(II) was successfully extracted from an aqueous solution into an organic phase (1,2-dichloroethane) using disulfonamide ligands together with a bi-pyridyl co-ligand in a synergistic fashion.⁹¹ These ligands have remarkable selectivity for Pb^(II) and were also used as sensors because upon complexation with Pb^(II) the color changes from colorless to yellow⁹¹. These ligands were also used to extract Cd^(II). Their selectivity for Pb^(II) is attributed to the stereochemically active lone pair and soft characteristics of the metal, features that also apply to Hg^(II).

Figure 1.13 shows some of the *o*-phenylenediamine-derived sulfonamide complexes with Pb^(II) and Cd^(II).⁹¹

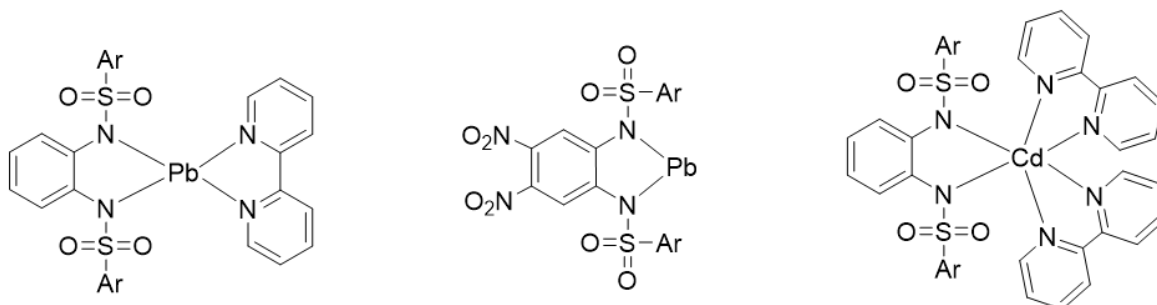


Figure 1.13: Lead and cadmium complexes of *o*-phenylenediamine-derived sulfonamide ligands.⁹¹

Fluorescent sulfonamides containing dansyl or quinoline moieties (Figure 1.14) have been widely studied for binding and detection of metals in different media^{92–95} including a seminal study for Pb^(II) reported by our research group.⁹²

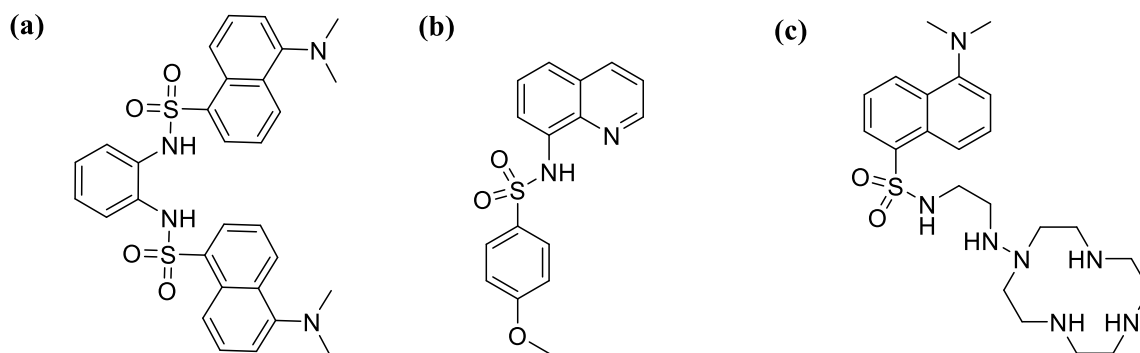


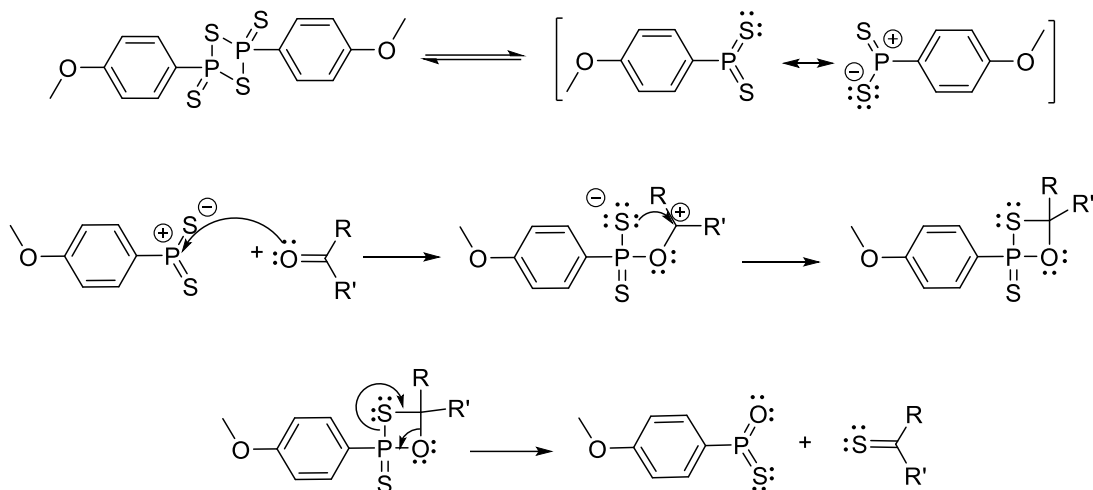
Figure 1.14: Some fluorescent sulfonamide ligands used for metal ion detection and complexation. Metal ions detected are; (a) Pb^(II)⁹² (b) Cu^(II), Cd^(II), Zn^(II), and Co(II)⁹⁵ (c) Zn^(II)⁹⁴

1.8 Thioamide ligands for toxic metal complexation

Thioamides are organosulfur compounds of great interest in various aspects of chemistry due to their unique structural features. Thioamide moieties have the general

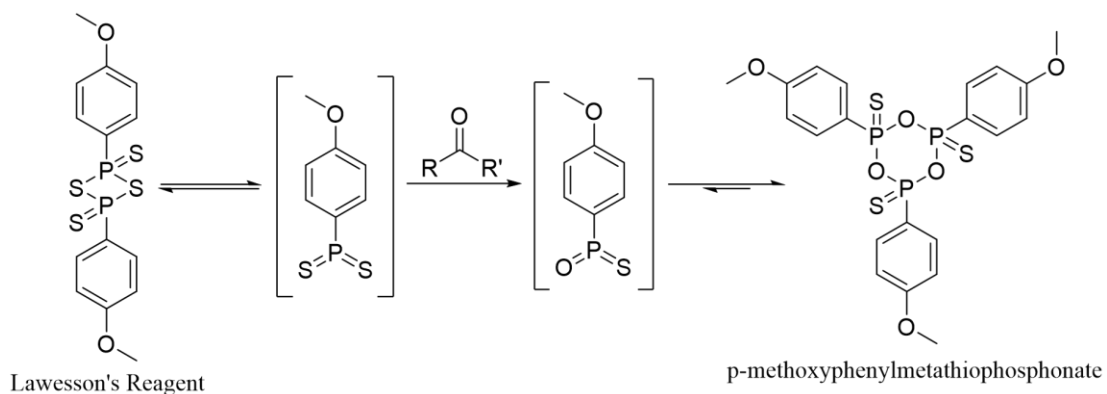
structure $R-C(=S)-NR'R''$ where R, R', and R'' are organic groups. Thioamides are used in several industrial applications. They have also found use in pharmacological applications due to their antitumor, thyrotoxic, and anthelmintic activities. Furthermore, their higher stability when compared to other thiocarbonyls (thioketones, thioaldehydes, and thioesters) and their unique binding properties toward soft metals, such as $Hg^{(II)}$, $Au^{(II)}$, and $Ag^{(I)}$, promote their organometallic and coordination chemistry.

Thioamide synthesis involves the chemistry of amides (carbonyl compounds with -N- heteroatom). Conventional amide thionation methods, such as the use of phosphorus pentasulfide, typically give very low yields. However, the thionation of amides to thioamides using Lawesson's reagent (LR) has gained recent attention due to improved yields.⁹⁶ Lawesson's reagent is commercially available or can be prepared by reacting phosphorus pentasulfide with anisole under high heat. A typical thionation using Lawesson's reagent involves refluxing under nitrogen using solvents such as toluene, acetonitrile, and THF. The reaction mechanism is shown in Scheme 1.2, where equilibrium is established between LR and dithiophosphine ylide (a decomposed form of LR under high heat). These ylides are quite reactive; they attack the carbonyl oxygen to form a P-O bond (thioxaphosphetane), which is the driving force for these reactions. The reaction step involving the formation of thioxaphosphetane, which eventually decomposes to thiocarbonyl, is similar to the Wittig reaction.



Scheme 1.2: Mechanism of Lawesson's reaction

In most cases, a trimer, *p*-methoxyphenylmetathiophosphonate is the isolated byproduct from these reactions (Scheme 1.3). This trimer makes the reaction work-up tedious due to solubility similarities with the compound of interest.⁹⁷



Scheme 1.3: Formation of the trimer by-product, *p*-methoxyphenylmetathiophosphonate

The reactivity of thioamides is very versatile due to their different resonance forms when deprotonated (Figure 1.15).

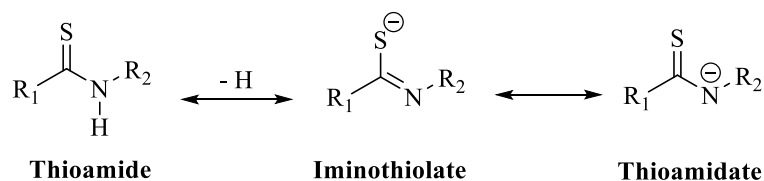


Figure 1.15: Secondary thioamide and its resonance structures

Several complexes of monodentate or multidentate thioamide ligands with various metals have been reported. Begum et al. in 2006 reported the complexation of Pd^(II) to a dithiopicolinamide through the S,C,S or S,N,S triad. Due to their charge versatility, these thioamide ligands derived from dipicolinamide tend to form metal pincer complexes that are considered thermally stable (Figure 1.16).⁹⁸

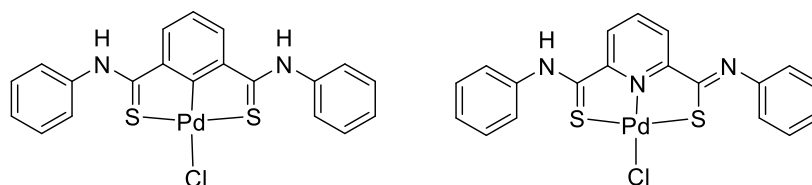


Figure 1.16: Pd^(II) pincer complexes of dithiopicolinamide.

1.9 Analytical methods: Instrumentation, methodology, and data analysis

1.9.1 Overview

Several analytical techniques are used to characterize and determine the properties of synthesized compounds and formed complexes. Properties such as light absorption or emission and mass-to-charge ratio are measured. These techniques include UV-Visible spectroscopy, fluorescence spectrophotometry, infrared spectroscopy, NMR spectroscopy, mass spectrometry, elemental analysis, and single-crystal X-ray diffraction. Most of these methods use various forms of electromagnetic radiation in the

wavelength range of 100 nm to 1 mm.⁹⁹ Interaction of electromagnetic waves with the matter may lead to their reflection or deflection, which is the major principle of analytical instrumentation. The following sections describe how these typical experimental methods were used in our studies.

1.9.2 Determination of complexation equilibria by titration

Titration is carried out to determine the complexation equilibria between ligands and the complexed metal. Techniques such as UV-Vis, fluorescence, and NMR spectroscopy are utilized. Typically, in UV-Vis or fluorescence, a solution of ligand and organic base (if required for ligand deprotonation) is titrated with metal salt solutions at constant ligand concentration. For spectra collection, a quartz cell of 1 cm optical path length filled with 2.300 mL of the ligand solution is titrated with the salt solution (prepared with the ligand solution) at gradual increments until saturation is observed. All the spectroscopic measurements are performed in triplicate and averaged. NMR titrations are quite similar, but deuterated solvents are used instead.

1.9.3 Determination of stoichiometry by Job plot

Information on the stoichiometry of the complexes can be obtained from the continuous variation method (Job plot)¹⁰⁰ using either UV-Vis or fluorescence spectrophotometry. Solutions containing varying Hg(II) and ligand concentrations are prepared in a suitable solvent. Stock solutions of the ligand of a certain concentration and metal salt (the same as the ligand) in the desired solvent are used. In a typical experiment, eleven vials are filled with 1.0 mL of solutions containing ligand and metal in the following volume ratios (mL) - 1.0/0, 0.9/0.1, 0.8/0.2, 0.7/0.3, 0.6/0.4, 0.5/0.5,

0.4/0.6, 0.3/0.7, 0.2/0.8, 0.1/0.9 and 0/1.0. Each of them is transferred to the cuvette, and absorbance or intensity spectra are recorded at the λ_{max} or emission wavelength of the complex. Afterward, the absorbance/intensity plot vs. mol ratio of the $[M^{(II)}]_t$ is obtained.

$$\text{Mol ratio of } M(\text{II}) = \frac{[M^{(II)}]}{[M^{(II)}] + [L]} \quad (\text{eq. 1.1})$$

where **L** is the ligand and $M^{(II)}$ is $\text{Hg}^{(II)}$.

1.9.4 Determination of complexation affinity and stoichiometry by non-linear regression analysis

Software programs such as Excel, Origin, MestRenova, and Hypspec are typically used for data analysis. Determination of error is performed by the standard deviation of triplicate measurements. Binding constants for metal-ligand complexation are calculated from fitting to the nonlinear regression equation (eq. 1.4). Data obtained from the plot of absorbance or intensity (at a particular wavelength) vs. the metal ion concentration are used.

In a simple equilibrium system, considering the interaction of a metal (M) with ligand (L) to give a complex ML we have:



And the stability constant, K_a as

$$K_a = \frac{[ML]}{[M][L]} \quad (\text{eq. 1.3})$$

At different complexation ratios, then we have the general equilibrium as:



$$K_a = K_{qp} = \frac{[M_q L_p]}{[M]^q [L]^p} \quad (\text{eq. 1.5})$$

From a UV-Vis or fluorescence titration, the non-linear fitting of the binding curves of each complex absorbance or intensity vs. the total metal concentration is used for the calculation of binding constants. The eq.1.6 shows the non-linear fitting equation for 1-1 thermodynamic binding;¹⁰¹

$$y = \frac{\pm(L+x+K^{-1}-\sqrt{(L+x+K^{-1})^2-4xL})*J}{2L} \quad (\text{eq. 1.6})$$

Where y = Cumulative change in absorbance

x = total metal concentration

L = Ligand concentration

J = $\Delta\text{Abs}_{\text{max}}$ or $\Delta\text{I}_{\text{max}}$

K = binding constant

For fluorescence titrations, the stability constant of 1-1 complexation can also be determined using the Stern-Volmer constant (quenching) or the Benesi-Hildebrand equation (enhancement). The Stern-Volmer constant (K_{sv}) is determined from the slope of a plot of I_0/I vs. $[Q]$ at lower concentrations of the analyte (eq. 1.7), where $[Q]$ is the concentration of the quencher, I_0 is the measured fluorescence intensity in the absence of the quencher, and I is the measured fluorescence intensity in the presence of the quencher.

$$I_0/I = 1 + K_{sv}[Q] \quad (\text{eq. 1.7})$$

1.9.5 Hg^(II) quantification by the dithizone method

Aqueous phases are analyzed through UV-Vis spectroscopy to determine the concentration of the residual unextracted Hg^(II) after extraction or recovered Hg^(II) after stripping. The Hg^(II) concentrations in the aqueous phases after extraction are determined by the dithizone UV-Vis spectrophotometric method for mercury quantification.¹⁰² This method involves the analysis of a solution prepared with dithizone as a ligand in a buffer solution at pH 1.0. The solution is then analyzed by measuring the absorbance of the dithizone-Hg^(II) complex at 490 nm. Calibration curves (2.0 – 10.0 μM) were prepared for each of the Hg^(II) quantification experiments using this method. For each experiment, the Hg concentration of the control measured corresponded to the original concentrations of prepared Hg^(II) solutions (from either weighed HgCl₂ or ICP-MS standards) within a +/-2% confidence margin.

1.9.6 Validation of analytical methods

The metrics of reliability for each analytical method used are:

Sensitivity (calibration sensitivity); measures the magnitude of the analyte response with the increase in its concentration.

Selectivity; measures how selective the instrumental response for one analyte is over another.

Precision; determination of the standard deviation in order to monitor the analytical method's random errors. It measures how reproducible the method is. Experiments are

replicated to determine this parameter, which was determined by triplicate measurements in all work described herein (unless noted otherwise).

Limit of detection(LOD); measures the smallest amount of the analyte that can be distinguished from the background. LOD is calculated by multiplying by three the standard deviation of the blank (σ) and dividing by the slope (k).¹⁰³

$$\text{LOD} = 3\sigma/k$$

Dynamic range; is defined as the concentration range over which the linear instrumental response is observed.

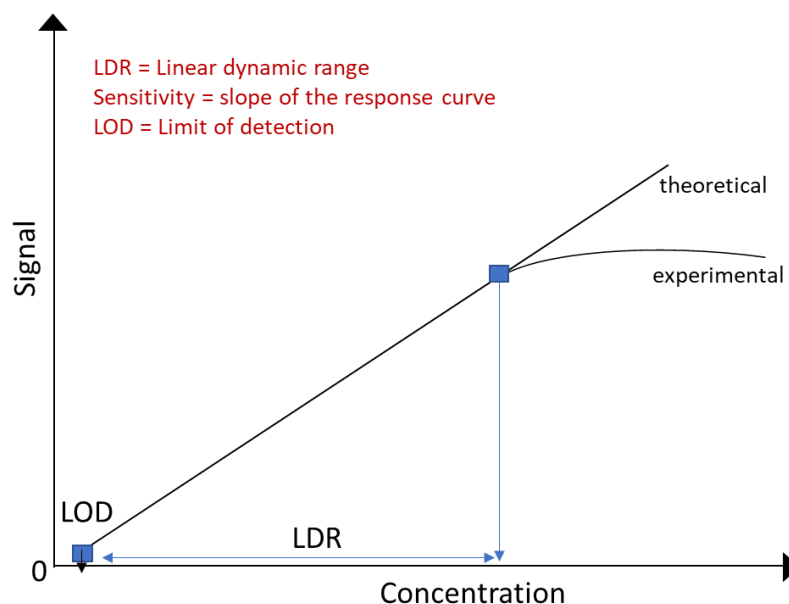


Figure 1.17: Schematic of a calibration curve plot showing the LOD and linear dynamic range.¹⁰³

1.10 References

- (1) Habashi, F. Mercury, Physical and Chemical Properties. In *Encyclopedia of Metalloproteins*; Kretsinger, R. H., Uversky, V. N., Permyakov, E. A., Eds.; Springer: New York, NY, 2013; 1375–1377.
- (2) Lacerda, L. D. Global Mercury Emissions from Gold and Silver Mining. *Water. Air. Soil Pollut.* **1997**, *97*, 209–221.
- (3) Selin, N. E. Global Biogeochemical Cycling of Mercury: A Review. *Annu. Rev. Environ. Resour.* **2009**, *34*, 43–63.
- (4) Liu, G.; Cai, Y.; O’Driscoll, N. *Environmental Chemistry, and Toxicology of Mercury*; John Wiley & Sons, 2011.
- (5) Nriagu, J. O. A Global Assessment of Natural Sources of Atmospheric Trace Metals. *Nature* **1989**, *338*, 47–49.
- (6) Ebinghaus, R.; Tripathi, R. M.; Wallschläger, D.; Lindberg, S. E. Natural and Anthropogenic Mercury Sources and Their Impact on the Air-Surface Exchange of Mercury on Regional and Global Scales. In *Mercury Contaminated Sites*, Springer Berlin Heidelberg: Berlin, Heidelberg, **1999**; 3–50.
- (7) Pirrone, N.; Keeler, G. J.; Nriagu, J. O. (Department of E. and I. H. Regional Differences in Worldwide Emissions of Mercury to the Atmosphere. *Atmospheric Environ. U. K.* **1996**. *30*, 2981-2987
- (8) Technical Background Report for the Global Mercury Assessment 2018 | Global Mercury Partnership <https://web.unep.org/globalmercurypartnership/technical-background-report-global-mercury-assessment-2018> (accessed 2021 -05 -17).
- (9) Hylander, L.; Meili, M. The Rise and Fall of Mercury: Converting a Resource to Refuse After 500 Years of Mining and Pollution. *Crit. Rev. Environ. Sci. Technol. - Crit Rev Env. Sci Technol* **2005**, *35*, 1–36.
- (10) McAuliffe, C. A. *The Chemistry of Mercury*. Ed.; Palgrave Macmillan UK: London, **1977**. <https://doi.org/10.1007/978-1-349-02489-6>.
- (11) Berlin, M.; Zalups, R. K.; Fowler, B. A. CHAPTER 33 - Mercury. In *Handbook on the Toxicology of Metals (Third Edition)*; Nordberg, G. F., Fowler, B. A., Nordberg, M., Friberg, L. T., Eds.; Academic Press: Burlington, **2007**; 675–729.
- (12) Pacyna, E. G.; Pacyna, J. M.; Sundseth, K.; Munthe, J.; Kindbom, K.; Wilson, S.; Steenhuisen, F.; Maxson, P. Global Emission of Mercury to the Atmosphere from Anthropogenic Sources in 2005 and Projections to 2020. *Atmos. Environ.* **2010**, *44*, 2487–2499.

- (13) Selin, N. E. Global Biogeochemical Cycling of Mercury: A Review. *Annu. Rev. Environ. Resour.* **2009**, *34*, 43–63.
- (14) O'Driscoll, N.; Rencz, A.; Lean, D. The Biogeochemistry and Fate of Mercury in the Environment. *Met. Ions Biol. Syst.* **2005**, *43*, 221–238.
- (15) King, J. K.; Kostka, J. E.; Frischer, M. E.; Saunders, F. M. Sulfate-Reducing Bacteria Methylate Mercury at Variable Rates in Pure Culture and in Marine Sediments. *Appl. Environ. Microbiol.* **2000**, *66*, 2430–2437.
- (16) Harada, M. Minamata Disease: Methylmercury Poisoning in Japan Caused by Environmental Pollution. *Crit. Rev. Toxicol.* **1995**, *25*, 1–24.
- (17) Pearson, R. G. Hard and Soft Acids and Bases. *J. Am. Chem. Soc.* **1963**, *85*, 3533–3539.
- (18) Bebout, D. C.; Bush II, J. F.; Crahan, K. K.; Bowers, E. V.; Butcher, R. J. Sterically Demanding Multidentate Ligand Tris[(2-(6-Methylpyridyl))Methyl]Amine Slows Exchange and Enhances Solution State Ligand Proton NMR Coupling to (199)Hg(II). *Inorg. Chem.* **2002**, *41*, 2529–2536.
- (19) Samie, A.; Salimi, A.; Garrison, J. C. Coordination Chemistry of Mercury (II) Halide Complexes: A Combined Experimental, Theoretical and (ICSD & CSD) Database Study on the Relationship between Inorganic and Organic Units. *Dalton Trans.* **2020**.
- (20) Bebout, D. C. Mercury: Inorganic & Coordination Chemistry Based in Part on the Article Mercury: Inorganic & Coordination Chemistry by Gregory J. Grant Which Appeared in the Encyclopedia of Inorganic Chemistry, First Edition. In *Encyclopedia of Inorganic and Bioinorganic Chemistry*; American Cancer Society, **2011**.
- (21) Crisponi, G.; Nurchi, V. M.; Crespo-Alonso, M.; Toso, L. Chelating Agents for Metal Intoxication. *Curr. Med. Chem.* **2012**, *19*, 2794–2815.
- (22) Bhardwaj, V.; Nurchi, V. M.; Sahoo, S. K. Mercury Toxicity and Detection Using Chromo-Fluorogenic Chemosensors. *Pharmaceuticals* **2021**, *14*, 23.
- (23) Bjørklund, G.; Crisponi, G.; Nurchi, V. M.; Cappai, R.; Buha Djordjevic, A.; Aaseth, J. A Review on Coordination Properties of Thiol-Containing Chelating Agents Towards Mercury, Cadmium, and Lead. *Molecules* **2019**, *24*, 3247.
- (24) Haitzer, M.; Aiken, G. R.; Ryan, J. N. Binding of Mercury(II) to Dissolved Organic Matter: The Role of the Mercury-to-DOM Concentration Ratio. *Environ. Sci. Technol.* **2002**, *36*, 3564–3570.
- (25) Coates, R. L.; Jones, M. M. Stability Constants of the Hg²⁺-BAL Complexes. *J. Inorg. Nucl. Chem.* **1977**, *39*, 677–678.

- (26) Shigemoto, A. K.; Killjoy, A. A.; Dayton, J.; Virca, C. N.; McCormick, T. M. Increased Binding of Thiophene-Based Ligands to Mercury(II) with Water Solubilizing Functional Groups. *Mol. Syst. Des. Eng.* **2020**, *5*, 1024–1036.
- (27) Kim, A.; Kim, S.; Kim, C. A Conjugated Schiff Base-Based Chemosensor for Selectively Detecting Mercury Ion. *J. Chem. Sci.* **2020**, *132*, 82.
- (28) Ngah, F.; Zakariah, E.; Hassan, N. I.; Yamin, B.; Sapari, S.; Hasbullah, A. Synthesis of Thiourea Derivatives and Binding Behavior towards the Mercury Ion. *Malays. J. Anal. Sci.* **2017**, *21*, 1226–1234.
- (29) Tsuchiya, T.; Shimizu, T.; Hirabayashi, K.; Kamigata, N. Formation and Structures of Mercury Complexes of 18-Membered Unsaturated and Saturated Thiocrown Ethers. *J. Org. Chem.* **2003**, *68*, 3480–3485.
- (30) Beckers, F.; Rinklebe, J. Cycling of Mercury in the Environment: Sources, Fate, and Human Health Implications: A Review. *Crit. Rev. Environ. Sci. Technol.* **2017**, *47*, 693–794.
- (31) National Risk Management Research Laboratory (US). Capsule Report: Aqueous Mercury Treatment. US Environmental Protection Agency; **1997**.
- (32) Martínez-Juárez, V. M.; Cárdenas-González, J. F.; Torre-Bouscoulet, M. E.; Acosta-Rodríguez, I. Biosorption of Mercury (II) from Aqueous Solutions onto Fungal Biomass. *Bioinorg. Chem. Appl.* **2012**, *2012*, e156190.
- (33) De Clercq, J. Removal of Mercury from Aqueous Solutions by Adsorption on a New Ultra Stable Mesoporous Adsorbent and on a Commercial Ion Exchange Resin. *Int. J. Ind. Chem.* **2012**, *3*, 1.
- (34) Chiarle, S.; Ratto, M.; Rovatti, M. Mercury Removal from Water by Ion Exchange Resins Adsorption. *Water Res.* **2000**, *34*, 2971–2978.
- (35) Mihaiela, A.; Dragomirescu, A.; Iovi, A.; Ursoiu, I.; Adina, N.; Lupa, L.; Negrea, P.; Mihaela, C. Use of Ion Exchange Resin to Remove the Mercury from Contaminated Waters. *Rev. Chim. -Buchar.- Orig. Ed.-* **2009**, *60*.
- (36) Fondeur, F. F. *Mercury Removal Performance of Amberlite(TM) GT-73A, Purolite(TM) S-920, Ionac(TM) SR-4 and SIR-200(TM) Resins*; WSRC-TR-2002-00046, 799695; **2002**; p WSRC-TR-2002-00046, 799695.
- (37) Manohar, D. M.; Anoop Krishnan, K.; Anirudhan, T. S. Removal of Mercury(II) from Aqueous Solutions and Chlor-Alkali Industry Wastewater Using 2-Mercaptobenzimidazole-Clay. *Water Res.* **2002**, *36*, 1609–1619.
- (38) Cyr, P. J.; Suri, R. P. S.; Helmig, E. D. A Pilot-Scale Evaluation of Removal of Mercury from Pharmaceutical Wastewater Using Granular Activated Carbon. *Water Res.* **2002**, *36*, 4725–4734.

- (39) Namasivayam, C.; Kadirvelu, K. Uptake of Mercury (II) from Wastewater by Activated Carbon from an Unwanted Agricultural Solid by-Product: Coirpith. *Carbon* **1999**, *37*, 79–84.
- (40) Parham, H.; Zargar, B.; Shiralipour, R. Fast and Efficient Removal of Mercury from Water Samples Using Magnetic Iron Oxide Nanoparticles Modified with 2-Mercaptobenzothiazole. *J. Hazard. Mater.* **2012**, *205–206*, 94–100.
- (41) Li, Q.; Liu, T.; Deng, P. Recovery of Mercury and Lead from Wastewater by Sulfide Precipitation-Flotation. In *Characterization of Minerals, Metals, and Materials 2015*; Carpenter, J. S., Bai, C., Escobedo, J. P., Hwang, J.-Y., Ikhmayies, S., Li, B., Li, J., Monteiro, S. N., Peng, Z., Zhang, M., Eds.; Springer International Publishing: Cham, **2016**; 667–674.
- (42) Toufik, M. Removal of Hg (II) Ions from Industrial Wastewaters Using Aluminum Sulfate. *Int. J. Eng. Res. Afr.* **2021**, *53*, 200–211.
- (43) Huang, Y.; Du, J. R.; Zhang, Y.; Lawless, D.; Feng, X. Removal of Mercury (II) from Wastewater by Polyvinylamine-Enhanced Ultrafiltration. *Sep. Purif. Technol.* **2015**, *154*, 1–10.
- (44) Kabiri, S.; Tran, D. N. H.; Cole, M. A.; Losic, D. Functionalized Three-Dimensional (3D) Graphene Composite for High-Efficiency Removal of Mercury. *Environ. Sci. Water Res. Technol.* **2016**, *2*, 390–402.
- (45) Mullett, M.; Mohamed, L. Removal of Mercury from Solution Using Reverse Osmosis Filtration. *Proc. 37th Chemeca Eng.* **2009**, 2207–2214.
- (46) Chen, G. Electrochemical Technologies in Wastewater Treatment. *Sep. Purif. Technol.* **2004**, *38*, 11–41.
- (47) Bazrafshan, E.; Mohammadi, L.; Ansari-Moghaddam, A.; Mahvi, A. H. Heavy Metals Removal from Aqueous Environments by Electrocoagulation Process– a Systematic Review. *J. Environ. Health Sci. Eng.* **2015**, *13*.
- (48) Bengtsson, M. K. O.; Tunsu, C.; Wickman, B. Decontamination of Mercury-Containing Aqueous Streams by Electrochemical Alloy Formation on Copper. *Ind. Eng. Chem. Res.* **2019**, *58*, 9166–9172.
- (49) Rydberg, J.; Choppin, G. R.; Musikas, C.; Sekine, T. Solvent Extraction Equilibria. In *Solvent Extraction Principles and Practice, Revised and Expanded*; CRC Press, **2004**.
- (50) Reddy, M. L. P.; Francis, T. Recent Advances in the Solvent Extraction of Mercury(Ii) with Calixarenes and Crown Ethers. *Solvent Extr. Ion Exch.* **2001**, *19*, 839–863.

- (51) Yordanov, A. T.; Mague, J. T.; Roundhill, D. M. Synthesis of Heavy Metal Ion Selective Calix[4]Arenes Having Sulfur-Containing Lower-Rim Functionalities. *Inorg. Chem.* **1995**, *34*, 5084–5087.
- (52) Yordanov, A. T.; Falana, O. M.; Koch, H. F.; Roundhill, D. M. (Methylthio)methyl and (*N,N* -Dimethylcarbamoyl)methyl Upper-Rim-Substituted Calix[4]Arenes as Potential Extractants for Ag(I), Hg(II), Ni(II), Pd(II), Pt(II), and Au(III). *Inorg. Chem.* **1997**, *36*, 6468–6471.
- (53) Talanova, G. G.; Talanov, V. S.; Bartsch, R. A. Calix[4]Arenes with Hard Donor Groups as Efficient Soft Cation Extractants. Remarkable Extraction Selectivity of Calix[4]Arene *N* -(X)Sulfonylcarboxamides for Hg II. *Chem. Commun.* **1998**, *0*, 1329–1330.
- (54) Deligöz, H.; Yilmaz, M. Liquid-Liquid Extraction of Transition Metal Cations by Calixarene-Based Cyclic Ligands. *Solvent Extr. Ion Exch.* **1995**, *13*, 19–26.
- (55) Vanifatova, N. G.; Isakova, N. V.; Petrukhin, O. M.; Zolotov, Y. A. Nitrogen- and sulfur-containing analogs of dibenzo-18-crown-6 as extractants. *Zhurnal Neorganicheskoi Khimii* **1991**, *36*, 792–798.
- (56) Vanifatova, N. G.; Isakova, N.; Petrukhin, O. M.; Zolotov, Y. A. Nitrogen- and sulfur-containing Analogs of Dibenzo-18-Crown-6 as Extracting Agents. *Russ. J. Inorg. Chem.* **1991**, *36*, 449–453.
- (57) Pasekova, N. A.; Pletnev, I. V.; Malkhasyan, E. V. Extraction Properties of azathia analogs of dibenzo-18-crown-6. *Zhurnal Neorganicheskoi Khimii* **1991**, *36*, 2971–2976.
- (58) Baumann, T. F.; Reynolds, J. G.; Fox, G. A. Polymer Pendant Crown Thioethers: Synthesis, Characterization and Hg²⁺ Extraction Studies of Polymer-Supported Thiacrowns ([14] AneS4 and [17] AneS5). *React. Funct. Polym.* **2000**, *44*, 111–120.
- (59) Gloe, K.; Kruger, T.; Stephan, H.; Wagner, M.; Drutkowski, U.; Olk, R. M.; Leckelt, U.; Richter, R.; Hoyer, E. Structure and Complex Formation of Small 1, 3-Dithiol Anellated Thia Crown Compounds. *Z. Anorg. Allg. Chem.* **1998**, *624*, 152–158.
- (60) Heitzsch, O.; Gloe, K.; Stephan, H.; Weber, E. Liquid-Liquid Extraction of Ag(I), Hg(II), Au(III) and Pd(II) By Some Oligothia Macrocyclic Ligands Incorporating Aromatic and Heteroaromatic Subunits. *Solvent Extr. Ion Exch.* **1994**, *12*, 475–496.
- (61) Moore, F. L. Liquid-Liquid Extraction of Mercury with High-Molecular-Weight Amines from Iodide and Bromide Solutions. *Sep. Sci.* **2006**, *7*, 505-512.
- (62) McDonald, C.; Pahlavan, G. H. Solvent Extraction of Mercury Using Alamine 304. *Mikrochim. Acta* **1982**, *78*, 77–82.

- (63) McDonald, C. W.; Pahlavan, G. H. Liquid-Liquid Extraction of Cadmium with Alamine 336 from Aqueous Chloride and Bromide Media. *Sep. Sci.* **1977**, *12*, 271–279.
- (64) Zuo, G.; Muhammed, M. Extraction of Mercury(II) by Thiourea-Based Reagents. *Solvent Extr. Ion Exch.* **1995**, *13*, 855–878.
- (65) Sekine, T.; Ishii, T. Studies of the Liquid-Liquid Partition Systems. VII. The Solvent Extraction of Mercury(II) Chloride, Bromide, Iodide, and Thiocyanate with Some Organic Solvents. *Bull. Chem. Soc. Jpn.* **1970**, *43*, 2422–2429.
- (66) Litman, Robert.; Williams, E. T.; Finston, H. L. Extraction of Mercury by Dithizone and Stability of the Extracted Complex. *Anal. Chem.* **1977**, *49*, 983–987.
- (67) Tigreros, A.; Portilla, J. Recent Progress in Chemosensors Based on Pyrazole Derivatives. *RSC Adv.* **2020**, *10*, 19693–19712.
- (68) Ebralidze, I. I.; Laschuk, N. O.; Poisson, J.; Zenkina, O. V. Chapter 1 - Colorimetric Sensors and Sensor Arrays. *Nanomaterials Design for Sensing Applications*, **2019**; 1–39.
- (69) Jablonski, A. Efficiency of Anti-Stokes Fluorescence in Dyes. *Nature* **1933**, *131*, 839–840.
- (70) Saleem, M.; Khang, C. H.; Kim, M.-H.; Lee, K. H. Chromo/Fluorogenic Detection of Co^{2+} , Hg^{2+} and Cu^{2+} by the Simple Schiff Base Sensor. *J. Fluoresc.* **2016**, *26*, 11–22.
- (71) P. Singh, A.; P. Murale, D.; Ha, Y.; Liew, H.; Mun Lee, K.; Segev, A.; Suh, Y.-H.; G. Churchill, D. A Novel, Selective, and Extremely Responsive Thienyl-Based Dual Fluorogenic Probe for Tandem Superoxide and Hg^{2+} Chemosensing. *Dalton Trans.* **2013**, *42*, 3285–3290.
- (72) Prodi, L.; Bargossi, C.; Montalti, M.; Zaccheroni, N.; Su, N.; Bradshaw, J. S.; Izatt, R. M.; Savage, P. B. An Effective Fluorescent Chemosensor for Mercury Ions. *J. Am. Chem. Soc.* **2000**, *122*, 6769–6770.
- (73) Chinna ayya Swamy P; Shanmugapriya, J.; Singaravadiel, S.; Sivaraman, G.; Chellappa, D. Anthracene-Based Highly Selective and Sensitive Fluorescent “Turn-on” Chemodosimeter for Hg^{2+} . *ACS Omega* **2018**, *3*, 12341–12348.
- (74) Dai, B.-N.; Cao, Q.-Y.; Wang, L.; Wang, Z.-C.; Yang, Z. A New Naphthalene-Containing Triazolophane for Fluorescence Sensing of Mercury(II) Ion. *Inorganica Chim. Acta* **2014**, *423*, 163–167.
- (75) Zareh Jonaghani, M.; Zali-Boeini, H. Highly Selective Fluorescent and Colorimetric Chemosensor for Detection of Hg^{2+} Ion in Aqueous Media. *Spectrochim. Acta. A. Mol. Biomol. Spectrosc.* **2017**, *178*, 66–70.

- (76) Wang, P.; An, Y.; Wu, J. Highly Sensitive Turn-on Detection of Mercury(II) in Aqueous Solutions and Live Cells with a Chemosensor Based on Tyrosine. *Spectrochim. Acta. A. Mol. Biomol. Spectrosc.* **2020**, *230*, 118004.
- (77) Sivaraman, G.; Anand, T.; Chellappa, D. Development of a Pyrene Based “Turn on” Fluorescent Chemosensor for Hg²⁺. *RSC Adv.* **2012**, *2*, 10605–10609.
- (78) Wilmarth, W. R.; Rosencrance, S. W. Studies of Mercury in High-Level Waste Systems (No. WSRC-TR-2003-00238). Savannah River Site (US).
<https://doi.org/10.2172/814850>
- (79) National Research Council. Tank waste retrieval, processing, and on-site disposal at three Department of Energy Sites. *National Academies Press*; **2006** Sep 12.
- (80) Edwards, R. E.; Jain, V.; Shah, H.; Occhipinti, J. E.; Wilmarth, W. R. Evaluation and Impacts of Mercury in the SRS Liquid Waste System – 1612. **2016**, 12.
- (81) Bannochie, C. J.; Fellingner, T. L.; Garcia-Strickland, P.; Shah, H. B.; Jain, V.; Wilmarth, W. R. Mercury in Aqueous Tank Waste at the Savannah River Site: Facts, Forms, and Impacts. *Sep. Sci. Technol.* **2018**, *53*, 1935–1947.
- (82) Jain, V.; Shah, H.; Occhipinti, J. E.; Wilmarth, W. R.; Edwards, R. E. Evaluation of Mercury in Liquid Waste Processing Facilities. **2015**, 71.
- (83) Boggess, A.J.; Jones, M.A.; White, T.L.; Bannochie, C.J.; Looney, B. Selective Capture and Analysis of Purgeable Mercury Species in High-Activity Tank Waste at Savannah River Site. *Separation Science and Technology.* **2019**, *54*, 1960–1969.
- (84) Zamecnik, J.; Choi, A. Modeling the Impact of Elevated Mercury in Defense Waste Processing Facility Melter Feed on the Melter Off-Gas System-Preliminary Report <https://sti.srs.gov/fulltext/SRNL-STI-2009-00149R1.pdf> (accessed 2018 -11 -07).
- (85) Janes, D. A. *DWPF Mercury Recovery Design Basis. [Steam Stripping End Point, Mercury Purge, and Gravity-Settled Mercury]*; DPST-82-893; Du Pont de Nemours (E.I.) and Co., Aiken, SC (USA). Savannah River Lab., **1982**.
- (86) Lewis, G. N. Acids and Bases. *J. Frankl. Inst.* **1938**, *226*, 293–313.
- (87) Chohan, Z. H. Metal-Based Sulfonamides: Their Preparation, Characterization and in-Vitro Antibacterial, Antifungal & Cytotoxic Properties. X-Ray Structure of 4-[(2-Hydroxybenzylidene) Amino] Benzenesulfonamide. *J. Enzyme Inhib. Med. Chem.* **2008**, *23*, 120–130.
- (88) Hossain, G. M. G.; Amoroso, A. J.; Banu, A.; Malik, K. M. A. Syntheses and Characterisation of Mercury Complexes of Sulfadiazine, Sulfamerazine, and Sulfamethazine. *Polyhedron* **2007**, *26*, 967–974.

- (89) Nesbitt, R. U.; Sandmann, B. J. Solubility Studies of Silver Sulfadiazine. *J. Pharm. Sci.* **1977**, *66*, 519–522.
- (90) Gutiérrez, L.; Alzuet, G.; Borrás, J.; Castiñeiras, A.; Rodríguez-Forteza, A.; Ruiz, E. Copper(II) Complexes with 4-Amino-N-[4,6-Dimethyl-2-Pyrimidinyl]Benzenesulfonamide. Synthesis, Crystal Structure, Magnetic Properties, EPR, and Theoretical Studies of a Novel Mixed μ -Carboxylato, NCN-Bridged Dinuclear Copper Compound. *Inorg. Chem.* **2001**, *40*, 3089–3096.
- (91) Alvarado, R. J.; Rosenberg, J. M.; Andreu, A.; Bryan, J. C.; Chen, W.-Z.; Ren, T.; Kavallieratos, K. Structural Insights into the Coordination and Extraction of Pb(II) by Disulfonamide Ligands Derived from o-Phenylenediamine. *Inorg. Chem.* **2005**, *44*, 7951–7959.
- (92) Kavallieratos, K.; Rosenberg, J. M.; Chen, W.-Z.; Ren, T. Fluorescent Sensing and Selective Pb(II) Extraction by a Dansylamide Ion-Exchanger. *J. Am. Chem. Soc.* **2005**, *127*, 6514–6515.
- (93) Wanichacheva, N.; Watpathomsub, S.; Lee, V. S.; Grudpan, K. Synthesis of a Novel Fluorescent Sensor Bearing Dansyl Fluorophores for the Highly Selective Detection of Mercury (II) Ions. *Molecules* **2010**, *15*, 1798–1810.
- (94) Jiang, P.; Guo, Z. Fluorescent Detection of Zinc in Biological Systems: Recent Development on the Design of Chemosensors and Biosensors. *Coord. Chem. Rev.* **2004**, *248*, 205–229.
- (95) Diaconu, D.; Mangalagiu, V.; Amariuca-Mantu, D.; Antoci, V.; Giuroiu, C.; Mangalagiu, I. Hybrid Quinoline-Sulfonamide Complexes (M^{2+}) Derivatives with Antimicrobial Activity. *Molecules* **2020**, *25*, 2946.
- (96) Okamoto, K.; Kuwabara, J.; Kanbara, T. Thioamide-Based Transition Metal Complexes. In *Chemistry of Thioamides*; Murai, T., Ed.; Springer: Singapore, **2019**; 157–191.
- (97) Wu, K.; Ling, Y.; Ding, A.; Jin, L.; Sun, N.; Hu, B.; Shen, Z.; Hu, X. A Column-Free and Aqueous Waste-Free Process for Thioamide Preparation with Lawesson's Reagent. *Beilstein Arch.* **2020**, *2020*, 126.
- (98) Begum, R. A.; Powell, D.; Bowman-James, K. Thioamide Pincer Ligands with Charge Versatility. *Inorg. Chem.* **2006**, *45*, 964–966.
- (99) Jaski, T.; Süsskind, C. Electromagnetic Radiation as a Tool in the Life Sciences. *Science* **1961**, *133*, 443–447.
- (100) Job, P. Formation and Stability of Inorganic Complexes in solution. *Ann Chim* **1928**, *9*, 113–134.

- (101) Ackermann, T. K. A. Connors: Binding Constants — the Measurement of Molecular Complex Stability, John Wiley & Sons, New York, Chichester, Brisbane, Toronto, Singapore 1987. 411 Seiten, Preis: £ 64.15. *Berichte Bunsenges. Für Phys. Chem.* **1987**, *91*, 1398–1398.
- (102) Khan, H.; Ahmed, M. J.; Bhangar, M. I. A Simple Spectrophotometric Determination of Trace Level Mercury Using 1,5-Diphenylthiocarbazone Solubilized in Micelle. *Anal. Sci.* **2005**, *21*, 507–512.
- (103) Armbruster, D. A.; Pry, T. Limit of Blank, Limit of Detection and Limit of Quantitation. *Clin. Biochem. Rev.* **2008**, *29*, 49–52.

CHAPTER II: Complexation and Efficient Extraction of Mercury(II) in Alkaline Conditions by a Family of Bis-Arylsulfonamide Ligands

Adenike O. Fasiku, Indranil Chakraborty, Rene Panzer, Raphael G. Raptis, and

Konstantinos Kavallieratos*

2.1 Abstract

Arylsulfonamide ligands with various alkyl substituents (**LH₂**) are shown to complex and extract Hg^(II) from water into dichloroethane under alkaline conditions. Coordination complexes of type [Et₃NH]₂[HgL₂], where **L** is the bis-deprotonated sulfonamide ligand, were synthesized from N,N'-(1,2-phenylene)bis(4-methylbenzenesulfonamide) (**L1H₂**), N,N'-(4,5-dimethyl-1,2-phenylene)bis(4-methylbenzenesulfonamide) (**L2H₂**), N,N'-(1,2-phenylene)bis(4-(tert-butyl)benzenesulfonamide) (**L3H₂**), and N,N'-(4,5-dimethyl-1,2-phenylene)bis(4-(tert-butyl)benzenesulfonamide) (**L4H₂**) with mercuric chloride in the presence of triethylamine. In solution, complexes consistent with both 1:2 and 1:1 Hg^(II)/**L** ratios are obtained, depending on the conditions. The isolated complexes were characterized by elemental analysis, FT-IR, UV-Vis, ¹H and ¹³C NMR, and, in one case, by X-ray diffraction. In all X-ray structures, it was shown that these bidentate ligands act as N-donors that coordinate to Hg^(II) through the sulfonamide nitrogens, with triethylammonium ions acting as counter cations in the outer coordination sphere. Solvent extraction of Hg^(II) from aqueous sodium hydroxide solutions using **L2H₂** and **L4H₂** as extractants in 1,2 dichloroethane (DCE) followed by stripping with 0.2 M HNO₃ showed up to 80 % and 90 % Hg^(II) recovery for **L2H₂** and **L4H₂** respectively at pH 12.0

even in the absence of an organic base. Extraction data analysis demonstrated that complexation stoichiometry varies depending on the conditions, with 1:1 and 1:2 Hg^(II)/L complexes involved in the presence *vs.* absence of Et₃N.

2.2 Introduction

Mercury (Hg) is a highly toxic environmental contaminant originating from both natural and anthropogenic sources, which can pose a severe threat to the health of living organisms and biodiversity because of its toxicity and bioaccumulation tendencies.¹ The use of mercury for several decades in mining and industrial applications explains its environmental exposure and contamination routes. Hg has also found use as a catalyst for nuclear fuel cladding dissolution leading to its accumulation in nuclear waste sites.² Hg^(II) in its divalent state is of particular concern, as it is environmentally mobile and could lead to renal failure or autoimmune diseases if ingested or absorbed by the body.^{3,4} Thus, new approaches towards *in-situ* Hg^(II) remediation have received significant attention in the scientific community. Various methods such as adsorption, ion exchange, membrane filtration, biological treatment, complexation, and solvent extraction have been developed for mercury sensing and removal processes from aqueous solutions.^{5,6} The use of adsorbents typically requires secondary waste disposal. Therefore, it is highly desirable to develop solvent extraction methods that remove mercury and recover the complexing agent via Hg^(II) complexation in the extraction step and subsequent decomplexation and recovery of the ligand during the stripping stage.⁷⁻¹² Such methods use ligands that can form organo-soluble metal complexes for mercury removal, with

minimal ligand partition in the aqueous phase. Soft S-donor and N-donor sites incorporated on the ligand framework can lead to selective and strong Hg^(II) complexation owing to mercury's soft Lewis acid characteristics and its affinity to softer Lewis bases.¹³ Several such studies on the use of organo-soluble ligands with S- or N-moieties for complexation and Hg^(II) extraction have been reported over the years.^{10,14–18} In this study, we are investigating for the first time the use of *o*-phenylenediamine-derived sulfonamide ligands for Hg^(II) complexation and extraction. As these ligands are easily obtainable in high yields in one synthetic step from commercially available amines and suitable sulfonyl chlorides, they present enormous potential for hydrometallurgical separation applications, with a variety of complexes reported.^{19–23} The sulfonamido group functionality (RSO₂-NH-) can be easily deprotonated (typical pK_a = 9-11)²⁴ forming stable anionic bis-N donor chelates for metal coordination, with two 5-member rings, per complexed ligand. Stripping of the organic phase and recovery of the metal in a new aqueous phase with the neutral ligand remaining in the organic phase can be obtained after contact with mildly acidic media.

Although several pharmacological, separations, and sensing applications of sulfonamides are known,^{7,8,21,25–29} few studies on mercury complexation and environmental remediation are reported. In an early report, sulfonamide derivatives of 8-hydroxyquinoline were found to yield insoluble chelates with six metals: Ag^(I), Hg^(II), Cu^(II), Pb^(II), Co^(II), and Zn^(II).³⁰ In 2005, our group pioneered an ion-exchange extraction method, in which *o*-phenylenediamine-derived disulfonamides were used in a synergistic fashion together with 2,2'-bipyridyl to sense, complex, and selectively extract Pb^(II) from the aqueous phase into an organic phase.^{7,31} Subsequently, upon contacting the organic

phase with a mildly acidic aqueous solution, the complexed $\text{Pb}^{\text{(II)}}$ was released to the aqueous phase, with ligand recovery. In the absence of a co-ligand or coordinating solvents, an insoluble polymeric, $\text{L-Pb}^{\text{(II)}}$ 1:1 complex was formed, while in the presence of N-donor co-ligands, or coordinating solvents, like DMSO, the crystal structures showed coordination patterns of 1:1:1 ($\text{L:Pb}^{\text{(II):2'2-bipyridyl}$), or 1:1:2 ($\text{L:Pb}^{\text{(II):DMSO}$). As we are especially interested in new methods for extraction and recovery of $\text{Hg}^{\text{(II)}}$ from alkaline high-level nuclear waste sites, such as the Savannah River Site, we have now undertaken the effort to explore $\text{Hg}^{\text{(II)}}$ complexation and extraction/recovery using the same family of ligands.

Herein, we report complexation and effective extraction in alkaline conditions of $\text{Hg}^{\text{(II)}}$ by these *o*-phenylenediamine-derived sulfonamide ligands. The crystal structure of the $\text{Hg}^{\text{(II):L2}}$ complex shows a 1:2 $\text{Hg}^{\text{(II):L2}}$ stoichiometry with two triethylammonium ions (Et_3NH^+) coordinating in the outer sphere. $\text{Hg}^{\text{(II)}}$ extraction and recovery under various pH conditions and in the presence and absence of an organic base showed promise for application of this ligand family as an efficient extractant for $\text{Hg}^{\text{(II)}}$ with over 90% recovery at pH 12.0 in the absence of an organic base. $^1\text{H-NMR}$ and UV-Vis spectroscopy of the organic phases confirmed the formation of $\text{Hg}^{\text{(II)}}$ complexes and provided insight into various coordination patterns depending on the extraction conditions. With over 90% recovery of extracted $\text{Hg}^{\text{(II)}}$, these ligands show promise for potential application in mercury complexation and recovery from alkaline high-level waste tanks.

2.3 Experimental section

2.3.1 Materials and methods

All chemicals and materials were purchased from Fisher Scientific or Sigma-Aldrich. All chemicals were standard reagent grade and were used without further purification. ^1H and ^{13}C -NMR spectra were recorded on a 400-MHz Bruker Avance NMR spectrometer with chemical shifts, δ , reported in ppm. The UV-Vis spectra were recorded on a CARY 100 Bio UV-Visible spectrophotometer, and FT-IR spectra were recorded on a Cary 600 series FT-IR spectrometer. X-ray diffraction studies were carried out on a Bruker D8 Quest with PHOTON 100 detector. Elemental analysis was provided by Atlantic Microlab Inc. All ligands (**L1H₂**-**L4H₂**) were synthesized as described previously^{7,25,31} and were found spectroscopically identical to the reported compounds.

2.3.2 Synthesis of Hg^(II) complexes of bis-arylsulfonamide ligands

(Et₃NH)₂Hg(L1)₂, (C1): Et₃N (40.47 mg, 55.79 μL , 0.4 mmol) was added dropwise to a solution of **L1H₂** (83.30 mg, 0.2 mmol) in CH₂Cl₂ (DCM) (5 mL) at room temperature (r.t.). After stirring for 5 min, HgCl₂ (27.52 mg, 0.1 mmol) was added. The reaction was stirred for 16 h at room temperature (r.t.), washed with H₂O (3 x 5 mL) and the organic phase was dried over MgSO₄. After evaporation of all volatiles, the complex was obtained as a yellow powder. Recrystallization from CH₂Cl₂/hexanes gave the analytically pure compound. Slow diffusion of hexanes into a saturated solution of the complex in CH₂Cl₂ yielded suitable crystals for single-crystal X-ray crystallography. 117.55 mg of **C1** is obtained as a light-yellow solid (0.095 mmol, 95% yield). ^1H NMR

(400 MHz, CDCl₃) δ (ppm); 7.99 (s, 4H- Ar), 7.09 (d, $J = 8.1$ Hz, 4H- Ar), 7.04 (s, 2H- Ar), 6.44 (s, 2H- Ar), 2.73 (q, $J = 7.3$ Hz, 6H -CH₂- (Et₃N)), 2.25 (s, 6H -CH₃), 0.89 (t, $J = 7.3$ Hz, 9H -CH₃ (Et₃N)). ¹³C NMR (101 MHz, CDCl₃) δ (ppm); 140.95 (Ar), 140.31 (Ar), 134.65 (Ar), 129.07 (Ar), 127.89 (Ar), 119.30 (Ar), 117.26 (Ar), 46.27 (-CH₂-, Et₃N), 21.36 (-CH₃), 8.53 (-CH₃, Et₃N). FT-IR (cm⁻¹); $\nu = 1255$ (asymSO₂), 1122 (symSO₂), 963 (S-N). Elemental analysis (%) calculated for [(C₆H₁₅NH)₂HgC₄₀H₃₂N₄O₈S₄]: C 50.78, H 5.25, N 6.83; Found: C 50.33, H 5.70, N 6.66.

(Et₃NH)₂Hg(L2)₂, (C2) was obtained by the same method as C1 above from **L2H₂** (88.91 mg, 0.2 mmol). 116.45 mg of **C2** was obtained as a light pink solid (0.090 mmol, 90% yield). ¹H NMR (400 MHz, CDCl₃) δ (ppm); 7.95 (s, 4H- Ar), 7.09 (d, $J = 8.1$ Hz, 4H- Ar), 6.90 (s, 2H- Ar), 2.73 (q, $J = 7.3$ Hz, 6H -CH₂- (Et₃N)), 2.25 (s, 6H -CH₃), 1.90 (s, 6H -CH₃), 0.95 (t, $J = 7.3$ Hz, 9H -CH₃ (Et₃N)). ¹³C NMR (101 MHz, CDCl₃) δ (ppm); 141.02 (Ar), 140.23 (Ar), 131.96 (Ar), 129.04 (Ar), 127.84 (Ar), 125.89 (Ar), 119.55 (Ar), 46.26 (-CH₂-, Et₃N), 21.35 (-CH₃), 19.44 (-CH₃), 9.00 (-CH₃, Et₃N). FT-IR (cm⁻¹); $\nu = 1227$ (asymSO₂), 1122 (symSO₂), 917 (S-N). Elemental analysis (%) calculated for [(C₆H₁₅NH)₂HgC₄₄H₄₄N₄O₈S₄]: C 49.79, H 5.72, N 6.11; Found: C 49.84, H 4.96, N 5.99.

(Et₃NH)₂Hg(L3)₂, (C3) was obtained by the same method as C1 above from **L3H₂** (100.13 mg, 0.2 mmol). 125.40 mg of **C3** was obtained as a pale-yellow solid (0.090 mmol, 90% yield). ¹H NMR (400 MHz, CDCl₃) δ (ppm); 7.98 (d, $J = 6.8$ Hz, 4H- Ar), 7.21 (d, $J = 8.5$ Hz, 4H- Ar), 6.92 (dd, $J = 5.8, 3.6$ Hz, 2H- Ar), 6.30 (s, 2H- Ar), 2.63 (q,

$J = 7.3$ Hz, 6H -CH₂- (Et₃N)), 1.10 (s, 18H -CH₃), 0.78 (t, $J = 7.3$ Hz, 9H -CH₃ (Et₃N)).
¹³C NMR (101 MHz, CDCl₃) δ (ppm); 131.04 (Ar), 127.72 (Ar), 125.51 (Ar), 46.21 (-
CH₂-, Et₃N), 31.18 (-CH₃), 8.62 (-CH₃, Et₃N). FT-IR (cm⁻¹); $\nu = 1255$ (asymSO₂), 1125
(symSO₂), 964 (S-N). Elemental analysis (%) calculated for [(C₆H₁₅NH)₂
HgC₅₂H₆₀N₄O₈S₄]: C 54.82, H 6.61, N 5.99; Found: C 54.56, H 6.41, N 5.85.

(Et₃NH)₂Hg(L4)₂, (C4) was obtained by the same method as C1 above from **L4H₂**
(105.75 mg, 0.2 mmol). 116.45 mg of **C4** is obtained as a very light-pink solid (0.085
mmol, 85% yield). ¹H NMR (400 MHz, CDCl₃) δ (ppm); 7.98 (s, 4H- Ar), 7.35 (d, $J =$
8.3 Hz, 4H- Ar), 6.91 (s, 2H- Ar), 2.84 (q, $J = 7.2$ Hz, 6H -CH₂- (Et₃N)), 1.94 (s, 6H -
CH₃), 1.24 (s, 18H -CH₃), 1.06 (t, $J = 7.3$ Hz, 9H -CH₃ (Et₃N)). ¹³C NMR (101 MHz,
CDCl₃) δ (ppm); 147.49 (Ar), 127.63 (Ar), 125.56 (Ar), 46.33 (-CH₂-, Et₃N), 34.89 (-
CH₃), 31.15 (-CH₃), 9.43 (-CH₃, Et₃N). FT-IR (cm⁻¹); $\nu = 1257$ (asymSO₂), 1136 (symSO₂),
920 (S-N). Elemental analysis (%) calculated for [(C₆H₁₅NH)₂ HgC₅₆H₆₈N₄O₈S₄]: C
56.00, H 6.91, N 5.76; Found: C 55.51, H 6.74, N 5.72.

2.3.3 UV-Vis titrations

Solutions of ligands **L1H₂-L4H₂** and Et₃N in MeOH were titrated with solutions
of HgCl₂ at constant ligand concentration. In a typical experiment, a solution of ligand
LH₂ (0.04 mM) and 2.2 eq. of Et₃N (0.088 mM) in MeOH (Solution A) was titrated with
a solution of HgCl₂ (0.4 mM) and LH₂ (0.04 mM) and Et₃N (0.088 mM) (Solution B)
prepared by weighing HgCl₂ and diluting with solution A. For spectra collection, a

quartz cell of 1.000 cm optical path length was filled with 2.300 mL of solution A, and the $\text{Hg}^{(\text{II})}$ solution B was added in 5-100 μL increments until a total of 1020 μL had been added. All the spectroscopic measurements were performed in triplicate and were averaged. The binding curves of each of the Hg-L ΔAbs vs. $[\text{Hg}^{(\text{II})}]_{\text{t}}$ were fitted to the 1-1 binding isotherm.³²

2.3.4 Extraction studies

$\text{Hg}^{(\text{II})}$ extraction at constant concentrations of **L4H₂** and Et_3N from aqueous phases of variable alkalinity was studied using aqueous solutions of HgCl_2 and NaOH . In a typical experiment, 5.00 mL of aqueous $\text{Hg}^{(\text{II})}$ solutions were prepared by adding various volumes of NaOH (10^{-6} – 1 M; pH 7, 8, 9, 10, 11, 12, 13, 14) to 0.5 mL of a 10 mM HgCl_2 solution and subsequently diluted up to 5.0 mL mark (final $[\text{Hg}^{(\text{II})}]$ in aqueous solution is 0.98 mM). The aqueous phases were then equilibrated with 5.00 mL solutions of 2.0 mM **L4** and Et_3N (2.2 eq.) in DCE by rotating on a wheel at 55 rpm. After contacting both phases for 20 h, the solutions were centrifuged for 5 min for proper separation of both layers. Similar experiments in the absence of Et_3N were also carried out. The aqueous phase was analyzed through UV-Vis spectroscopy to determine the concentration of the residual unextracted $\text{Hg}^{(\text{II})}$ after extraction or recovered $\text{Hg}^{(\text{II})}$ after stripping. The $\text{Hg}^{(\text{II})}$ concentrations in the aqueous phases after extraction were determined by the dithizone UV-Vis spectrophotometric method for mercury quantification.³³ This method involves the analysis of a solution prepared with dithizone as a ligand in a buffer solution at pH 2.0. Typically, an aliquot (0.1 mL) of the aqueous solution obtained after extraction or stripping was added to a mixed solution containing

1.00 mL of 1.0 M H₂SO₄, 4.00 mL of 0.6 M sodium dodecyl sulfate, and 1.00 mL of 0.39 mM dithizone. The obtained solution was diluted to 10.0 mL with DI water. The solution was then analyzed by measuring the absorbance of the dithizone-Hg^(II) complex at 490 nm. This Hg^(II) quantification method shows reliable results after triplicate experiments. The calibration curve for the quantification of Hg^(II) (Figure 2.7) was linear in the range of 1.99 – 9.97 μM with R² = 0.9993 (n=4)

The % extraction (% E) of Hg^(II) was calculated as follows;

$$\% E = \frac{C_0 - C}{C_0} \times 100 \quad (1)$$

C₀ is the concentration in the absence of ligand, and C denotes the concentration in the aqueous phase after extraction.

For stripping, 2.00 mL of 0.2 M HNO₃ was contacted with 2.00 mL of the organic phases. The samples were rotated on a wheel at 55 rpm for 20 h and then centrifuged for 5 min for suitable phase separation. The concentration of Hg^(II) in the aqueous phases was determined spectroscopically. The distribution ratio (D_{Hg}) of Hg^(II) after stripping was calculated using the following equation;

$$D_{\text{Hg(II)}} = \frac{[\text{Hg(II)}]_{\text{org.}}}{[\text{Hg(II)}]_{\text{aq.}}} \quad (2)$$

The % Hg^(II) recovered after stripping is calculated as:

$$\% [\text{Hg(II)}]_{\text{recovered}} = \frac{[\text{Hg(II)}]_{\text{found}}}{[\text{Hg(II)}]_{\text{initial}}} \times 100 \quad (3)$$

Where [Hg^(II)]_{initial} is the concentration in the absence of ligand and [Hg^(II)]_{found} denotes the concentration in the aqueous phase after stripping.

Slope analysis experiments were performed at pH 12.0 by preparing solutions of various concentrations of **LH₂** (**L2H₂** or **L4H₂**) in DCE both in the presence and absence of

triethylamine and contact with HgCl₂ solutions. The **LH₂** dependence was determined by preparing 5.00 mL DCE solutions of various concentrations of **LH₂** (0.30 – 2.0 mM) and 5 mM of triethylamine and contacting them with 5.00 mL of aqueous solutions of HgCl₂ (1.0 mM) at pH 12.0 (NaOH; 10⁻² M). Experiments in the absence of Et₃N were also performed in a similar manner. All reported errors were determined by standard deviations from independently prepared triplicate samples.

2.3.5 ¹H-NMR titrations - Determination of complexation equilibria

Solutions of **L₂H₂** in MeOD were titrated with HgCl₂ at constant ligand concentration. In a typical experiment, a solution of ligand (4.0 x 10⁻³ M) and 2.2 equiv. of triethylamine (Et₃N) in MeOD was transferred to an NMR tube and titrated with solutions of HgCl₂ (prepared by diluting with the ligand/Et₃N) solutions at various concentrations (0.1 – 2 equiv.). Spectra were acquired at 298 K on a 400-MHz Bruker Avance NMR spectrometer with chemical shifts, δ , reported in ppm.

2.3.6 Determination of stoichiometry by the continuous variation method (Job Plot)

Information on the stoichiometry of the complexes was obtained from the continuous variation method.³⁴ Solutions containing varying concentrations of Hg^(II) and ligand (0.02 – 0.2 mM) were prepared in methanol. A stock solution of ligand (0.20 mM) and HgCl₂ (0.20 mM) was used. UV-Vis absorbances were measured at the λ_{max} of the complexes ($\lambda_{\text{max}} = 304$ nm). Afterward, the absorbances at 304 nm was plotted vs. the mol ratio of the [Hg^(II)]_t as shown below.

$$\text{Mol ratio of Hg}^{(\text{II})} = \frac{[\text{Hg}^{(\text{II})}]}{[\text{Hg}^{(\text{II})}] + [\text{L}]} \quad (5)$$

2.3.7 X-ray crystallography for C2

Light pink block-shaped crystals of the complex were obtained by slow diffusion of hexanes into its dichloromethane solution. Data collection and structure refinement details are summarized in Table 2.3. A suitable crystal was selected and mounted on a Bruker D8 Quest diffractometer equipped with PHOTON II detector operating at $T = 298 \text{ K}$. The structure was solved in the trigonal space group $P3_2$ (# 145) determined by the *ShelXS*³⁵ structure solution program using Direct Methods and refined by Least Squares using version 2018/3 of *ShelXL*.³⁶ All non-hydrogen atoms were refined anisotropically. Calculations and molecular graphics were performed using the *SHELXTL 2014* and *Olex2*³⁷ programs.

2.4. Results and discussion

2.4.1 Isolation and characterization of Hg^(II) complexes

2.4.1.1 Synthesis

All ligands, **L1H₂**, **L2H₂**, **L3H₂**, and **L4H₂** (Figure 2.1), were synthesized in one step according to a modified literature procedure.⁷ Typically, the ligand synthesis involves the reaction of the *o*-phenylenediamine derivative with two equivalents of the appropriate sulfonyl chloride derivative in a halogenated solvent and pyridine. All ligands were found spectroscopically identical to the reported compounds.^{7,25}

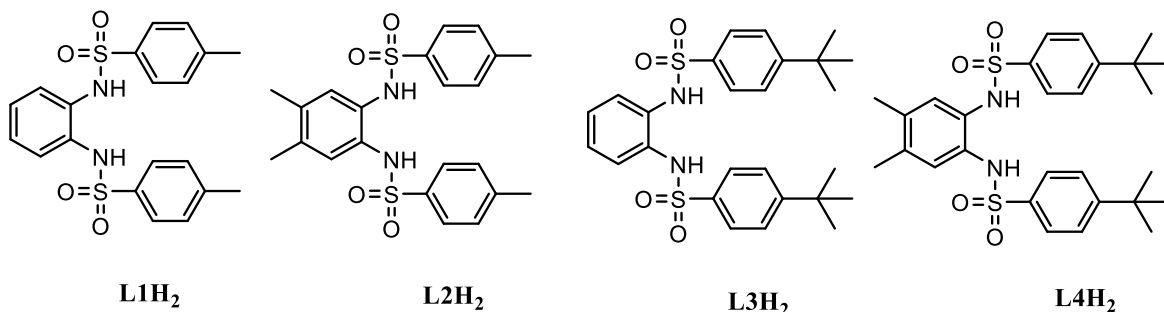
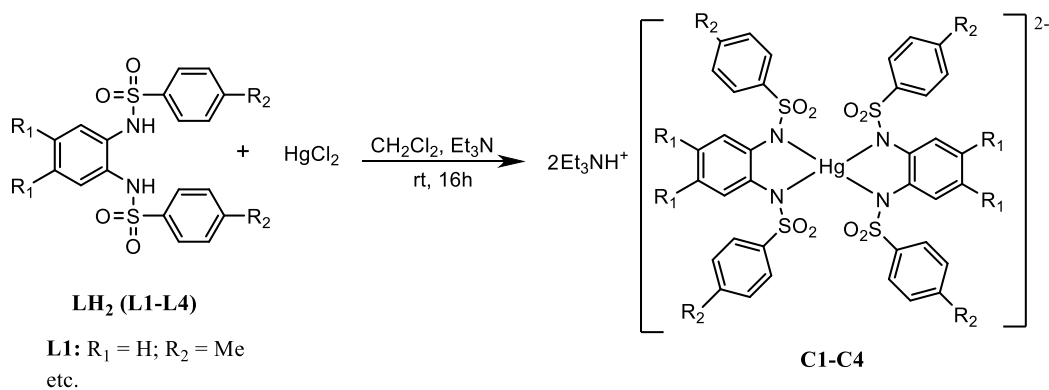


Figure 2.1. Structures of bis-arylsulfonamide ligands

The synthesis of complexes was carried out in one step by reacting solutions of ligands in Et₃N with HgCl₂ solutions in CH₂Cl₂ (Scheme 2.1). All isolated complexes were found to be 1:2 anionic complexes of the type [HgL₂]²⁻ isolated as (Et₃NH)₂HgL₂ with two triethylammonium counteranions. Unlike previous work for Pb^(II), triethylamine was not involved in coordination to the metal, and 1:1 M^(II)-L complexes were not isolated. X-ray crystallography for the **C2** (Figure 2.17), ¹H and ¹³C-NMR spectroscopy (Figures 2.4 and 2.5b), and elemental analysis are all consistent with this 1:2 formulation.



C1: R₁ = H; R₂ = Me **C2:** R₁ = Me; R₂ = Me
C3: R₁ = H; R₂ = t-Bu **C4:** R₁ = Me; R₂ = t-Bu

Scheme 2.1: Synthesis of Hg^(II)-bis-arylsulfonamide complexes

2.4.1.2 FT-IR studies

Table 2.1 shows the main FT-IR spectral bands for the ligands **L1H₂** – **L4H₂** vs. their Hg^(II) complexes **C1** – **C4**. There are two potential N-donor sites in each ligand, due to deprotonation of the sulfonamidic nitrogens (RSO₂NH⁻), with N-H stretching bands appearing around 3314 cm⁻¹. The disappearance of these N-H bands on the spectra of the complexes is evidence of ligand deprotonation, necessary for complexation. The bands which appear at 1330 - 1301 cm⁻¹ and 1164 - 1143 cm⁻¹ in the ligand spectra are due to $\nu_{\text{asym}}(\text{SO}_2)$ and $\nu_{\text{sym}}(\text{SO}_2)$, respectively. These bands shift to lower frequencies in the complexes at 1257 - 1227 cm⁻¹ and 1136 - 1122 cm⁻¹, respectively.

Table 2.1. Selected IR bands of the bis-arylsulfonamide ligands and their corresponding Hg^(II) complexes

Compounds	$\nu_{\text{asym}}(\text{SO}_2)$	$\nu_{\text{sym}}(\text{SO}_2)$	$\nu(\text{S-N})$	$\nu(\text{N-H})$
	Wavenumber (cm ⁻¹)			
L1	1301	1143	917	3314
C1	1255	1122	963	-
L2	1326	1157	908	3261
C2	1227	1122	917	-
L3	1330	1159	907	3316
C3	1255	1125	964	-
L4	1319	1164	902	3328
C4	1257	1136	920	-

Complexation is also evident by the shifts to a higher frequency observed in $\nu(\text{S-N})$ from the spectra of the ligands (917 - 902 cm⁻¹) to the spectra of the complexes (964 - 917 cm⁻¹). These shifts can be explained due to the resonance form for the

deprotonated sulfonamide directing electron density to the S-N bond, which is thus strengthened and shortened after complexation.^{38,39} FT-IR spectra for all complexes are provided in Figure 2.2 (a) – (d).

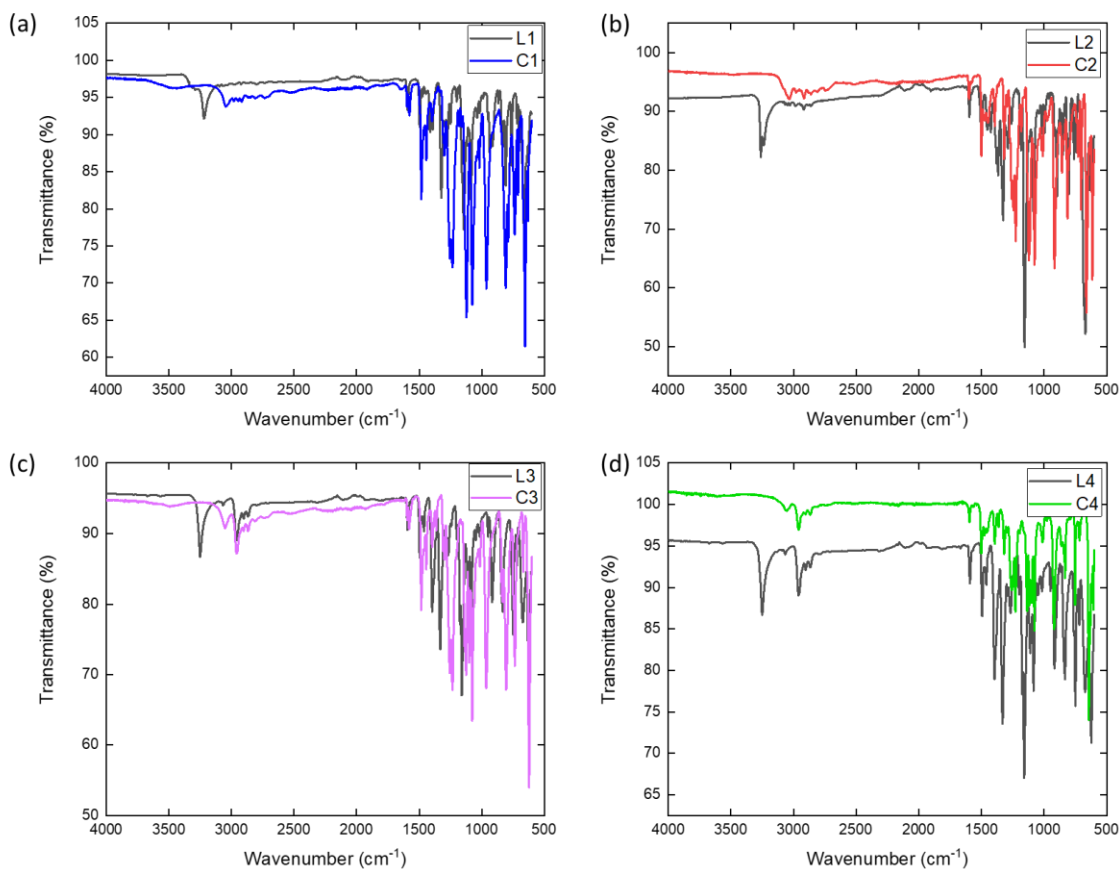


Figure 2.2: FT-IR Spectra of (a) C1 (b) C2 (c) C3 (d) C4

2.4.1.3 NMR studies

The ¹H-NMR spectra for the ligands **L1H₂** – **L4H₂** and their Hg^(II) complexes were collected in CDCl₃. N-H Signals were observed at δ 6.56, 9.25, 6.45, and 6.36 ppm for **L1H₂**, **L2H₂**, **L3H₂**, and **L4H₂**, respectively, and completely disappeared in the

spectra of the complexes, thus confirming the deprotonation and involvement of the sulfonamidic N in coordination. More importantly, significant upfield or downfield chemical shift changes for the aromatic protons by 0.3 – 1 ppm were observed for all spectra upon complexation. The aromatic protons for **L2** (Figure 2.3; H_c and H_e) closest to the sulfonamidic N shifted downfield due to the conjugation of the sulfonamidic N, while all other protons shifted upfield (See Figure 2.3 for the **L2**-Hg^(II) complex, and Figure 2.4 for spectra of the other complexes). The signals appearing at δ 0.78 – 1.06 ppm and δ 2.28 – 2.73 ppm in the complex spectra correspond respectively to the three (-CH₃) and two (-CH₂-) protons attributed to the triethylammonium counteranion.

The ¹³C NMR spectra for the ligands and their complexes were also obtained in CDCl₃. The spectral assignments for all complexes are given in the experimental section, and the spectra are provided in Figure 2.5. The carbon signals were found to be in their expected region, supporting the binding modes evidenced by the FT-IR and ¹H NMR spectral data. Signals due to the aromatic carbons are found in the δ 90-180 ppm region and the aliphatic carbons around δ 20-50 ppm.

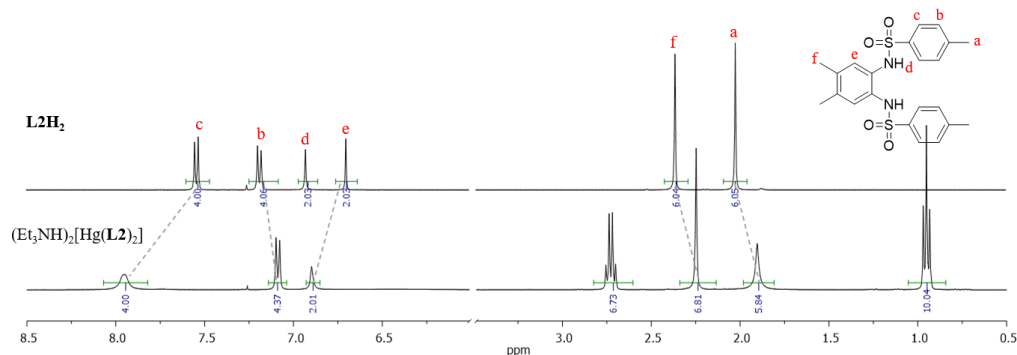


Figure 2.3. ¹H-NMR of **L2H₂** and isolated $(Et_3NH)_2[Hg(L_2)_2]$ in CDCl₃.

The carbons of sulfonamidic S and N (-C-SO₂-HN-C-) in all complexes were observed at 140.2 – 147.5 ppm and 140.0 – 140.3 ppm, respectively. The resonances around 46.2 ppm and 9.0 ppm are assigned to carbons of the methylene and methyl groups of triethylammonium, indicating the presence and involvement of triethylammonium in these complexes (Figure 2.5).

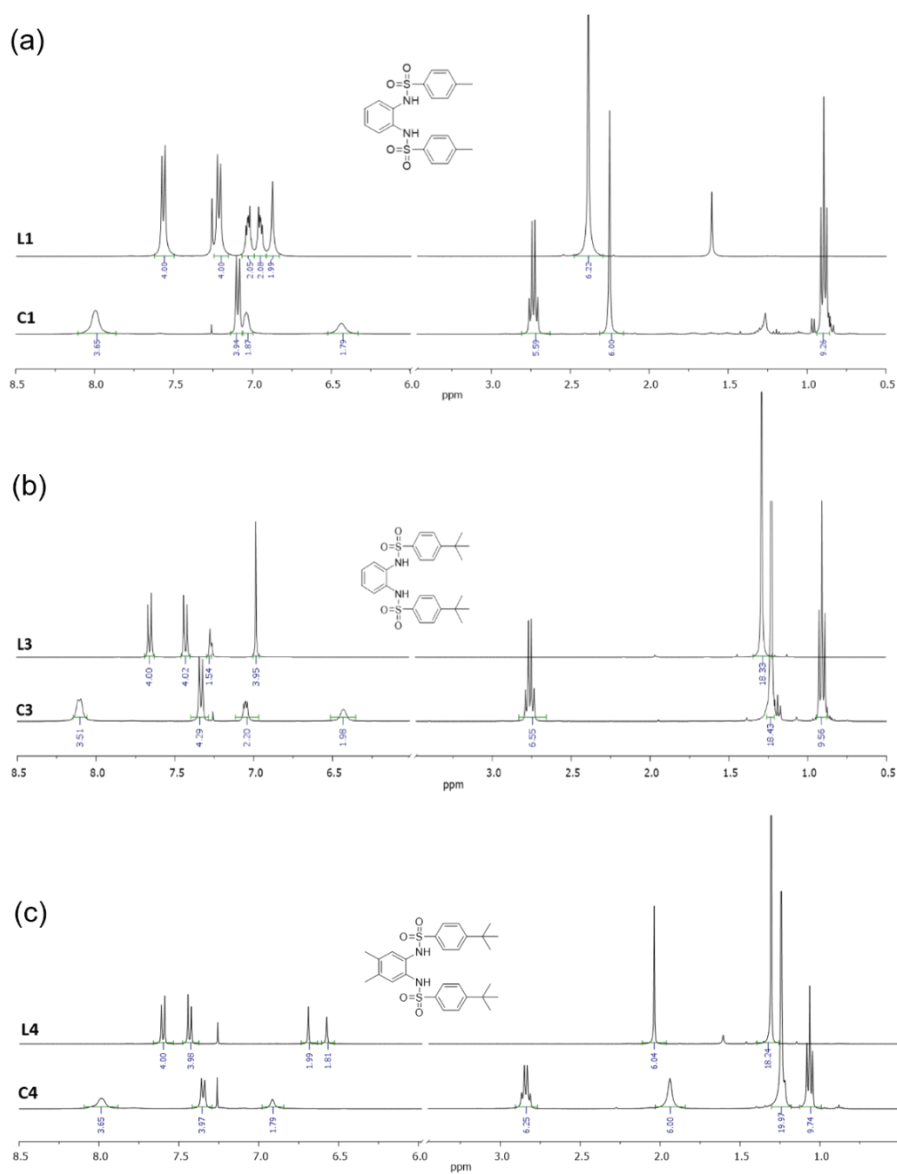


Figure 2.4: ¹H-NMR of (a) L1 and (Et₃NH)₂[Hg(L1)₂] (b) L3 and (Et₃NH)₂[Hg(L3)₂] (c) L4 and (Et₃NH)₂[Hg(L4)₂] in CDCl₃.

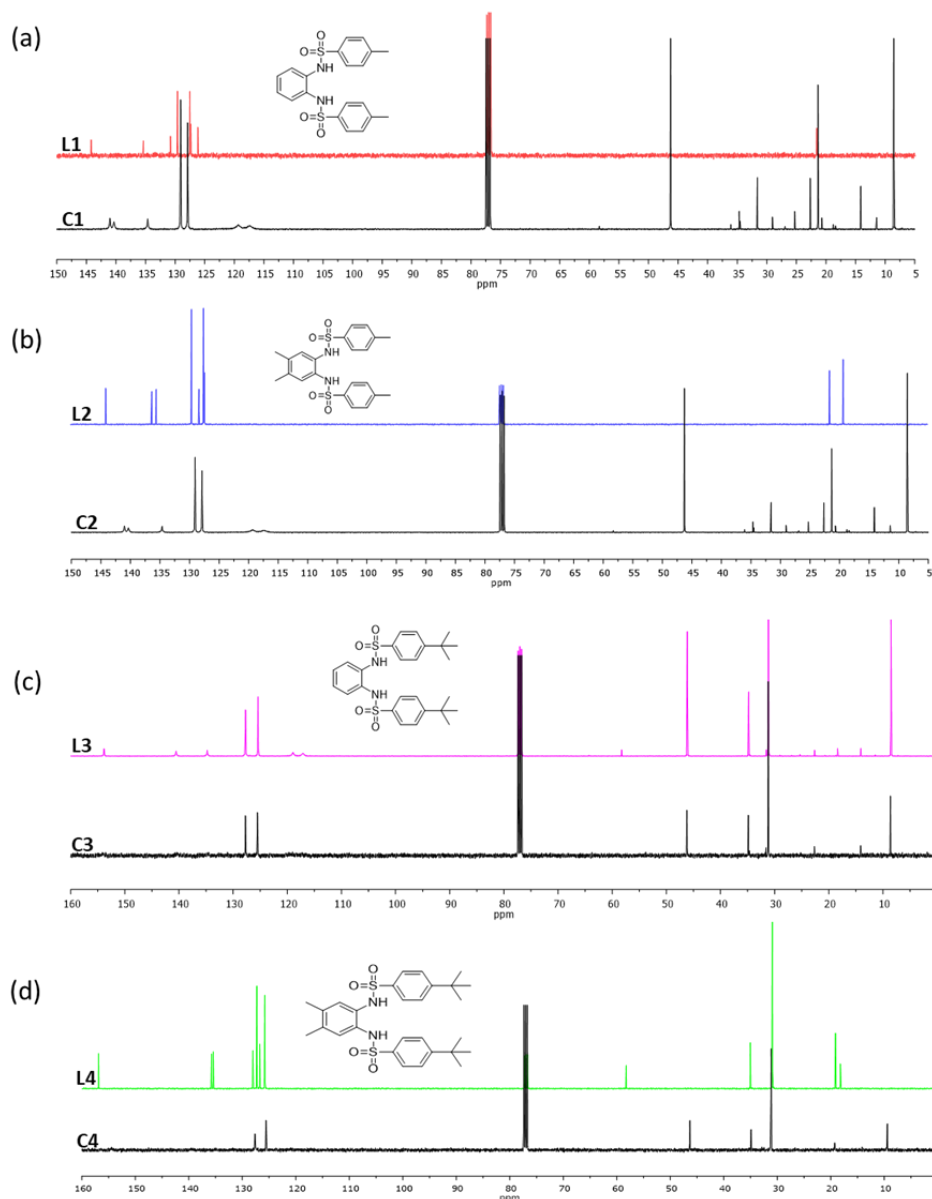


Figure 2.5: ^{13}C -NMR of (a) **L1** and $(\text{Et}_3\text{NH})_2[\text{Hg}(\text{L1})_2]$ (b) **L2** and $(\text{Et}_3\text{NH})_2[\text{Hg}(\text{L2})_2]$ (c) **L3** and $(\text{Et}_3\text{NH})_2[\text{Hg}(\text{L3})_2]$ (d) **L4** and $(\text{Et}_3\text{NH})_2[\text{Hg}(\text{L4})_2]$ in CDCl_3 .

Complexation equilibria were determined by performing ^1H -NMR titrations. Aliquots of HgCl_2 (prepared in MeOD) were added to 4.0 mM solution of **L2H₂** and Et_3N (2.2 eq.) in MeOD at 298 K. There were significant changes in the chemical shifts

of the free ligand **L2H₂**, the deprotonated ligand **L2²⁻** and the complexes formed (Figures 2.6 (a) and (b)). After the addition of 0.25 – 0.5 equivalents of Hg^(II), the ¹H-NMR spectrum is consistent with a 1:2 M-L stoichiometry of type [Hg(**L2**)₂]²⁻, as also observed in the crystal structure (Figure 2.17). Although a complex was formed at these ratios, the peaks are broad, and the residual signals for the deprotonated ligand are still slightly noticeable. Likewise, the simultaneous growth of new signals attributed to the 1:1 complex was also observed. This can be explained by slow exchange under the NMR timescale for these concentration levels, indicating covalent bond formation. Upon further additions of Hg^(II) (1 – 2 eq. of Hg^(II)), there were noticeable chemical shift changes and sharpening of the signals, with final disappearance of the resonances for both the deprotonated ligand and the 1:2 complex, indicating a complete formation of a 1:1 complex. Comparison of the ¹H-NMR spectra after titration of Hg^(II) to **L2H₂** shows evidence of conversion of triethylamine to triethylammonium and effects due to second-sphere interactions with Hg^(II). This is corroborated by the significant chemical shift changes of the triethylammonium resonances at 0.5 eq. of Hg^(II) (Figure 2.6b), while no shift changes for the same resonances were observed at other equivalent ratios of Hg^(II).

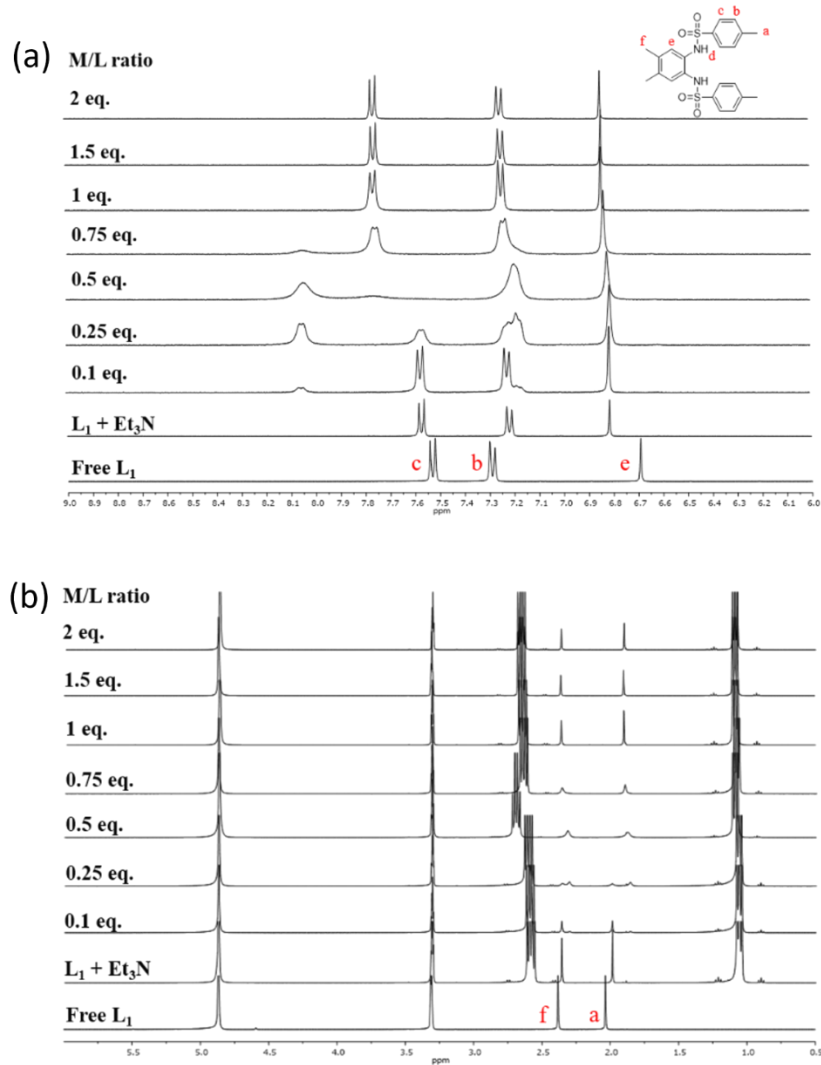


Figure 2.6: 1H -NMR titration of $HgCl_2$ ($4.0 \times 10^{-2} M$ stock solution) into a solution of L_2H_2 ($4.0 \times 10^{-3} M$) and Et_3N (2.2 equiv.) in MeOD (various equiv. of $Hg^{(II)}$ are labelled on each spectrum). The effect of $Hg^{(II)}$ addition is shown in (a) the aromatic proton region of L_2H_2 and (b) the aliphatic proton region of L_2H_2 .

2.4.2 Extraction studies

2.4.2.1 General remarks

Solutions of ligands L_2H_2 or L_4H_2 (2.0 mM) in DCE with or without Et_3N (2.2 eq.) were contacted with aqueous $HgCl_2$ (1.0 mM) at pH range 7.0 – 14.0 in order to determine

extraction efficiency for $\text{Hg}^{(\text{II})}$ by those ligands. The amount of $\text{Hg}^{(\text{II})}$ extracted from aqueous solutions into 1,2-dichloroethane by L2H_2 or L4H_2 , both in the presence or absence of triethylamine (Et_3N), was determined and quantified using the dithizone spectrophotometric method of $\text{Hg}^{(\text{II})}$ determination.¹⁵ This method was successfully used to determine $\text{Hg}^{(\text{II})}$ concentrations in the aqueous phases for all samples after extraction and after stripping in order to quantify $\text{Hg}^{(\text{II})}$ recovery. Measurements of the amounts of total $\text{Hg}^{(\text{II})}$ before extraction provided satisfactory mass balances (Figures 2.12 and 2.13) that corresponded to the original concentrations of prepared $\text{Hg}^{(\text{II})}$ solutions. The limit of detection (LOD) was determined to be $0.36 \mu\text{M}$.⁴⁰

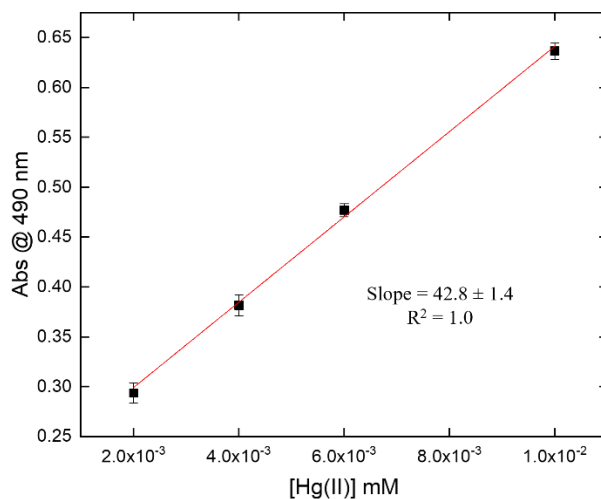


Figure 2.7: Calibration curve for the quantification of $\text{Hg}^{(\text{II})}$ using the dithizone- Hg complex absorbance at 490 nm

2.4.2.2 Extraction dependence on pH

$\text{Hg}^{(\text{II})}$ was extracted from pH -adjusted solutions ranging from pH 7.0 to 14.0 using various sodium hydroxide concentrations. Figure 2.8 displays the influence of pH on the

extraction of $\text{Hg}^{(\text{II})}$ from these alkaline aqueous solutions after contact with an organic phase containing 2.0 mM of **L2H₂** or **L4H₂** (with or without triethylamine). The pH value of the aqueous phase played a significant role in the extraction process. In the presence of triethylamine, about 98% of $\text{Hg}^{(\text{II})}$ was recovered from the solution at a pH range of 7.0 to 10.0 for **L4H₂**, while about 85% was recovered for **L2H₂**. The recovered amount was gradually lower for pH 11.0 and higher. For experiments at higher pH (12.0 – 14.0), precipitation was observed at the interface in the presence of trimethylamine, which was even more pronounced at pH 13.0 and 14.0, thus explaining the lower recovery of $\text{Hg}^{(\text{II})}$ at very high alkalinity. In the absence of triethylamine, low extraction efficiency was observed for mercury by **L2H₂** from pH 7.0 to 11.0 (about 19.7 %) and by **L4H₂** from pH 7.0 to 10.0 (about 9.7 %) until pH 11.0 (26.2 %). Optimum recovery of mercury was observed at pH 12.0 (82.7%) for **L2H₂** and (90.7%) for **L4H₂**, suggesting that the equilibrium at pH 12.0 is favorable for the formation of a coordination complex. At pH 13.0 and 14.0, recovery was low, presumably due to precipitation, which was also observed in the aqueous-organic interface for pH > 12.0. The overall results indicate that deprotonation of the ligand is necessary for the extraction of mercury into the organic phase, and pH 12.0 is the optimal pH in which ligand deprotonation is sufficient, while precipitation is minimal.

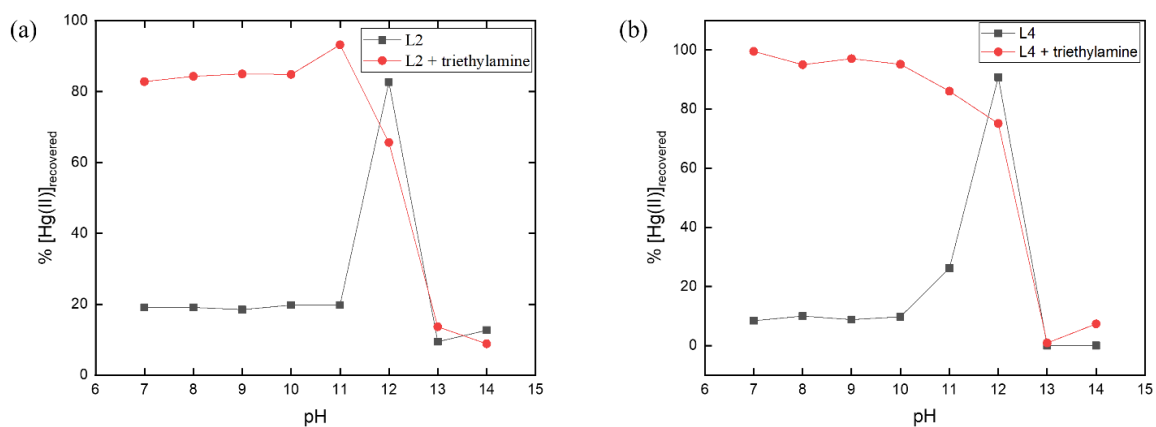


Figure 2.8. pH-dependent extraction of $\text{Hg}^{(II)}$ by (a) L2H_2 and (b) L4H_2 into DCE both in the absence (black) and presence (red) of triethylamine. ($[\text{Hg}^{(II)}] = 1.0 \text{ mM}$, $[\text{L2H}_2]$ or $[\text{L4H}_2] = 2.0 \text{ mM}$, $[\text{Et}_3\text{N}] = 4.0 \text{ mM}$).

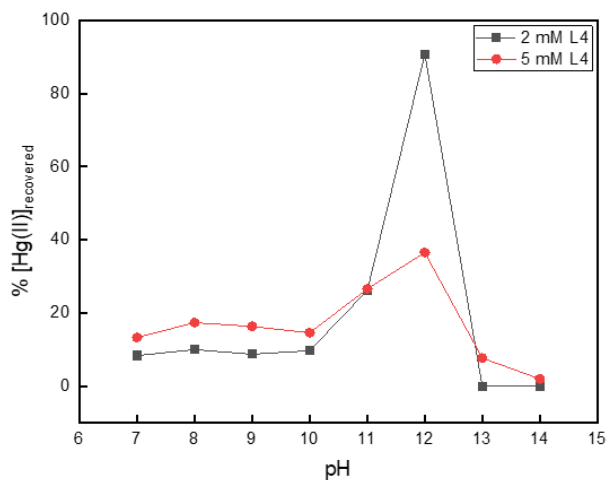


Figure 2.9. pH-dependent extraction of $\text{Hg}^{(II)}$ by 2.0 mM (black) or 5.0 mM (red) L4 into DCE in the absence of trimethylamine. ($[\text{Hg}^{(II)}] = 1.0 \text{ mM}$)

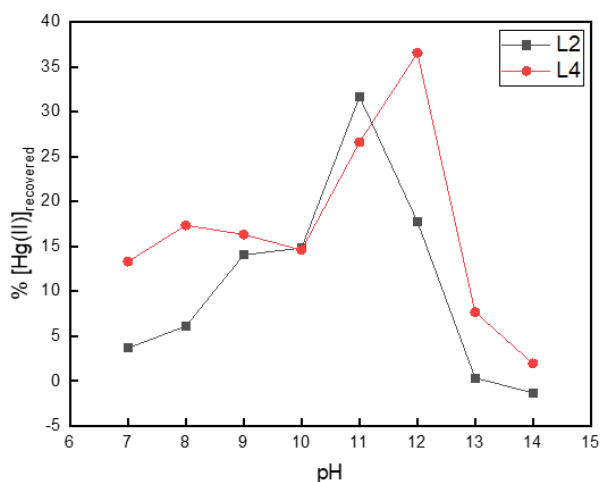


Figure 2.10. pH-dependent extraction of $\text{Hg}^{\text{(II)}}$ by **L2** and **L4** into DCE in the absence of triethylamine. ($[\text{Hg}^{\text{(II)}}] = 1.0 \text{ mM}$, $[\text{L2}] = 5.0 \text{ mM}$, $[\text{L4}] = 5.0 \text{ mM}$)

2.4.2.3 Extraction dependence on ligand concentration

$\text{Hg}^{\text{(II)}}$ was extracted at pH 12.0 with varying **L2H₂** or **L4H₂** concentrations in the presence or absence of triethylamine. At $[\text{L4H}_2] = 2.0 \text{ mM}$ and 2.2 eq. of Et_3N , 98.6% extraction (Figure 2.13) of $\text{Hg}^{\text{(II)}}$ with 82.6% recovery after stripping (Figure 2.11c) was recorded. Likewise, approximately the same amount was extracted and stripped (97.6% extraction and 82.8% recovery) in the absence of triethylamine (Figures 2.11a and 2.12). The results show that as the ligand concentration increases from 0.3 to 2.0 mM at constant $[\text{Et}_3\text{N}]_i$ (5 mM) and pH 12.0, the % extraction of $\text{Hg}^{\text{(II)}}$ increases and becomes essentially quantitative for 2.0 mM of ligand in the presence of triethylamine. This result is consistent with the hypothesis that two complexes can form under these conditions (presumably 1:1 and 1:2 $\text{Hg}:\text{L4}$ complexes). Interestingly, extraction studies in the absence of triethylamine and pH 12.0 show the deprotonation, coordination, and subsequent extraction of mercury from the aqueous phase to the organic phase as a 1:2

Hg:**L4** complex (less dominant) or 1:1 Hg:**L4** complex that saturates at 1.0 mM instead of 2.0 mM of the ligand, clearly indicating that the 1:1 complex is dominant in the absence of Et₃N. A possible formulation for the 1:1 complex is Hg**L4** and the 1:2 complex as [Hg**L4**₂]²⁻ with two Na⁺ (in the absence of Et₃N) as counterions, which would be in agreement with the X-ray structure obtained for the **L2** analog **C2**. Formation of this type of ion-paired complexes in dichloromethane has been reported to be favorable for Ln(III) complexation by these sulfonamides²⁵ by DFT calculations and has also been shown to form for other ligands as well.^{41,42} As **L4** is quite lipophilic, this complex is expected to be present mainly in the 1,2-dichloroethane phase. Extraction studies with concentrations of **L4H₂** > 2 mM showed a decrease in the recovery of Hg^(II) (Figure 2.9), presumably due to increased precipitation. **L2H₂** showed similar extraction efficiency as **L4H₂**, however, at 2.0 mM **L2H₂** in the absence of triethylamine, both the extraction efficiency and the recovery of Hg^(II) were low (56 %), probably indicating a complex partition of the less lipophilic 1:2 complex Na₂[Hg**L2**] to the aqueous phase. This observation is consistent with the hypothesis that the more lipophilic **L4** forms a more lipophilic organosoluble 1:2 complex than **L2**, with only minimal partition to the aqueous phase.

Slope analysis to confirm the complex stoichiometry in the organic phase both in the presence and absence of triethylamine was performed by determining the relationship between the logarithm of D_{Hg} and the logarithm of [**L**] (Figure 2.11b or 2.11d). The slope of the straight line between log D_{Hg} and log [**L2**] or [**L4**] obtained is 1.8 or 2.1 respectively for the extraction with triethylamine and 2.3 or 1.9 respectively for the extraction without triethylamine. This suggests the higher contribution of the 1:2 Hg/**L**

complex stoichiometries. It is presumed that triethylammonium is involved in stronger outer sphere coordination with the anionic complex formed than Na^+ , further stabilizing these complexes. This hypothesis is further supported by the findings from the $^1\text{H-NMR}$ titration (Figure 2.6a and 2.6b), clearly indicating the formation of both complexes and the involvement of triethylammonium counteractions in outer sphere complexation.

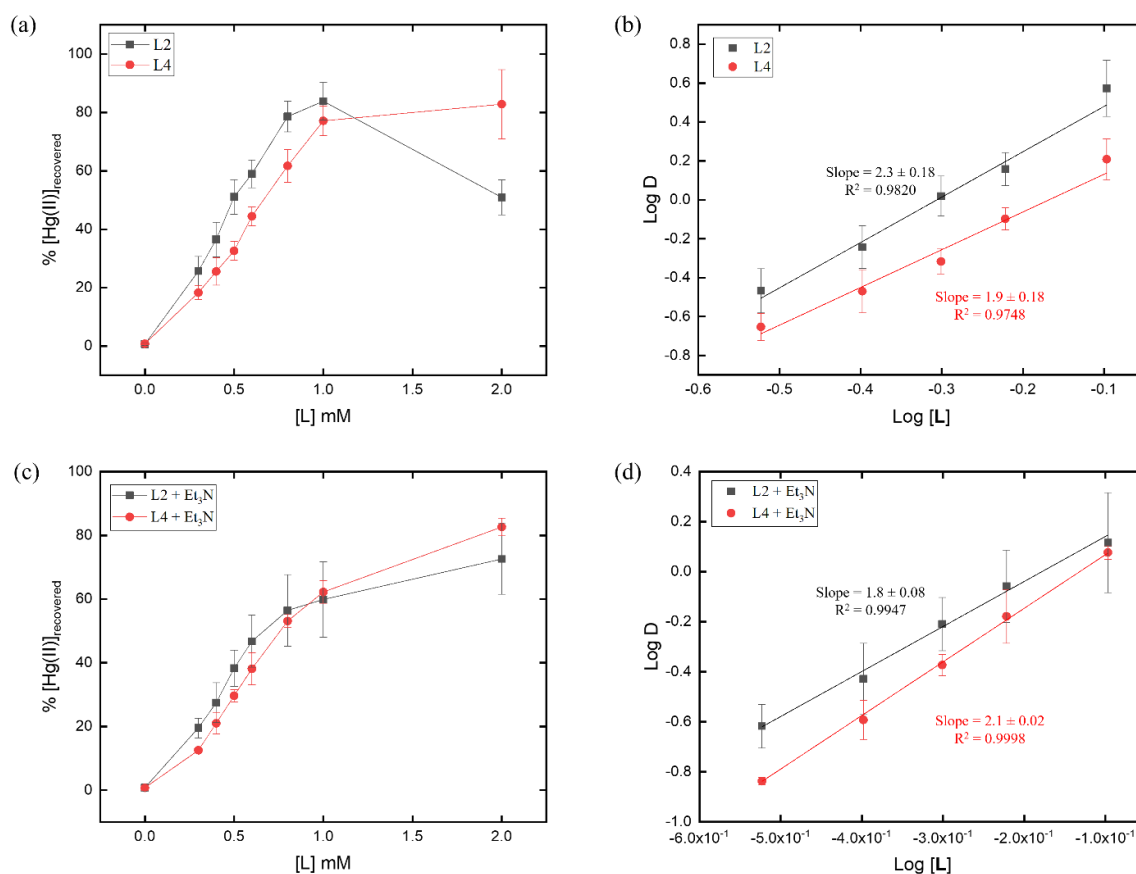


Figure 2.11. Distribution experiments (% recovery after stripping) showing: (a) Influence of L2H_2 or L4H_2 concentration on $\text{Hg}^{(II)}$ extraction efficiency in the absence of triethylamine. Conditions: $\text{pH} = 12.0$, $[\text{Hg}^{(II)}] = 1.0 \text{ mM}$, $[\text{L2H}_2]$ or $[\text{L4H}_2] = 0.30 - 2.0 \text{ mM}$, $[\text{Et}_3\text{N}] = 5.0 \text{ mM}$ (b) Relationship between $\log D_{\text{Hg}}$ and $\log [\text{L2H}_2]$ or $[\text{L4H}_2]$ showing the stoichiometry of the $\text{Hg}^{(II)}:\text{L}$ complexes that are formed at various $\text{Hg}^{(II)}:\text{L}$ ratios. (c) Influence of L2H_2 or L4H_2 concentration on $\text{Hg}^{(II)}$ extraction efficiency in the presence of triethylamine. Conditions: $\text{pH} = 12$, $[\text{Hg}^{(II)}] = 1.0 \text{ mM}$, $[\text{L2H}_2]$ or $[\text{L4H}_2] = 0.30 - 2.0 \text{ mM}$, $[\text{Et}_3\text{N}] = 5.0 \text{ mM}$ (d) Relationship between $\log D_{\text{Hg}}$ and $\log [\text{L2H}_2]$ or $[\text{L4H}_2]$ showing the stoichiometry of the $\text{Hg}^{(II)}:\text{L}$ complexes that are formed at various $\text{Hg}^{(II)}:\text{L}$ ratios.

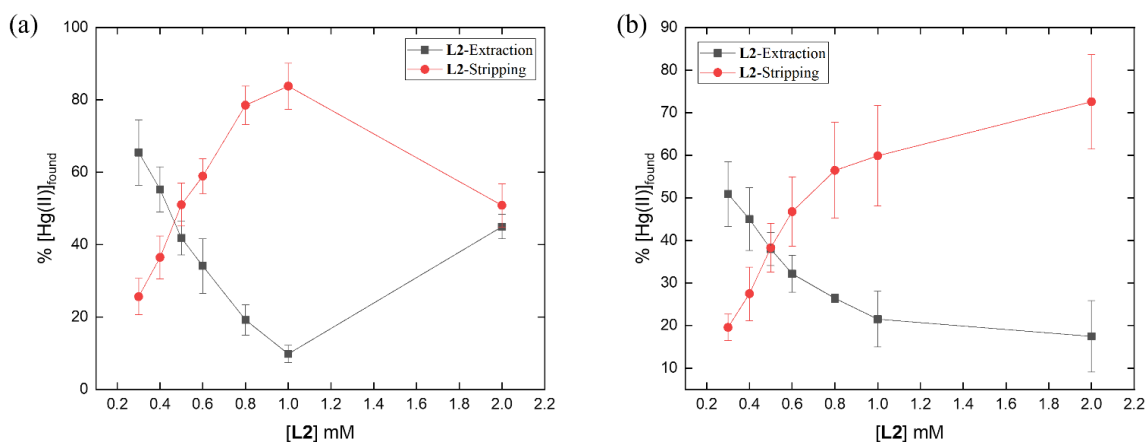


Figure 2.12. Amount of $\text{Hg}^{\text{(II)}}$ found in the aqueous phases after **L2** extraction and stripping experiments in the (a) absence of triethylamine and (b) presence of triethylamine (5.0 mM) ($[\text{Hg}^{\text{(II)}}] = 1.0 \text{ mM}$, $[\text{L2}] = 0.30 - 2.0 \text{ mM}$, $\text{pH} = 12.0$)

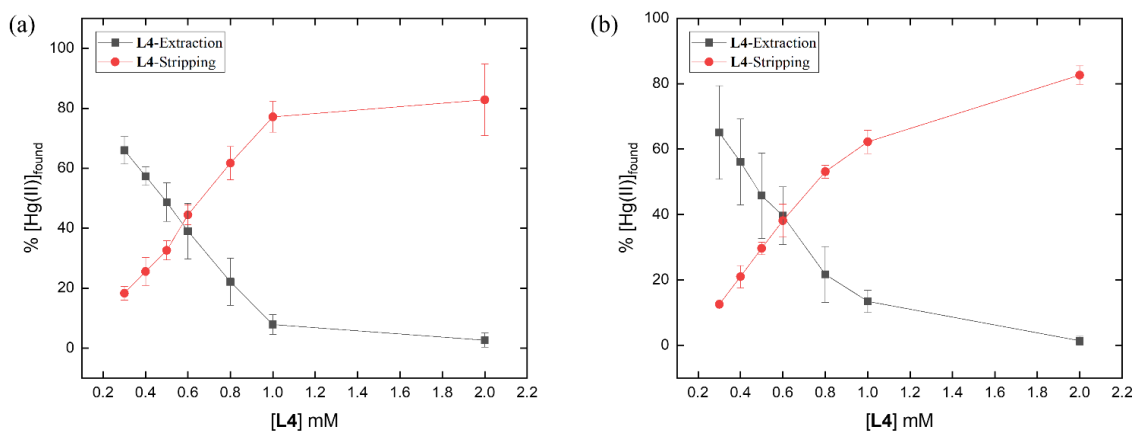


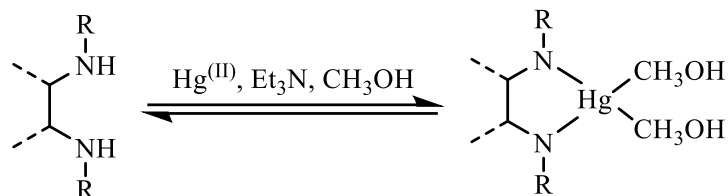
Figure 2.13. Amount of $\text{Hg}^{\text{(II)}}$ found in the aqueous phases after **L4** extraction and stripping experiments in the (a) absence of triethylamine and (b) presence of triethylamine (5.0 mM) ($[\text{Hg}^{\text{(II)}}] = 1.0 \text{ mM}$, $[\text{L4}] = 0.30 - 2.0 \text{ mM}$, $\text{pH} = 12.0$)

2.4.3 UV-Vis binding studies

UV-Vis titrations of the bis-arylsulfonamide ligands with $\text{Hg}^{\text{(II)}}$ in methanol provided binding information and quantitative data for complexation. The UV-Vis spectral changes for methanol solutions of disulfonamides **L** (0.040 mM) and Et_3N

(0.088 mM) upon titrating with HgCl₂ (0 – 0.140 mM) at constant **L** concentration are shown in Figure 2.15. With the gradual additions of Hg^(II) (0 – 0.140 mM) to the methanolic solutions of **L1H₂**, **L2H₂**, **L3H₂**, or **L4H₂** (0.040 mM) and triethylamine (2.2 eq.), a new absorption band was observed at around ca. 300 nm. It is attributed to charge transfer transition arising from π electron interactions between Hg and the ligand, indicating complexation. The absorption band at 220 nm (due to π - π^* transitions) is enhanced, broadened, and slightly blue-shifted upon Hg^(II) addition (Figure 2.14). Initial isosbestic points formed at 209 nm are masked after subsequent additions due to the spectrum of excess HgCl₂ in the solution (240 nm). A control experiment in the absence of ligand showed that mercury addition does not show any absorption in the 300-350 nm region (Figure 2.15). The plot of the absorbance at 304 nm vs. [Hg^(II)]_t revealed a significant change in absorbance that plateaus at 0.04 mM of [Hg^(II)]_t, suggesting a 1:1 **L** to Hg^(II) complexation ratio. Even though this result seems inconsistent with the crystal structure, it can be explained because methanol is a coordinating solvent that can satisfy the Hg^(II) coordination sphere in a similar fashion as Et₃N (*vide infra*). The binding constants were determined from the increase in the absorption band at ca 300 nm (Table 2.2). The results show similarities in the Hg^(II) binding strength for all four ligands. The continuous variations method³⁴ (Job plot) experiment in methanol (0.20 mM) for the binding of **L2** to Hg^(II) (monitored at 304 nm) is shown in Figure 2.16. The bell-shaped curve and maximum at a molar fraction of 0.5 is strongly indicative of 1:1 complexation between **L2** and Hg^(II). The experimental observation of 1:1 stoichiometry from methanolic solution studies by UV-Vis titrations and Job plots indicate likely formation of Hg^(II)L(CH₃OH)₂ complexes in methanol, instead of the 1:2 [HgL₂]²⁻ isolated in solid-

state. This coordination difference can be attributed to methanol coordinating ability to $\text{Hg}^{(\text{II})}$ (Scheme 2.2).



Scheme 2.2: Proposed 1:1 coordination of $\text{Hg}^{(\text{II})}$ to **L** in a methanolic solution in the presence of triethylamine, which is consistent with the UV-Vis experiments

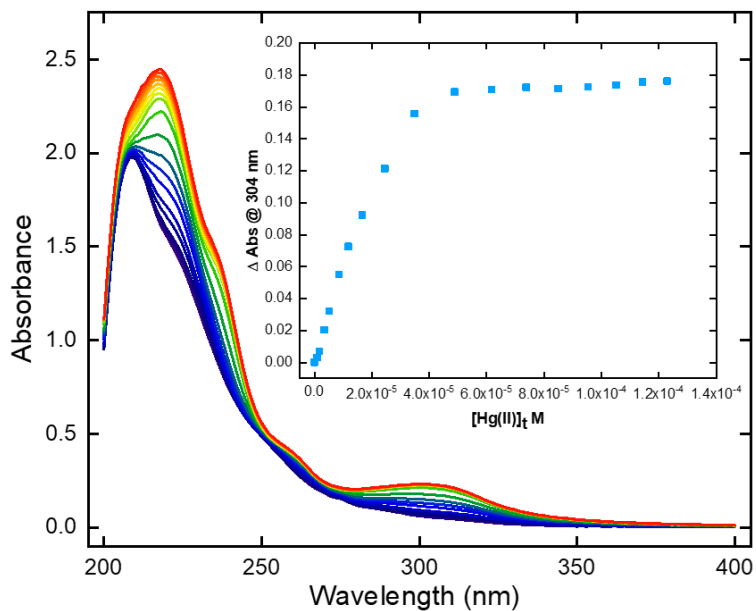


Figure 2.14. UV-Vis titration of ligand **L2H₂** ($4.0 \times 10^{-5} \text{ M}$) and Et_3N (2.2 eq) in CH_3OH upon gradual addition of HgCl_2 ($4.0 \times 10^{-4} \text{ M}$). The concentration of the ligand was constant during the titration. Inset: UV-Vis titration binding curve of **L2** with $\text{Hg}^{(\text{II})}$ at 304 nm.

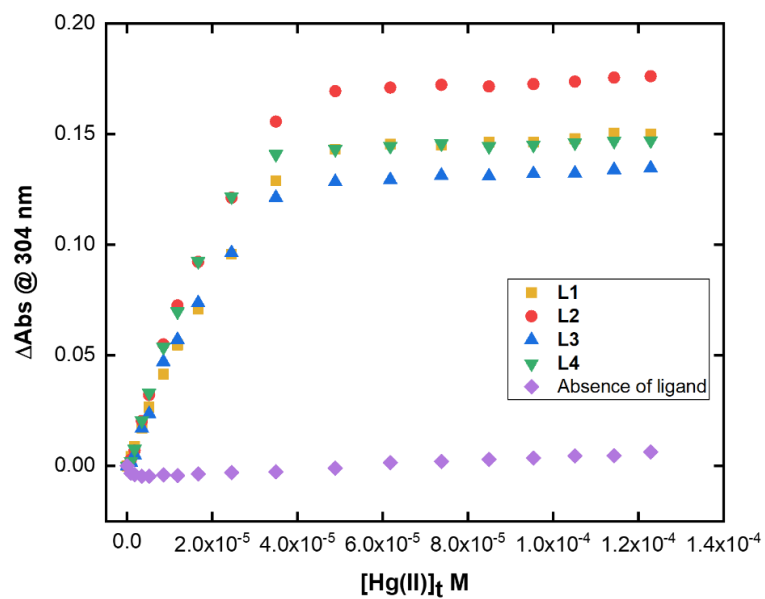


Figure 2.15. UV-Vis titration curves for bis-arylsulfonamide ligands (*L1H₂* - *L4H₂*) ($4.0 \times 10^{-5} \text{ M}$) and Et_3N (2.2 eq.) with $\text{Hg}^{(\text{II})}$ at 304 nm ($4.0 \times 10^{-4} \text{ M}$). Titration in the absence of ligand (purple diamond) indicates no complexation between triethylamine and mercury.

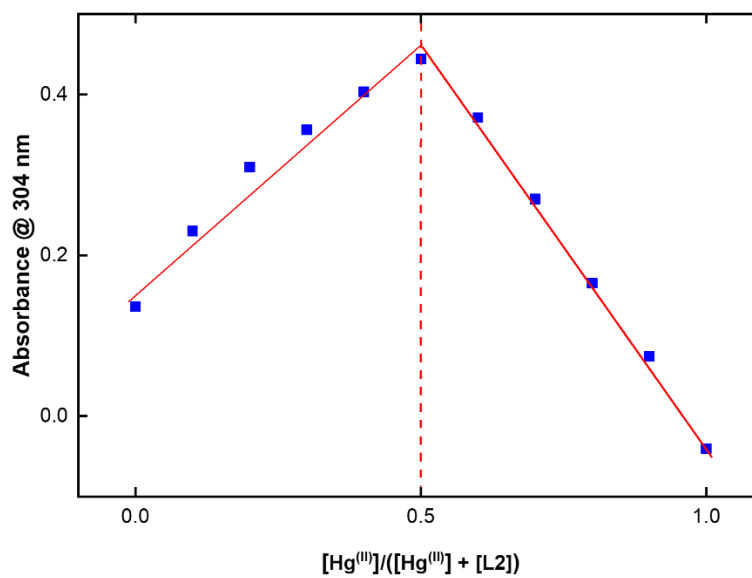


Figure 2.16. Job plot of *L2* ($2.0 \times 10^{-4} \text{ M}$) and Et_3N ($4.8 \times 10^{-4} \text{ M}$) with $\text{Hg}^{(\text{II})}$ ($2.0 \times 10^{-4} \text{ M}$) in methanol.

Table 2.2: Association constants of the complexes obtained from titrating the corresponding ligands with HgCl₂ in methanol.

	Log K
L1-Hg	5.77 ± 0.05
L2-Hg	5.34 ± 0.09
L3-Hg	5.19 ± 0.06
L4-Hg	5.87 ± 0.09

2.4.4 Single-crystal X-ray crystallography

Single crystal X-ray crystallographic analysis reveals the molecular structure for complex (C2). The perspective view of the structure is depicted in Figure, and selected metric parameters are listed in the figure caption.

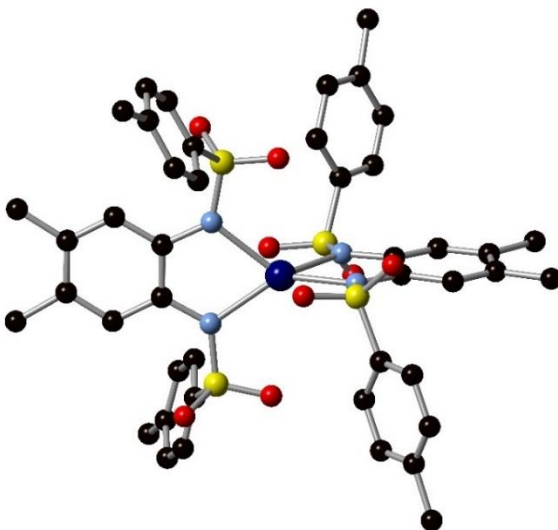


Figure 2.17. Perspective view of the molecular structure of the anion of complex C2. The counter cations and the H atoms are not shown for the sake of clarity. Color code: deep blue = Hg, blue = N, red = O, yellow = S and black = C atoms. Selected bond distance (Å): Hg-N, 2.176(7), 2.292(10), 2.202(7), 2.248(7); selected bond angles (°): 138.6(3), 134.0(4), 124.5(4), 118.7(3), 74.1(3), 73.8(3).

Table 2.3. Crystal data and structure refinement parameters for the complex

	Complex C2
Formula	C ₄₄ H ₄₄ HgN ₄ O ₈ S ₄ · 2(C ₆ H ₁₆ N)
<i>F</i> _w	1288.04
<i>D</i> _{calc.} / g cm ⁻³	1.380
μ /mm ⁻¹	2.670
Shape	Block
<i>T</i> /K	298(2)
Crystal System	Trigonal
Space Group	P3 ₂
<i>a</i> /Å	17.172(4)
<i>b</i> /Å	17.172(4)
<i>c</i> /Å	18.210(8)
α /°	90
β /°	90
γ /°	120
<i>V</i> /Å ³	4650(3)
<i>Z</i>	3
Wavelength/Å	0.71073
Radiation type	Mo-K α
<i>T</i> _{min} /°	2.959
<i>T</i> _{max} /°	24.781
Measured Refl.	40190
Independent Refl.	10532
Reflections Used	10125
<i>R</i> _{int}	0.0484
Parameters	757
Restraints	124
Largest peak	0.922
Deepest hole	-0.410
Flack parameter	0.020(3)
Hooft parameter	0.069(5)
^a GooF	1.050
^c <i>wR</i> ₂	0.0680
^b <i>R</i> ₁	0.0293

The X-ray structure of **C2** (Figure 2.17) shows a mononuclear Hg^(II) complex where the metal center resides in a distorted tetrahedral coordination environment. Two **L2** ligands bind the metal center through the N atoms in a bidentate fashion forming two five-membered chelate rings that are satisfactorily planar (mean deviations, 0.015(3) and 0.017(3) Å). The dihedral angle between the two chelate planes is 87.8° suggests a

distorted tetrahedral coordination geometry around the Hg^(II) center. The dihedral angles between the two chelate planes and the two planes formed by two aryl rings connected to the S atoms in each **L2** ligand are 83.9 and 78.6°. Following an established method,⁴³, a more detailed assessment was performed on this geometry of tetra-coordination. Three parameters θ , τ_{tet} and τ_4 clearly delineate the extent of distortion from ideal tetrahedral geometry. θ is the dihedral angle between the two chelate planes, while α and β is the two largest interatomic angles within the coordination sphere in this species (Table 2.3).

Table 2.4. Selected geometrical parameters to assess the distortion of the geometry of **C2** from idealized tetrahedral and square planar

Geometry	θ	$\tau_{\text{tet}} = \theta/90^\circ$	$\tau_4 = [360-(\alpha+\beta)]/141^\circ$
Tetrahedral	90	1	1
Square planar	0	0	0
Complex 1	87.8	0.98	0.62

By comparing the parameters listed in Table 2.4, it is evident that in complex **C2**, the Hg^(II) center resides in a pseudo tetrahedral environment. The deviation of the dihedral angle (θ) from 90° lowers the point group symmetry of the molecule (complex **C2**) from achiral D_{2d} to chiral D₂. Six- and five-coordination are most abundant in literature within the discrete mercury (II) complexes. A thorough Cambridge Structural Database (accessed on Feb 3, 2019) survey revealed 202 structures of Hg^(II) coordination complex with all N-donor ligands. However, only eight structures show homoleptic tetra-coordination around Hg^(II) centers. Among these eight structures, one reveals square planar geometry⁴⁴ while the rest exhibit pseudo-tetrahedral coordination around the

central metal. Conspicuously, all these 4-coordinated Hg^(II) complexes are either cationic or neutral in charge, whereas the present Hg^(II) complex is the sole example of anionic species under this category. The cationic complexes are of type [Hg(L)₂]²⁺ where L = 2,2'-bipyridine⁴⁵, 1,10-phenanthroline-2-one⁴⁶, carbohydrazone blocked with Rhodamine 6G⁴⁷, and 2,3,4,6,7,9,10,11-Octahydro-pyrazino[1,2- α ; 4,3- α']dipyrimidine⁴⁸, while the homoleptic neutral complexes are of type [Hg(L)₂]⁰ where L = N-(fluorinatedphenyl)-2-pyrazinocarboxamides⁴⁴, tetraarylazadipyromethane⁴⁹, 1,3-di(2-methoxy)benzene]triazene⁵⁰, and N-(2,3,4-trimethoxybenzyl)-2-aminomalonitrile⁵¹. The average Hg-N bond lengths in these compounds are comparable to those in the present complex (average Hg-N, 2.230(7) Å).

Complex **C2** crystallized in a chiral, P3₂ space group with a full molecule in the asymmetric unit. Upon completion of the refinement, the Flack parameter of 0.020(3) in this structure suggested that the crystal investigated was enantiopure (homochiral). A Flack parameter close to zero excluded the possibility of erroneously assigned absolute structure in the present case. Taken together, complex **C2** represents the first example of an anionic homoleptic and homochiral structure with a pseudo-tetrahedral coordination sphere.

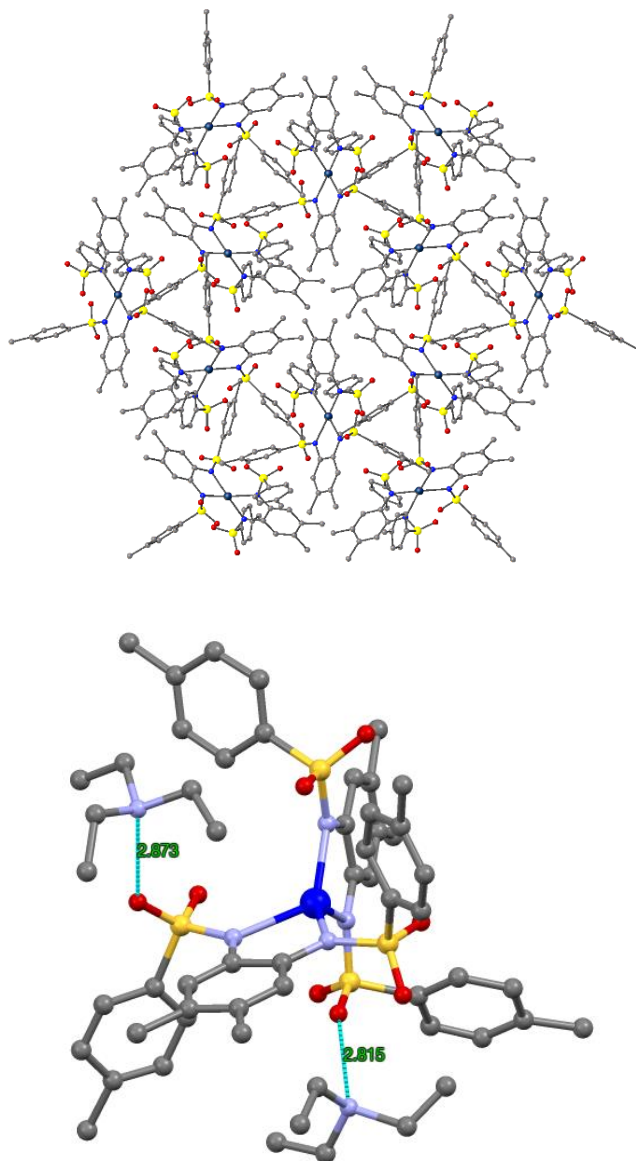


Figure 2.18. Packing pattern of complex **C2** along *c* axis (top) and *H*-bonding interactions involving the *N* atoms of Et_3NH^+ ions and *O* atoms of sulfonamide moieties (bottom).

The packing pattern of **C2** (Figure 2.18a) reveals few moderate non-classical C-H...O interactions (with C...O span the range, 2.88(2) - 3.55(2) Å), which consolidated its extended structure. Moreover, significant hydrogen bonding interactions (2.87(2) and 2.82(2) Å) involving the *N* atoms of the triethylammonium counteranions and the *O*

atoms of sulfonamide moieties are also quite evident (Figure 2.18b, right). A detailed listing of the C-H...O hydrogen bonding interactions can be found in Table 2.7. No C-H... π and π - π interactions were observed upon careful analysis of the extended structure. Though complex **C2** is achiral in a molecular sense, the plausible explanation of its crystallization in a chiral space group is most likely due to the way the molecules are aligned in the lattice. A simplified polyhedral representation of the packing patterns clearly displays the site of the 3-fold axis within the crystal (Figure 2.19).

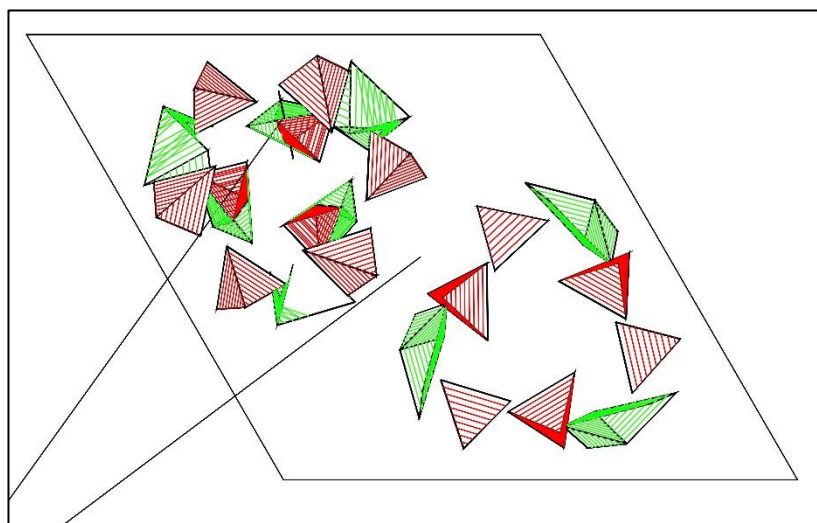


Figure 2.19. Polyhedral representation of the packing pattern revealing the site of the 3-fold axis

Table 2.5: Fractional atomic coordinates and isotropic or equivalent isotropic displacement parameters (\AA^2)

	<i>x</i>	<i>y</i>	<i>z</i>	$U_{\text{iso}}^*/U_{\text{eq}}$	Occ. (<1)
Hg1	0.55261 (2)	0.53761 (3)	0.2100 (2)	0.06458 (13)	
S7	0.56173 (17)	0.70620 (19)	0.3119 (3)	0.0566 (6)	
S8	0.71515 (18)	0.56209 (19)	0.1060 (3)	0.0613 (6)	
S111	0.37667 (16)	0.48517 (19)	0.1058 (2)	0.0555 (6)	
N12	0.6842 (5)	0.6146 (6)	0.1588 (5)	0.055 (2)	
C9BA	0.2141 (7)	0.2463 (7)	0.2514 (8)	0.077 (3)	
C1	0.2539 (8)	0.2286 (8)	0.3085 (8)	0.074 (3)	
C4	0.3440 (7)	0.2837 (7)	0.3202 (7)	0.060 (2)	
H4	0.371267	0.271011	0.358864	0.073*	
C4CA	0.3971 (6)	0.3596 (6)	0.2754 (6)	0.054 (2)	
C10	0.3564 (5)	0.3797 (5)	0.2189 (5)	0.0455 (19)	

C9	0.2642 (8)	0.3210 (7)	0.2065 (7)	0.067 (3)
H9	0.235975	0.332175	0.167633	0.080*
O666	0.6464 (6)	0.4700 (5)	0.1097 (5)	0.073 (2)
O23	0.4523 (6)	0.5652 (6)	0.0770 (5)	0.079 (2)
C6BA	0.8200 (7)	0.7651 (9)	0.1461 (7)	0.064 (3)
H6BA	0.842177	0.743558	0.109530	0.077*
C0AA	0.8699 (6)	0.8531 (7)	0.1670 (6)	0.061 (3)
C4AA	0.8380 (9)	0.8879 (8)	0.2216 (6)	0.072 (3)
C45	0.7542 (7)	0.8294 (8)	0.2515 (7)	0.064 (3)
H45	0.731580	0.852001	0.286721	0.077*
C3CA	0.7027 (6)	0.7406 (7)	0.2325 (6)	0.053 (2)
C5AA	0.7359 (6)	0.7058 (7)	0.1781 (6)	0.051 (2)
O93	0.5612 (6)	0.7857 (7)	0.2880 (5)	0.075 (2)
O94	0.4755 (6)	0.6274 (6)	0.3211 (5)	0.079 (2)
N16	0.6173 (7)	0.6788 (7)	0.2601 (5)	0.061 (2)
N17	0.4106 (4)	0.4581 (5)	0.1767 (5)	0.0523 (17)
O0AA	0.3317 (6)	0.4136 (6)	0.0531 (5)	0.079 (2)
O1AA	0.8058 (6)	0.5818 (7)	0.1180 (6)	0.080 (2)
C5BA	0.7154 (6)	0.6012 (8)	0.0158 (6)	0.059 (2)
C6AA	0.6470 (8)	0.6147 (10)	-0.0068 (6)	0.074 (3)
H6AA	0.601518	0.605657	0.025810	0.088*
C1AA	0.6453 (9)	0.6416 (10)	-0.0779 (7)	0.080 (3)
H1AA	0.599217	0.651466	-0.092817	0.097*
C2AA	0.7120 (10)	0.6540 (12)	-0.1271 (7)	0.091 (4)
CXE	0.7781 (16)	0.641 (2)	-0.1045 (11)	0.148 (11)
HXE	0.824416	0.652090	-0.136691	0.177*
C2	0.7797 (11)	0.6124 (17)	-0.0330 (9)	0.125 (7)
H2	0.825027	0.600867	-0.018910	0.150*
C4BA	0.6778 (15)	0.8351 (17)	0.5005 (9)	0.130 (7)
H4BA	0.696665	0.891499	0.520839	0.157*
C8AA	0.6432 (11)	0.8142 (10)	0.4320 (8)	0.094 (4)
H8AA	0.639897	0.858467	0.404976	0.113*
C7AA	0.6131 (7)	0.7328 (7)	0.4002 (6)	0.058 (2)
C3AA	0.6186 (11)	0.6670 (10)	0.4372 (7)	0.086 (4)
H3AA	0.599333	0.610834	0.416316	0.103*
C6CA	0.6560 (14)	0.6886 (17)	0.5108 (9)	0.118 (7)
H6CA	0.660376	0.645362	0.538468	0.142*
CXF	0.6840 (14)	0.7697 (19)	0.5389 (10)	0.112 (6)

S1	0.54918 (17)	0.41317 (18)	0.3500 (3)	0.0578 (6)
N10	0.4899 (5)	0.4180 (5)	0.2855 (5)	0.0580 (19)
O8	0.6391 (5)	0.4864 (6)	0.3369 (6)	0.082 (2)
O10	0.5133 (6)	0.4089 (6)	0.4214 (5)	0.083 (2)
C2BA	0.8897 (11)	0.9854 (9)	0.2484 (9)	0.105 (5)
H2BA	0.943124	0.995803	0.273624	0.157*
H2BB	0.852470	0.996368	0.281194	0.157*
H2BC	0.905931	1.025257	0.207024	0.157*
C0BA	0.9616 (8)	0.9154 (10)	0.1314 (9)	0.096 (5)
H0BA	0.966445	0.889200	0.086289	0.144*
H0BB	1.008681	0.923214	0.164224	0.144*
H0BC	0.966890	0.972769	0.121414	0.144*
C1BA	0.5540 (7)	0.3127 (7)	0.3393 (6)	0.061 (2)
C13	0.5470 (12)	0.2605 (9)	0.3981 (7)	0.098 (4)
H13	0.537795	0.276725	0.444601	0.117*
C5	0.5532 (14)	0.1860 (10)	0.3901 (10)	0.116 (5)
H5	0.550436	0.153524	0.431855	0.139*
C7BA	0.5629 (11)	0.1568 (11)	0.3254 (11)	0.100 (4)
C3BA	0.5694 (13)	0.2079 (13)	0.2637 (12)	0.118 (6)
H3BA	0.575534	0.189028	0.217259	0.142*
C15	0.5666 (11)	0.2885 (11)	0.2718 (9)	0.092 (4)
H15	0.573257	0.324208	0.231187	0.110*
C17	0.7069 (15)	0.6855 (17)	-0.2041 (8)	0.130 (7)
H17A	0.746714	0.749272	-0.207693	0.194*
H17B	0.646454	0.671763	-0.214042	0.194*
H17C	0.724409	0.655415	-0.239265	0.194*
C0CA	0.1994 (11)	0.1494 (10)	0.3585 (11)	0.113 (6)
H0CA	0.153100	0.156399	0.381756	0.170*
H0CB	0.237972	0.146609	0.395227	0.170*
H0CC	0.172501	0.094988	0.330148	0.170*
C9AA	0.2939 (8)	0.5426 (8)	0.2046 (6)	0.063 (2)
H9AA	0.334433	0.544094	0.239158	0.075*
C3	0.2324 (11)	0.5676 (10)	0.2241 (7)	0.080 (4)
H3	0.230534	0.583305	0.272663	0.096*
C1CA	0.2956 (7)	0.5154 (7)	0.1339 (6)	0.056 (2)
C2CA	0.1742 (10)	0.5701 (10)	0.1751 (8)	0.086 (4)
C16	0.1782 (11)	0.5448 (14)	0.1052 (9)	0.108 (5)
H16	0.137911	0.544522	0.070882	0.129*
C20	0.2399 (10)	0.5189 (10)	0.0820 (8)	0.083 (4)
H20	0.242873	0.504787	0.033206	0.099*
C5CA	0.1071 (14)	0.5975 (16)	0.1950 (11)	0.136 (7)
H5CA	0.127435	0.635340	0.237712	0.204*
H5CB	0.050253	0.544914	0.205325	0.204*
H5CC	0.100321	0.629875	0.154869	0.204*
C7CA	0.5645 (17)	0.0707 (15)	0.3112 (17)	0.178 (10)
H7CA	0.574443	0.048545	0.356567	0.266*
H7CB	0.612088	0.082464	0.277424	0.266*
H7CC	0.508006	0.026586	0.290576	0.266*
C8CA	0.1147 (10)	0.1883 (11)	0.2348 (12)	0.127 (7)
H8CA	0.095961	0.126507	0.244832	0.190*
H8CB	0.103999	0.194787	0.184037	0.190*
H8CC	0.081157	0.206899	0.265100	0.190*

N3DA	0.8276 (8)	0.5683 (10)	0.3448 (7)	0.099 (3)	
C4DA	0.8558 (10)	0.5837 (12)	0.4213 (7)	0.100 (3)	
H4DA	0.847663	0.527983	0.441782	0.120*	
H4DB	0.919457	0.627545	0.423202	0.120*	
C5DA	0.8446 (12)	0.6473 (15)	0.3051 (10)	0.123 (5)	
H5DA	0.804463	0.667005	0.324055	0.148*	
H5DB	0.828176	0.630357	0.254170	0.148*	
C6	0.8092 (13)	0.6144 (18)	0.4657 (9)	0.136 (6)	
H6A	0.745607	0.574104	0.461028	0.203*	
H6B	0.823447	0.673493	0.450139	0.203*	
H6C	0.826728	0.616385	0.515980	0.203*	
C6DA	0.8211 (17)	0.4519 (17)	0.2613 (13)	0.146 (8)	
H6DA	0.768693	0.402763	0.283130	0.218*	
H6DB	0.857339	0.430016	0.239413	0.218*	
H6DC	0.803052	0.479440	0.224173	0.218*	
C7DA	0.8704 (15)	0.5148 (18)	0.3147 (13)	0.142 (6)	
H7DA	0.928947	0.556919	0.294532	0.170*	
H7DB	0.880056	0.484076	0.355381	0.170*	
C8DA	0.9344 (16)	0.723 (2)	0.306 (2)	0.27 (2)	
H8DA	0.946555	0.755376	0.260959	0.399*	
H8DB	0.976504	0.702212	0.312769	0.399*	
H8DC	0.940170	0.761971	0.346394	0.399*	
C7	0.718 (2)	0.790 (3)	0.6188 (13)	0.232 (19)	
H7A	0.782408	0.828135	0.618826	0.348*	
H7B	0.702727	0.734522	0.643431	0.348*	
H7C	0.690980	0.819371	0.643765	0.348*	
N1	0.5138 (16)	0.8281 (16)	0.1483 (12)	0.067 (5)	0.5
C9CA	0.5577 (15)	0.9226 (16)	0.1406 (16)	0.064 (5)	0.5
H9CA	0.521652	0.944249	0.164541	0.077*	0.5
H9CB	0.560808	0.937101	0.088828	0.077*	0.5
C1DA	0.4096 (19)	0.787 (2)	0.1592 (10)	0.077 (6)	0.5
H1DA	0.386487	0.809584	0.121498	0.093*	0.5
H1DB	0.380038	0.721835	0.153841	0.093*	0.5
C8BA	0.6513 (18)	0.972 (2)	0.172 (2)	0.077 (9)	0.5
H8BA	0.682363	1.032378	0.153649	0.115*	0.5
H8BB	0.683339	0.941703	0.158131	0.115*	0.5
H8BC	0.647994	0.973137	0.224717	0.115*	0.5
C0DA	0.388 (2)	0.809 (2)	0.2338 (11)	0.096 (9)	0.5
H0DA	0.326707	0.794918	0.235011	0.145*	0.5
H0DB	0.426765	0.872350	0.243146	0.145*	0.5
H0DC	0.398155	0.775154	0.270629	0.145*	0.5
C3DA	0.6112 (16)	0.797 (2)	0.0649 (19)	0.108 (9)	0.5
H3DA	0.608854	0.752552	0.031379	0.162*	0.5
H3DB	0.640074	0.795302	0.109522	0.162*	0.5
H3DC	0.644572	0.855408	0.043030	0.162*	0.5
C2DA	0.5170 (15)	0.777 (2)	0.0816 (15)	0.103 (7)	0.5
H2DA	0.478947	0.712869	0.090173	0.124*	0.5
H2DB	0.493340	0.792798	0.039411	0.124*	0.5
N1A	0.549 (2)	0.832 (2)	0.1528 (16)	0.107 (8)	0.5
C9CB	0.587 (3)	0.926 (2)	0.141 (3)	0.119 (12)	0.5
H9CC	0.544832	0.944667	0.155746	0.142*	0.5
H9CD	0.600996	0.939488	0.089710	0.142*	0.5

C1DB	0.447 (3)	0.778 (2)	0.135 (2)	0.120 (9)	0.5
H1DC	0.436168	0.796250	0.087299	0.144*	0.5
H1DD	0.428051	0.714185	0.131659	0.144*	0.5
C2DB	0.590 (3)	0.788 (3)	0.1075 (15)	0.115 (8)	0.5
H2DC	0.560430	0.724389	0.119709	0.137*	0.5
H2DD	0.652897	0.814653	0.119346	0.137*	0.5
C8BB	0.673 (4)	0.976 (3)	0.187 (3)	0.14 (2)	0.5
H8BD	0.723424	0.983484	0.158314	0.204*	0.5
H8BE	0.667866	0.942845	0.230464	0.204*	0.5
H8BF	0.682147	1.034395	0.199816	0.204*	0.5
C0DB	0.391 (2)	0.791 (3)	0.193 (2)	0.118 (11)	0.5
H0DD	0.333053	0.775282	0.172338	0.177*	0.5
H0DE	0.420953	0.852665	0.207892	0.177*	0.5
H0DF	0.382555	0.753139	0.234156	0.177*	0.5
C3DB	0.579 (4)	0.798 (3)	0.0259 (16)	0.17 (2)	0.5
H3DD	0.560819	0.841929	0.018471	0.251*	0.5
H3DE	0.534662	0.741424	0.005908	0.251*	0.5
H3DF	0.635693	0.817608	0.001721	0.251*	0.5

Table 2.6: Atomic displacement parameters (\AA^2)

	U^{11}	U^{22}	U^{33}	U^{12}	U^{13}	U^{23}
Hg1	0.04451 (19)	0.0523 (2)	0.07335 (17)	0.0065 (2)	0.0055 (2)	0.0075 (2)
S7	0.0455 (12)	0.0647 (15)	0.0487 (13)	0.0193 (11)	0.0037 (10)	0.0050 (11)
S8	0.0596 (16)	0.0653 (15)	0.0590 (14)	0.0312 (13)	0.0029 (11)	0.0023 (11)
S111	0.0529 (12)	0.0597 (17)	0.0555 (12)	0.0294 (12)	0.0012 (9)	0.0019 (11)
N12	0.036 (4)	0.052 (5)	0.050 (4)	0.003 (4)	0.010 (3)	0.005 (4)
C9BA	0.037 (6)	0.036 (5)	0.128 (9)	-0.004 (4)	-0.003 (6)	0.004 (6)
C1	0.061 (7)	0.048 (6)	0.107 (8)	0.023 (5)	0.007 (6)	0.013 (6)
C4	0.044 (5)	0.048 (5)	0.084 (7)	0.019 (4)	0.008 (4)	0.016 (5)
C4CA	0.042 (5)	0.042 (5)	0.076 (6)	0.019 (4)	0.003 (4)	0.001 (4)
C10	0.031 (4)	0.030 (4)	0.071 (5)	0.012 (4)	0.005 (4)	-0.004 (4)
C9	0.059 (6)	0.049 (6)	0.089 (7)	0.025 (5)	-0.013 (5)	-0.005 (5)
O666	0.080 (6)	0.062 (5)	0.070 (5)	0.031 (4)	0.007 (4)	0.002 (4)
O23	0.072 (5)	0.104 (6)	0.071 (5)	0.050 (5)	0.015 (4)	0.032 (4)
C6BA	0.037 (5)	0.085 (8)	0.065 (6)	0.025 (6)	0.007 (5)	0.013 (5)
C0AA	0.036 (5)	0.057 (6)	0.068 (6)	0.007 (5)	-0.004 (4)	0.008 (5)
C4AA	0.085 (8)	0.056 (7)	0.056 (6)	0.020 (6)	-0.008 (5)	-0.003 (5)
C45	0.050 (5)	0.055 (6)	0.069 (6)	0.012 (5)	0.001 (4)	-0.007 (5)
C3CA	0.038 (5)	0.050 (6)	0.050 (5)	0.007 (4)	0.005 (4)	0.009 (4)
C5AA	0.038 (5)	0.056 (6)	0.044 (5)	0.013 (4)	0.000 (3)	0.011 (4)
O93	0.084 (6)	0.093 (6)	0.065 (4)	0.057 (5)	-0.005 (4)	0.013 (4)
O94	0.054 (5)	0.094 (6)	0.068 (4)	0.023 (4)	0.015 (4)	0.005 (4)
N16	0.048 (5)	0.060 (5)	0.050 (5)	0.008 (5)	0.009 (4)	-0.001 (4)
N17	0.034 (3)	0.043 (4)	0.068 (4)	0.010 (3)	-0.005 (3)	0.007 (3)
O0AA	0.089 (5)	0.084 (5)	0.075 (4)	0.051 (5)	-0.027 (4)	-0.024 (4)
O1AA	0.066 (5)	0.106 (7)	0.080 (5)	0.052 (5)	0.003 (4)	0.002 (5)
C5BA	0.042 (5)	0.076 (7)	0.056 (6)	0.027 (5)	0.005 (4)	-0.006 (5)
C6AA	0.073 (7)	0.112 (9)	0.056 (6)	0.062 (7)	0.013 (5)	0.008 (6)
C1AA	0.082 (8)	0.110 (10)	0.072 (7)	0.065 (8)	0.000 (6)	0.006 (6)
C2AA	0.085 (9)	0.118 (12)	0.059 (6)	0.043 (8)	0.009 (6)	0.007 (7)
CXE	0.122 (15)	0.28 (3)	0.081 (11)	0.129 (19)	0.036 (11)	0.041 (15)

C2	0.087 (10)	0.23 (2)	0.087 (10)	0.106 (13)	0.012 (7)	0.011 (12)
C4BA	0.17 (2)	0.167 (17)	0.075 (10)	0.095 (16)	-0.037 (10)	-0.047 (11)
C8AA	0.108 (12)	0.093 (10)	0.074 (8)	0.044 (9)	-0.012 (7)	-0.014 (7)
C7AA	0.050 (5)	0.073 (6)	0.051 (5)	0.031 (5)	0.003 (4)	0.001 (4)
C3AA	0.089 (9)	0.105 (10)	0.075 (8)	0.057 (9)	0.005 (7)	0.018 (7)
C6CA	0.140 (15)	0.19 (2)	0.074 (9)	0.121 (16)	0.008 (9)	0.039 (11)
CXF	0.102 (14)	0.143 (19)	0.073 (9)	0.047 (13)	-0.017 (8)	-0.019 (11)
S1	0.0494 (13)	0.0591 (14)	0.0656 (14)	0.0276 (11)	-0.0063 (11)	-0.0010 (11)
N10	0.040 (4)	0.052 (4)	0.066 (4)	0.011 (3)	0.011 (4)	0.022 (3)
O8	0.056 (4)	0.076 (5)	0.115 (6)	0.033 (4)	-0.018 (4)	0.004 (4)
O10	0.097 (6)	0.100 (6)	0.066 (4)	0.062 (5)	-0.003 (4)	-0.013 (4)
C2BA	0.084 (9)	0.061 (8)	0.118 (11)	-0.002 (7)	0.001 (8)	-0.033 (7)
C0BA	0.057 (7)	0.080 (9)	0.107 (9)	0.001 (6)	0.008 (6)	0.007 (7)
C1BA	0.051 (5)	0.060 (6)	0.072 (6)	0.027 (5)	-0.001 (5)	-0.009 (5)
C13	0.148 (13)	0.082 (8)	0.073 (7)	0.065 (9)	-0.005 (8)	0.015 (6)
C5	0.161 (17)	0.082 (9)	0.128 (13)	0.078 (11)	-0.014 (11)	0.012 (8)
C7BA	0.090 (9)	0.079 (9)	0.131 (13)	0.043 (8)	-0.017 (9)	-0.020 (9)
C3BA	0.119 (14)	0.116 (13)	0.120 (14)	0.059 (12)	0.031 (11)	-0.028 (11)
C15	0.100 (11)	0.089 (10)	0.090 (9)	0.049 (9)	0.013 (8)	-0.001 (8)
C17	0.133 (15)	0.19 (2)	0.065 (8)	0.079 (14)	0.011 (9)	0.028 (10)
C0CA	0.083 (10)	0.064 (8)	0.169 (15)	0.020 (7)	0.032 (10)	0.051 (9)
C9AA	0.069 (6)	0.061 (6)	0.062 (6)	0.036 (6)	0.000 (5)	-0.002 (4)
C3	0.112 (11)	0.082 (8)	0.077 (7)	0.072 (9)	0.001 (7)	-0.002 (6)
C1CA	0.044 (5)	0.040 (5)	0.078 (7)	0.015 (4)	-0.006 (5)	0.004 (4)
C2CA	0.092 (9)	0.093 (9)	0.089 (9)	0.058 (8)	0.020 (7)	0.019 (7)
C16	0.097 (10)	0.148 (15)	0.115 (12)	0.090 (11)	-0.017 (8)	0.013 (11)
C20	0.086 (9)	0.108 (10)	0.080 (7)	0.068 (8)	-0.008 (6)	-0.004 (7)
C5CA	0.138 (16)	0.175 (19)	0.158 (15)	0.125 (15)	0.046 (13)	0.037 (14)
C7CA	0.16 (2)	0.100 (14)	0.30 (3)	0.087 (15)	-0.01 (2)	-0.018 (17)
C8CA	0.062 (9)	0.068 (9)	0.21 (2)	0.000 (7)	-0.010 (10)	0.035 (11)
N3DA	0.061 (6)	0.135 (8)	0.094 (5)	0.043 (6)	0.002 (5)	0.013 (5)
C4DA	0.073 (8)	0.127 (11)	0.094 (5)	0.046 (8)	0.000 (5)	0.023 (6)
C5DA	0.088 (8)	0.165 (11)	0.113 (10)	0.060 (7)	-0.017 (8)	0.033 (8)
C6	0.110 (12)	0.205 (19)	0.106 (8)	0.089 (13)	-0.011 (9)	-0.011 (11)
C6DA	0.154 (18)	0.166 (16)	0.158 (14)	0.111 (15)	-0.024 (13)	-0.013 (11)
C7DA	0.115 (13)	0.167 (14)	0.150 (11)	0.076 (12)	0.012 (10)	-0.010 (9)
C8DA	0.118 (11)	0.23 (2)	0.35 (4)	0.011 (13)	-0.050 (19)	0.18 (3)
C7	0.24 (4)	0.36 (6)	0.091 (14)	0.15 (4)	-0.072 (18)	-0.05 (2)
N1	0.082 (10)	0.064 (8)	0.046 (9)	0.030 (8)	-0.009 (7)	0.001 (7)
C9CA	0.075 (11)	0.066 (8)	0.048 (11)	0.033 (7)	-0.014 (9)	0.007 (7)
C1DA	0.082 (10)	0.079 (13)	0.057 (13)	0.030 (8)	-0.005 (8)	0.013 (11)
C8BA	0.081 (12)	0.068 (12)	0.08 (2)	0.038 (9)	-0.028 (12)	-0.004 (13)
C0DA	0.089 (17)	0.14 (3)	0.065 (13)	0.057 (18)	-0.002 (11)	0.006 (13)
C3DA	0.155 (19)	0.11 (2)	0.068 (17)	0.074 (17)	0.022 (15)	0.002 (18)
C2DA	0.143 (18)	0.093 (13)	0.071 (11)	0.057 (13)	0.009 (11)	-0.013 (11)
N1A	0.145 (18)	0.080 (11)	0.082 (13)	0.045 (13)	-0.027 (13)	0.016 (10)
C9CB	0.15 (2)	0.078 (12)	0.11 (3)	0.041 (13)	-0.02 (2)	0.018 (12)
C1DB	0.148 (18)	0.075 (14)	0.12 (2)	0.045 (13)	-0.040 (15)	0.014 (17)
C2DB	0.16 (2)	0.097 (17)	0.076 (14)	0.057 (18)	-0.037 (14)	0.001 (13)
C8BB	0.15 (3)	0.10 (2)	0.12 (3)	0.04 (2)	-0.03 (3)	-0.01 (2)
C0DB	0.13 (2)	0.10 (2)	0.11 (3)	0.042 (17)	-0.058 (16)	0.00 (2)
C3DB	0.32 (6)	0.11 (2)	0.074 (13)	0.10 (3)	-0.067 (19)	-0.024 (16)

Table 2.7: Geometric parameters (Å, °)

Hg1—N12	2.176 (7)	C0CA—H0CC	0.9600
Hg1—N16	2.292 (10)	C9AA—H9AA	0.9300
Hg1—N17	2.202 (7)	C9AA—C3	1.369 (18)
Hg1—N10	2.248 (7)	C9AA—C1CA	1.374 (16)
S7—O93	1.438 (9)	C3—H3	0.9300
S7—O94	1.431 (9)	C3—C2CA	1.36 (2)
S7—N16	1.572 (12)	C1CA—C20	1.367 (16)
S7—C7AA	1.780 (10)	C2CA—C16	1.36 (2)
S8—N12	1.581 (11)	C2CA—C5CA	1.49 (2)
S8—O666	1.426 (9)	C16—H16	0.9300
S8—O1AA	1.434 (9)	C16—C20	1.40 (2)
S8—C5BA	1.774 (11)	C20—H20	0.9300
S111—O23	1.438 (9)	C5CA—H5CA	0.9600
S111—N17	1.579 (8)	C5CA—H5CB	0.9600
S111—O0AA	1.442 (8)	C5CA—H5CC	0.9600
S111—C1CA	1.786 (11)	C7CA—H7CA	0.9600
N12—C5AA	1.405 (14)	C7CA—H7CB	0.9600
C9BA—C1	1.360 (18)	C7CA—H7CC	0.9600
C9BA—C9	1.396 (17)	C8CA—H8CA	0.9600
C9BA—C8CA	1.516 (18)	C8CA—H8CB	0.9600
C1—C4	1.368 (17)	C8CA—H8CC	0.9600
C1—C0CA	1.509 (17)	N3DA—C4DA	1.455 (17)
C4—H4	0.9300	N3DA—C5DA	1.43 (2)
C4—C4CA	1.416 (14)	N3DA—C7DA	1.54 (2)
C4CA—C10	1.381 (14)	C4DA—H4DA	0.9700
C4CA—N10	1.408 (12)	C4DA—H4DB	0.9700
C10—C9	1.406 (14)	C4DA—C6	1.41 (2)
C10—N17	1.420 (12)	C5DA—H5DA	0.9700
C9—H9	0.9300	C5DA—H5DB	0.9700
C6BA—H6BA	0.9300	C5DA—C8DA	1.44 (3)
C6BA—C0AA	1.366 (18)	C6—H6A	0.9600
C6BA—C5AA	1.411 (14)	C6—H6B	0.9600
C0AA—C4AA	1.406 (17)	C6—H6C	0.9600
C0AA—C0BA	1.536 (15)	C6DA—H6DA	0.9600
C4AA—C45	1.388 (16)	C6DA—H6DB	0.9600
C4AA—C2BA	1.531 (17)	C6DA—H6DC	0.9600
C45—H45	0.9300	C6DA—C7DA	1.38 (3)
C45—C3CA	1.371 (16)	C7DA—H7DA	0.9700
C3CA—C5AA	1.415 (11)	C7DA—H7DB	0.9700
C3CA—N16	1.405 (13)	C8DA—H8DA	0.9600
C5BA—C6AA	1.369 (16)	C8DA—H8DB	0.9600
C5BA—C2	1.354 (17)	C8DA—H8DC	0.9600
C6AA—H6AA	0.9300	C7—H7A	0.9600
C6AA—C1AA	1.379 (17)	C7—H7B	0.9600
C1AA—H1AA	0.9300	C7—H7C	0.9600
C1AA—C2AA	1.384 (18)	N1—C9CA	1.41 (2)
C2AA—CXE	1.32 (2)	N1—C1DA	1.57 (3)
C2AA—C17	1.52 (2)	N1—C2DA	1.52 (3)
CXE—HXE	0.9300	C9CA—H9CA	0.9700
CXE—C2	1.40 (3)	C9CA—H9CB	0.9700
C2—H2	0.9300	C9CA—C8BA	1.507 (18)

C4BA—H4BA	0.9300	C1DA—H1DA	0.9700
C4BA—C8AA	1.35 (2)	C1DA—H1DB	0.9700
C4BA—CXF	1.37 (3)	C1DA—C0DA	1.507 (18)
C8AA—H8AA	0.9300	C8BA—H8BA	0.9600
C8AA—C7AA	1.355 (17)	C8BA—H8BB	0.9600
C7AA—C3AA	1.359 (17)	C8BA—H8BC	0.9600
C3AA—H3AA	0.9300	C0DA—H0DA	0.9600
C3AA—C6CA	1.45 (2)	C0DA—H0DB	0.9600
C6CA—H6CA	0.9300	C0DA—H0DC	0.9600
C6CA—CXF	1.33 (3)	C3DA—H3DA	0.9600
CXF—C7	1.54 (3)	C3DA—H3DB	0.9600
S1—N10	1.584 (9)	C3DA—H3DC	0.9600
S1—O8	1.442 (9)	C3DA—C2DA	1.507 (18)
S1—O10	1.424 (8)	C2DA—H2DA	0.9700
S1—C1BA	1.778 (11)	C2DA—H2DB	0.9700
C2BA—H2BA	0.9600	N1A—C9CB	1.42 (3)
C2BA—H2BB	0.9600	N1A—C1DB	1.55 (4)
C2BA—H2BC	0.9600	N1A—C2DB	1.51 (3)
C0BA—H0BA	0.9600	C9CB—H9CC	0.9700
C0BA—H0BB	0.9600	C9CB—H9CD	0.9700
C0BA—H0BC	0.9600	C9CB—C8BB	1.53 (3)
C1BA—C13	1.363 (17)	C1DB—H1DC	0.9700
C1BA—C15	1.349 (18)	C1DB—H1DD	0.9700
C13—H13	0.9300	C1DB—C0DB	1.52 (3)
C13—C5	1.34 (2)	C2DB—H2DC	0.9700
C5—H5	0.9300	C2DB—H2DD	0.9700
C5—C7BA	1.32 (2)	C2DB—C3DB	1.52 (3)
C7BA—C3BA	1.40 (3)	C8BB—H8BD	0.9600
C7BA—C7CA	1.51 (3)	C8BB—H8BE	0.9600
C3BA—H3BA	0.9300	C8BB—H8BF	0.9600
C3BA—C15	1.42 (2)	C0DB—H0DD	0.9600
C15—H15	0.9300	C0DB—H0DE	0.9600
C17—H17A	0.9600	C0DB—H0DF	0.9600
C17—H17B	0.9600	C3DB—H3DD	0.9600
C17—H17C	0.9600	C3DB—H3DE	0.9600
C0CA—H0CA	0.9600	C3DB—H3DF	0.9600
C0CA—H0CB	0.9600		
N12—Hg1—N16	73.8 (3)	C1CA—C9AA—H9AA	120.0
N12—Hg1—N17	138.6 (3)	C9AA—C3—H3	118.8
N12—Hg1—N10	134.0 (4)	C2CA—C3—C9AA	122.3 (13)
N17—Hg1—N16	124.5 (4)	C2CA—C3—H3	118.8
N17—Hg1—N10	74.1 (3)	C9AA—C1CA—S111	121.3 (8)
N10—Hg1—N16	118.7 (3)	C20—C1CA—S111	118.6 (9)
O93—S7—N16	113.4 (6)	C20—C1CA—C9AA	119.8 (11)
O93—S7—C7AA	105.5 (5)	C3—C2CA—C16	116.7 (13)
O94—S7—O93	116.0 (6)	C3—C2CA—C5CA	123.2 (15)
O94—S7—N16	106.5 (5)	C16—C2CA—C5CA	120.0 (15)
O94—S7—C7AA	106.4 (5)	C2CA—C16—H16	118.3
N16—S7—C7AA	108.7 (5)	C2CA—C16—C20	123.4 (13)
N12—S8—C5BA	106.5 (5)	C20—C16—H16	118.3
O666—S8—N12	106.1 (5)	C1CA—C20—C16	117.6 (13)

O666—S8—O1AA	117.0 (6)	C1CA—C20—H20	121.2
O666—S8—C5BA	107.8 (5)	C16—C20—H20	121.2
O1AA—S8—N12	114.1 (5)	C2CA—C5CA—H5CA	109.5
O1AA—S8—C5BA	104.8 (5)	C2CA—C5CA—H5CB	109.5
O23—S111—N17	106.9 (4)	C2CA—C5CA—H5CC	109.5
O23—S111—O0AA	114.5 (5)	H5CA—C5CA—H5CB	109.5
O23—S111—C1CA	106.8 (5)	H5CA—C5CA—H5CC	109.5
N17—S111—C1CA	107.9 (5)	H5CB—C5CA—H5CC	109.5
O0AA—S111—N17	114.4 (5)	C7BA—C7CA—H7CA	109.5
O0AA—S111—C1CA	105.9 (5)	C7BA—C7CA—H7CB	109.5
S8—N12—Hg1	117.2 (5)	C7BA—C7CA—H7CC	109.5
C5AA—N12—Hg1	117.1 (7)	H7CA—C7CA—H7CB	109.5
C5AA—N12—S8	125.6 (6)	H7CA—C7CA—H7CC	109.5
C1—C9BA—C9	120.4 (10)	H7CB—C7CA—H7CC	109.5
C1—C9BA—C8CA	122.1 (12)	C9BA—C8CA—H8CA	109.5
C9—C9BA—C8CA	117.4 (12)	C9BA—C8CA—H8CB	109.5
C9BA—C1—C4	119.0 (11)	C9BA—C8CA—H8CC	109.5
C9BA—C1—C0CA	120.5 (12)	H8CA—C8CA—H8CB	109.5
C4—C1—C0CA	120.4 (12)	H8CA—C8CA—H8CC	109.5
C1—C4—H4	118.9	H8CB—C8CA—H8CC	109.5
C1—C4—C4CA	122.1 (10)	C4DA—N3DA—C7DA	103.6 (13)
C4CA—C4—H4	118.9	C5DA—N3DA—C4DA	114.8 (15)
C10—C4CA—C4	119.0 (9)	C5DA—N3DA—C7DA	117.1 (15)
C10—C4CA—N10	116.9 (8)	N3DA—C4DA—H4DA	108.6
N10—C4CA—C4	124.0 (9)	N3DA—C4DA—H4DB	108.6
C4CA—C10—C9	118.0 (9)	H4DA—C4DA—H4DB	107.6
C4CA—C10—N17	117.8 (8)	C6—C4DA—N3DA	114.7 (13)
C9—C10—N17	124.2 (9)	C6—C4DA—H4DA	108.6
C9BA—C9—C10	121.3 (10)	C6—C4DA—H4DB	108.6
C9BA—C9—H9	119.4	N3DA—C5DA—H5DA	107.9
C10—C9—H9	119.4	N3DA—C5DA—H5DB	107.9
C0AA—C6BA—H6BA	118.9	N3DA—C5DA—C8DA	117.7 (16)
C0AA—C6BA—C5AA	122.1 (11)	H5DA—C5DA—H5DB	107.2
C5AA—C6BA—H6BA	118.9	C8DA—C5DA—H5DA	107.9
C6BA—C0AA—C4AA	120.4 (9)	C8DA—C5DA—H5DB	107.9
C6BA—C0AA—C0BA	120.7 (11)	C4DA—C6—H6A	109.5
C4AA—C0AA—C0BA	119.0 (10)	C4DA—C6—H6B	109.5
C0AA—C4AA—C2BA	123.6 (11)	C4DA—C6—H6C	109.5
C45—C4AA—C0AA	116.9 (10)	H6A—C6—H6B	109.5
C45—C4AA—C2BA	119.4 (12)	H6A—C6—H6C	109.5
C4AA—C45—H45	117.8	H6B—C6—H6C	109.5
C3CA—C45—C4AA	124.4 (11)	H6DA—C6DA—H6DB	109.5
C3CA—C45—H45	117.8	H6DA—C6DA—H6DC	109.5
C45—C3CA—C5AA	118.2 (9)	H6DB—C6DA—H6DC	109.5
C45—C3CA—N16	126.9 (10)	C7DA—C6DA—H6DA	109.5
N16—C3CA—C5AA	114.9 (9)	C7DA—C6DA—H6DB	109.5
N12—C5AA—C6BA	123.3 (10)	C7DA—C6DA—H6DC	109.5
N12—C5AA—C3CA	118.8 (8)	N3DA—C7DA—H7DA	108.4
C6BA—C5AA—C3CA	117.9 (10)	N3DA—C7DA—H7DB	108.4
S7—N16—Hg1	120.7 (5)	C6DA—C7DA—N3DA	115.3 (19)
C3CA—N16—Hg1	115.3 (8)	C6DA—C7DA—H7DA	108.4
C3CA—N16—S7	123.3 (8)	C6DA—C7DA—H7DB	108.4

S111—N17—Hg1	120.0 (4)	H7DA—C7DA—H7DB	107.5
C10—N17—Hg1	115.9 (6)	C5DA—C8DA—H8DA	109.5
C10—N17—S111	123.9 (6)	C5DA—C8DA—H8DB	109.5
C6AA—C5BA—S8	120.2 (7)	C5DA—C8DA—H8DC	109.5
C2—C5BA—S8	120.6 (10)	H8DA—C8DA—H8DB	109.5
C2—C5BA—C6AA	119.1 (11)	H8DA—C8DA—H8DC	109.5
C5BA—C6AA—H6AA	119.9	H8DB—C8DA—H8DC	109.5
C5BA—C6AA—C1AA	120.1 (10)	CXF—C7—H7A	109.5
C1AA—C6AA—H6AA	119.9	CXF—C7—H7B	109.5
C6AA—C1AA—H1AA	119.8	CXF—C7—H7C	109.5
C6AA—C1AA—C2AA	120.3 (12)	H7A—C7—H7B	109.5
C2AA—C1AA—H1AA	119.8	H7A—C7—H7C	109.5
C1AA—C2AA—C17	117.4 (15)	H7B—C7—H7C	109.5
CXE—C2AA—C1AA	119.0 (13)	C9CA—N1—C1DA	111 (2)
CXE—C2AA—C17	123.5 (15)	C9CA—N1—C2DA	116 (2)
C2AA—CXE—HXE	119.4	C2DA—N1—C1DA	101.6 (19)
C2AA—CXE—C2	121.3 (15)	N1—C9CA—H9CA	108.6
C2—CXE—HXE	119.4	N1—C9CA—H9CB	108.6
C5BA—C2—CXE	120.1 (15)	N1—C9CA—C8BA	114.4 (19)
C5BA—C2—H2	120.0	H9CA—C9CA—H9CB	107.6
CXE—C2—H2	120.0	C8BA—C9CA—H9CA	108.6
C8AA—C4BA—H4BA	121.4	C8BA—C9CA—H9CB	108.6
C8AA—C4BA—CXF	117.1 (19)	N1—C1DA—H1DA	109.4
CXF—C4BA—H4BA	121.4	N1—C1DA—H1DB	109.4
C4BA—C8AA—H8AA	118.0	H1DA—C1DA—H1DB	108.0
C4BA—C8AA—C7AA	124.0 (17)	C0DA—C1DA—N1	111 (2)
C7AA—C8AA—H8AA	118.0	C0DA—C1DA—H1DA	109.4
C8AA—C7AA—S7	122.4 (10)	C0DA—C1DA—H1DB	109.4
C8AA—C7AA—C3AA	119.8 (11)	C9CA—C8BA—H8BA	109.5
C3AA—C7AA—S7	117.8 (9)	C9CA—C8BA—H8BB	109.5
C7AA—C3AA—H3AA	121.6	C9CA—C8BA—H8BC	109.5
C7AA—C3AA—C6CA	116.9 (15)	H8BA—C8BA—H8BB	109.5
C6CA—C3AA—H3AA	121.6	H8BA—C8BA—H8BC	109.5
C3AA—C6CA—H6CA	119.9	H8BB—C8BA—H8BC	109.5
CXF—C6CA—C3AA	120.3 (16)	C1DA—C0DA—H0DA	109.5
CXF—C6CA—H6CA	119.9	C1DA—C0DA—H0DB	109.5
C4BA—CXF—C7	118 (2)	C1DA—C0DA—H0DC	109.5
C6CA—CXF—C4BA	121.9 (17)	H0DA—C0DA—H0DB	109.5
C6CA—CXF—C7	120 (3)	H0DA—C0DA—H0DC	109.5
N10—S1—C1BA	108.2 (5)	H0DB—C0DA—H0DC	109.5
O8—S1—N10	105.5 (4)	H3DA—C3DA—H3DB	109.5
O8—S1—C1BA	106.2 (5)	H3DA—C3DA—H3DC	109.5
O10—S1—N10	114.0 (5)	H3DB—C3DA—H3DC	109.5
O10—S1—O8	116.3 (6)	C2DA—C3DA—H3DA	109.5
O10—S1—C1BA	106.2 (5)	C2DA—C3DA—H3DB	109.5
C4CA—N10—Hg1	115.2 (6)	C2DA—C3DA—H3DC	109.5
C4CA—N10—S1	126.0 (6)	N1—C2DA—H2DA	109.2
S1—N10—Hg1	118.3 (4)	N1—C2DA—H2DB	109.2
C4AA—C2BA—H2BA	109.5	C3DA—C2DA—N1	112 (2)
C4AA—C2BA—H2BB	109.5	C3DA—C2DA—H2DA	109.2
C4AA—C2BA—H2BC	109.5	C3DA—C2DA—H2DB	109.2
H2BA—C2BA—H2BB	109.5	H2DA—C2DA—H2DB	107.9

H2BA—C2BA—H2BC	109.5	C9CB—N1A—C1DB	114 (3)
H2BB—C2BA—H2BC	109.5	C9CB—N1A—C2DB	115 (3)
C0AA—C0BA—H0BA	109.5	C2DB—N1A—C1DB	104 (2)
C0AA—C0BA—H0BB	109.5	N1A—C9CB—H9CC	109.7
C0AA—C0BA—H0BC	109.5	N1A—C9CB—H9CD	109.7
H0BA—C0BA—H0BB	109.5	N1A—C9CB—C8BB	110 (3)
H0BA—C0BA—H0BC	109.5	H9CC—C9CB—H9CD	108.2
H0BB—C0BA—H0BC	109.5	C8BB—C9CB—H9CC	109.7
C13—C1BA—S1	121.4 (9)	C8BB—C9CB—H9CD	109.7
C15—C1BA—S1	119.4 (10)	N1A—C1DB—H1DC	109.3
C15—C1BA—C13	119.2 (13)	N1A—C1DB—H1DD	109.3
C1BA—C13—H13	119.4	H1DC—C1DB—H1DD	107.9
C5—C13—C1BA	121.3 (15)	C0DB—C1DB—N1A	112 (3)
C5—C13—H13	119.4	C0DB—C1DB—H1DC	109.3
C13—C5—H5	118.6	C0DB—C1DB—H1DD	109.3
C7BA—C5—C13	122.8 (15)	N1A—C2DB—H2DC	109.3
C7BA—C5—H5	118.6	N1A—C2DB—H2DD	109.3
C5—C7BA—C3BA	117.7 (15)	N1A—C2DB—C3DB	111 (3)
C5—C7BA—C7CA	126 (2)	H2DC—C2DB—H2DD	108.0
C3BA—C7BA—C7CA	116 (2)	C3DB—C2DB—H2DC	109.3
C7BA—C3BA—H3BA	120.0	C3DB—C2DB—H2DD	109.3
C7BA—C3BA—C15	119.9 (16)	C9CB—C8BB—H8BD	109.5
C15—C3BA—H3BA	120.0	C9CB—C8BB—H8BE	109.5
C1BA—C15—C3BA	119.0 (16)	C9CB—C8BB—H8BF	109.5
C1BA—C15—H15	120.5	H8BD—C8BB—H8BE	109.5
C3BA—C15—H15	120.5	H8BD—C8BB—H8BF	109.5
C2AA—C17—H17A	109.5	H8BE—C8BB—H8BF	109.5
C2AA—C17—H17B	109.5	C1DB—C0DB—H0DD	109.5
C2AA—C17—H17C	109.5	C1DB—C0DB—H0DE	109.5
H17A—C17—H17B	109.5	C1DB—C0DB—H0DF	109.5
H17A—C17—H17C	109.5	H0DD—C0DB—H0DE	109.5
H17B—C17—H17C	109.5	H0DD—C0DB—H0DF	109.5
C1—C0CA—H0CA	109.5	H0DE—C0DB—H0DF	109.5
C1—C0CA—H0CB	109.5	C2DB—C3DB—H3DD	109.5
C1—C0CA—H0CC	109.5	C2DB—C3DB—H3DE	109.5
H0CA—C0CA—H0CB	109.5	C2DB—C3DB—H3DF	109.5
H0CA—C0CA—H0CC	109.5	H3DD—C3DB—H3DE	109.5
H0CB—C0CA—H0CC	109.5	H3DD—C3DB—H3DF	109.5
C3—C9AA—H9AA	120.0	H3DE—C3DB—H3DF	109.5
C3—C9AA—C1CA	120.1 (11)		
Hg1—N12—C5AA—C6BA	-176.1 (8)	C6AA—C1AA—C2AA—CXE	-1 (3)
Hg1—N12—C5AA—C3CA	3.9 (10)	C6AA—C1AA—C2AA—C17	-178.8 (17)
S7—C7AA—C3AA—C6CA	-176.5 (11)	C1AA—C2AA—CXE—C2	3 (4)
S8—N12—C5AA—C6BA	7.1 (15)	C2AA—CXE—C2—C5BA	-3 (5)
S8—N12—C5AA—C3CA	-172.9 (7)	C2—C5BA—C6AA—C1AA	-2 (2)
S8—C5BA—C6AA—C1AA	-177.4 (11)	C4BA—C8AA—C7AA—S7	176.0 (15)
S8—C5BA—C2—CXE	179 (2)	C4BA—C8AA—C7AA—C3AA	-1 (2)
S111—C1CA—C20—C16	-178.6 (13)	C8AA—C4BA—CXF—C6CA	-1 (4)
N12—S8—C5BA—C6AA	-41.7 (12)	C8AA—C4BA—CXF—C7	-177 (2)
N12—S8—C5BA—C2	142.6 (15)	C8AA—C7AA—C3AA—C6CA	1.1 (19)
C9BA—C1—C4—C4CA	1.0 (18)	C7AA—S7—N16—Hg1	118.1 (6)

C1—C9BA—C9—C10	0.0 (19)	C7AA—S7—N16—C3CA	-72.1 (10)
C1—C4—C4CA—C10	1.3 (16)	C7AA—C3AA—C6CA—CXF	-1 (3)
C1—C4—C4CA—N10	-179.9 (11)	C3AA—C6CA—CXF—C4BA	1 (3)
C4—C4CA—C10—C9	-2.8 (13)	C3AA—C6CA—CXF—C7	176 (2)
C4—C4CA—C10—N17	177.7 (8)	CXF—C4BA—C8AA—C7AA	1 (3)
C4—C4CA—N10—Hg1	-175.9 (8)	S1—C1BA—C13—C5	-178.1 (15)
C4—C4CA—N10—S1	-3.9 (14)	S1—C1BA—C15—C3BA	-179.4 (14)
C4CA—C10—C9—C9BA	2.3 (15)	N10—C4CA—C10—C9	178.3 (9)
C4CA—C10—N17—Hg1	-1.1 (10)	N10—C4CA—C10—N17	-1.2 (12)
C4CA—C10—N17—S111	173.9 (7)	N10—S1—C1BA—C13	-138.5 (11)
C10—C4CA—N10—Hg1	2.9 (11)	N10—S1—C1BA—C15	42.8 (12)
C10—C4CA—N10—S1	174.9 (7)	O8—S1—N10—Hg1	-8.2 (7)
C9—C9BA—C1—C4	-1.6 (19)	O8—S1—N10—C4CA	180.0 (9)
C9—C9BA—C1—C0CA	178.2 (14)	O8—S1—C1BA—C13	108.7 (12)
C9—C10—N17—Hg1	179.4 (7)	O8—S1—C1BA—C15	-70.0 (12)
C9—C10—N17—S111	-5.6 (13)	O10—S1—N10—Hg1	120.6 (6)
O666—S8—N12—Hg1	-3.9 (7)	O10—S1—N10—C4CA	-51.2 (10)
O666—S8—N12—C5AA	172.9 (9)	O10—S1—C1BA—C13	-15.7 (13)
O666—S8—C5BA—C6AA	71.8 (12)	O10—S1—C1BA—C15	165.6 (11)
O666—S8—C5BA—C2	-103.9 (15)	C2BA—C4AA—C45—C3CA	-179.0 (13)
O23—S111—N17—Hg1	-2.0 (7)	C0BA—C0AA—C4AA—C45	179.1 (11)
O23—S111—N17—C10	-176.8 (7)	C0BA—C0AA—C4AA—C2BA	0 (2)
O23—S111—C1CA—C9AA	-92.0 (10)	C1BA—S1—N10—Hg1	-121.5 (6)
O23—S111—C1CA—C20	82.0 (11)	C1BA—S1—N10—C4CA	66.7 (10)
C6BA—C0AA—C4AA—C45	-1.0 (18)	C1BA—C13—C5—C7BA	-3 (3)
C6BA—C0AA—C4AA—C2BA	179.8 (13)	C13—C1BA—C15—C3BA	2 (2)
C0AA—C6BA—C5AA—N12	-178.6 (10)	C13—C5—C7BA—C3BA	2 (3)
C0AA—C6BA—C5AA—C3CA	1.3 (14)	C13—C5—C7BA—C7CA	-176 (2)
C0AA—C4AA—C45—C3CA	1.8 (19)	C5—C7BA—C3BA—C15	1 (3)
C4AA—C45—C3CA—C5AA	-0.9 (17)	C7BA—C3BA—C15—C1BA	-3 (3)
C4AA—C45—C3CA—N16	-179.2 (12)	C15—C1BA—C13—C5	1 (3)
C45—C3CA—C5AA—N12	179.3 (11)	C17—C2AA—CXE—C2	180 (2)
C45—C3CA—C5AA—C6BA	-0.7 (12)	C0CA—C1—C4—C4CA	-178.8 (12)
C45—C3CA—N16—Hg1	177.9 (9)	C9AA—C3—C2CA—C16	1 (2)
C45—C3CA—N16—S7	7.6 (16)	C9AA—C3—C2CA—C5CA	-179.7 (16)
C5AA—C6BA—C0AA—C4AA	-0.5 (17)	C9AA—C1CA—C20—C16	-4 (2)
C5AA—C6BA—C0AA—C0BA	179.4 (11)	C3—C9AA—C1CA—S111	178.3 (10)
C5AA—C3CA—N16—Hg1	-0.4 (10)	C3—C9AA—C1CA—C20	4.3 (18)
C5AA—C3CA—N16—S7	-170.7 (7)	C3—C2CA—C16—C20	-2 (3)
O93—S7—N16—Hg1	-124.9 (6)	C1CA—S111—N17—Hg1	-116.6 (5)
O93—S7—N16—C3CA	44.9 (11)	C1CA—S111—N17—C10	68.6 (8)
O93—S7—C7AA—C8AA	-0.4 (12)	C1CA—C9AA—C3—C2CA	-3 (2)
O93—S7—C7AA—C3AA	177.1 (10)	C2CA—C16—C20—C1CA	3 (3)
O94—S7—N16—Hg1	3.7 (8)	C5CA—C2CA—C16—C20	179.4 (18)
O94—S7—N16—C3CA	173.6 (9)	C7CA—C7BA—C3BA—C15	178.7 (18)
O94—S7—C7AA—C8AA	-124.1 (11)	C8CA—C9BA—C1—C4	180.0 (15)
O94—S7—C7AA—C3AA	53.4 (11)	C8CA—C9BA—C1—C0CA	0 (2)
N16—S7—C7AA—C8AA	121.5 (11)	C8CA—C9BA—C9—C10	178.5 (14)
N16—S7—C7AA—C3AA	-61.0 (11)	C4DA—N3DA—C5DA—C8DA	53 (3)
N16—C3CA—C5AA—N12	-2.2 (10)	C4DA—N3DA—C7DA—C6DA	147 (2)
N16—C3CA—C5AA—C6BA	177.8 (11)	C5DA—N3DA—C4DA—C6	65 (2)

N17—S111—C1CA—C9AA	22.6 (10)	C5DA—N3DA—C7DA—C6DA	-86 (3)
N17—S111—C1CA—C20	-163.4 (10)	C7DA—N3DA—C4DA—C6	-166.6
N17—C10—C9—C9BA	-178.3 (10)	C7DA—N3DA—C5DA—C8DA	(19)
			-69 (3)
O0AA—S111—N17—Hg1	125.7 (5)	C9CA—N1—C1DA—C0DA	-71 (3)
O0AA—S111—N17—C10	-49.1 (9)	C9CA—N1—C2DA—C3DA	66 (3)
O0AA—S111—C1CA—C9AA	145.5 (9)	C1DA—N1—C9CA—C8BA	147 (2)
O0AA—S111—C1CA—C20	-40.5 (11)	C1DA—N1—C2DA—C3DA	-173 (3)
O1AA—S8—N12—Hg1	-134.2 (6)	C2DA—N1—C9CA—C8BA	-98 (3)
O1AA—S8—N12—C5AA	42.6 (11)	C2DA—N1—C1DA—C0DA	165 (3)
O1AA—S8—C5BA—C6AA	-162.9 (11)	C9CB—N1A—C1DB—C0DB	-73 (4)
O1AA—S8—C5BA—C2	21.4 (16)	C9CB—N1A—C2DB—C3DB	-61 (4)
C5BA—S8—N12—Hg1	110.8 (6)	C1DB—N1A—C9CB—C8BB	158 (4)
C5BA—S8—N12—C5AA	-72.4 (10)	C1DB—N1A—C2DB—C3DB	64 (4)
C5BA—C6AA—C1AA—C2AA	1 (2)	C2DB—N1A—C9CB—C8BB	-82 (5)
C6AA—C5BA—C2—CXE	3 (3)	C2DB—N1A—C1DB—C0DB	161 (3)

2.5 Conclusions

We have presented a comprehensive spectroscopic, structural, and extraction study of bis-arylsulfonamide ligands derived from *o*-phenylenediamine for mercury extraction and complexation using experimental and structural techniques. These bis-arylsulfonamides are shown to extract Hg^(II) from alkaline aqueous media at pH 12.0 with potential application to high-level waste processing for Hg^(II) extraction and removal. An advantage of these ligands is the low ligand concentration required for quantitative extraction from alkaline conditions and that the recovery of extracted metal is straightforward. The titration studies in methanolic solutions, together with the solid-state findings and structural results, indicate the formation of 1:1 complexes when additional coordinating ligands and solvents are present, while 1:2 complexes dominate in the absence of this additional coordination. Our research is currently being directed towards the development of modified sulfonamide ligands that can form organosoluble complexes of mercury in highly lipophilic solvents, such as dodecane, that are more applicable for extraction processes for mercury removal from high-level alkaline waste, with no ligand partition and complete ligand and Hg^(II) recovery.

2.6 Acknowledgments

This research project was supported by the US Department of Energy Minority Serving Institution Partnership Program (MSIPP) managed by the Savannah River National Laboratory under SRNS contract BOA No: 541, TOA No. 0000332972 and 0000403067 to FIU. We also acknowledge the financial support of the Florida

International University Dissertation Year Fellowship for Adenike Fasiku (DYF Spring/Summer 2021 Fellow).

2.7 References

- (1) Clifton, J. C. Mercury Exposure and Public Health. *Pediatr. Clin. North Am.* **2007**, *54*, 237.e1-237.e45.
- (2) Bannochie, C. J.; Fellingner, T. L.; Garcia-Strickland, P.; Shah, H. B.; Jain, V.; Wilmarth, W. R. Mercury in Aqueous Tank Waste at the Savannah River Site: Facts, Forms, and Impacts. *Sep. Sci. Technol.* **2018**, *53*, 1935–1947.
- (3) Saturday, A.; Saturday, A.; Internationals, O. Mercury and Its Associated Impacts on Environment and Human Health: A Review. *J. Environ. Health Sci.* **2018**, *4*, 37–43.
- (4) Stejskal, V. Allergy and Autoimmunity Caused by Metals: A Unifying Concept. In *Vaccines and Autoimmunity*; 2015; 57–64.
- (5) Sharma, A.; Sharma, A.; Arya, R. K. Removal of Mercury(II) from Aqueous Solution: A Review of Recent Work. *Sep. Sci. Technol.* **2015**, *50*, 1310–1320.
- (6) Hua, K.; Xu, X.; Luo, Z.; Fang, D.; Yi, J.; Bao, R. Effective Removal of Mercury Ions in Aqueous Solutions: A Review. *Current Nanoscience*; **2020**, *16*, 363-375.
- (7) Alvarado, R. J.; Rosenberg, J. M.; Andreu, A.; Bryan, J. C.; Chen, W.-Z.; Ren, T.; Kavallieratos, K. Structural Insights into the Coordination and Extraction of Pb(II) by Disulfonamide Ligands Derived from o-Phenylenediamine. *Inorg. Chem.* **2005**, *44*, 7951–7959.
- (8) Kavallieratos, K.; Rosenberg, J. M.; Bryan, J. C. Pb(II) Coordination and Synergistic Ion-Exchange Extraction by Combinations of Sulfonamide Chelates and 2,2'-Bipyridine. *Inorg. Chem.* **2005**, *44*, 2573–2575.
- (9) Mane, C.; Mahamuni, S.; Gaikwad, A.; Shejwal, R.; Kolekar, S.; Anuse, M. Extraction and Separation of Mercury(II) from Succinate Media with High Molecular Weight Amine as an Extractant. *J. Saudi Chem. Soc.* **2015**, *140*.
- (10) Fábrega, F. M.; Guimarães, A. S.; Resende, G. P. S.; Mansur, M. B. Solvent Extraction of Mercury(II) from Aqueous Chloride Solutions Using Cyanex 302. *Miner. Process. Extr. Metall.* **2017**, *126*, 193–198.

- (11) McDonald, C.; Pahlavan, G. H. Solvent Extraction of Mercury Using Alamine 304. *Mikrochim. Acta* **1982**, *78*, 77–82.
- (12) Moore, F. L. Liquid-Liquid Extraction of Mercury with High-Molecular-Weight Amines from Iodide and Bromide Solutions. *Sep. Sci.* **2006**.
- (13) Pearson, R. G. Hard, and Soft Acids and Bases. *J. Am. Chem. Soc.* **1963**, *85*, 3533–3539.
- (14) Abbasi, Y.; Shahida, S.; Ali, A.; Khan, M. Liquid-Liquid Extraction of Mercury(II) from Aqueous Solution Using Furosemide in Benzyl Alcohol. *J. Radioanal. Nucl. Chem.* **2019**, *319*.
- (15) Francis, T.; Meera, R.; Reddy, M. L. P. Extraction and Separation of Mercury (II) from the Brine Sludge of a Chlor-Alkali Industry Using Thio-Substituted Organophosphinic Acids. In *Proceedings of International Symposium of Solvent Extraction (ISSE 2002)*; Allied Publishers Pvt. Ltd New Delhi, **2002**, 169–178.
- (16) Hutchison, A.; Atwood, D.; Santilliann-Jiminez, Q. E. The Removal of Mercury from Water by Open Chain Ligands Containing Multiple Sulfurs. *J. Hazard. Mater.* **2008**, *156*, 458–465.
- (17) Barron-Zambrano, J.; Laborie, S.; Viers, Ph.; Rakib, M.; Durand, G. Mercury Removal from Aqueous Solutions by Complexation—Ultrafiltration. *Desalination* **2002**, *144*, 201–206.
- (18) Marinho, O. R.; Kamogawa, M. Y.; Ferreira, J. R.; Reis, B. F. Automated Liquid-Liquid Extraction Procedure for the Photometric Determination of Nanogram Levels of Hg(II) in Soil and Sediment Extracts. *Microchem. J.* **2020**, *156*, 104978.
- (19) Matsumoto, M.; Yoshizuka, K.; Kondo, K.; Nakashio, F. Extraction Equilibria of Copper and Zinc with N-8-Quinolylsulfonamides. *J. Chem. Eng. Jpn.* **1984**, *17*, 89–93.
- (20) Takagi, M.; Omori, T.; Matsuo, S.; Matsuno, S.; Ueno, K.; Ide, S. Sulfonamides. a New Class of Chelating Agents of Potential Utility in Analytical and Separation Chemistry. *Chem. Lett.* **1980**, *9*, 387–390.
- (21) Hirayama, N.; Taga, J.; Oshima, S.; Honjo, T. Sulfonamide-Type Di-Schiff Base Ligands as Chelate Extraction Reagents for Divalent Metal Cations. *Anal. Chim. Acta* **2002**, *466*, 295–301.
- (22) Şenkal, B. F.; Yavuz, E.; Bicak, N. Poly(Acrylamide) Grafts on Spherical Polymeric Sulfonamide Based Resin for Selective Removal of Mercury Ions from Aqueous Solutions. *Macromol. Symp.* **2004**, *217*, 169–178.

- (23) Matsumiya, M.; Sumi, M.; Uchino, Y.; Yanagi, I. Recovery of Indium Based on the Combined Methods of Ionic Liquid Extraction and Electrodeposition. *Sep. Purif. Technol.* **2018**, *201*, 25–29.
- (24) Remko, M. Molecular Structure, PKa, Lipophilicity, Solubility and Absorption of Biologically Active Aromatic and Heterocyclic Sulfonamides. *J. Mol. Struct. THEOCHEM* **2010**, *944*, 34–42.
- (25) Govor, E. V.; Morozov, A. N.; Rains, A. A.; Mebel, A. M.; Kavallieratos, K. Spectroscopic and Theoretical Insights into Surprisingly Effective Sm(III) Extraction from Alkaline Aqueous Media by o-Phenylenediamine-Derived Sulfonamides. *Inorg. Chem.* **2020**, *59*, 6884–6894.
- (26) Agertt, V. A.; Bonez, P. C.; Rossi, G. G.; Flores, V. da C.; Siqueira, F. dos S.; Mizdal, C. R.; Marques, L. L.; de Oliveira, G. N. M.; de Campos, M. M. A. Identification of Antimicrobial Activity among New Sulfonamide Metal Complexes for Combating Rapidly Growing Mycobacteria. *BioMetals* **2016**, *29*, 807–816.
- (27) Chohan, Z. H. Metal-Based Sulfonamides: Their Preparation, Characterization and in-Vitro Antibacterial, Antifungal & Cytotoxic Properties. X-Ray Structure of 4-[(2-Hydroxybenzylidene) Amino] Benzenesulfonamide. *J. Enzyme Inhib. Med. Chem.* **2008**, *23*, 120–130.
- (28) Pervaiz, M.; Riaz, A.; Munir, A.; Saeed, Z.; Hussain, S.; Rashid, A.; Younas, U.; Adnan, A. Synthesis and Characterization of Sulfonamide Metal Complexes as Antimicrobial Agents. *J. Mol. Struct.* **2020**, *1202*, 127284.
- (29) Zhang, W.; Cai, Y.; Kavallieratos, K. Investigation of Disulfonamide Ligands Derived from O-Phenylenediamine and Their Pb(II) Complexes by Electrospray Ionization Mass Spectrometry. *Rapid Commun. Mass Spectrom. RCM* **2006**, *20* (2), 303–308.
- (30) Billman, J. H.; Chernin, R. 8-Sulfonamidoquinolines as a New Class of Organic Reagents. *Anal. Chem.* **1962**, *34*, 408–410.
- (31) Kavallieratos, K.; Rosenberg, J. M.; Alvarado, R. J.; Zhang, W.; Chen, W.-Z.; Ren, T. Pb(II) Coordination, Extraction, and Sensing by Disulfonamide Ion-Exchangers.
- (32) Ackermann, T. K. A. Connors: Binding Constants — the Measurement of Molecular Complex Stability, John Wiley & Sons, New York, Chichester, Brisbane, Toronto, Singapore 1987. 411 Seiten, Preis: £ 64.15. *Berichte Bunsenges. Für Phys. Chem.* **1987**, *91*, 1398–1398.

- (33) Khan, H.; Ahmed, M. J.; Bhanger, M. I. A Simple Spectrophotometric Determination of Trace Level Mercury Using 1,5-Diphenylthiocarbazone Solubilized in Micelle. *Anal. Sci.* **2005**, *21*, 507–512.
- (34) Job, P. Formation and stability of inorganic complexes in solution. *Ann Chim* **1928**, *9*, 113–134.
- (35) Sheldrick, G. M. A Short History of SHELX. *Acta Crystallogr.* **2008**, *64*, 112–122.
- (36) Sheldrick, G. M. Crystal Structure Refinement with SHELXL. *Acta Crystallogr. Sect. C Struct. Chem.* **2015**, *71*, 3–8.
- (37) Dolomanov, O. V.; Bourhis, L. J.; Gildea, R. J.; Howard, J. a. K.; Puschmann, H. OLEX2: A Complete Structure Solution, Refinement and Analysis Program. *J. Appl. Crystallogr.* **2009**, *42*, 339–341.
- (38) Hossain, G. M. G.; Amoroso, A. J.; Banu, A.; Malik, K. M. A. Syntheses and Characterisation of Mercury Complexes of Sulfadiazine, Sulfamerazine and Sulfamethazine. *Polyhedron* **2007**, *26*, 967–974.
- (39) Diaconu, D.; Mangalagiu, V.; Amariuca-Mantu, D.; Antoci, V.; Giuroiu, C.; Mangalagiu, I. Hybrid Quinoline-Sulfonamide Complexes (M^{2+}) Derivatives with Antimicrobial Activity. *Molecules* **2020**, *25*, 2946.
- (40) Zorn, M. E.; Gibbons, R. D.; Sonzogni, W. C. Evaluation of Approximate Methods for Calculating the Limit of Detection and Limit of Quantification. *Environ. Sci. Technol.* **1999**, *33*, 2291–2295.
- (41) Morozov, A. N.; Govor, E. V.; Anagnostopoulos, V. A.; Kavallieratos, K.; Mebel, A. M. 1,3,5-Tris-(4-(Iso-Propyl)-Phenylsulfamoylmethyl)Benzene as a Potential Am(III) Extractant: Experimental and Theoretical Study of Sm(III) Complexation and Extraction and Theoretical Correlation with Am(III). *Mol. Phys.* **2018**, *116*, 2719–2727.
- (42) Panetti, G. B.; Robinson, J. R.; Carroll, P. J.; Gau, M. R.; Manor, B. C.; Walsh, P. J.; Schelter, E. J. Synthesis of Novel Copper-Rare Earth Binolate Frameworks from a Hydrogen Bonding DBU-H Rare Earth BINOLate Complex. *Dalton Trans.* **2018**, *47*, 14408–14410.
- (43) Enamullah, M.; Vasylyeva, V.; Quddus, M. A.; Islam, M. K.; Höfert, S.-P.; Janiak, C. Spontaneous Resolution of a Δ/Λ -Chiral-at-Metal Pseudo-Tetrahedral Schiff-Base Zinc Complex to a Racemic Conglomerate with C–H \cdots O Organized 41- and 43-Helices. *CrystEngComm* **2018**, *20*, 4724–4734.

- (44) Khavasi, H. R.; Rahimi, N. Coordination Polymers with Intramolecular Fluorine-Involved Contacts in Two-Dimensional Sheet Windows. *Cryst. Growth Des.* **2017**, *17*, 834–845.
- (45) Grdenić, D.; Kamenar, B.; Hergold-Brundić, A. Crystal and Molecular Structure of Bis (2, 2'-Bipyridyl) Mercury (II) Nitrate Dihydrate. *Croat. Chem. Acta* **1979**, *52*, 339–346.
- (46) Zheng, S.-L.; Zhang, J.-P.; Chen, X.-M.; Huang, Z.-L.; Lin, Z.-Y.; Wong, W.-T. Syntheses, Structures, Photoluminescence, and Theoretical Studies of a Novel Class of D10 Metal Complexes of 1H-[1, 10] Phenanthroline-2-one. *Chem. Eur. J.* **2003**, *9*, 3888–3896.
- (47) Wu, D.; Huang, W.; Duan, C.; Lin, Z.; Meng, Q. Highly Sensitive Fluorescent Probe for Selective Detection of Hg²⁺ in DMF Aqueous Media. *Inorg. Chem.* **2007**, *46*, 1538–1540.
- (48) Li, J.; Widlicka, D. W.; Fichter, K.; Reed, D. P.; Weisman, G. R.; Wong, E. H.; DiPasquale, A.; Heroux, K. J.; Golen, J. A.; Rheingold, A. L. Comparative Structural Coordination Chemistry of Two Tricyclic Bisamidines. *Inorganica Chim. Acta* **2010**, *364*, 185–194.
- (49) Teets, T. S.; Partyka, D. V.; Updegraff Iii, J. B.; Gray, T. G. Homoleptic, Four-Coordinate Azadipyrromethene Complexes of D10 Zinc and Mercury. *Inorg. Chem.* **2008**, *47*, 2338–2346.
- (50) Rofouei, M. K.; Hematyar, M.; Ghoulipour, V.; Gharamaleki, J. A. Syntheses, Structures, Thermal Behavior and Solution Studies of Two Types of Hg (II) Complexes with [1, 3-Di (2-Methoxy) Benzene] Triazene. *Inorganica Chim. Acta* **2009**, *362*, 3777–3784.
- (51) Huo, Y.; Wang, S.; Lu, T.; Pan, C.; Lu, Y.; Yang, X.; Hu, D.; Hu, S. Highly Selective and Sensitive Colorimetric Chemosensors for Hg²⁺ Based on Novel Diaminomaleonitrile Derivatives. *RSC Adv.* **2016**, *6*, 5503–5511.

CHAPTER III: A bis-Dansylamide Derivative of *o*-Phenylenediamine as a Fluorescent Chemosensor for the Detection of Hg(II) in Alkaline Solutions

Adenike O. Fasiku, Indranil Chakraborty, Laura M. Garcia, and Konstantinos

Kavallieratos*

3.1 Abstract

Mercury (Hg) separation and sensing is of significance due to Hg^(II) environmental mobility and toxicity. Furthermore, the use of Hg in nuclear applications has resulted to its accumulation in several DOE sites, such as in Oak Ridge and Savannah River (SRS) reservations. A bis-dansylamide ligand (**L_D**) derived from substituted *o*-phenylenediamine, and dansyl chloride has been synthesized and tested for extraction and sensing of Hg^(II). This bidentate ligand acts as an N-donor that coordinates to Hg^(II) through the amine group after deprotonation. The presence of the fluorogenic dansyl moiety on this ligand enhances its sensing abilities. **L_D** was shown to be an effective Hg^(II) sensor, as fluorescence quenching was observed upon gradual addition of a HgCl₂ solution with complete quenching at 1:1 Hg^(II):**L_D** ratio. When compared with other prevalent metals in SRS, such as Na^(I), Ca^(II), Cs^(I), Sr^(II), and K^(I), only for the addition of Hg^(II), a spectroscopic change was observed, including complete quenching of the **L_D** fluorescence. **L_D** was also shown to extract Hg^(II) from aqueous phases into dichloroethane in the presence of diisopropylethylamine (DIPEA), with extraction efficiency as high as 99.2 %.

3.2 Introduction

Interest in mercury detection from different sources by new practical analytical and sensitive methods has increased because of the well-known mercury toxicity and mobility in the environment. The presence of mercury at the high-level alkaline waste (HLW) tanks at the Savannah River Site (SRS) due to its use over time as a dissolution catalyst for aluminum nuclear fuel cladding has led to increased accumulation of very toxic organic mercury forms in saltstone, which pose significant risks to the workers and the surrounding environment.¹ As a result, the design, and synthesis of chemosensors that can complex, extract, and detect $\text{Hg}^{(\text{II})}$ in alkaline environments with high sensitivity and selectivity in the presence of a wide range of concentration of metals that are abundant both in these sites and in biological systems, such as $\text{Na}^{(\text{I})}$, $\text{Ca}^{(\text{II})}$, $\text{Cs}^{(\text{I})}$, $\text{Sr}^{(\text{II})}$, and $\text{K}^{(\text{I})}$, is an area of broad interest.

The use of fluorescent chemosensors for the detection of $\text{Hg}^{(\text{II})}$ has greatly increased due to their high relevance in industrial and biological processes, low cost, and easy usability.²⁻⁴ In most of these fluorescent sensors, fluorescent quenching is observed in the presence of $\text{Hg}^{(\text{II})}$ due to enhanced spin-orbit coupling associated with a heavy atom, which facilitates the intersystem crossing process.⁵ Dansyl-based chemosensors are common compounds used for the detection of metal ions due to their large Stokes shifts.^{2,6-13} Recently, a tetrapeptide-based dansyl fluorescent “turn-on” response chemosensor was reported for $\text{Hg}^{(\text{II})}$ with a limit of detection of 7.59 nM.¹⁴ In 2015, Zhou et al. reported a dansyl and morpholine-based sensor, which shows fluorescent quenching upon addition of $\text{Hg}^{(\text{II})}$.¹⁵ A fluorescent tris-dansyl trisulfonamide derived from dansyl chloride and 1,3,5-tris(2-aminomethyl)-2,4,6-triethylbenzene was shown by

our group to sense $\text{Hg}^{\text{(II)}}$ added as either HgCl_2 or $\text{Hg}(\text{OAc})_2$, also by fluorescence quenching, while no response was observed to the addition of $\text{Co}^{\text{(II)}}$, $\text{Ca}^{\text{(II)}}$, $\text{Cu}^{\text{(II)}}$, $\text{Ag}^{\text{(I)}}$, and $\text{Cd}^{\text{(II)}}$.¹⁶ The crystal structures of the $\text{Hg}^{\text{(II)}}$ complexes formed with $\text{Hg}(\text{OAc})_2$ and HgCl_2 show remarkably different coordination patterns with 3:1 and 1:2 metal:ligand stoichiometries, respectively. In 2005, our group showed that a bis-dansyl chemosensor derived from *o*-phenylenediamine senses $\text{Pb}^{\text{(II)}}$ by selectively extracting it into an organic phase.¹⁷ Based on these promising results, we decided to undertake a study with a bis-methyl derivative of this ligand for $\text{Hg}^{\text{(II)}}$ extraction and sensing.

Herein, we report a bis-dansylamide ligand (**LD**) derived from *o*-phenylenediamine that selectively senses $\text{Hg}^{\text{(II)}}$ in alkaline aqueous solutions via complexation and extraction to 1,2-dichloroethane (DCE). No response was observed after the addition of several metal salts that are present in HLW (Ca^{2+} , K^+ , Cs^+ , Na^+ , and Sr^{2+}). The ligand, which was synthesized in one step with good yields, was shown to extract $\text{Hg}^{\text{(II)}}$ at 99.2 % efficiency at pH 7.0 and at 51.9 % efficiency at pH 11.0. The slope analysis from the $\log D$ vs. $\log[\text{LD}]$ suggests a 1:2 $\text{Hg}:\text{LD}$ binding stoichiometry for the extracted species in 1,2-dichloroethane, while titrations in solvents with higher coordinating ability, such as methanol, showed dominant 1:1 stoichiometry. The 1:1 $\text{Hg}:\text{LD}$ binding in methanol was confirmed by the UV-Vis and fluorescence titrations, Job plots, and the $^1\text{H-NMR}$ titration that shows complete coordination of $\text{Hg}^{\text{(II)}}$ to the ligand without residual peaks after the addition of 1 eq. of $\text{Hg}^{\text{(II)}}$ to 1 eq. of the ligand. The association constant obtained from the UV-Vis titration of **LD** in methanol was $K_{11} = 3.6 (\pm 1.1) \times 10^5 \text{ M}^{-1}$. The Stern-Volmer constant, K_{SV} obtained from fluorescence intensity quenching of **LD** by $\text{Hg}^{\text{(II)}}$ was $2.9 (\pm 0.7) \times 10^5 \text{ M}^{-1}$. **LD** was able to detect $\text{Hg}^{\text{(II)}}$

at a detection limit of 0.78 μM with linearity ranging from 0 – 13.4 μM . The X-ray structure of the chemosensor **L_D** is also reported herein.

3.3 Experimental section

3.3.1 Materials and methods

All chemicals and materials were purchased from Fisher Scientific or Sigma-Aldrich. All chemicals were standard reagent grade and were used without further purification. ^1H and ^{13}C -NMR spectra were recorded on a 400-MHz Bruker Avance NMR spectrometer with chemical shifts, δ , reported in ppm. The fluorescence spectra were recorded on a Cary Eclipse fluorescence spectrophotometer, and UV-Vis spectra were recorded on a CARY 100 Bio UV-Vis spectrophotometer. FT-IR spectra were recorded on a Cary 600 series FT-IR spectrometer. Single crystal X-ray diffraction studies were carried out on a Bruker D8 Quest with PHOTON 100 detector. Elemental analysis was provided by Atlantic Microlab Inc.

3.3.2 Synthesis of N,N'-(4,5-dimethyl-1,2-phenylene)bis(5-(dimethylamino)naphthalene-1-sulfonamide) (L_D**)**

The ligand **L_D** was synthesized by a modification of a method for similar ligands reported by Alvarado et al.¹⁸ To a stirring solution of 4,5-dimethyl-1,2-*o*-phenylenediamine (0.461 g, 3.38 mmol) in methylene chloride, 2.2 eq. (0.60 mL) of pyridine was added and left to stir for a while. Then, dansyl chloride (2.0 g, 7.42 mmol) dissolved in methylene chloride is dropwise added to the stirring solution and left to stir at room temperature for 24 hrs. The reaction was monitored with TLC. After completion,

the solution was washed three times with 1M HCl, 0.2 M NaHCO₃, and deionized water. The product was dried *in vacuo* and recrystallized initially from hot ethanol and subsequently from methylene chloride/hexanes. Yield: 0.952 g, 1.58 mmol (46.7 %). ¹H-NMR (400 MHz, MeOD) δ 8.51 (d, *J* = 8.5 Hz, 2H), 8.31 (d, *J* = 8.7 Hz, 2H), 7.95 (d, *J* = 6.5 Hz, 2H), 7.63 – 7.53 (m, 2H), 7.45 – 7.36 (m, 2H), 7.28 (d, *J* = 7.5 Hz, 2H), 6.43 (s, 2H), 2.86 (s, 12H), 1.80 (s, 6H). ¹³C-NMR (101 MHz, MeOD) δ 151.34 (s), 138.14 (s), 131.22 (s), 130.07 (s), 129.76 (s), 129.08 (s), 128.29 (s), 127.43 (s), 127.16 (s), 122.82 (s), 120.42 (s), 114.67 (s), 44.52 (s), 17.91 (s). ¹H-NMR (400 MHz, CDCl₃) δ 8.50 (d, *J* = 8.5 Hz, 2H), 8.27 (d, *J* = 8.6 Hz, 2H), 7.97 (d, *J* = 7.3 Hz, 2H), 7.62 (t, *J* = 7.8 Hz, 2H), 7.37 (t, *J* = 7.6 Hz, 2H), 7.22 (d, *J* = 7.5 Hz, 2H), 6.61 (s, 2H), 6.49 (s, 2H), 2.88 (s, 12H), 1.87 (s, 6H). FT-IR (cm⁻¹); ν(N-H) = 3299.0, ν_{asym}(SO₂) = 1319.1, ν_{sym}(SO₂) = 1139.7, ν(S – N) = 904.5. UV/Vis. Elemental analysis (%) calculated for C₃₂H₃₄N₄O₄S₂: C 63.76, H 5.69, N 9.30; Found: C 63.50, H 5.72, N 9.19.

3.3.3 Synthesis of Hg-L_D complex

A solution of HgCl₂ (30.3 mg, 0.112 mmol) in 10 mL methanol was added dropwise to a 25 mL dichloromethane (DCM) solution of L_D (56.0 mg, 0.093 mmol) and DIPEA (41.5 μL, 0.233 mmol). Instantaneous precipitation was observed. The precipitate was filtered under vacuum and washed with methanol and then DCM. The brownish yellow product obtained was dried under vacuum at room temperature (19.7 mg). FT-IR (cm⁻¹); ν_{asym}(SO₂) = 1315.2, ν_{sym}(SO₂) = 1114.6, ν(S – N) = 912.2. Solubility of the isolated complex is poor in most solvents, hence, solution state spectroscopic data of the complex are provided below from the low concentration

¹H-NMR titration end points rather than the isolated solid: ¹H-NMR (400 MHz, MeOD) δ 8.67 (d, *J* = 8.7 Hz, 2H), 8.41 (d, *J* = 8.5 Hz, 2H), 8.11 (d, *J* = 7.1 Hz, 2H), 7.49 (t, *J* = 8.1 Hz, 2H), 7.39 (t, *J* = 7.9 Hz, 2H), 7.20 (d, *J* = 7.5 Hz, 2H), 6.83 (s, 2H), 3.22 (dd, *J* = 30.7, 24.5 Hz, 12H), 2.81 (s, 12H), 2.72 (t, *J* = 15.9 Hz, 14H), 1.85 (s, 6H). ¹³C-¹H-NMR (101 MHz, MeOD) δ 152.74 (s), 140.59 (s), 131.59 (s), 131.33 (s), 129.56 (s), 129.41 (s), 128.49 (s), 128.04 (s), 124.29 (s), 122.17 (s), 120.08 (s), 116.04 (s), 45.84 (s), 19.25 (s).

3.3.4 UV-Visible titrations

Solutions of ligand **L_D** in MeOH were titrated with HgCl₂ at constant ligand concentration. In a typical experiment, a ligand solution (2.0 × 10⁻⁵ M) and 2.2 eq. of diisopropylethylamine (DIPEA) in MeOH was titrated with a solution of HgCl₂ prepared by diluting with the ligand/DIPEA solution. For spectra collection, 2.300 mL of ligand solution was added to the cuvette, and HgCl₂ (4.0 × 10⁻⁴ M) prepared in ligand solution was added in 5-100 μL increments until a total of 950 μL had been added. The binding constants were determined by non-linear regression fitting to the 1-1 binding isotherm.¹⁹ All spectroscopic measurements were performed in triplicate, and the binding constants obtained were averages of three independent experiments.

3.3.5 Fluorescence titrations

Solutions of ligand in methanol were titrated with HgCl₂ at constant ligand concentration, as above. Fluorescence emission was measured at increments of 0.5 nm and integration time of 0.1 secs, excitation and emission slit width of 10 nm and 5 nm, respectively. Excitation at 334 nm produced an emission at 533 nm. In a typical

experiment, a solution of **LD** (2.0×10^{-5} M) and 2.5 eq. of DIPEA (5.0×10^{-5} M) in methanol was titrated with a solution of HgCl_2 (4.0×10^{-4} M) prepared by weighing 1.086 mg of HgCl_2 and diluting with the ligand solution in a 10.0 mL volumetric flask. For spectra collection, 2.300 mL of ligand solution was added to the cuvette and $\text{Hg}^{(\text{II})}$ solution prepared was added in 5-100 μL increments until a total of 950 μL had been added. The binding constant was determined by Stern-Volmer linear analysis.²⁰ All spectroscopic measurements were performed in triplicate, and the binding constants obtained were averages of three independent experiments.

3.3.6 Determination of stoichiometry by the continuous variation method (Job Plot)

Information on the stoichiometry of the complex was obtained from the continuous variation method.²¹ Solutions containing varying concentrations of $\text{Hg}^{(\text{II})}$ and **LD** were prepared in methanol. Stock solutions of i) ligand (0.020 mM)/DIPEA (0.050 mM) and ii) HgCl_2 (0.020 mM) were used. Both solutions were mixed from the molar fractions of 0.1 to 0.9 while maintaining a constant overall concentration of 0.020 mM. Fluorescence intensities of the solutions were measured at 533 nm (excited at 334 nm). Afterward, the plot of the delta intensity at 533 nm vs. mol ratio of the [**LD**] was obtained.

$$\text{Mol ratio of } \mathbf{LD} = \frac{[\mathbf{LD}]}{[\text{Hg}^{(\text{II})}] + [\mathbf{LD}]} \quad (1)$$

3.3.7 Comparative experiments

Methanol solutions (3.0 mL) of chloride salts of several metals ($\text{Ca}^{(\text{II})}$, $\text{K}^{(\text{I})}$, $\text{Cs}^{(\text{I})}$, $\text{Na}^{(\text{I})}$, $\text{Hg}^{(\text{II})}$, and $\text{Sr}^{(\text{II})}$, 0.20 mM) were added to 3.0 mL methanolic solutions of **LD** (0.10

mM) and DIPEA (0.25 mM). After contact of the two solutions the emission spectra were recorded at 533 nm ($\lambda_{\text{exc}} = 334$ nm).

3.3.8 Extraction studies

Hg^(II) extraction at constant concentrations of **LD** from aqueous phases of variable alkalinity was studied using aqueous solutions of HgCl₂ and NaOH. In a typical experiment, 5.00 mL of aqueous Hg^(II) solutions were prepared by adding various volumes of NaOH (10^{-6} – 1 M; pH 7, 8, 9, 10, 11, 12, 13, 14) to 0.50 mL of a 10.0 mM HgCl₂ solution and subsequently diluted up to 5.00 mL mark (final [Hg^(II)] in aqueous solution is 0.98 mM). The aqueous phases were then equilibrated with 5.00 mL solutions of 2.00 mM **LD** in 1,2-dichloroethane (DCE) by rotating on a wheel at 55 rpm. After contacting both phases for 20 h, the solutions were centrifuged for 5 min for proper separation of both layers.

Slope analysis experiments were performed at pH 11.0 and pH 7.0. At pH 11.0, solutions of various concentrations of **LD** in DCE were prepared and contacted with HgCl₂ solutions. The **LD** dependence was determined by preparing 5.00 mL solutions of various concentrations of **LD** (0.30 – 2.0 mM) in DCE and contacting with 5.00 mL of aqueous solutions of HgCl₂ (1.0 mM) at pH 11.0 (NaOH; 10^{-3} M). Experiments at pH = 7.0 were carried out by preparing 5.00 mL solutions of various concentrations of **LD** (0.3 - 2 mM) and DIPEA in DCE and contacting with 5.00 mL of aqueous solutions of HgCl₂ (carried out in the absence of NaOH).

The concentration of the residual unextracted Hg^(II) in the aqueous phase after extraction was determined using the dithizone method of mercury quantification.²²

The % Extraction (% E) of Hg^(II) is calculated as follows

$$\% E = \frac{C_0 - C}{C_0} \times 100 \quad (2)$$

C₀ is the initial concentration in the aqueous phase before extraction, and C denotes the concentration in the aqueous phase after extraction.

The Distribution coefficient D, is calculated as

$$D = \frac{C_0 - C}{C} \quad (3)$$

3.3.9 X-ray crystallography for LD

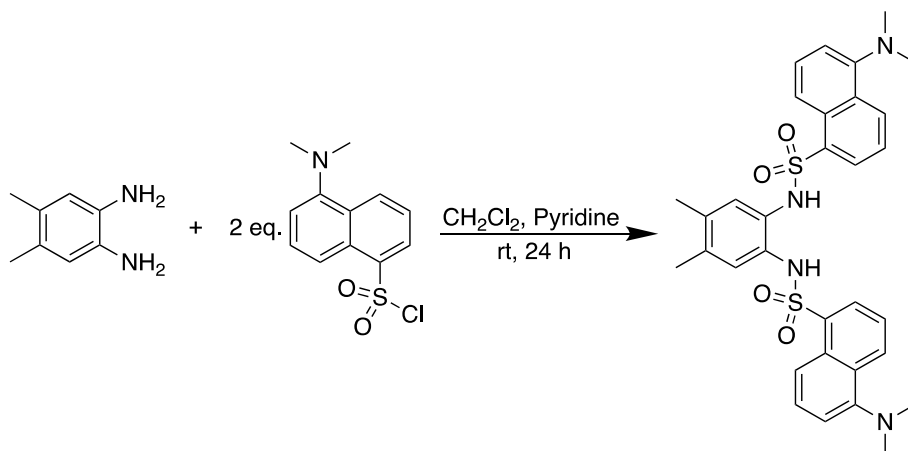
Reddish orange block-shaped crystals of the ligand were obtained by slow diffusion of hexanes into a dichloromethane solution. Data collection and structure refinement details are summarized in Table 3.1. A suitable crystal was selected and mounted on a Bruker D8 Quest diffractometer equipped with PHOTON II detector operating at T = 298 K. The structure was solved in space group *P*3₂ (# 145) determined by the *ShelXS*²³ structure solution program using Direct Methods and refined by Least Squares using version 2018/3 of *ShelXL*.²⁴ All non-hydrogen atoms were refined anisotropically. Calculations and molecular graphics were performed using *SHELXTL 2014* and *Olex2*²⁵ programs.

3.4 Results and discussion

3.4.1 Synthesis

The bis-dansylamide ligand **LD** was synthesized from the corresponding 4,5-dimethyl-*o*-phenylenediamine and dansyl chloride in pyridine (Scheme 3.1) by a

modification of a reported method for analogous compounds.¹⁸ The ligand was fully characterized by ¹H and ¹³C-NMR, FT-IR, and elemental analysis, and its structure was determined by X-ray crystallography (Figure 3.11).



Scheme 3.1: Synthesis of *N,N'*-(4,5-dimethyl-1,2-phenylene)bis(5-(dimethylamino)naphthalene-1-sulfonamide) (**LD**)

3.4.2 FT-IR studies

The important IR spectral bands of the ligand **LD** vs. its complex with $\text{Hg}^{\text{(II)}}$ are shown in Figure 3.1. The disappearance of the sulfonamide N-H band on the complex spectra is evidence of the deprotonation of the ligand, which is necessary for complexation. The ligand band due to $\nu_{\text{asym}}(\text{SO}_2)$ and $\nu_{\text{sym}}(\text{SO}_2)$ appear at 1319.1 and 1139.7 cm^{-1} , respectively. These bands shift to lower frequencies, $\nu_{\text{asym}}(\text{SO}_2)$ and $\nu_{\text{sym}}(\text{SO}_2)$, for the $\text{Hg}^{\text{(II)}}$ complex now appearing at 1315.2 and 1114.6 cm^{-1} , respectively. The $\nu(\text{S} - \text{N})$ band also shifted from 904.5 cm^{-1} in the ligand to 912.2 cm^{-1} in the complex. These shifts to a higher frequency for S-N and lower frequency for S-O are expected due to the increased contribution of the $\text{N}=\text{S}-\text{O}$ vs $\text{N}-\text{S}=\text{O}$ resonance forms in

the complex vs. the ligand. A strong band observed at 430 cm^{-1} is assigned to N-Hg stretches.

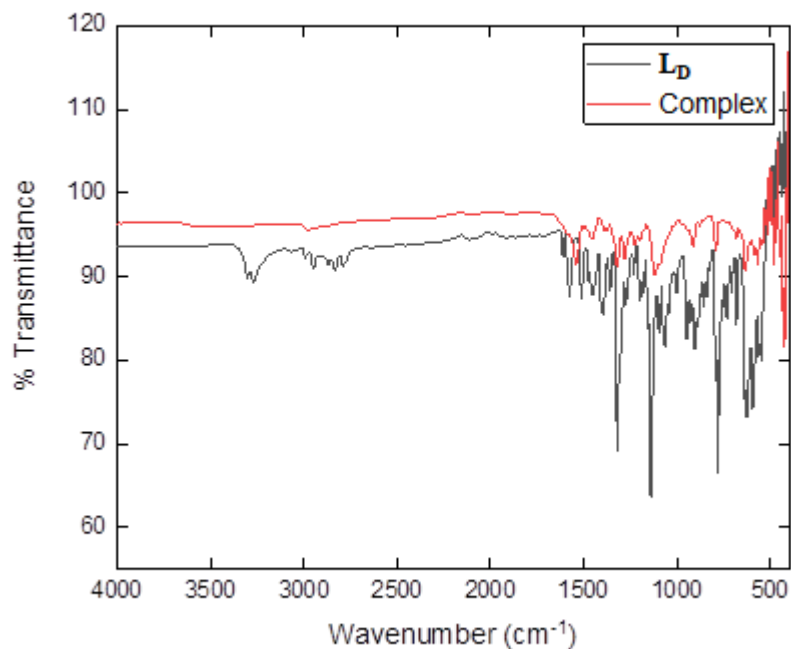


Figure 3.1: FT-IR spectra of L_D vs its $Hg^{(II)}$ complex.

3.4.3 1H and ^{13}C NMR studies

1H -NMR spectra of the free ligand and its $Hg^{(II)}$ complexes at various equivalent additions of $Hg^{(II)}$ were recorded in MeOD (Figure 3.2). Aliquots of $HgCl_2$ (prepared in MeOD) were added to 4.0 mM solutions of L_D and DIPEA (2.5 eq.) in MeOD at 298 K. After the addition of 0.5 equivalents of $Hg^{(II)}$, which corresponds to a 1:2 $Hg^{(II)}:L_D$ ratio, distinct signals for a formed complex were observed, although, the residual ligand signals could still be observed. The additions of more aliquots of $Hg^{(II)}$ resulted in the formation of a L_D -Hg 1-1 complex at one equivalent of $Hg^{(II)}$ with no residual signals for

either the ligand or the 1:2 complex. All the protons due to heteroaromatic/aromatic groups were found to be in their expected region. Due to the increased conjugation and coordination with the metal, there is noticeable chemical shift changes for the aromatic protons H4, H6, and H7 of the deprotonated ligand from δ 8.56 ppm, δ 7.79 ppm, δ 6.82 ppm to δ 8.70 ppm, δ 8.14 ppm, δ 6.86 ppm in the complex respectively. In addition, the three signals attributed to DIPEA appearing at δ 3.17 ppm, δ 2.64 ppm, and δ 1.11 ppm for the deprotonated ligand were seen to undergo significant chemical shift changes after addition of 0.5 eq. of Hg^(II) to δ 3.21 ppm, δ 2.72 ppm and δ 1.13 ppm respectively, indicating the presence of the diisopropylethylammonium ions as counter cations to the 1:2 complex with presumed formulation [Hg(L_D)₂]²⁻ (Figure 3.3). The fact that the signals for the complexes and the ligand appear at the same spectra indicates slow exchange at the NMR timescale.

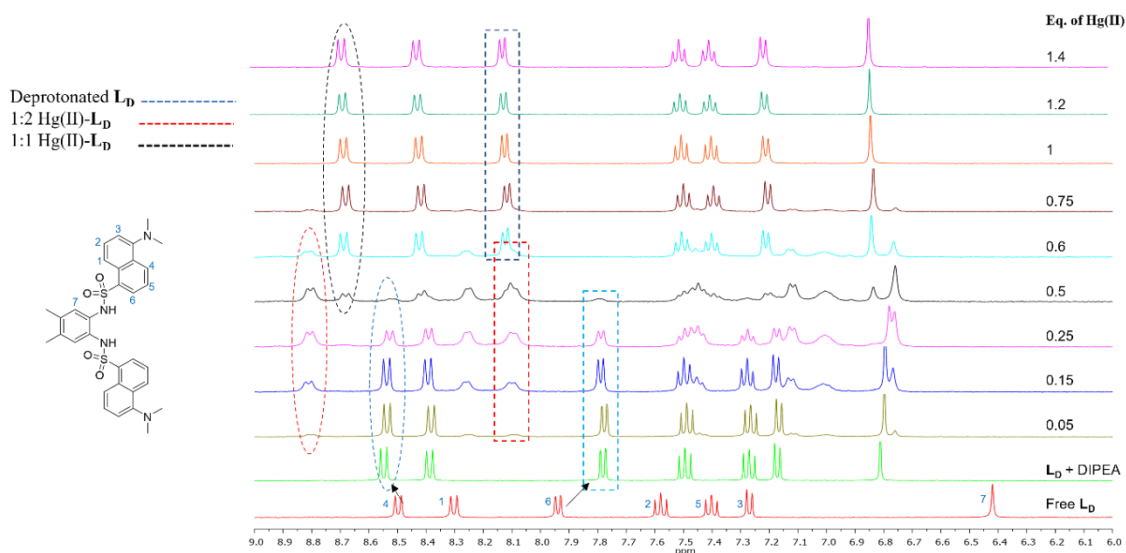


Figure 3.2: ¹H-NMR titration of L_D (4.0 mM) and 2.2 eq. of DIPEA with HgCl₂ in MeOD. Concurrent decrease in ligand signals and the appearance of new complex signals indicates initial 1-2 Hg:L_D complex formation, followed by 1-1 Hg:L_D complex formation.

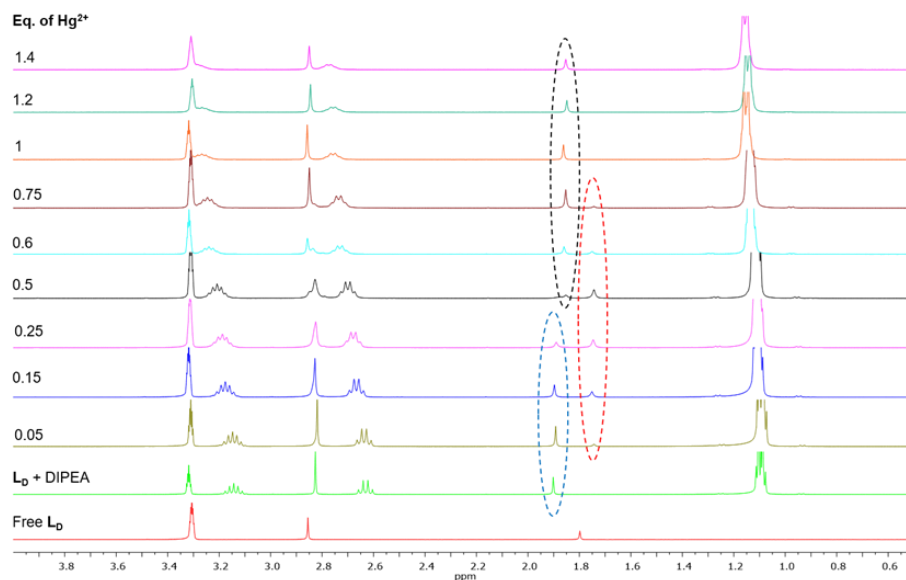


Figure 3.3: Aliphatic region of the ^1H -NMR spectra from the titration of L_D (4.0 mM) and 2.2 eq. of DIPEA with HgCl_2 in MeOD.

The proton-decoupled ^{13}C -NMR spectra for the ligand vs. complex were obtained in MeOD at 298 K. The spectral assignments for both the ligand and the complex are given in the experimental section, and their spectra are provided in Figure 3.4. The carbon signals were found to be in their expected region, supporting the binding modes evidenced by the FT-IR and ^1H -NMR spectral data. Signals due to the aromatic carbons are found in the δ 110-160 ppm region and the aliphatic carbons around δ 20-50 ppm. The carbons of sulfonamidic S and N (-C-SO₂-HN-C-) observed for the ligand at δ 151.34 and δ 138.14 ppm, respectively shifted to δ 152.74 and δ 140.59 ppm in the complex spectra, confirming complex formation.

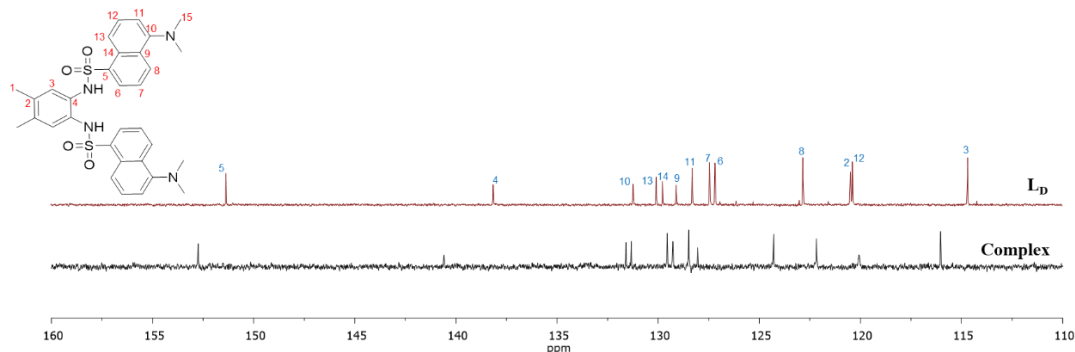


Figure 3.4: $^{13}\text{C}\{-^1\text{H}\}$ -NMR of L_D vs Hg-L_D complex in MeOD at 298 K

3.4.4. UV-Vis spectroscopy

Figure 3.5 (a) and (b) shows the UV-Vis spectra of the titrations of L_D (2.0×10^{-5} M) and DIPEA (5.0×10^{-5} M) with HgCl_2 (4.0×10^{-4} M) in CH_3OH . The ligand maximum absorbance at 252 nm showed an increase, broadening, and a slight blue-shift after titration with $\text{Hg}^{(\text{II})}$ (Figure 3.5a). Furthermore, an absorbance increase was observed at 310 nm, which is attributed to ligand to metal charge transfer. Non-linear regression analysis of the plot of $A_{310\text{nm}}$ vs. $[\text{Hg}^{(\text{II})}]$ (Figure 3.5b) and fitting into the 1:1 binding isotherm gave a binding constant of $K_{11} = 3.6 (\pm 1.1) \times 10^5 \text{ M}^{-1}$ for the formation of the Hg-L_D complex.

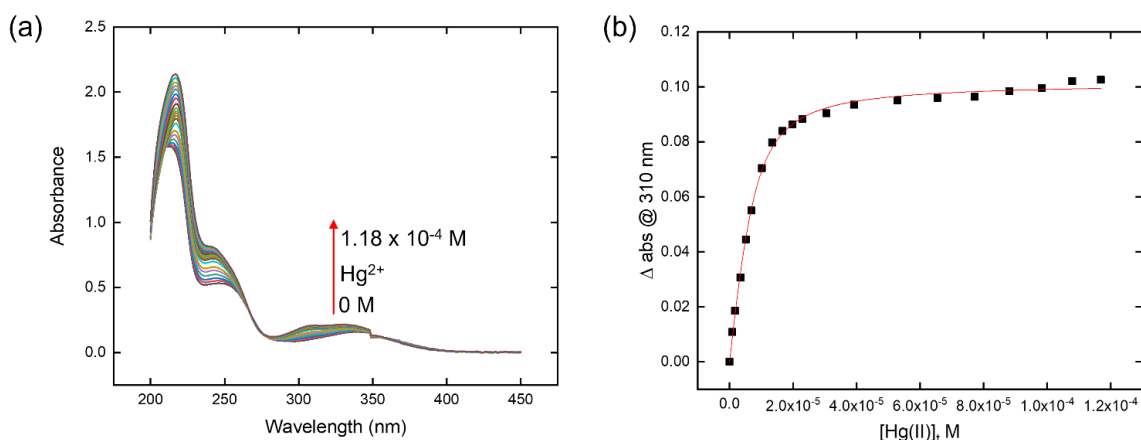


Figure 3.5: UV-Vis spectra of L_D ($2.0 \times 10^{-5} M$) in the presence of DIPEA ($5.0 \times 10^{-5} M$) with gradual addition of $HgCl_2$ (0 - 950 μL of $4.0 \times 10^{-4} M$) in methanol.

3.4.5. Fluorescence spectroscopy

Figure 3.6a shows the fluorescence emission spectrum of L_D and DIPEA at increasing concentrations of $Hg^{(II)}$ when titrating L_D /DIPEA solutions in methanol with $HgCl_2$ solutions. The fluorescence spectrum of L_D ($2.0 \times 10^{-5} M$) and DIPEA (2.5 eq.) in methanolic solution shows emission at 533 nm ($\lambda_{exc} = 334$ nm). The addition of $Hg^{(II)}$ to this solution resulted in the gradual decrease in fluorescence intensity for this emission (fluorescence quenching). This quenching is potentially due to the formation of only a slightly fluorescent $Hg^{(II)}$ complex as a new weak fluorescence emission is observed at 463 nm. Figure 3.6b shows the plot of the fluorescence intensity change at 533 nm vs. the concentration of $Hg^{(II)}$. A well-fitted curve obtained from fitting this plot to the 1-1 binding isotherm shows saturation at $2.0 \times 10^{-5} M$ of $Hg^{(II)}$ ($[L_D] = 2.0 \times 10^{-5} M$), which is indicative of 1:1 $Hg:L_D$ binding stoichiometry. As fluorescence quenching was observed upon the addition of $Hg^{(II)}$, the binding constant was obtained from the Stern-

Volmer equation (Eq. 3). The equation is obtained from the plot of I_0/I ratio as a function of $Hg^{(II)}$ concentration (Figure 3.6c) where I_0 and I are the fluorescence emission intensities at 533 nm in the absence and presence of $Hg^{(II)}$ respectively, $[Q]$ is the concentration of the quencher ($Hg^{(II)}$), K_{SV} is the Stern-Volmer quenching constant, K_q is the bimolecular quenching rate constant and τ_0 is the average lifetime of the fluorophore (**LD**) in the absence of the quencher.

$$I_0/I = K_{SV} [Q] + 1 = K_q \tau_0 [Q] + 1 \quad (3)$$

The obtained K_{SV} from the slope of the linear fit by Eq. (3) gives a value of $2.9 (\pm 0.7) \times 10^5 \text{ M}^{-1}$, which is reasonably close to the association constant, $K_{11} = 3.6 (\pm 1.1) \times 10^5 \text{ M}^{-1}$, obtained from the UV-Vis titration of **LD** with $Hg^{(II)}$. This suggests that there is significant interaction of **LD** with $Hg^{(II)}$, which leads to the quenching of the fluorescence intensity. From the fluorescence titration experiments, an accurate linear equation ($R^2 = 0.9902$) was obtained from the plot of the fluorescence intensity at 533 nm *vs.* the metal concentration (Figure 3.6d). The detection limit for $Hg^{(II)}$ sensing was determined to be $0.78 \mu\text{M}$, with linear range of $0 - 13.4 \mu\text{M}$. The LOD value for $Hg^{(II)}$ is lower than the WHO acceptable limit of inorganic mercury in drinking water ($2.5 \mu\text{M}$),²⁷; therefore, **LD** can be considered a suitable sensor for monitoring of $Hg^{(II)}$ in water samples.

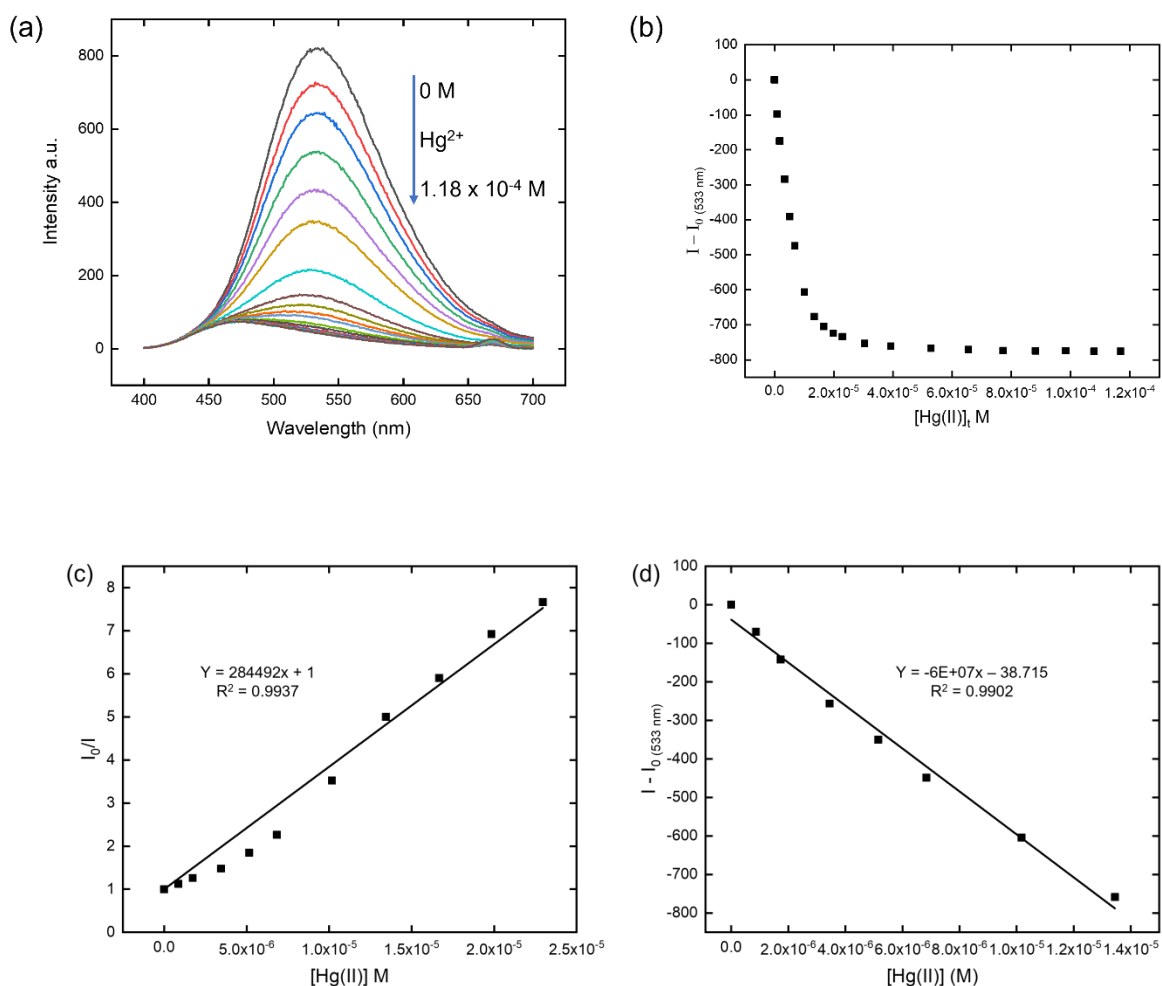


Figure 3.6: Results showing (a) Fluorescence titration spectra of L_D ($2.0 \times 10^{-5} M$) and 2.5 eq. DIPEA with $HgCl_2$ in methanol. $\lambda_{exc} = 334 nm$. (b) Plot of ΔI at 533 nm vs. $Hg^{(II)}$ concentration (c) Stern-Volmer plot for fluorescence quenching of L_D by $Hg^{(II)}$ in methanol, $K_{SV} = 2.8 \times 10^5 M^{-1}$ (d) Linear curve of the fluorescence intensity at 533 nm vs $Hg^{(II)}$ concentration ($0 - 13.4 \mu M$)

The fluorescence responses of L_D with different metals ($0.20 mM$ of Ca^{2+} , K^+ , Cs^+ , Na^+ , and Sr^{2+} added as chloride salts) in comparison to $Hg^{(II)}$ were measured in methanol (Figure 3.7). When various metal chloride salts were added into the ligand solution, only $HgCl_2$ resulted in quenching of the fluorescence emission at 533 nm (λ_{exc}

= 334 nm), whereas none of the other metals had any notable impact on the fluorescence intensity.

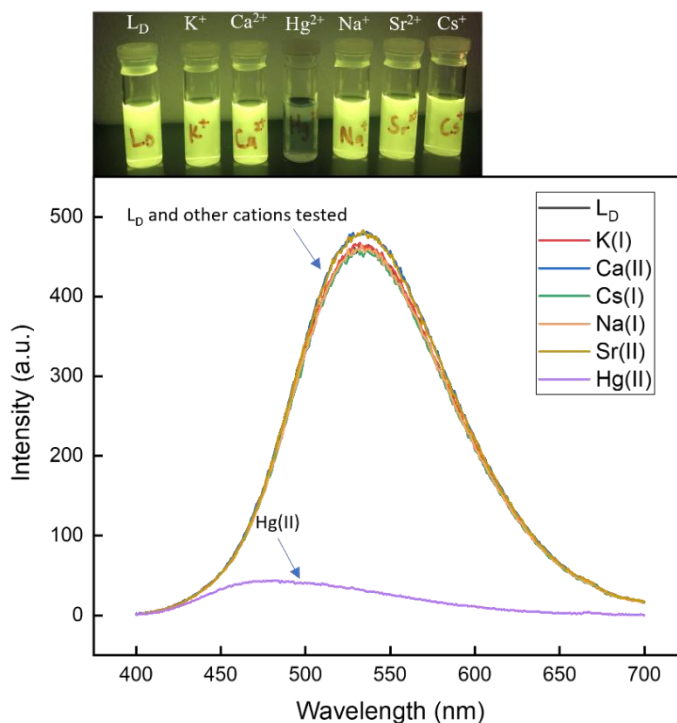


Figure 3.7: Fluorescence spectra of **L_D** (0.10 mM) and 2.5 eq. DIPEA before and after addition of various metals (0.20 mM, added as chloride salts) in methanol. $\lambda_{exc} = 334$ nm.

The continuous variations method²¹ (Job plot) experiment in methanol (0.20 mM) for the binding of **L_D** to Hg^(II) was carried out by monitoring the fluorescence emission at 538 nm ($\lambda_{exc} = 334$ nm) (Figure 3.8). The bell-shaped curve and a maximum at a molar fraction of 0.5 is indicative of 1:1 interaction between **L_D** and Hg^(II). This strongly supports our initial results from both the ¹H-NMR titrations and UV-Vis titrations showing a 1:1 Hg^(II):**L_D** complex formation in CH₃OH.

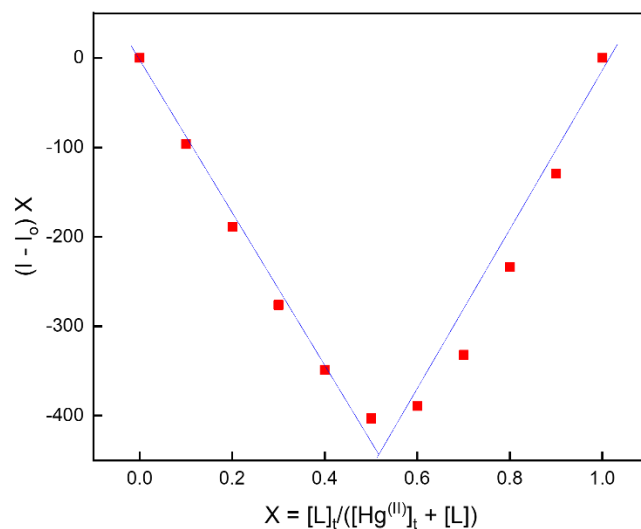


Figure 3.8: Job plot of L_D - $Hg^{(II)}$ complex in methanol. $L_D = 2.0 \times 10^{-3} M$; 2.5 eq. DIPEA; $[Hg^{(II)}]_t = 2.0 \times 10^{-3} M$; $\lambda_{exc} = 334 nm$

3.4.6. Extraction studies

$Hg^{(II)}$ extraction experiments into DCE were carried out either from neutral aqueous phases (in the presence of DIPEA in the organic phase) or at pH 11.0 (NaOH = $10^{-3} M$) with varying concentrations of L_D in dichloroethane. A pH-dependent experiment was also carried out by varying NaOH concentrations in the aqueous phase (pH 7.0 – 14.0) (Figure 3.9a). At 1.0 mM $Hg^{(II)}$ and 2.0 mM L_D , the highest recovery of $Hg^{(II)}$ after stripping was recorded at pH 11.0 with a % recovery of 51.8 %; the low percentage of recovery is attributed to precipitation of the complex in the interphase during the extraction experiments (Figure 3.9b). Further experiments were carried out to determine the binding stoichiometry of L_D to $Hg^{(II)}$ in the absence of an organic base at pH 11.0. At 2.0 mM of L_D , 50.2% of $Hg^{(II)}$ was recovered after only one extraction/stripping cycle (Figure 3.9b).

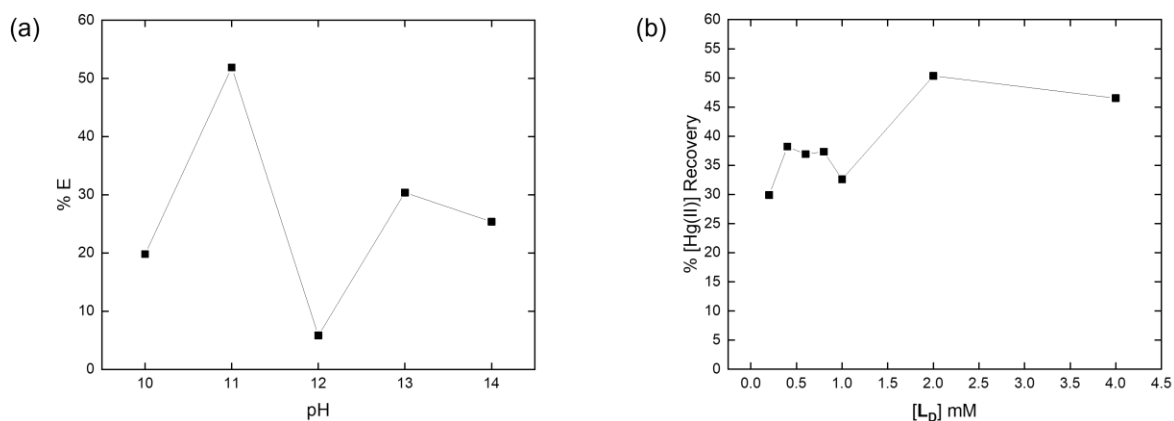


Figure 3.9: Results showing (a) the pH dependent extraction of $\text{Hg}^{(\text{II})}$ by L_D into DCE . Conditions; $[\text{Hg}^{(\text{II})}] = 1.0 \text{ mM}$, $[\text{L}_\text{D}]_i = 2.0 \text{ mM}$ (b) % recovery of $\text{Hg}^{(\text{II})}$ after extraction into DCE and subsequent stripping at various concentrations of L_D . Conditions; $[\text{Hg}^{(\text{II})}]_i = 1.0 \text{ mM}$, $[\text{L}_\text{D}]_i = 0.20 - 4.0 \text{ mM}$, $\text{pH} = 11.0$

Extraction experiments at neutral pH (Figure 3.10 (a) and (b)) in the presence of DIPEA were carried out, with DIPEA used in order to facilitate ligand deprotonation. At 1.0 mM of L_D at neutral pH, 99.2 % of $\text{Hg}^{(\text{II})}$ was extracted. The saturation and maximum extraction at 1.0 mM of the ligand is indicative of 1:1 complex formation. As the ligand concentration increases from 0.3 to 1.0 mM at a constant DIPEA concentration of 5.0 mM, the % Extraction of $\text{Hg}^{(\text{II})}$ increases and becomes essentially quantitative for 1.0 mM of ligand. This result is consistent with the Job plot, $^1\text{H-NMR}$ titration, fluorescence, and the UV-Vis titration results indicating a 1:1 $\text{Hg}:\text{L}_\text{D}$ complex. However, the slope analysis (Figure 3.10b) shows a complex stoichiometry of 1:2, as the slope of the straight line of $\log D_{\text{Hg}}$ vs. $\log [\text{L}_\text{D}]$ was 2.14.

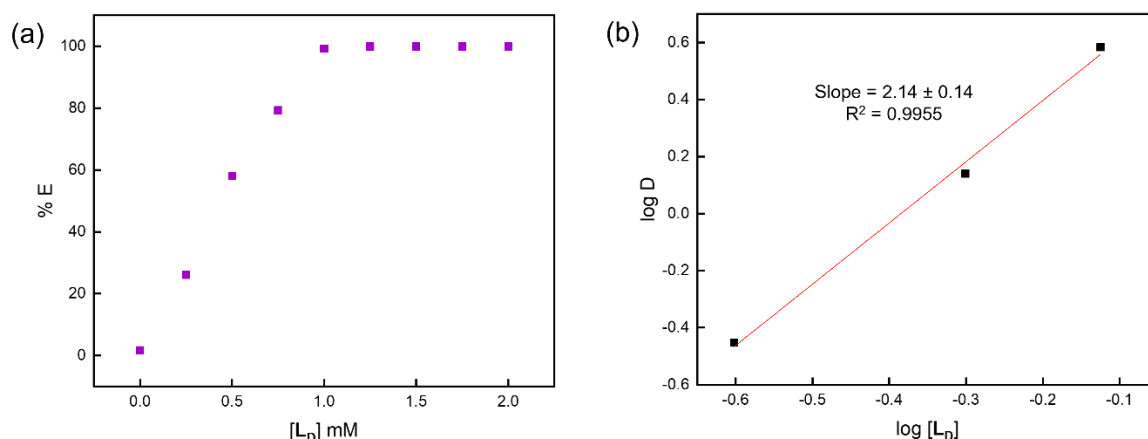


Figure 3.10: Extraction results showing (a) Influence of L_D concentration on $Hg^{(II)}$ extraction efficiency. Conditions; $[Hg^{(II)}]_i = 1.0$ mM, $[L_D]_i = 0.30 - 2.0$ mM, $[DIPEA]_i = 5.0$ mM (b) Relationship between $\log D_{Hg}$ and $\log [L_D]_i$, showing the stoichiometry of the $Hg^{(II)}-L_D$ complexes that are formed at various $Hg^{(II)}:L_D$ ratios.

3.4.7. X-Ray crystallography of L_D

Crystals of L_D suitable for X-ray crystallography were obtained by slow diffusion of hexanes into a dichloromethane solution. Table 3.1 shows the summary of the single-crystal X-ray crystallographic data of L_D , while its structure is shown in Figure 3.11. All bond lengths are within the normal range as expected for L_D . In the structure L_D , all bond lengths were within normal ranges.

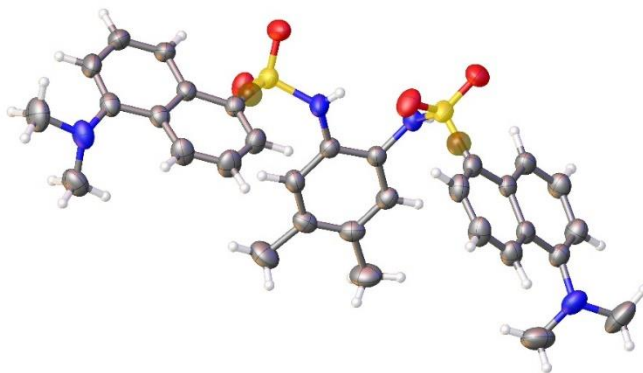


Figure 3.11: ORTEP representation of the X-ray Structure of L_D (50 % probability ellipsoids)

Table 3.1: Crystal data and structure refinement parameters for the complex

Crystal data	
Chemical formula	C ₃₂ H ₃₄ N ₄ O ₄ S ₂
<i>Mr</i>	602.75
Temperature (K)	298
Crystal System , space group	Monoclinic, P2 1/n
<i>a</i> , <i>b</i> , <i>c</i> (Å)	13.6542 (5), 11.1789 (4), 19.5631 (8)
μ (mm ⁻¹)	0.22
β (°)	94.917 (1)
V(Å ³)	2975.10 (19)
<i>Z</i>	4
Crystal size (mm)	0.25 × 0.20 × 0.10
Radiation type	Mo-K α
Data collection	
Diffractometer	Bruker APEX-II CCD Absorption
Absorption correction	Multi-scan SADABS2016/2 (Bruker,2016/2) was used for absorption correction. wR2(int) was 0.0475 before and 0.0386 after correction. The Ratio of minimum to maximum transmission is 0.9584. The $\lambda/2$ correction factor is not present.
<i>T</i> _{min} , <i>T</i> _{max}	0.714, 0.745
Measured Refl.	33127
Independent Refl.	5376
Reflections Used	4977
<i>R</i> _{int}	0.020
Refinement	
<i>R</i> [<i>F</i> ² > 2 σ (<i>F</i> ²)], w <i>R</i> (<i>F</i> ²), <i>S</i>	0.034, 0.095, 1.07
$\Delta\rho_{\max}$, $\Delta\rho_{\min}$ (e Å ⁻³)	0.23, -0.31

Table 3.2: Fractional atomic coordinates and isotropic or equivalent isotropic displacement parameters (Å²)

	<i>x</i>	<i>y</i>	<i>z</i>	<i>U</i> _{iso} */ <i>U</i> _{eq}
S1	0.01447 (3)	0.46944 (3)	0.30752 (2)	0.04541 (12)
S2	0.19346 (3)	0.71061 (3)	0.49198 (2)	0.04196 (12)
O4	0.17562 (8)	0.69148 (11)	0.56213 (6)	0.0531 (3)
O2	0.09954 (10)	0.54409 (11)	0.30554 (6)	0.0590 (3)
O1	-0.07712 (10)	0.50892 (11)	0.27513 (7)	0.0641 (4)
O3	0.15464 (9)	0.81438 (10)	0.45736 (7)	0.0601 (3)
N2	-0.00329 (10)	0.45204 (12)	0.38820 (7)	0.0406 (3)
N3	0.14960 (10)	0.59792 (12)	0.44777 (8)	0.0456 (3)
C30	0.38063 (11)	0.79440 (13)	0.52761 (7)	0.0372 (3)
N1	-0.00800 (11)	-0.09683 (13)	0.23378 (8)	0.0556 (4)
N4	0.64883 (10)	0.84195 (15)	0.57376 (7)	0.0534 (4)
C18	0.14132 (10)	0.47871 (13)	0.47048 (7)	0.0370 (3)
C25	0.48448 (11)	0.78480 (13)	0.52712 (7)	0.0399 (3)

C13	0.06946 (10)	0.40478 (13)	0.43827 (7)	0.0358 (3)
C1	0.04584 (11)	0.32834 (14)	0.27449 (7)	0.0410 (3)
C10	-0.02170 (11)	0.23023 (13)	0.27239 (7)	0.0374 (3)
C5	0.01385 (11)	0.11739 (14)	0.25139 (7)	0.0391 (3)
C21	0.32249 (11)	0.70832 (13)	0.48804 (7)	0.0382 (3)
C14	0.06266 (11)	0.28724 (14)	0.45969 (8)	0.0419 (3)
C26	0.54632 (11)	0.86403 (14)	0.56909 (8)	0.0433 (3)
C15	0.12140 (12)	0.24168 (14)	0.51475 (8)	0.0458 (4)
C29	0.34098 (13)	0.88768 (14)	0.56544 (9)	0.0455 (4)
C9	-0.12021 (12)	0.23870 (15)	0.28924 (8)	0.0447 (4)
C22	0.36368 (13)	0.62552 (15)	0.44811 (8)	0.0478 (4)
C17	0.20202 (11)	0.43242 (15)	0.52481 (8)	0.0432 (3)
C6	-0.04852 (12)	0.01476 (14)	0.25126 (8)	0.0429 (3)
C16	0.19109 (11)	0.31666 (15)	0.54848 (8)	0.0453 (4)
C4	0.10925 (12)	0.10991 (16)	0.22840 (8)	0.0483 (4)
C7	-0.14367 (13)	0.02815 (16)	0.26675 (9)	0.0497 (4)
C27	0.50426 (13)	0.95557 (15)	0.60230 (9)	0.0509 (4)
C2	0.13804 (13)	0.31649 (17)	0.25302 (8)	0.0501 (4)
C24	0.52377 (13)	0.69946 (17)	0.48402 (9)	0.0518 (4)
C28	0.40206 (14)	0.96682 (15)	0.60005 (10)	0.0534 (4)
C8	-0.17884 (12)	0.14013 (16)	0.28551 (9)	0.0500 (4)
C3	0.16883 (13)	0.20692 (18)	0.22835 (9)	0.0551 (4)
C23	0.46574 (13)	0.62284 (18)	0.44505 (9)	0.0568 (4)
C19	0.25440 (19)	0.2760 (2)	0.61089 (12)	0.0688 (6)
C20	0.1072 (2)	0.11394 (19)	0.53673 (15)	0.0706 (6)
C32	0.67665 (15)	0.7320 (2)	0.61066 (12)	0.0640 (5)
C31	0.71087 (17)	0.9407 (3)	0.60011 (13)	0.0740 (6)
C11	0.0580 (2)	-0.1468 (2)	0.28906 (15)	0.0814 (7)
C12	-0.0787 (2)	-0.1863 (2)	0.20748 (18)	0.0852 (8)
H9	-0.1465 (13)	0.3162 (17)	0.3023 (9)	0.053 (5)*
H14	0.0149 (14)	0.2378 (17)	0.4383 (9)	0.052 (5)*
H3	0.1282 (15)	0.6124 (19)	0.4115 (11)	0.061 (6)*
H22	0.3237 (14)	0.5683 (17)	0.4220 (10)	0.055 (5)*
H28	0.3745 (14)	1.0290 (18)	0.6281 (10)	0.062 (5)*
H7	-0.1898 (15)	-0.0391 (18)	0.2656 (10)	0.062 (5)*
H29	0.2754 (14)	0.8948 (16)	0.5663 (9)	0.053 (5)*
H2A	0.1792 (13)	0.3840 (17)	0.2552 (9)	0.053 (5)*
H4	0.1290 (12)	0.0326 (16)	0.2108 (9)	0.045 (4)*

H27	0.5428 (14)	1.0105 (18)	0.6291 (10)	0.057 (5)*
H2	-0.0572 (15)	0.4274 (17)	0.3923 (10)	0.053 (5)*
H24	0.5913 (17)	0.6974 (19)	0.4821 (11)	0.071 (6)*
H3A	0.2314 (17)	0.1994 (19)	0.2140 (11)	0.075 (6)*
H17	0.2517 (13)	0.4826 (16)	0.5478 (9)	0.047 (4)*
H23	0.4948 (15)	0.5650 (19)	0.4145 (11)	0.068 (6)*
H8	-0.2450 (15)	0.1506 (17)	0.2960 (10)	0.060 (5)*
H31A	0.7032 (16)	0.957 (2)	0.6540 (13)	0.083 (7)*
H32A	0.6338 (18)	0.665 (2)	0.5953 (12)	0.085 (7)*
H32B	0.6686 (16)	0.744 (2)	0.6603 (12)	0.074 (6)*
H32C	0.7443 (19)	0.713 (2)	0.6049 (12)	0.084 (7)*
H31B	0.689 (2)	1.014 (3)	0.5757 (16)	0.109 (10)*
H31C	0.780 (2)	0.915 (2)	0.5954 (14)	0.103 (8)*
H19A	0.295 (2)	0.212 (3)	0.5986 (15)	0.107 (9)*
H19B	0.3073 (19)	0.334 (2)	0.6266 (12)	0.085 (7)*
H19C	0.218 (2)	0.257 (3)	0.6464 (16)	0.109 (9)*
H20A	0.164 (3)	0.072 (3)	0.5378 (17)	0.124 (11)*
H20B	0.061 (3)	0.074 (3)	0.5043 (18)	0.131 (12)*
H20C	0.089 (2)	0.105 (3)	0.5811 (19)	0.125 (11)*
H12A	-0.125 (2)	-0.145 (2)	0.1703 (15)	0.097 (9)*
H12B	-0.121 (2)	-0.213 (2)	0.2435 (15)	0.100 (9)*
H11A	0.108 (2)	-0.088 (3)	0.3090 (17)	0.127 (12)*
H12C	-0.0433 (19)	-0.250 (3)	0.1893 (14)	0.095 (8)*
H11B	0.024 (2)	-0.174 (3)	0.3322 (17)	0.117 (10)*
H11C	0.092 (2)	-0.212 (3)	0.2726 (16)	0.119 (10)*

Table 3.3: Atomic displacement parameters (\AA^2)

	U^{11}	U^{22}	U^{33}	U^{12}	U^{13}	U^{23}
S1	0.0577 (3)	0.0359 (2)	0.0406 (2)	-0.00319 (16)	-0.00710 (17)	0.00136 (15)
S2	0.0383 (2)	0.0372 (2)	0.0492 (2)	-0.00221 (14)	-0.00281 (15)	-0.00540 (15)
O4	0.0466 (6)	0.0614 (7)	0.0523 (7)	-0.0094 (5)	0.0100 (5)	-0.0143 (6)
O2	0.0794 (9)	0.0458 (7)	0.0517 (7)	-0.0203 (6)	0.0043 (6)	0.0009 (5)
O1	0.0773 (9)	0.0503 (7)	0.0596 (8)	0.0118 (6)	-0.0242 (6)	0.0028 (6)
O3	0.0522 (7)	0.0388 (6)	0.0854 (9)	0.0014 (5)	-0.0173 (6)	-0.0005 (6)
N2	0.0364 (7)	0.0414 (7)	0.0430 (7)	-0.0007 (5)	-0.0030 (5)	-0.0041 (5)
N3	0.0520 (8)	0.0382 (7)	0.0439 (7)	-0.0068 (6)	-0.0122 (6)	0.0012 (6)
C30	0.0398 (7)	0.0359 (7)	0.0349 (7)	0.0007 (6)	-0.0019 (6)	0.0029 (6)
N1	0.0626 (9)	0.0416 (7)	0.0635 (9)	-0.0009 (7)	0.0114 (7)	-0.0131 (7)
N4	0.0384 (7)	0.0708 (10)	0.0501 (8)	-0.0096 (7)	-0.0005 (6)	-0.0001 (7)
C18	0.0371 (7)	0.0353 (7)	0.0384 (7)	0.0002 (6)	0.0029 (6)	-0.0022 (6)
C25	0.0409 (8)	0.0437 (8)	0.0347 (7)	-0.0016 (6)	0.0002 (6)	0.0035 (6)
C13	0.0335 (7)	0.0380 (7)	0.0358 (7)	0.0020 (6)	0.0029 (5)	-0.0033 (6)
C1	0.0471 (8)	0.0426 (8)	0.0322 (7)	-0.0040 (7)	-0.0031 (6)	-0.0015 (6)
C10	0.0398 (8)	0.0417 (8)	0.0296 (7)	-0.0008 (6)	-0.0032 (5)	-0.0027 (6)
C5	0.0404 (8)	0.0448 (8)	0.0315 (7)	-0.0009 (6)	-0.0003 (6)	-0.0049 (6)
C21	0.0406 (8)	0.0372 (7)	0.0360 (7)	-0.0015 (6)	-0.0009 (6)	-0.0003 (6)
C14	0.0399 (8)	0.0377 (8)	0.0485 (8)	-0.0027 (6)	0.0060 (6)	-0.0035 (6)
C26	0.0430 (8)	0.0477 (8)	0.0384 (7)	-0.0067 (7)	-0.0020 (6)	0.0058 (7)
C15	0.0468 (9)	0.0403 (8)	0.0517 (9)	0.0060 (7)	0.0115 (7)	0.0055 (7)

C29	0.0435 (9)	0.0380 (8)	0.0530 (9)	0.0066 (7)	-0.0065 (7)	-0.0051 (7)
C9	0.0416 (8)	0.0469 (9)	0.0450 (8)	0.0042 (7)	-0.0009 (6)	-0.0076 (7)
C22	0.0508 (9)	0.0504 (9)	0.0418 (8)	-0.0035 (7)	0.0026 (7)	-0.0109 (7)
C17	0.0392 (8)	0.0475 (9)	0.0417 (8)	-0.0006 (7)	-0.0024 (6)	-0.0019 (7)
C6	0.0489 (9)	0.0419 (8)	0.0378 (8)	-0.0020 (7)	0.0031 (6)	-0.0065 (6)
C16	0.0433 (8)	0.0504 (9)	0.0426 (8)	0.0089 (7)	0.0050 (6)	0.0052 (7)
C4	0.0440 (8)	0.0569 (10)	0.0444 (8)	0.0020 (7)	0.0053 (7)	-0.0118 (7)
C7	0.0479 (9)	0.0479 (9)	0.0536 (9)	-0.0087 (7)	0.0061 (7)	-0.0043 (7)
C27	0.0540 (10)	0.0420 (9)	0.0538 (10)	-0.0072 (7)	-0.0118 (8)	-0.0032 (7)
C2	0.0474 (9)	0.0585 (10)	0.0439 (8)	-0.0147 (8)	0.0013 (7)	-0.0037 (7)
C24	0.0420 (9)	0.0684 (11)	0.0457 (9)	0.0014 (8)	0.0073 (7)	-0.0075 (8)
C28	0.0584 (10)	0.0383 (8)	0.0610 (10)	0.0082 (7)	-0.0098 (8)	-0.0096 (7)
C8	0.0383 (8)	0.0560 (10)	0.0560 (9)	-0.0016 (7)	0.0059 (7)	-0.0049 (8)
C3	0.0411 (9)	0.0730 (12)	0.0520 (10)	-0.0074 (8)	0.0094 (7)	-0.0125 (9)
C23	0.0540 (10)	0.0680 (11)	0.0496 (9)	0.0033 (9)	0.0104 (8)	-0.0185 (9)
C19	0.0674 (13)	0.0784 (15)	0.0585 (12)	0.0076 (12)	-0.0064 (10)	0.0211 (11)
C20	0.0811 (15)	0.0472 (11)	0.0837 (16)	0.0028 (11)	0.0075 (13)	0.0191 (10)
C32	0.0439 (10)	0.0817 (14)	0.0650 (12)	0.0108 (10)	-0.0026 (9)	0.0007 (11)
C31	0.0527 (12)	0.0922 (17)	0.0757 (15)	-0.0252 (12)	-0.0026 (10)	-0.0047 (13)
C11	0.0955 (18)	0.0586 (13)	0.0905 (17)	0.0281 (13)	0.0104 (14)	0.0026 (12)
C12	0.0921 (18)	0.0546 (13)	0.112 (2)	-0.0181 (13)	0.0266 (17)	-0.0375 (14)

Table 3.4: Geometric parameters (Å, °)

S1—O2	1.4334 (13)	C9—C8	1.360 (2)
S1—O1	1.4228 (13)	C9—H9	0.980 (19)
S1—N2	1.6289 (14)	C22—C23	1.400 (2)
S1—C1	1.7710 (16)	C22—H22	0.959 (19)
S2—O4	1.4302 (12)	C17—C16	1.387 (2)
S2—O3	1.4226 (12)	C17—H17	0.962 (18)
S2—N3	1.6139 (13)	C6—C7	1.367 (2)
S2—C21	1.7704 (15)	C16—C19	1.505 (2)
N2—C13	1.4348 (18)	C4—C3	1.356 (3)
N2—H2	0.80 (2)	C4—H4	0.978 (18)
N3—C18	1.412 (2)	C7—C8	1.401 (2)
N3—H3	0.76 (2)	C7—H7	0.98 (2)
C30—C25	1.423 (2)	C27—C28	1.398 (3)
C30—C21	1.432 (2)	C27—H27	0.94 (2)
C30—C29	1.413 (2)	C2—C3	1.395 (3)
N1—C6	1.418 (2)	C2—H2A	0.940 (19)
N1—C11	1.459 (3)	C24—C23	1.356 (3)
N1—C12	1.454 (3)	C24—H24	0.93 (2)
N4—C26	1.416 (2)	C28—H28	0.98 (2)
N4—C32	1.459 (3)	C8—H8	0.95 (2)
N4—C31	1.459 (3)	C3—H3A	0.93 (2)

C18—C13	1.392 (2)	C23—H23	0.99 (2)
C18—C17	1.390 (2)	C19—H19A	0.95 (3)
C25—C26	1.433 (2)	C19—H19B	1.00 (3)
C25—C24	1.409 (2)	C19—H19C	0.91 (3)
C13—C14	1.385 (2)	C20—H20A	0.90 (4)
C1—C10	1.431 (2)	C20—H20B	0.97 (4)
C1—C2	1.367 (2)	C20—H20C	0.93 (4)
C10—C5	1.425 (2)	C32—H32A	0.98 (3)
C10—C9	1.415 (2)	C32—H32B	1.00 (2)
C5—C6	1.429 (2)	C32—H32C	0.96 (3)
C5—C4	1.417 (2)	C31—H31A	1.08 (3)
C21—C22	1.363 (2)	C31—H31B	0.98 (3)
C14—C15	1.384 (2)	C31—H31C	1.00 (3)
C14—H14	0.927 (19)	C11—H11A	1.00 (3)
C26—C27	1.365 (2)	C11—H11B	1.05 (3)
C15—C16	1.391 (2)	C11—H11C	0.94 (3)
C15—C20	1.509 (2)	C12—H12A	1.03 (3)
C29—C28	1.356 (2)	C12—H12B	1.00 (3)
C29—H29	0.900 (19)	C12—H12C	0.95 (3)
O2—S1—N2	106.49 (7)	N1—C6—C5	117.51 (14)
O2—S1—C1	106.67 (8)	C7—C6—N1	123.19 (15)
O1—S1—O2	119.39 (8)	C7—C6—C5	119.29 (14)
O1—S1—N2	105.69 (8)	C15—C16—C19	121.64 (17)
O1—S1—C1	110.16 (7)	C17—C16—C15	119.52 (14)
N2—S1—C1	107.93 (7)	C17—C16—C19	118.84 (17)
O4—S2—N3	108.16 (7)	C5—C4—H4	117.0 (10)
O4—S2—C21	106.95 (7)	C3—C4—C5	121.42 (16)
O3—S2—O4	119.44 (8)	C3—C4—H4	121.6 (10)
O3—S2—N3	105.99 (7)	C6—C7—C8	120.63 (15)
O3—S2—C21	108.82 (7)	C6—C7—H7	122.1 (12)
N3—S2—C21	106.87 (7)	C8—C7—H7	117.2 (12)
S1—N2—H2	110.8 (14)	C26—C27—C28	120.79 (15)
C13—N2—S1	123.62 (11)	C26—C27—H27	121.1 (12)
C13—N2—H2	113.3 (14)	C28—C27—H27	118.0 (12)
S2—N3—H3	115.4 (16)	C1—C2—C3	120.28 (16)
C18—N3—S2	127.15 (11)	C1—C2—H2A	118.1 (11)
C18—N3—H3	117.3 (16)	C3—C2—H2A	121.6 (11)
C25—C30—C21	116.89 (13)	C25—C24—H24	118.2 (13)
C29—C30—C25	119.08 (14)	C23—C24—C25	121.99 (16)
C29—C30—C21	124.02 (14)	C23—C24—H24	119.8 (13)
C6—N1—C11	112.79 (16)	C29—C28—C27	121.77 (16)
C6—N1—C12	115.42 (17)	C29—C28—H28	119.5 (12)
C12—N1—C11	110.4 (2)	C27—C28—H28	118.4 (12)
C26—N4—C32	113.11 (14)	C9—C8—C7	121.64 (15)
C26—N4—C31	115.57 (17)	C9—C8—H8	117.0 (12)
C31—N4—C32	110.13 (17)	C7—C8—H8	121.3 (12)
C13—C18—N3	119.35 (13)	C4—C3—C2	120.24 (16)
C17—C18—N3	122.21 (13)	C4—C3—H3A	119.8 (14)

C17—C18—C13	118.43 (14)	C2—C3—H3A	119.9 (14)
C30—C25—C26	119.22 (14)	C22—C23—H23	119.5 (12)
C24—C25—C30	119.06 (14)	C24—C23—C22	119.88 (16)
C24—C25—C26	121.70 (14)	C24—C23—H23	120.6 (12)
C18—C13—N2	120.69 (13)	C16—C19—H19A	109.3 (17)
C14—C13—N2	119.71 (13)	C16—C19—H19B	113.7 (14)
C14—C13—C18	119.30 (13)	C16—C19—H19C	111.8 (18)
C10—C1—S1	121.17 (12)	H19A—C19—H19B	98 (2)
C2—C1—S1	117.14 (12)	H19A—C19—H19C	113 (2)
C2—C1—C10	121.66 (15)	H19B—C19—H19C	110 (2)

C5—C10—C1	116.88 (13)	C15—C20—H20A	111 (2)
C9—C10—C1	124.40 (14)	C15—C20—H20B	110 (2)
C9—C10—C5	118.72 (14)	C15—C20—H20C	115 (2)
C10—C5—C6	119.58 (13)	H20A—C20—H20B	107 (3)
C4—C5—C10	119.28 (14)	H20A—C20—H20C	103 (3)
C4—C5—C6	121.09 (14)	H20B—C20—H20C	110 (3)
C30—C21—S2	118.32 (11)	N4—C32—H32A	111.7 (14)
C22—C21—S2	119.72 (12)	N4—C32—H32B	109.0 (13)
C22—C21—C30	121.95 (14)	N4—C32—H32C	109.6 (14)
C13—C14—H14	119.5 (11)	H32A—C32—H32B	106.6 (19)
C15—C14—C13	122.37 (15)	H32A—C32—H32C	111 (2)
C15—C14—H14	118.0 (11)	H32B—C32—H32C	109.2 (18)
N4—C26—C25	117.37 (14)	N4—C31—H31A	111.5 (13)
C27—C26—N4	123.62 (15)	N4—C31—H31B	108.3 (17)
C27—C26—C25	119.01 (14)	N4—C31—H31C	106.0 (16)
C14—C15—C16	118.33 (14)	H31A—C31—H31B	107 (2)
C14—C15—C20	119.36 (18)	H31A—C31—H31C	108 (2)
C16—C15—C20	122.31 (17)	H31B—C31—H31C	116 (2)
C30—C29—H29	120.1 (12)	N1—C11—H11A	113.0 (19)
C28—C29—C30	119.73 (16)	N1—C11—H11B	114.7 (16)
C28—C29—H29	120.2 (12)	N1—C11—H11C	109.7 (19)
C10—C9—H9	119.8 (11)	H11A—C11—H11B	102 (3)
C8—C9—C10	120.00 (15)	H11A—C11—H11C	108 (3)
C8—C9—H9	120.2 (11)	H11B—C11—H11C	109 (2)
C21—C22—C23	120.00 (15)	N1—C12—H12A	106.6 (15)
C21—C22—H22	120.9 (11)	N1—C12—H12B	111.6 (16)
C23—C22—H22	119.1 (11)	N1—C12—H12C	107.6 (16)
C18—C17—H17	119.4 (10)	H12A—C12—H12B	106 (2)
C16—C17—C18	121.90 (15)	H12A—C12—H12C	112 (2)
C16—C17—H17	118.7 (10)	H12B—C12—H12C	113 (2)
S1—N2—C13—C18	84.18 (16)	C1—C10—C5—C6	177.13 (13)
S1—N2—C13—C14	-102.09 (15)	C1—C10—C5—C4	-5.3 (2)
S1—C1—C10—C5	-173.87 (10)	C1—C10—C9—C8	179.87 (15)
S1—C1—C10—C9	6.5 (2)	C1—C2—C3—C4	-3.0 (3)
S1—C1—C2—C3	178.08 (13)	C10—C1—C2—C3	-0.1 (2)
S2—N3—C18—C13	154.09 (12)	C10—C5—C6—N1	-176.43 (13)
S2—N3—C18—C17	-25.1 (2)	C10—C5—C6—C7	4.5 (2)
S2—C21—C22—C23	-179.67 (14)	C10—C5—C4—C3	2.5 (2)
O4—S2—N3—C18	-29.99 (16)	C10—C9—C8—C7	1.5 (3)
O4—S2—C21—C30	-59.72 (13)	C5—C10—C9—C8	0.3 (2)
O4—S2—C21—C22	120.07 (13)	C5—C6—C7—C8	-2.8 (2)
O2—S1—N2—C13	-56.60 (14)	C5—C4—C3—C2	1.8 (3)
O2—S1—C1—C10	176.90 (11)	C21—S2—N3—C18	84.85 (15)
O2—S1—C1—C2	-1.29 (14)	C21—C30—C25—C26	-176.25 (13)
O1—S1—N2—C13	175.46 (12)	C21—C30—C25—C24	5.3 (2)
O1—S1—C1—C10	-52.13 (14)	C21—C30—C29—C28	-178.37 (15)
O1—S1—C1—C2	129.68 (13)	C21—C22—C23—C24	2.7 (3)
O3—S2—N3—C18	-159.20 (14)	C14—C15—C16—C17	-2.2 (2)
O3—S2—C21—C30	70.58 (13)	C14—C15—C16—C19	176.95 (18)
O3—S2—C21—C22	-109.63 (14)	C26—C25—C24—C23	178.85 (17)
N2—S1—C1—C10	62.80 (13)	C26—C27—C28—C29	0.4 (3)

N2—S1—C1—C2	-115.39 (13)	C29—C30—C25—C26	4.8 (2)
N2—C13—C14—C15	-170.18 (14)	C29—C30—C25—C24	-173.69 (15)
N3—S2—C21—C30	-175.38 (11)	C29—C30—C21—S2	-5.4 (2)
N3—S2—C21—C22	4.42 (15)	C29—C30—C21—C22	174.84 (16)
N3—C18—C13—N2	-7.5 (2)	C9—C10—C5—C6	-3.3 (2)
N3—C18—C13—C14	178.74 (14)	C9—C10—C5—C4	174.28 (14)
N3—C18—C17—C16	177.57 (14)	C17—C18—C13—N2	171.73 (13)
C30—C25—C26—N4	172.31 (13)	C17—C18—C13—C14	-2.0 (2)
C30—C25—C26—C27	-7.5 (2)	C6—C5—C4—C3	179.97 (16)
C30—C25—C24—C23	-2.7 (3)	C6—C7—C8—C9	-0.2 (3)
C30—C21—C22—C23	0.1 (3)	C4—C5—C6—N1	6.1 (2)
C30—C29—C28—C27	-3.2 (3)	C4—C5—C6—C7	-172.98 (15)
N1—C6—C7—C8	178.21 (16)	C2—C1—C10—C5	4.2 (2)
N4—C26—C27—C28	-174.79 (16)	C2—C1—C10—C9	-175.35 (15)
C18—C13—C14—C15	3.6 (2)	C24—C25—C26—N4	-9.3 (2)
C18—C17—C16—C15	3.8 (2)	C24—C25—C26—C27	170.87 (16)
C18—C17—C16—C19	-175.36 (17)	C20—C15—C16—C17	178.57 (18)
C25—C30—C21—S2	175.68 (10)	C20—C15—C16—C19	-2.3 (3)
C25—C30—C21—C22	-4.1 (2)	C32—N4—C26—C25	-68.30 (19)
C25—C30—C29—C28	0.5 (2)	C32—N4—C26—C27	111.5 (2)
C25—C26—C27—C28	5.0 (2)	C31—N4—C26—C25	163.46 (16)
C25—C24—C23—C22	-1.4 (3)	C31—N4—C26—C27	-16.7 (2)
C13—C18—C17—C16	-1.7 (2)	C11—N1—C6—C5	75.6 (2)
C13—C14—C15—C16	-1.5 (2)	C11—N1—C6—C7	-105.3 (2)
C13—C14—C15—C20	177.76 (17)	C12—N1—C6—C5	-156.2 (2)
C1—S1—N2—C13	57.62 (14)	C12—N1—C6—C7	22.8 (3)

3.4 Conclusions

In conclusion, a bis-dansylamide ligand **L_D** was reported as a fluorescence chemosensor for detecting Hg^(II) at a detection limit as low as 0.78 μM. Fluorescence quenching was observed after the addition of Hg^(II) to **L_D** in the presence of DIPEA, while no changes were observed when competing metals, such as Sr^(II), Cs^(I), K^(I), Na^(I), and Ca^(II) were added. Furthermore, we investigated the Hg^(II) extraction behavior for this chemosensor and obtained efficient Hg^(II) extraction at both neutral and alkaline pHs with up to 99.9% of Hg^(II) recovered into 1,2-dichloroethane. We obtained NMR spectroscopic evidence for the formation of both 1:1 and 1:2 complexes in CD₃OD. Non-linear regression analysis of UV-Vis titration curves and Stern-Volmer plot analysis of fluorescence titrations gave binding constants in the range of 10⁵ M⁻¹ for 1:1 complex formation.

3.5 Acknowledgments

This research project was supported by the US Department of Energy Minority Serving Institution Partnership Program (MSIPP) managed by the Savannah River National Laboratory under SRNS contract BOA No: 541, TOA No. 0000332972 and 0000403067 to FIU. We also acknowledge the financial support of the Florida International University Dissertation Year Fellowship for Adenike Fasiku (DYF Spring/Summer 2021 Fellow).

3.6 References

- (1) Bannochie, C. J.; Fellingner, T. L.; Garcia-Strickland, P.; Shah, H. B.; Jain, V.; Wilmarth, W. R. Mercury in Aqueous Tank Waste at the Savannah River Site: Facts, Forms, and Impacts. *Sep. Sci. Technol.* **2018**, *53*, 1935–1947.

- (2) Wanichacheva, N.; Watpathomsub, S.; Lee, V. S.; Grudpan, K. Synthesis of a Novel Fluorescent Sensor Bearing Dansyl Fluorophores for the Highly Selective Detection of Mercury (II) Ions. *Molecules* **2010**, *15*, 1798–1810.
- (3) Shankar, B. H.; Ramaiah, D. Dansyl—Naphthalimide Dyads As Molecular Probes: Effect of Spacer Group on Metal Ion Binding Properties. *J. Phys. Chem. B* **2011**, *115*, 13292–13299.
- (4) Tharmaraj, V.; Pitchumani, K. An Acyclic, Dansyl Based Colorimetric and Fluorescent Chemosensor for Hg(II) via Twisted Intramolecular Charge Transfer (TICT). *Anal. Chim. Acta* **2012**, *751*, 171–175.
- (5) Zhao, Y.; Lin, Z.; He, C.; Wu, H.; Duan, C. A “Turn-On” Fluorescent Sensor for Selective Hg(II) Detection in Aqueous Media Based on Metal-Induced Dye Formation. *Inorg. Chem.* **2006**, *45*, 10013–10015.
- (6) Wu, H.; Zhou, P.; Wang, J.; Zhao, L.; Duan, C. Dansyl-Based Fluorescent Chemosensors for Selective Responses of Cr(III). *New J. Chem.* **2009**, *33*, 653–658.
- (7) Chae, J. B.; Yun, D.; Lee, H.; Lee, H.; Kim, K.-T.; Kim, C. Highly Sensitive Dansyl-Based Chemosensor for Detection of Cu²⁺ in Aqueous Solution and Zebrafish. *ACS Omega* **2019**, *4*, 12537–12543.
- (8) Piao, J.; Lv, J.; Zhou, X.; Zhao, T.; Wu, X. A Dansyl–Rhodamine Chemosensor for Fe(III) Based on off–on FRET. *Spectrochim. Acta. A. Mol. Biomol. Spectrosc.* **2014**, *128*, 475–480.
- (9) Wang, P.; Zhou, D.; Chen, B. High Selective and Sensitive Detection of Zn(II) Using Tetrapeptide-Based Dansyl Fluorescent Chemosensor and Its Application in Cell Imaging. *Spectrochim. Acta. A. Mol. Biomol. Spectrosc.* **2018**, *204*, 735–742.
- (10) Maity, D.; Govindaraju, T. Pyrrolidine Constrained Bipyridyl-Dansyl Click Fluoroionophore as Selective Al³⁺-sensor. *Chem. Commun.* **2010**, *46*, 4499–4501.
- (11) Fu, L.; Mei, J.; Zhang, J.-T.; Liu, Y.; Jiang, F.-L. Selective and Sensitive Fluorescent Turn-off Chemosensors for Fe³⁺. *Luminescence* **2013**, *28*, 602–606.
- (12) Nishiyabu, R.; Kobayashi, H.; Kubo, Y. Dansyl-Containing Boronate Hydrogel Film as Fluorescent Chemosensor of Copper Ions in Water. *RSC Adv.* **2012**, *2*, 6555–6561.
- (13) Li, G.-K.; Liu, M.; Yang, G.-Q.; Chen, C.-F.; Huang, Z.-T. An Effective Hg²⁺-Selective Fluorescent Chemosensor Based on a Calix[4]Arene Bearing Four Dansyl Amides. *Chin. J. Chem.* **2008**, *26*, 1440–1446.

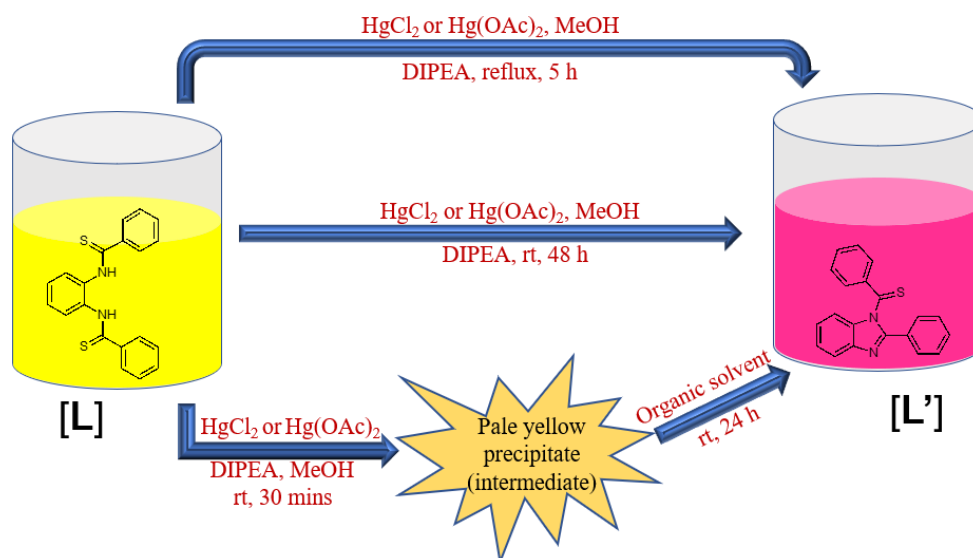
- (14) Xue, S.; Wang, P.; Chen, K. A Novel Fluorescent Chemosensor for Detection of Mercury(II) Ions Based on Dansyl-Peptide and Its Application in Real Water Samples and Living LNcap Cells. *Spectrochim. Acta. A. Mol. Biomol. Spectrosc.* **2020**, *226*, 117616.
- (15) Zhou, S.; Zhou, Z.-Q.; Zhao, X.-X.; Xiao, Y.-H.; Xi, G.; Liu, J.-T.; Zhao, B.-X. A Dansyl Based Fluorescence Chemosensor for Hg²⁺ and Its Application in the Complicated Environment Samples. *Spectrochim. Acta. A. Mol. Biomol. Spectrosc.* **2015**, *148*, 348–354.
- (16) Jonah, T.; Currie, R. A.; Flores, G. A.; Mathivathanan, L.; Chakraborty, I.; Raptis, R. G.; Kavallieratos, K. A Selective Tripodal Tris-Dansylamide Hg(II) Sensor with Unusual Counteranion-Dependent Hg(II) Coordination Patterns. *Manuscript in Preparation*
- (17) Kavallieratos, K.; Rosenberg, J. M.; Chen, W.-Z.; Ren, T. Fluorescent Sensing and Selective Pb(II) Extraction by a Dansylamide Ion-Exchanger. *J. Am. Chem. Soc.* **2005**, *127*, 6514–6515.
- (18) Alvarado, R. J.; Rosenberg, J. M.; Andreu, A.; Bryan, J. C.; Chen, W.-Z.; Ren, T.; Kavallieratos, K. Structural Insights into the Coordination and Extraction of Pb(II) by Disulfonamide Ligands Derived from o-Phenylenediamine. *Inorg. Chem.* **2005**, *44*, 7951–7959.
- (19) Ackermann, T. K. A. Connors: Binding Constants — the Measurement of Molecular Complex Stability, John Wiley & Sons, New York, Chichester, Brisbane, Toronto, Singapore 1987. 411 Seiten, Preis: £ 64.15. *Berichte Bunsenges. Für Phys. Chem.* **1987**, *91*, 1398–1398.
- (20) Stern, O. Über Die Abklingungszeit Der Fluoreszenz. *Phys Z* **1919**, *20*, 183–188.
- (21) Job, P. Formation and stability of inorganic complexes in solution. *Ann Chim* **1928**, *9*, 113–134.
- (22) Khan, H.; Ahmed, M. J.; Bhangar, M. I. A Simple Spectrophotometric Determination of Trace Level Mercury Using 1,5-Diphenylthiocarbazon Solubilized in Micelle. *Anal. Sci.* **2005**, *21*, 507–512.
- (23) Sheldrick, G. M. A Short History of SHELX. *Acta Crystallogr.* **2008**, *64*, 112–122.
- (24) Sheldrick, G. M. Crystal Structure Refinement with SHELXL. *Acta Crystallogr. Sect. C Struct. Chem.* **2015**, *71*, 3–8.

- (25) Dolomanov, O. V.; Bourhis, L. J.; Gildea, R. J.; Howard, J. a. K.; Puschmann, H. OLEX2: A Complete Structure Solution, Refinement and Analysis Program. *J. Appl. Crystallogr.* **2009**, *42*, 339–341.
- (26) Al-Jibori, S. A.; Ahmed, S. A. O.; Wagner, C.; Schmidt, H.; Hogarth, G. Synthesis and Molecular Structure of the Twelve-Membered Metallamacrocycle [Hg₂(μ-2,6-Dapy)₂] (2,6-DapyH₂=2,6-Diacetamidopyridine). *Inorganica Chim. Acta* **2014**, *410*, 118–121.
- (27) *Guidelines for Drinking-Water Quality*, 4th ed.; World Health Organization, Ed.; World Health Organization: Geneva, 2011.

CHAPTER IV: Mercury (II) Sensing via Cyclization of a Dithioamide into a Benzimidazole Derivative: A Structural and Spectroscopic Study.

Adenike O. Fasiku, Matthew T. Fortunato, Indranil Chakraborty*, and Konstantinos Kavallieratos*

(Chapter is a slight modification from the published paper: A. O. Fasiku, M. T. Fortunato, I. Chakraborty,* K. Kavallieratos Mercury (II) sensing via cyclization of a dithioamide into a benzimidazole derivative: A structural and spectroscopic study. *Inorganica Chimica Acta*, **2020**, *510*, 119680).



4.1 Abstract

An *o*-phenylenediamine-derived dithioamide **L** was found to sense Hg^(II) in the UV-visible via Hg^(II)-mediated cyclization leading to a new benzimidazole derivative (**L'**). Both **L** and **L'** have been characterized by single-crystal X-ray crystallography. The structure of **L** reveals relatively strong intramolecular H-bonding interactions of N—H---S type. The extended structure is consolidated by several classical hydrogen bonding interactions. For **L'**, analysis of the packing pattern reveals few non-classical H-bonding contacts. Spectroscopic study of both compounds using FT-IR, UV-Visible, ¹H- and ¹³C-NMR support the single-crystal X-ray crystallography results and confirm the formation of the new benzimidazole derivative. UV-Vis titrations suggest, and NMR confirms that the cyclization reaction occurs via an initial formation of a Hg^(II) complex, which is too transient to be fully characterized. As this reaction is Hg^(II)-mediated, dithioamide **L** acts as a selective Hg^(II) sensor as shown by UV-Visible titrations and a selectivity study against Pb^(II), Cd^(II), Ca^(II), Zn^(II), Ag^(I), and Cr^(III): For Hg^(II), but not for other metals, a distinct color change from yellow to pink is observed with corresponding UV-Vis spectroscopic changes and an isosbestic point at 270 nm.

4.2 Introduction

Mercury is a pollutant arising from both natural and anthropogenic sources, mainly through medicinal and industrial applications. The very toxic organic forms of mercury have some lipophilicity. They can pass through the blood-brain barrier, thus causing short-term and long-term detrimental effects on the human brain and also to the

lungs and kidneys.¹ Hg^(II) is an environmentally mobile form of Hg and can be transformed into more toxic organic forms. Hence, developing methods to sense both Hg^(II) and organic mercury in the environment is of great importance. Over the years, various detection methods for mercury in the environment have been widely studied, including atomic absorption, fluorescence sensing, electrochemical sensing, and other colorimetric methods.² Low-cost colorimetric and fluorescence sensors offer the potential for high sensitivity and selectivity for detection of Hg^(II) in the environment.³⁻⁸

Our group has been engaged in developing sulfonamide and carboxamide-based extractants for sequestration and sensing of toxic metal ions, such as Pb^(II)⁹⁻¹¹ and f-elements.¹² As we were studying the Hg^(II) complexation properties of dithioamide (**L**) with HgCl₂/Hg(CH₃COO)₂, we noticed that no Hg^(II) complex with **L** could be isolated from the reaction, but instead, a new benzimidazole derivative (**L'**) formed via Hg^(II)-mediated cyclization.

Owing to their wide range of applications in pharmaceutical industries, benzimidazole derivatives are considered as an important class of heterocyclic compounds. One of the most common examples of the existence of benzimidazole derivative in nature is *N*-ribosyl-dimethylbenzimidazole, which binds the Cobalt center axially in Vitamin B₁₂.¹³ Based on their biological evaluations, several benzimidazole derivatives have also found their place as antimicrobial, anti-hypertensive, anti-viral, and anti-ulcer agents within clinical settings.¹⁴⁻¹⁹ In recent times, the prevailing antimicrobial resistance is an alarming issue worldwide, especially as a sizeable number of multi drug-resistant (MDR) pathogens have been found to render the action of some crucial antimicrobial agents (like β -lactam-based antibiotics,

vancomycin, quinolones *etc.*) ineffective. This situation has triggered various research groups to develop smart ways of designing antibacterial agents to alleviate the resistance mechanisms inherent to these MDR pathogens. Due to structural similarity with purines, there is a considerable research interest in developing antimicrobial agents based on benzimidazole ligand frameworks. Although the direct synthetic methodology for the preparation of benzimidazoles which involves *ortho*-di-arylamine and an aldehyde, is well known, this procedure often leads to several undesirable side products. Various metal-based catalysts, namely Cu, Co, Ru, Pd, Zn, and Rh, are known to afford much cleaner and sustainable results.²⁰⁻²⁴ Mercury has also been reported as a catalyst that mediates these cyclization reactions.^{6,25,26} For instance, Su et al. developed a microwave-assisted technique for a HgCl₂-mediated synthesis of benzimidazole by intermolecular cyclization using triethylamine.²⁷ Wang et al. synthesized polysubstituted benzimidazoles from *ortho*-di-arylcarboxamides through electrophilic activation of amides with trifluoromethanesulfonic anhydride and 2-chloropyridine.²⁸

Herein, we are exploiting the capability of Hg^(II) to catalyze the cyclization reaction of *o*-phenylenediamine-derived diamides to benzimidazoles to report a unique sensing method for Hg^(II), which is reasonably selective against several competing metals. Furthermore, we have shown the utility of this Hg^(II)-mediated reaction for facile synthesis of a new fully characterized benzimidazole thioamide derivative, which is not straightforward by other conventional synthetic pathways.

4.3 Experimental

4.3.1 Materials and methods

All chemicals and materials were purchased from Fisher Scientific or Sigma-Aldrich. All chemicals were standard reagent grade and were used without further purification except for toluene, which was distilled from CaH₂ before use. NMR spectra were recorded on either a 400-MHz Bruker Avance or a 600-MHz Bruker Avance NMR spectrometer. The UV-Visible spectra were recorded on a CARY 100 Bio UV-Visible spectrophotometer. X-ray diffraction studies were carried out on a Bruker D8 Quest with PHOTON 100 detector. Elemental analysis was provided by Atlantic Microlab Inc. The diamide precursor (*N,N'*-(1,2-phenylene)dibenzamide) of **L** was synthesized by a modification of a previously-reported procedure²⁹ and was found spectroscopically identical to the reported compound.³⁰ The dithioamide ligand **L** has been previously reported,³¹ yet we have now synthesized it by a different method³² and report its NMR characterization and X-ray structure.

4.3.2. Synthesis of *N,N'*-(1,2-phenylene)dibenzothioamide (**L**)

N,N'-(1,2-phenylene)dibenzamide (0.506 g (1.60 mmol)) was dissolved in distilled dry toluene (100 mL). To this solution, 1.424 g (3.52 mmol, 2.2 eq.) of 2,4-Bis(4-methoxyphenyl)-1,3,2,4,-dithiadiphosphetane-2,4-disulfide (Lawesson's Reagent) was added. The reaction mixture was then heated to reflux under nitrogen with constant stirring. After 30 min, the solution turned yellow. After 12 h, the volatiles were evaporated to dryness. A small volume of dichloromethane was used to dissolve the

residue, which was subjected to *silica gel* column chromatography with hexane/ethyl acetate (7:3) as the eluent. The yellow-band eluted fraction was dried *in vacuo* and dissolved in a small volume of dichloromethane. Dropwise addition of hexanes and cooling at 4 °C gave a crystalline yellow precipitate, which was filtered, washed with hexanes, and dried under vacuum. Yield: 0.244 g (0.70 mmol, 43.8%); FT-IR (cm⁻¹): 3263, 1508, 1444, 1361, 1216, 987, 921; ¹H-NMR (600 MHz, CDCl₃) δ 9.38 (s, 2H), 7.86 (d, *J* = 7.7 Hz, 4H), 7.64 – 7.60 (m, 2H), 7.56 – 7.51 (m, 2H), 7.48 (t, *J* = 7.4 Hz, 2H), 7.39 (t, *J* = 7.7 Hz, 4H); ¹³C-NMR (101 MHz, CDCl₃) δ 200.04 (s), 141.05 (s), 134.85 (s), 131.87 (s), 129.18 (s), 128.68 (s), 127.95 (s), 127.08 (s).

4.3.3. Synthesis of phenyl(2-phenyl-1H-benzimidazol-1-yl)methanethione (L')

N,N'-(1,2-phenylene)dibenzothioamide (**L**) (0.041 g, 0.12 mmol) was dissolved in methanol (20 mL) in a round-bottom flask. 42 μL (0.264 mmol) of *N,N'*-diisopropylethylamine (DIPEA) was added and the solution was left to stir for 5 min. A solution of HgCl₂ (0.032 g, 0.12 mmol) or Hg(OAc)₂ (0.038g, 0.12 mmol) in methanol (5 mL) was added dropwise to the stirring solution of **L**. A pale yellow precipitate immediately formed. The reaction mixture was then heated to reflux. After 5h, the reaction contained a pink solution with a black precipitate, which was filtered off by gravity filtration. The volatiles were evaporated under reduced pressure, and the pink residue was dissolved in methylene chloride and subjected to a silica gel column chromatography using methylene chloride as the mobile phase. The fraction containing the pink band was collected, dried under reduced pressure, and the resulting purple

powder was recrystallized in CH₂Cl₂/hexanes, washed with hexanes, and dried under vacuum. Yield (based on HgCl₂): 0.025 g, (0.08 mmol, 66.6 %); FT-IR (cm⁻¹): 1587, 1446, 1313, 1309, 1267, 1164, 1033; ¹H-NMR (600 MHz, CDCl₃) δ 7.95 (d, J = 7.8 Hz, 1H), 7.68 (dd, J = 14.6, 7.3 Hz, 4H), 7.53 (d, J = 7.4 Hz, 1H), 7.42 (t, J = 7.7 Hz, 1H), 7.39 (d, J = 8.2 Hz, 1H), 7.34 – 7.27 (m, 6H); ¹³C-NMR (101 MHz, MeOD) δ 209.63 (s), 145.70 (s), 143.82 (s), 137.90 (s), 135.47 (s), 131.34 (s), 130.88 (s), 130.61 (s), 130.15 (s), 129.76 (s), 126.12 (s), 126.00 (s), 120.59 (s), 118.17 (s), 113.79 (s); *Anal.* Calc. for C₂₀H₁₄N₂S·1/6CH₂Cl₂ (%): C 73.72, H 4.40, N 8.53. Found (%): C 73.83, H 4.43, N 8.53.

4.3.4. X-ray crystallography

The isolated **L** and **L'** were dissolved in methylene chloride, and the solutions were layered carefully with hexanes. Yellow crystals of the dithioamide were formed after several days. Light purple crystals of the benzimidazole derivative were formed within a week. X-ray structure determination experimental details are summarized in Table 1. The non-H atoms are located through intrinsic phasing using *SHELXT*³³ integrated in the *Olex2* graphical user interface.³⁴ H-atoms are included in calculated positions riding on the C atoms to which they bonded, with C—H = 0.93 Å and *U*_{iso}(H) = 1.2U_{eq}(C). The N-H hydrogen atoms are located within the difference map.

4.4 Results and discussion

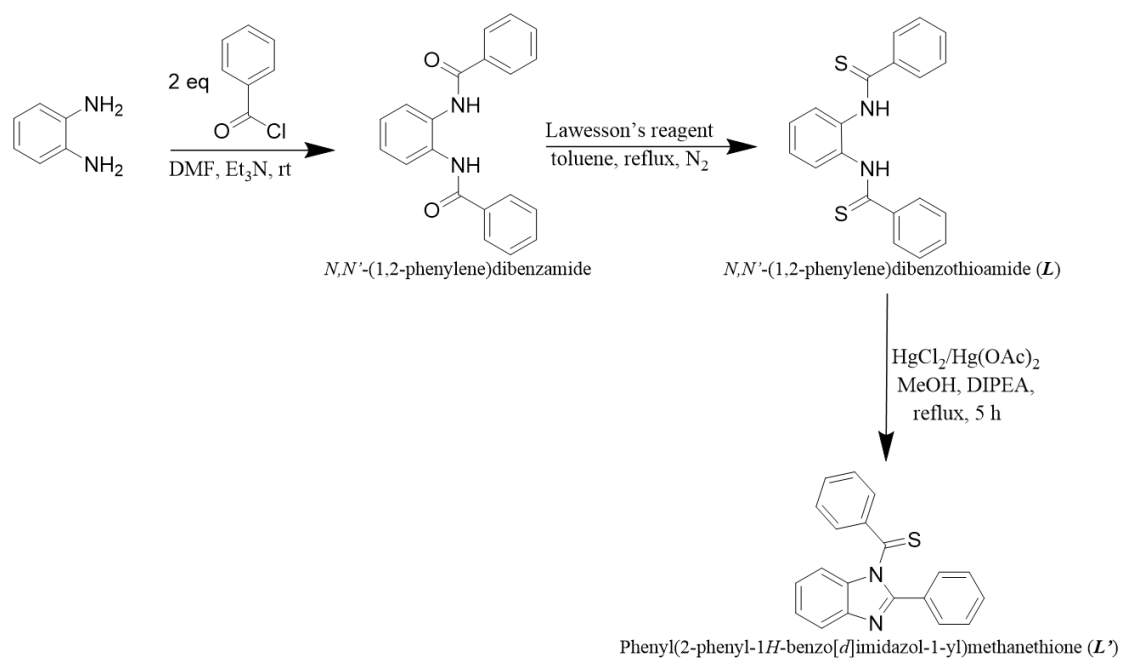
4.4.1. Synthesis

The dithioamide **L**³¹ was synthesized in two steps (Scheme 4.1) from commercially available *o*-phenylenediamine and benzoyl chloride in DMF²⁹ to give

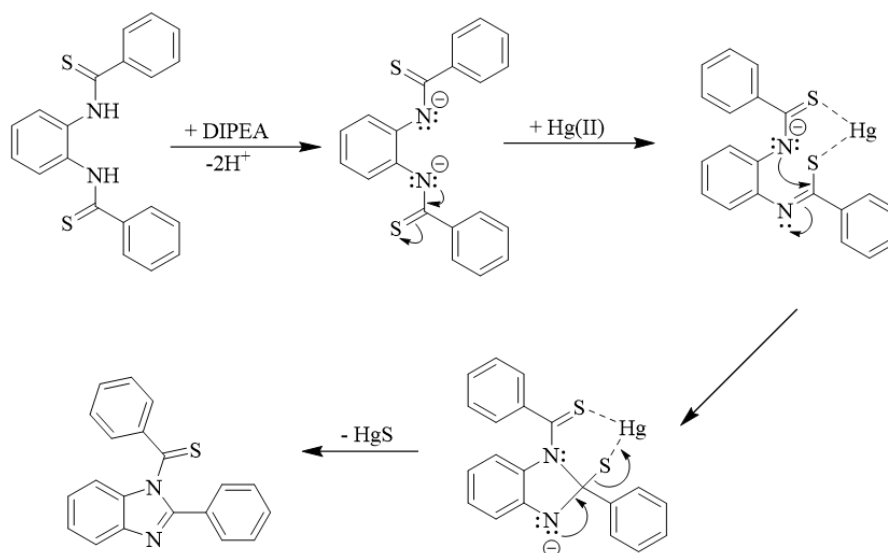
initially the diamide, which was subsequently reacted³² with Lawesson's Reagent in dry toluene to give a yellow product, which was characterized by FT-IR, ¹H/¹³C-NMR, and X-ray crystallography. Even though **L** is known,³¹ the report is not easily accessible, and its X-ray structure is also reported here for the first time.

The benzimidazole thioamide derivative **L'** was synthesized by a Hg^(II)-mediated cyclization reaction after reflux in CH₃OH using 1.2 eq. of HgCl₂ or Hg(OAc)₂. In a reaction similar to ours, Wang et al. have successfully synthesized different polysubstituted benzimidazoles from ortho-di-arylcarboxamides using trifluoromethanesulfonic anhydride and 2-chloropyridine as the reaction mediator.²⁸ Su et al. have also used a microwave-assisted Hg^(II)-mediated cyclization to synthesize benzimidazoles using HgCl₂ and triethylamine.²⁷ The reported cyclization reaction has now resulted to a new thioamide-benzimidazole derivative and also provided evidence -for the first time for this type of reactions- on the formation of a transient Hg^(II)-**L** dithioamide complex. The reaction was carried out by dropwise addition of HgX₂ (X = Cl⁻ or CH₃COO⁻) in methanol to a stirring solution of ligand and DIPEA in methanol. The transient Hg^(II) complex was formed immediately as a yellow powder and filtered, while the pink filtrate was dried *in vacuo* and recrystallized to obtain the cyclized product. The stability of the isolated transient Hg^(II) complex both in solution and in solid state is poor, yet we were able to record the UV-Vis, FT-IR (Figure 4.2), and ¹H-NMR spectra (Figure 4.9) immediately after synthesis, which already show the transient complex being transformed gradually to the cyclized benzimidazole product. As our group focuses on the complexation and sensing of mercury by sulfonamides and thioamides, this mercury-mediated cyclization reaction was further exploited for

Hg^(II)-selective sensing. For synthesis in a larger scale, we found out that refluxing the reaction mixture for 5 h gives higher yields (up to 66.6 %) for the formation of the benzimidazole derivative (**L'**) (Scheme 4.1). For growing suitable crystals for X-ray diffraction: Methylene chloride solutions of reaction mixtures of HgCl₂ and **L** were layered with hexanes. The solution color turned initially yellow, and eventually pink, with a black precipitate settled at the bottom of the tubes. This is presumably due to demetallation of the transient Hg^(II)-**L** species, with the black precipitate being HgS (Scheme 4.2).



Scheme 4.1: Synthesis of *N,N'*-(1,2-phenylene)dibenzothioamide (**L**) and Phenyl(2-phenyl-1H-benzo[*d*]imidazol-1-yl)methanethione (**L'**)



Scheme 4.2: Proposed mechanism of $\text{Hg}^{(II)}$ -catalyzed cyclization reaction transforming **L** into **L'**

4.4.2. FT-IR studies

The infrared spectrum of the new benzimidazole derivative (**L'**) is characterized by the presence of three distinct bands at 1585, 1309, and 1162 cm^{-1} (Figure 4.1). These bands are attributed to the stretching vibrations of the C=N, C-N, and C=S, respectively. Strong and medium intensity bands at 1600–1400 cm^{-1} correspond to the C=N and C=C stretching vibrations. The disappearance of the band corresponding to N-H stretching vibrations in the 3300-3000 cm^{-1} region of the ligand (**L**) spectra and the appearance of a new $\nu(\text{C}=\text{N})$ band of medium intensity at 1585 cm^{-1} for **L'** indicates the formation of the benzimidazole ring. In addition, shifts to lower frequency are observed for the $\nu(\text{C}=\text{S})$ from 1216 cm^{-1} , in **L** to 1162 cm^{-1} in **L'**. A shift for the $\nu(\text{C}-\text{N})$ band is also observed from 1365 cm^{-1} , in **L** to 1309 cm^{-1} in **L'**, which is also consistent with the formation of the benzimidazole.

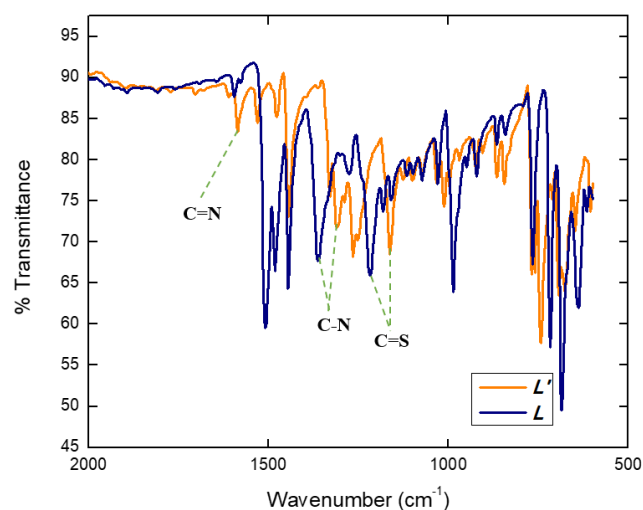


Figure 4.1. FT-IR spectra of the dithioamide ligand (**L**) and the cyclized benzimidazole (**L'**)

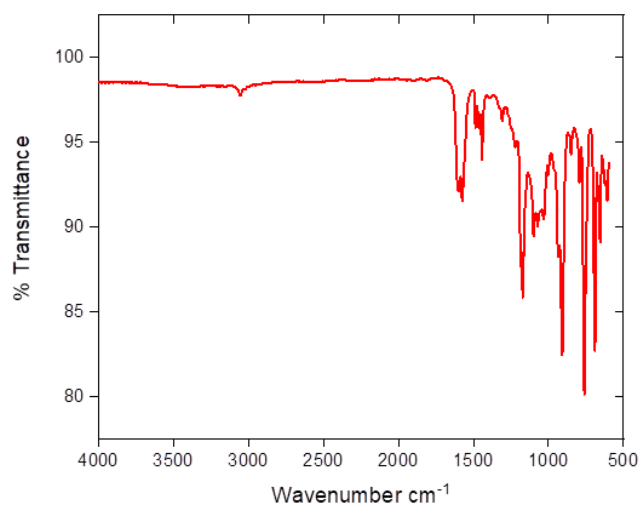


Figure 4.2. FT-IR spectra of the transient $\text{Hg}^{(\text{II})}$ -**L** complex

4.4.3. UV-Visible sensing studies - titrations

The formation of the new benzimidazole derivative **L'** was also confirmed by UV-Vis spectroscopy. The absorption spectra of **L** and isolated **L'** were recorded in 0.1 mM MeOH solutions using a quartz cuvette of 1 cm path length (Figure 4.3). Response to $\text{Hg}^{(\text{II})}$ addition was monitored by gradual addition of various amounts of $\text{Hg}^{(\text{II})}$

(0.005-1.600 mL of 0.5 mM HgCl₂) to solutions of **L** (0.02 mM) and DIPEA (0.044 mM) in MeOH (at constant concentration of **L** and DIPEA). A 10 min interval was used before each reading to ensure the reaction was under thermodynamic control. The UV-Vis spectra of dithioamide **L** in MeOH solution show an absorption band at 248 nm. The addition of Hg^(II) resulted in a red shift and a gradual disappearance of this absorption band (Figure 4.5). Two new bands appeared at 286 nm and 328 nm, an observation consistent with the formation of the benzimidazole. Very similar spectra were obtained after the addition of Hg(OAc)₂ (Figure 4.4). The ratio changes observed in the titration plot (Figure 4.5) produced a linear function for a Hg^(II) concentration up to 10.63 μM. The detection limit was calculated to be 0.69 μM, with a 1.08 - 10.63 μM dynamic range. It is notable that the spectra of i) isolated benzimidazole product ii) the reaction mixture after 24h, and iii) the titration spectra after Hg^(II) addition, are virtually identical. This observation is consistent with the hypothesis that the UV-Vis sensing of Hg^(II) is a direct result of the Hg^(II)-mediated cyclization reaction.

Selectivity for Hg^(II) sensing by **L** compares favorably vs. various other metals, including Cd^(II), Pb^(II), Zn^(II), Ca^(II), Ag^(I), and Cr^(III). One equivalent of these metals (added as chloride salts) was added to solutions of **L** (0.1 mM) and 2.2 eq of DIPEA and the solutions were left to stand for 24 h. The UV-Vis spectra were collected and are shown in Figure 4.6 (for Cd^(II), Pb^(II), Zn^(II), and Hg^(II)), and in Fig. 4.7 (for Ca^(II), Ag^(I), Cr^(III) and Hg^(II)). Only for mercury addition do the new benzimidazole bands at 286 nm and 328 nm appear prominently. Pb^(II) and Cd^(II), show some increases in absorption (Figure 4.6), which are more consistent with complex formation rather than benzimidazole formation, while Zn^(II), Ca^(II), Ag^(I), and Cr^(III) show no interference

(Figure 4.6 and 4.7).

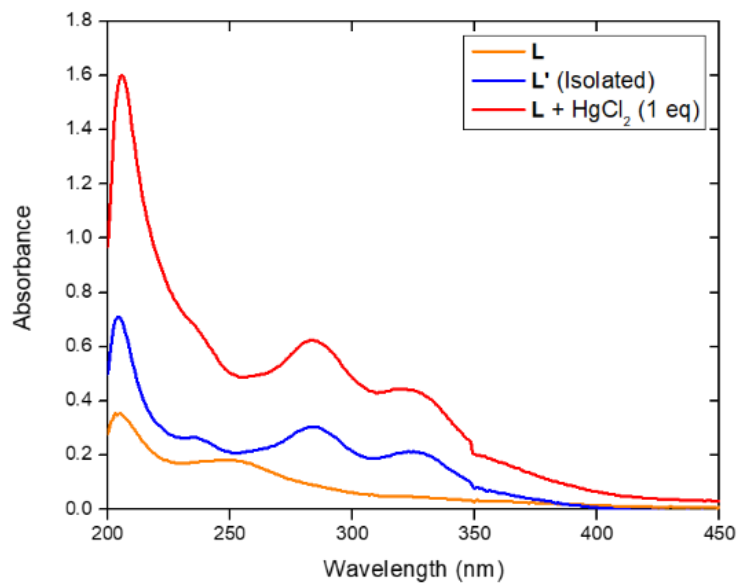


Figure 4.3. UV-Vis spectra of i) **L** (0.1 mM) in MeOH, ii) isolated **L'** (0.1 mM) in MeOH and iii) reaction mixture after addition of HgCl₂ (1 eq., 0.1 mM) to **L** in MeOH, after standing for 24 h.

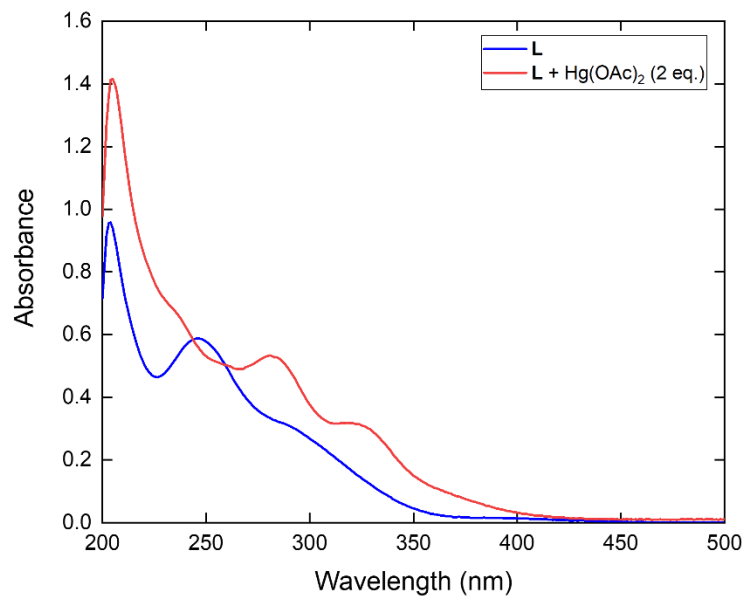


Figure 4.4. UV-Vis spectra of **L** (0.02 mM) in CH₃OH vs **L** + Hg(OAc)₂ (2 eq.). No organic base was added.

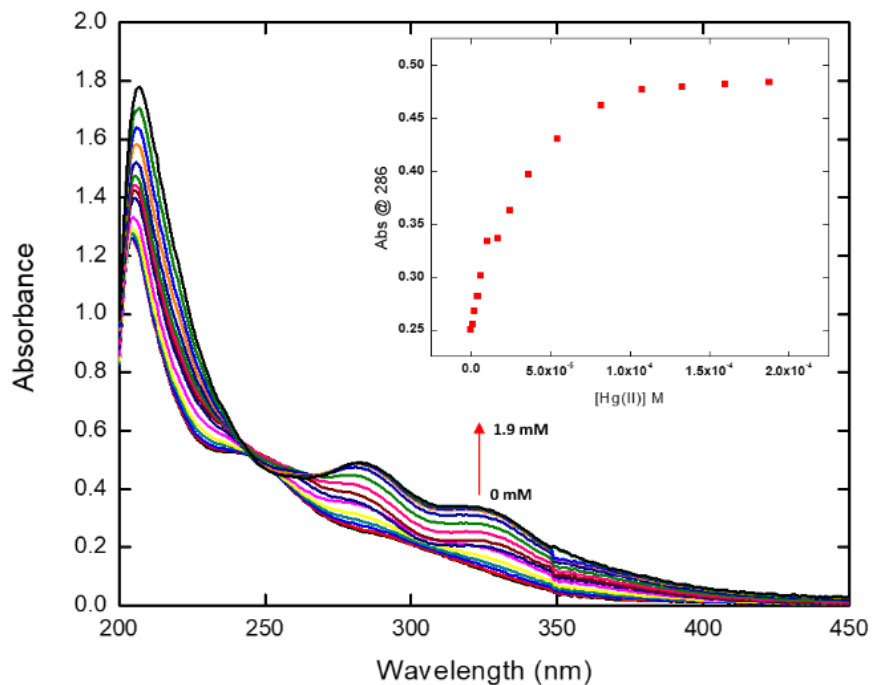


Figure 4.5. UV-Vis titration of **L** (0.02 mM) and DIPEA (2.2 eq.) in CH_3OH after gradual addition of HgCl_2 (0.5 mM) at constant **L** and DIPEA concentration.

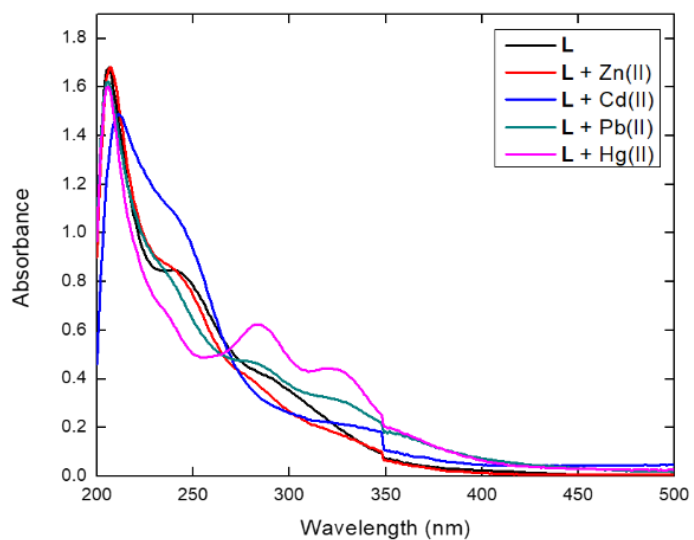


Figure 4.6. UV-Vis spectra of **L** (0.1 mM) before and after addition of chloride salts of $\text{Zn}^{(II)}$, $\text{Pb}^{(II)}$, $\text{Cd}^{(II)}$, or $\text{Hg}^{(II)}$ (1 eq.) in MeOH after standing for 24 h.

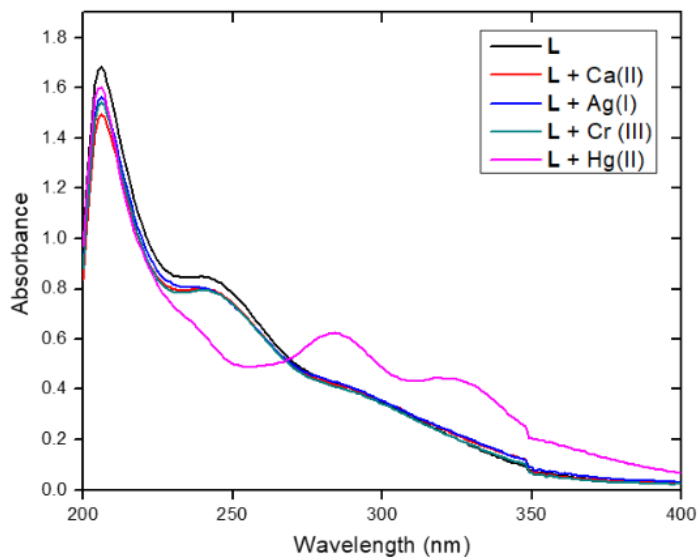


Figure 4.7. UV-Vis spectra of **L** (0.1 mM) before and after addition of chloride salts of Ca(II), Ag^(I), Cr^(III), and Hg^(II) (1 eq.) in MeOH, after standing for 24 h.

4.4.4. NMR spectroscopy

The ¹H-NMR spectrum of benzimidazole **L'** differs significantly from the spectrum of dithioamide **L** (Figure 4.8). There is a multiplet at δ 7.34-7.27 which is assigned to the phenyl protons. The N-H resonance for **L** at δ 9.38 is no longer present at **L'**. The ortho-aryl protons of **L** are assigned as d and e (δ 7.62 and 7.53), both split into d and g (δ 7.95 and 7.39) and e, f (δ 7.53 and 7.42), for **L'** (Fig. 4.8). Figure 4.9 depicts the ¹H-NMR spectrum of **L** after the addition of HgCl₂ (1.2 eq.), in comparison with the spectra of **L** (3.2 mM) and **L** with DIPEA (7.0 mM) (bottom, top and middle respectively). After Hg^(II) addition, the formation of a new species is clearly indicated, with chemical shifts at 8.06, 7.45, and 7.28 ppm, which are substantially different than the benzimidazole **L'**. Resonances for the deprotonated ligand are still prominent,

however, indicating that the formation of the transient Hg^{II} complex (Scheme 4.2) is a slow step in the process.

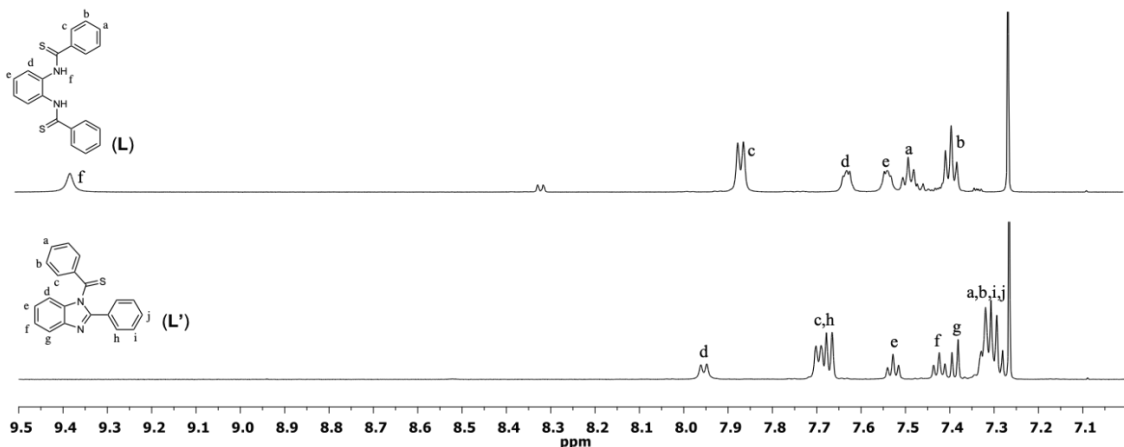


Figure 4.8. $^1\text{H-NMR}$ spectra of di-thioamide (**L**) and the cyclized benzimidazole product (**L'**) in CDCl_3 .

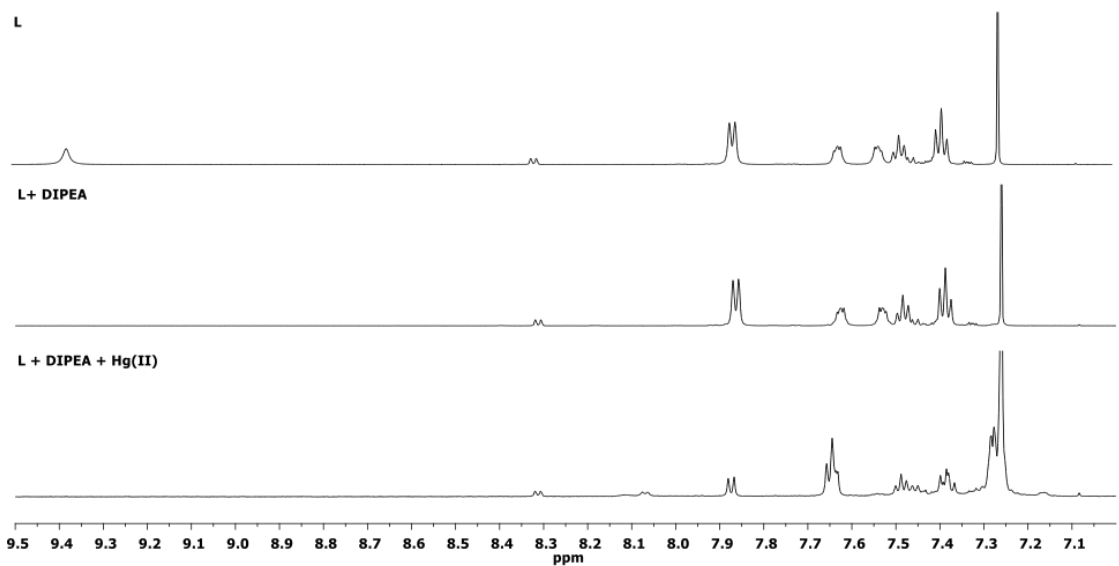


Figure 4.9. $^1\text{H-NMR}$ spectra of **L** (3.2 mM) (top) in comparison with **L** + DIPEA (2.2 eq.) (middle) and the reaction mixture after addition of HgCl_2 (1.2 eq.) showing the transient Hg^{II} -**L** complex formation at 8.06, 7.45, and 7.28 ppm (bottom).

4.4.5 Single-crystal X-ray crystallography

Crystal data, data collection, and structure refinement details are summarized in Table 4.1. The dithioamide compound **L** was solved and refined in a Triclinic, *P*-1 space group, with a full molecule in the asymmetric unit (as shown in Figure 4.10). The phenyl group of the *o*-phenylenediamine motif (constituted by C1, C2, C3, C4, C5, C6 atoms) is satisfactorily planar with a mean deviation of 0.11 (3) Å. The two other dangling phenyl groups constituted by C8, C9, C10, C11, C12, C13, and C15, C16, C17, C18, C19, C20 atoms show excellent planarity (mean deviation, 0.003 (2) Å). The dihedral angles between the two planes constituted by these two phenyl rings with the phenyl ring of the *o*-phenylenediamine motif are 55.8 and 82.8°, respectively. The asymmetric unit displays an intramolecular H-bonding interaction of N—H...S, type involving an S atom associated with a thioamide and an amide N-H, that is a part of another thioamide. Examination of the packing pattern for **L** (Figure 4.11) revealed that its extended structure is consolidated by several classical H-bonding interactions (N1—H1—S2, with H—S, 2.39 Å; N2—H2—S1, with H—S, 2.67 Å; C5—H5—S1, with H—S, 2.87 Å; C9—H9—S1, with H—S, 2.65 Å; C16—H16—S2, with H—S, 2.74 Å; Symmetry code: (i) $-x + 1, -y + 2, -z + 1$). The cyclized benzimidazole **L'** (Figure 4.12) was obtained from compound **L** through a mercury (II) mediated cyclization process (*vide infra*). The benzimidazole fragment (constituted by C1, C2, C3, C4, C5, C6, C7, N2, N1 atoms) in this compound is satisfactorily planar with mean deviation of 0.017 (3) Å. The conjoining phenyl ring (constituted by C8, C9, C10, C11, C12, C13 atoms) shows excellent planarity (mean deviation, 0.005 (3) Å) and the dihedral angle between this plane and the benzimidazole fragment is

43.0 °. The other phenyl ring (constituted by C15, C16, C17, C18, C19, C20 atoms) is also highly planar (mean deviation, 0.004 (3) Å) and the dihedral angle between this plane and the plane of benzimidazole ring is 72.7 °. In case of **L'**, its extended structure (Fig. 4.13) is consolidated by few non-classical H-bonding interactions (C16—H16—N1, with H—N, 2.54 Å; C19—H19—N2, with H—N, 2.61 Å; C20—H20—S1, with H—S, 2.76 Å; Symmetry code: (i)x, y, z - 1).

Table 4.1: Experimental details for X-ray structure determination.

	L	L'
Chemical formula	C ₂₀ H ₁₆ N ₂ S ₂	C ₂₀ H ₁₄ N ₂ S
Mr	348.47	314.39
Crystal system, space group	Triclinic, P-1	Triclinic, P-1
Temperature (K)	273	293
a, b, c (Å)	8.7208 (4), 10.0905 (5), 11.4131 (5)	8.9989 (7), 9.8812 (8), 9.9587 (8)
α, β, γ (°)	66.506 (1), 72.172 (1), 89.016 (1)	111.313 (2), 97.350 (2), 98.663 (2)
V (Å ³)	870.49 (7)	799.35 (11)
Z	2	2
Radiation type	Mo Kα	Mo Kα
μ (mm ⁻¹)	0.31	0.20
Crystal size (mm)	0.30 × 0.25 × 0.20	0.15 × 0.10 × 0.08
Data collection		
Diffractometer	Bruker D8 Quest with PHOTON 100 detector	Bruker D8 Quest with PHOTON 100 detector
Absorption correction	Multi-scan SADABS2016/2 (Bruker,2016/2) was used for absorption correction. wR2(int) was 0.0430 before and 0.0379 after correction. The Ratio of minimum to maximum transmission is 0.9450. The λ/2 correction factor is not present.	Multi-scan SADABS2016/2 (Bruker,2016/2) was used for absorption correction. wR2(int) was 0.0598 before and 0.0480 after correction. The Ratio of minimum to maximum transmission is 0.8939. The λ/2 correction factor is not present.
T _{min} , T _{max}	0.705, 0.746	0.650, 0.745
No. of measured, independent and observed [I > 2σ(I)] reflections	17250, 4321, 3533	10067, 2726, 2003
R _{int}	0.020	0.031

$(\sin \theta/\lambda)_{\max}$ (\AA^{-1})	0.668	0.589
Refinement		
$R[F^2 > 2\sigma(F^2)]$, $wR(F^2)$, S	0.037, 0.102, 1.04	0.048, 0.135, 1.05
No. of reflections	4321	2726
No. of parameters	225	208
H-atom treatment	H-atoms treated by a mixture of independent and constrained refinement	H-atom parameters constrained
$\Delta\rho_{\max}$, $\Delta\rho_{\min}$ (e \AA^{-3})	0.26, -0.37	0.32, -0.48

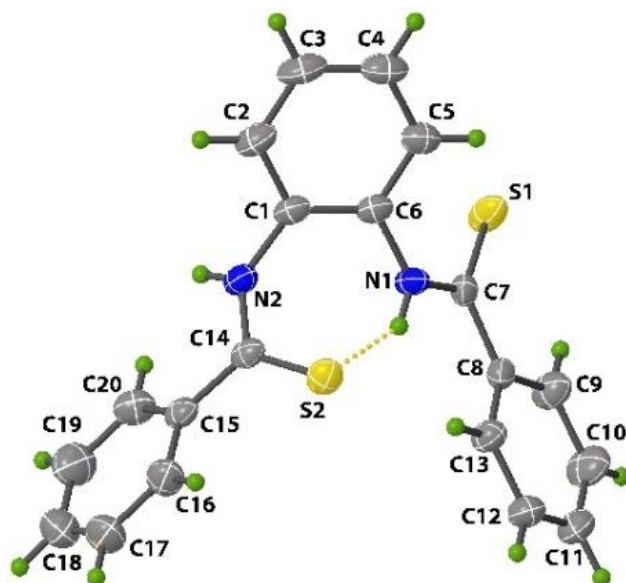


Figure 4.10. ORTEP representation (50% probability ellipsoids) for the X-ray crystal structure of dithioamide **L**, with atom labeling scheme, showing an N-H...S intramolecular hydrogen bonding interaction.

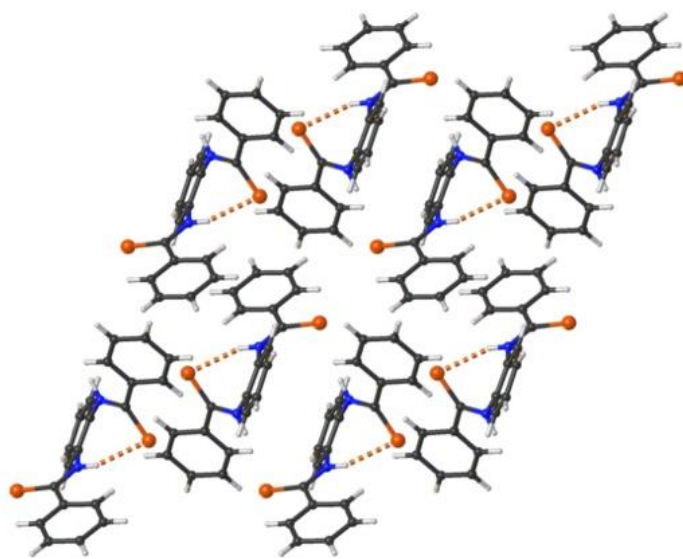


Figure 4.11. Packing pattern of **L** along *a* axis. The dotted lines indicate both intra- and inter-molecular H-bonding interactions

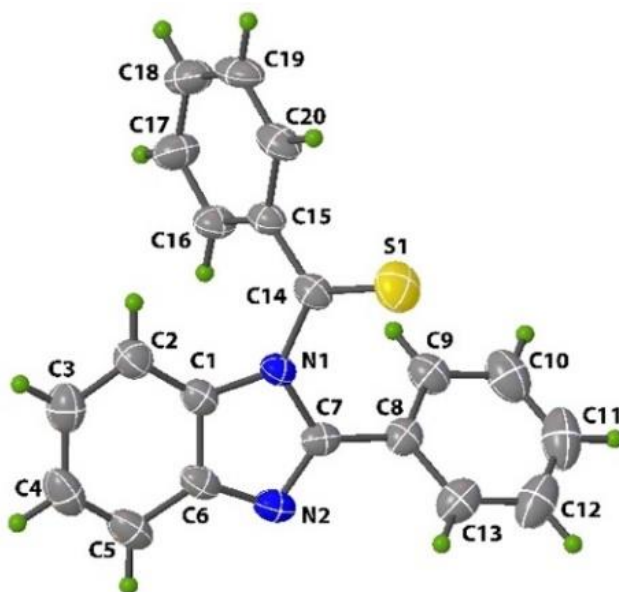


Figure 4.12. ORTEP representation (50% probability ellipsoids) for the X-ray crystal structure of benzimidazole **L'**, with atom labeling scheme.

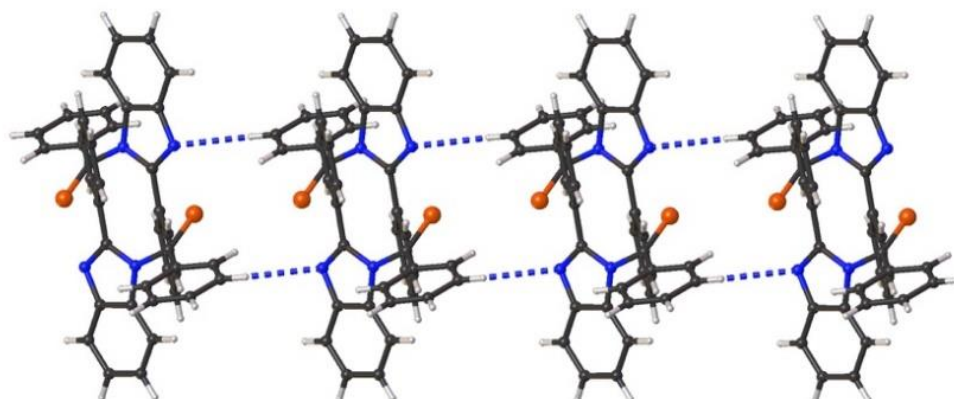


Figure 4.13. Packing pattern of L' along b axis. The dotted lines indicate intermolecular H-bonding interactions.

Table 4.2: Fractional atomic coordinates and isotropic or equivalent isotropic displacement parameters (\AA^2) for L

	x	y	z	$U_{\text{iso}}^*/U_{\text{eq}}$
S2	0.56389 (5)	0.51699 (4)	0.63790 (4)	0.04697 (12)
S1	0.39713 (6)	0.95414 (5)	0.84411 (4)	0.05764 (14)
N2	0.55531 (15)	0.78761 (13)	0.47136 (12)	0.0410 (3)
H2	0.605480	0.864942	0.401315	0.049*
N1	0.45992 (14)	0.75402 (13)	0.74660 (12)	0.0406 (3)
H1	0.520899	0.688787	0.736641	0.049*
C8	0.60039 (16)	0.74222 (15)	0.90040 (13)	0.0356 (3)
C14	0.63810 (17)	0.67163 (15)	0.50039 (14)	0.0378 (3)
C15	0.80144 (18)	0.69073 (15)	0.40046 (14)	0.0396 (3)
C7	0.48563 (16)	0.81245 (14)	0.82630 (13)	0.0355 (3)
C6	0.34601 (17)	0.78461 (15)	0.67611 (15)	0.0390 (3)
C1	0.39325 (17)	0.79580 (15)	0.54444 (15)	0.0401 (3)
C13	0.66337 (19)	0.61498 (17)	0.89852 (16)	0.0459 (3)
H13	0.636467	0.572527	0.847432	0.055*
C12	0.7654 (2)	0.55106 (19)	0.97175 (17)	0.0524 (4)
H12	0.807057	0.466508	0.968911	0.063*
C16	0.8731 (2)	0.56864 (19)	0.39223 (17)	0.0531 (4)
H16	0.817123	0.476203	0.447835	0.064*
C5	0.18467 (18)	0.79337 (16)	0.74032 (17)	0.0477 (4)
H5	0.151429	0.781217	0.829939	0.057*
C9	0.6442 (2)	0.8015 (2)	0.97781 (18)	0.0552 (4)
H9	0.604319	0.886522	0.980924	0.066*

C11	0.8057 (2)	0.6110 (2)	1.04822 (17)	0.0575 (4)
H11	0.873004	0.566732	1.098380	0.069*
C20	0.8876 (2)	0.82669 (19)	0.31484 (18)	0.0539 (4)
H20	0.842119	0.909679	0.318213	0.065*
C4	0.0741 (2)	0.81990 (18)	0.6720 (2)	0.0566 (4)
H4	-0.033134	0.826807	0.715066	0.068*
C2	0.2804 (2)	0.82327 (18)	0.47597 (18)	0.0530 (4)
H2A	0.311895	0.832879	0.387133	0.064*
C3	0.1223 (2)	0.8362 (2)	0.5396 (2)	0.0619 (5)
H3	0.047886	0.856047	0.493101	0.074*
C17	1.0254 (2)	0.5839 (2)	0.3027 (2)	0.0654 (5)
H17	1.072060	0.501398	0.299132	0.079*
C10	0.7464 (3)	0.7363 (2)	1.0505 (2)	0.0681 (5)
H10	0.774929	0.778205	1.101307	0.082*
C18	1.1093 (2)	0.7181 (3)	0.2191 (2)	0.0692 (5)
H18	1.212450	0.727110	0.158785	0.083*
C19	1.0403 (2)	0.8403 (2)	0.2244 (2)	0.0707 (5)
H19	1.096750	0.932217	0.167054	0.085*

Table 4.3: Atomic displacement parameters (\AA^2) for **L**

S2	0.0596 (2)	0.03729 (19)	0.0481 (2)	0.01264 (16)	-0.02086 (18)	-0.01949 (16)
S1	0.0870 (3)	0.0529 (2)	0.0556 (3)	0.0356 (2)	-0.0402 (2)	-0.0334 (2)
N2	0.0477 (7)	0.0402 (6)	0.0406 (6)	0.0146 (5)	-0.0218 (5)	-0.0169 (5)
N1	0.0422 (6)	0.0473 (7)	0.0464 (7)	0.0202 (5)	-0.0237 (5)	-0.0271 (6)
C8	0.0348 (6)	0.0402 (7)	0.0292 (6)	0.0034 (5)	-0.0096 (5)	-0.0123 (5)
C14	0.0477 (8)	0.0392 (7)	0.0427 (7)	0.0139 (6)	-0.0273 (6)	-0.0240 (6)
C15	0.0478 (8)	0.0435 (7)	0.0403 (7)	0.0139 (6)	-0.0258 (6)	-0.0219 (6)
C7	0.0382 (7)	0.0372 (6)	0.0276 (6)	0.0049 (5)	-0.0083 (5)	-0.0116 (5)
C6	0.0399 (7)	0.0351 (6)	0.0486 (8)	0.0112 (5)	-0.0227 (6)	-0.0181 (6)
C1	0.0442 (7)	0.0360 (7)	0.0496 (8)	0.0134 (6)	-0.0261 (6)	-0.0194 (6)
C13	0.0505 (8)	0.0518 (8)	0.0466 (8)	0.0156 (7)	-0.0251 (7)	-0.0248 (7)
C12	0.0506 (9)	0.0589 (10)	0.0521 (9)	0.0196 (7)	-0.0244 (7)	-0.0222 (8)
C16	0.0616 (10)	0.0487 (8)	0.0530 (9)	0.0177 (7)	-0.0189 (8)	-0.0254 (7)
C5	0.0407 (8)	0.0440 (8)	0.0573 (9)	0.0098 (6)	-0.0176 (7)	-0.0187 (7)
C9	0.0682 (11)	0.0595 (10)	0.0591 (10)	0.0194 (8)	-0.0357 (8)	-0.0350 (8)
C11	0.0526 (9)	0.0752 (12)	0.0489 (9)	0.0155 (8)	-0.0289 (8)	-0.0209 (8)
C20	0.0534 (9)	0.0478 (8)	0.0644 (10)	0.0102 (7)	-0.0254 (8)	-0.0227 (8)
C4	0.0385 (8)	0.0493 (9)	0.0808 (12)	0.0096 (7)	-0.0251 (8)	-0.0218 (9)
C2	0.0608 (10)	0.0541 (9)	0.0605 (10)	0.0176 (8)	-0.0397 (8)	-0.0257 (8)
C3	0.0536 (10)	0.0592 (10)	0.0884 (14)	0.0177 (8)	-0.0479 (10)	-0.0280 (10)
C17	0.0672 (11)	0.0728 (12)	0.0623 (11)	0.0287 (10)	-0.0190 (9)	-0.0364 (10)
C10	0.0795 (13)	0.0860 (14)	0.0703 (12)	0.0220 (11)	-0.0487 (10)	-0.0460 (11)
C18	0.0540 (10)	0.0911 (15)	0.0604 (11)	0.0168 (10)	-0.0145 (9)	-0.0328 (11)
C19	0.0593 (11)	0.0678 (12)	0.0698 (12)	-0.0009 (9)	-0.0170 (9)	-0.0160 (10)

Table 4.4: Geometric parameters (\AA , $^\circ$) for **L**

S2—C14	1.6664 (15)	C16—H16	0.9300
S1—C7	1.6670 (14)	C16—C17	1.372 (3)
N2—H2	0.8600	C5—H5	0.9300
N2—C14	1.3450 (17)	C5—C4	1.377 (2)
N2—C1	1.4245 (19)	C9—H9	0.9300
N1—H1	0.8600	C9—C10	1.382 (2)
N1—C7	1.3350 (17)	C11—H11	0.9300
N1—C6	1.4178 (17)	C11—C10	1.365 (3)
C8—C7	1.4950 (19)	C20—H20	0.9300
C8—C13	1.393 (2)	C20—C19	1.382 (3)
C8—C9	1.386 (2)	C4—H4	0.9300

C14—C15	1.485 (2)	C4—C3	1.378 (3)
C15—C16	1.395 (2)	C2—H2A	0.9300
C15—C20	1.385 (2)	C2—C3	1.380 (3)
C6—C1	1.389 (2)	C3—H3	0.9300
C6—C5	1.393 (2)	C17—H17	0.9300
C1—C2	1.3943 (19)	C17—C18	1.362 (3)
C13—H13	0.9300	C10—H10	0.9300
C13—C12	1.383 (2)	C18—H18	0.9300
C12—H12	0.9300	C18—C19	1.378 (3)
C12—C11	1.366 (2)	C19—H19	0.9300
C14—N2—H2	116.6	C6—C5—H5	119.8
C14—N2—C1	126.83 (12)	C4—C5—C6	120.42 (16)
C1—N2—H2	116.6	C4—C5—H5	119.8
C7—N1—H1	115.5	C8—C9—H9	119.5
C7—N1—C6	128.97 (12)	C10—C9—C8	121.07 (16)
C6—N1—H1	115.5	C10—C9—H9	119.5
C13—C8—C7	122.58 (12)	C12—C11—H11	120.2
C9—C8—C7	119.92 (13)	C10—C11—C12	119.52 (15)
C9—C8—C13	117.48 (13)	C10—C11—H11	120.2
N2—C14—S2	122.84 (11)	C15—C20—H20	119.7
N2—C14—C15	115.14 (13)	C19—C20—C15	120.70 (17)
C15—C14—S2	122.02 (10)	C19—C20—H20	119.7
C16—C15—C14	119.65 (14)	C5—C4—H4	120.0
C20—C15—C14	122.24 (13)	C5—C4—C3	120.03 (16)
C20—C15—C16	118.10 (15)	C3—C4—H4	120.0
N1—C7—S1	123.18 (11)	C1—C2—H2A	119.9
N1—C7—C8	115.58 (12)	C3—C2—C1	120.19 (16)
C8—C7—S1	121.24 (10)	C3—C2—H2A	119.9
C1—C6—N1	119.50 (12)	C4—C3—C2	120.26 (15)
C1—C6—C5	119.52 (13)	C4—C3—H3	119.9
C5—C6—N1	120.82 (14)	C2—C3—H3	119.9
C6—C1—N2	123.27 (12)	C16—C17—H17	119.5
C6—C1—C2	119.50 (14)	C18—C17—C16	120.93 (18)
C2—C1—N2	117.16 (14)	C18—C17—H17	119.5
C8—C13—H13	119.6	C9—C10—H10	119.7
C12—C13—C8	120.77 (14)	C11—C10—C9	120.55 (16)
C12—C13—H13	119.6	C11—C10—H10	119.7
C13—C12—H12	119.7	C17—C18—H18	120.2
C11—C12—C13	120.60 (16)	C17—C18—C19	119.58 (18)
C11—C12—H12	119.7	C19—C18—H18	120.2
C15—C16—H16	119.7	C20—C19—H19	119.9
C17—C16—C15	120.53 (17)	C18—C19—C20	120.15 (19)
C17—C16—H16	119.7	C18—C19—H19	119.9

Table 4.5: Fractional atomic coordinates and isotropic or equivalent isotropic displacement parameters (\AA^2) for **L'**

	<i>x</i>	<i>y</i>	<i>z</i>	$U_{\text{iso}}^*/U_{\text{eq}}$
S1	0.10388 (14)	0.49270 (14)	0.16903 (13)	0.0928 (5)
N1	0.2274 (3)	0.3274 (3)	0.2868 (3)	0.0473 (6)
C14	0.2176 (4)	0.3852 (4)	0.1748 (3)	0.0526 (8)
C15	0.3186 (4)	0.3387 (4)	0.0699 (3)	0.0502 (8)
C8	0.2674 (4)	0.5677 (4)	0.5079 (3)	0.0528 (8)
C9	0.3837 (4)	0.6552 (4)	0.4782 (4)	0.0631 (9)
H9	0.440062	0.611365	0.408610	0.076*
C20	0.2850 (4)	0.3464 (4)	-0.0676 (4)	0.0653 (10)
H20	0.195323	0.374693	-0.094851	0.078*
C13	0.1855 (4)	0.6355 (5)	0.6135 (4)	0.0703 (11)
H13	0.108753	0.577601	0.635543	0.084*
C16	0.4513 (4)	0.2945 (4)	0.1060 (4)	0.0608 (9)
H16	0.474476	0.286744	0.196139	0.073*
C7	0.2321 (3)	0.4060 (4)	0.4363 (3)	0.0500 (8)
C19	0.3846 (5)	0.3122 (4)	-0.1627 (4)	0.0750 (12)
H19	0.362094	0.317699	-0.253909	0.090*
N2	0.2089 (3)	0.3163 (3)	0.5045 (3)	0.0572 (7)
C1	0.1963 (3)	0.1764 (4)	0.2626 (4)	0.0510 (8)
C17	0.5501 (5)	0.2617 (5)	0.0098 (4)	0.0744 (11)
H17	0.640263	0.233452	0.035925	0.089*
C12	0.2173 (6)	0.7868 (6)	0.6849 (5)	0.0908 (15)
H12	0.161343	0.831794	0.754461	0.109*
C6	0.1840 (4)	0.1743 (4)	0.4000 (4)	0.0554 (9)
C18	0.5162 (5)	0.2704 (5)	-0.1236 (4)	0.0796 (12)
H18	0.583153	0.247623	-0.188233	0.095*
C10	0.4149 (5)	0.8071 (5)	0.5526 (5)	0.0854 (13)
H10	0.493335	0.866036	0.533558	0.102*
C3	0.1359 (5)	-0.0846 (5)	0.1565 (5)	0.0772 (12)
H3	0.116318	-0.173648	0.075056	0.093*
C2	0.1713 (4)	0.0479 (4)	0.1390 (4)	0.0653 (10)
H2	0.177962	0.050511	0.047737	0.078*
C11	0.3318 (7)	0.8724 (5)	0.6541 (6)	0.0976 (16)
H11	0.352892	0.975381	0.702548	0.117*
C5	0.1523 (4)	0.0382 (5)	0.4146 (5)	0.0738 (11)
H5	0.147436	0.034532	0.505713	0.089*
C4	0.1287 (5)	-0.0883 (5)	0.2938 (6)	0.0813 (12)
H4	0.107286	-0.179789	0.302366	0.098*

Table 4.6: Atomic displacement parameters (\AA^2) for L'

	U^{11}	U^{22}	U^{33}	U^{12}	U^{13}	U^{23}
S1	0.0940 (9)	0.0988 (9)	0.0925 (9)	0.0366 (7)	0.0024 (6)	0.0442 (7)
N1	0.0481 (15)	0.0554 (17)	0.0454 (15)	0.0132 (12)	0.0072 (11)	0.0274 (13)
C14	0.0504 (19)	0.057 (2)	0.0490 (18)	0.0036 (15)	-0.0043 (14)	0.0265 (16)
C15	0.0557 (19)	0.0519 (19)	0.0408 (17)	0.0023 (15)	0.0029 (14)	0.0211 (15)
C8	0.0467 (18)	0.062 (2)	0.0466 (18)	0.0134 (16)	-0.0016 (14)	0.0196 (16)
C9	0.056 (2)	0.070 (3)	0.066 (2)	0.0091 (18)	-0.0002 (17)	0.034 (2)
C20	0.072 (2)	0.071 (2)	0.051 (2)	0.0001 (19)	-0.0086 (17)	0.0342 (18)
C13	0.052 (2)	0.085 (3)	0.061 (2)	0.0171 (19)	0.0010 (17)	0.015 (2)
C16	0.066 (2)	0.077 (2)	0.0473 (19)	0.0178 (19)	0.0094 (16)	0.0324 (18)
C7	0.0374 (16)	0.072 (2)	0.0464 (18)	0.0168 (15)	0.0066 (13)	0.0280 (17)
C19	0.101 (3)	0.079 (3)	0.0406 (19)	-0.007 (2)	0.006 (2)	0.0299 (19)
N2	0.0537 (17)	0.075 (2)	0.0544 (17)	0.0144 (14)	0.0128 (13)	0.0371 (17)
C1	0.0407 (17)	0.059 (2)	0.059 (2)	0.0107 (15)	0.0067 (14)	0.0306 (18)
C17	0.073 (3)	0.099 (3)	0.062 (2)	0.028 (2)	0.024 (2)	0.036 (2)
C12	0.081 (3)	0.095 (4)	0.071 (3)	0.039 (3)	-0.005 (2)	0.003 (3)
C6	0.0455 (18)	0.070 (2)	0.064 (2)	0.0131 (16)	0.0109 (15)	0.042 (2)
C18	0.092 (3)	0.087 (3)	0.058 (2)	0.007 (2)	0.028 (2)	0.026 (2)
C10	0.075 (3)	0.076 (3)	0.100 (3)	0.007 (2)	-0.014 (2)	0.043 (3)
C3	0.069 (3)	0.058 (3)	0.094 (3)	0.0102 (19)	0.010 (2)	0.022 (2)
C2	0.068 (2)	0.064 (2)	0.065 (2)	0.0132 (18)	0.0113 (18)	0.027 (2)
C11	0.098 (4)	0.065 (3)	0.101 (4)	0.023 (3)	-0.030 (3)	0.014 (3)
C5	0.065 (2)	0.084 (3)	0.093 (3)	0.012 (2)	0.020 (2)	0.058 (3)
C4	0.071 (3)	0.069 (3)	0.120 (4)	0.011 (2)	0.021 (2)	0.055 (3)

Table 4.7: Geometric parameters (\AA , $^\circ$) for L'

S1—C14	1.585 (3)	C19—C18	1.364 (6)
N1—C14	1.425 (4)	N2—C6	1.375 (4)
N1—C7	1.404 (4)	C1—C6	1.398 (5)
N1—C1	1.396 (4)	C1—C2	1.376 (5)
C14—C15	1.468 (5)	C17—H17	0.9300
C15—C20	1.399 (4)	C17—C18	1.364 (5)
C15—C16	1.377 (5)	C12—H12	0.9300
C8—C9	1.387 (5)	C12—C11	1.371 (7)
C8—C13	1.392 (5)	C6—C5	1.392 (5)
C8—C7	1.456 (5)	C18—H18	0.9300
C9—H9	0.9300	C10—H10	0.9300
C9—C10	1.375 (6)	C10—C11	1.366
C20—H20	0.9300	C3—H3	0.9300

C20—C19	1.376 (5)	C3—C2	1.376
C13—H13	0.9300	C3—C4	1.394
C13—C12	1.366 (6)	C2—H2	0.9300
C16—H16	0.9300	C11—H11	0.9300
C16—C17	1.377 (5)	C5—H5	0.9300
C7—N2	1.306 (4)	C5—C4	1.351
C19—H19	0.9300	C4—H4	0.9300
C7—N1—C14	126.8 (3)	C2—C1—N1	133.3
C1—N1—C14	125.0 (3)	C2—C1—C6	122.1
C1—N1—C7	106.5 (2)	C16—C17—H17	119.9
N1—C14—S1	120.5 (3)	C18—C17—C16	120.2
N1—C14—C15	115.5 (3)	C18—C17—H17	119.9
C15—C14—S1	124.0 (2)	C13—C12—H12	120.0
C20—C15—C14	119.9 (3)	C13—C12—C11	120.0
C16—C15—C14	121.5 (3)	C11—C12—H12	120.0
C16—C15—C20	118.5 (3)	N2—C6—C1	111.1 (3)
C9—C8—C13	119.3 (4)	N2—C6—C5	129.5
C9—C8—C7	122.1 (3)	C5—C6—C1	119.4 (4)
C13—C8—C7	118.6 (3)	C19—C18—H18	119.8
C8—C9—H9	120.3	C17—C18—C19	120.3
C10—C9—C8	119.5 (4)	C17—C18—H18	119.8
C10—C9—H9	120.3	C9—C10—H10	119.7
C15—C20—H20	120.0	C11—C10—C9	120.6
C19—C20—C15	120.1 (4)	C11—C10—H10	119.7
C19—C20—H20	120.0	C2—C3—H3	119.3
C8—C13—H13	119.9	C2—C3—C4	121.5
C12—C13—C8	120.3 (4)	C4—C3—H3	119.3
C12—C13—H13	119.9	C1—C2—H2	121.5
C15—C16—H16	119.7	C3—C2—C1	116.9 (4)
C15—C16—C17	120.6 (3)	C3—C2—H2	121.5
C17—C16—H16	119.7	C12—C11—H11	119.8
N1—C7—C8	124.1 (3)	C10—C11—C12	120.4
N2—C7—N1	111.6 (3)	C10—C11—H11	119.8
N2—C7—C8	124.2 (3)	C6—C5—H5	120.7
C20—C19—H19	119.9	C4—C5—C6	118.7 (4)
C18—C19—C20	120.3 (3)	C4—C5—H5	120.7
C18—C19—H19	119.9	C3—C4—H4	119.3
C7—N2—C6	106.2 (3)	C5—C4—C3	121.3
N1—C1—C6	104.5 (3)	C5—C4—H4	119.3

4.5 Conclusions

In conclusion, we have reported selective Hg^(II) sensing via Hg^(II)-mediated cyclization of a dithioamide, leading to a new benzimidazole derivative. Both the dithioamide and benzimidazole compounds were fully characterized by X-ray

crystallography. The Hg^(II)-mediated cyclization is presumed to occur via the formation of a transient Hg^(II)-thioamide species, which was characterized tentatively by ¹H-NMR. We expect to continue this study in the future with detailed selectivity studies under competitive conditions in the presence of more complicated metal mixtures and also perform similar studies with substituted derivatives, such as N,N'-(4,5-dimethyl-1,2-phenylene)dibenzothioamide.

4.6 Acknowledgements

We would like to thank Mr. Omar Fernandez, Mr. Yatfung Chiu, Ms. Maria Fabiola Alvarado-Yepes, and Ms. Naivys Rodriguez for synthetic assistance and an anonymous reviewer for constructive comments and suggestions. This research project was supported by the US Department of Energy Minority Serving Institution Partnership Program (MSIPP) managed by the Savannah River National Laboratory under SRNS contract BOA No: 541, TOA No. 0000332972 and 0000403067 to FIU. MTF was supported with a scholarship from Nuclear Energy University Programs, Office of Nuclear Energy, US Dept. of Energy, under the DE-NE 0008365 cooperative agreement with FIU.

4.7 References

- (1) Bernhoft, R. A. Mercury Toxicity and Treatment: A Review of the Literature. *J. Environ. Public Health* **2012**, 2012.
- (2) Puk, R.; Weber, J. H. Critical Review of Analytical Methods for Determination of Inorganic Mercury and Methylmercury Compounds. *Appl. Organomet. Chem.* **1994**, 8, 293–302.
- (3) Tian, K.; Siegel, G.; Tiwari, A. A Simple and Selective Colorimetric Mercury (II) Sensing System Based on Chitosan Stabilized Gold Nanoparticles and 2,6-Pyridinedicarboxylic Acid. *Mater. Sci. Eng. C* **2017**, 71, 195–199.

- (4) Suvarapu, L. N.; Baek, S.-O. Recent Developments in the Speciation and Determination of Mercury Using Various Analytical Techniques. *J. Anal. Methods Chem.* **2015**, *2015*.
- (5) Chen, G.-H.; Chen, W.-Y.; Yen, Y.-C.; Wang, C.-W.; Chang, H.-T.; Chen, C.-F. Detection of Mercury(II) Ions Using Colorimetric Gold Nanoparticles on Paper-Based Analytical Devices. *Anal. Chem.* **2014**, *86*, 6843–6849.
- (6) Atta, A. K.; Kim, S.-B.; Heo, J.; Cho, D.-G. Hg(II)-Mediated Intramolecular Cyclization Reaction in Aqueous Media and Its Application as Hg(II) Selective Indicator. *Org. Lett.* **2013**, *15*, 1072–1075.
- (7) Che, Y.; Wu, D.; Deng, C.; Liu, L.; Jia, D. 5-Bromoindole-3-Carboxaldehyde Ethylthiosemicarbazone for Hg(II) Sensing and Removal. *Chem. Phys. Lett.* **2016**, *644*, 171–175.
- (8) Song, K.; Mo, J.; Lu, C. Hg(II) Sensing Platforms with Improved Photostability: The Combination of Rhodamine Derived Chemosensors and up-Conversion Nanocrystals. *Spectrochim. Acta. A. Mol. Biomol. Spectrosc.* **2017**, *179*, 125–131.
- (9) Kavallieratos, K.; Rosenberg, J. M.; Chen, W.-Z.; Ren, T. Fluorescent Sensing and Selective Pb(II) Extraction by a Dansylamide Ion-Exchanger. *J. Am. Chem. Soc.* **2005**, *127*, 6514–6515.
- (10) Alvarado, R. J.; Rosenberg, J. M.; Andreu, A.; Bryan, J. C.; Chen, W.-Z.; Ren, T.; Kavallieratos, K. Structural Insights into the Coordination and Extraction of Pb(II) by Disulfonamide Ligands Derived from o-Phenylenediamine. *Inorg. Chem.* **2005**, *44*, 7951–7959.
- (11) Kavallieratos, K.; Rosenberg, J. M.; Bryan, J. C. Pb(II) Coordination and Synergistic Ion-Exchange Extraction by Combinations of Sulfonamide Chelates and 2,2'-Bipyridine. *Inorg. Chem.* **2005**, *44*, 2573–2575.
- (12) Lehman-Andino, I.; Su, J.; Papathanasiou, K. E.; Eaton, T. M.; Jian, J.; Dan, D.; Albrecht-Schmitt, T. E.; Dares, C. J.; Batista, E. R.; Yang, P.; Gibson, J. K.; Kavallieratos, K. Soft-Donor Dipicolinamide Derivatives for Selective Actinide(III)/Lanthanide(III) Separation: The Role of S- vs. O-Donor Sites. *Chem. Commun.* **2019**, *55*, 2441–2444.
- (13) Barker, H. A.; Smyth, R. D.; Weissbach, H.; Toohey, J. I.; Ladd, J. N.; Volcani, B. E. Isolation and Properties of Crystalline Cobamide Coenzymes Containing Benzimidazole or 5, 6-Dimethylbenzimidazole. *J. Biol. Chem.* **1960**, *235*, 480–488.

- (14) Spasov, A. A.; Yozhitsa, I. N.; Bugaeva, L. I.; Anisimova, V. A. Benzimidazole Derivatives: Spectrum of Pharmacological Activity and Toxicological Properties (a Review). *Pharm. Chem. J.* **1999**, *33*, 232–243.
- (15) Arjmand, F.; Mohani, B.; Ahmad, S. Synthesis, Antibacterial, Antifungal Activity and Interaction of CT-DNA with a New Benzimidazole Derived Cu(II) Complex. *Eur. J. Med. Chem.* **2005**, *40*, 1103–1110.
- (16) Tariq Khan, M.; Tahir Razi, M.; Jan, S.; Mukhtiar, M.; Gul, R.; Hussain, A.; Mehmood Hashmi, A.; Taufiq Ahmad, M.; Ahmed Shahwani, N.; Rabbani, I. Synthesis, Characterization and Antihypertensive Activity of 2-Phenyl Substituted Benzimidazoles. *Pak. J. Pharm. Sci.* **2018**, *31*.
- (17) Tonelli, M.; Simone, M.; Tasso, B.; Novelli, F.; Boido, V.; Sparatore, F.; Paglietti, G.; Pricl, S.; Giliberti, G.; Blois, S.; Ibba, C.; Sanna, G.; Loddo, R.; La Colla, P. Antiviral Activity of Benzimidazole Derivatives. II. Antiviral Activity of 2-Phenylbenzimidazole Derivatives. *Bioorg. Med. Chem.* **2010**, *18*, 2937–2953.
- (18) Tonelli, M.; Novelli, F.; Tasso, B.; Vazzana, I.; Sparatore, A.; Boido, V.; Sparatore, F.; La Colla, P.; Sanna, G.; Giliberti, G.; Busonera, B.; Farci, P.; Ibba, C.; Loddo, R. Antiviral Activity of Benzimidazole Derivatives. III. Novel Anti-CVB-5, Anti-RSV and Anti-Sb-1 Agents. *Bioorg. Med. Chem.* **2014**, *22*, 4893–4909.
- (19) Yerragunta, V.; Patil, P.; Srujana, S.; Devi, R.; Gayathri, R.; Srujana; Divya, A. Benzimidazole Derivatives and Its Biological Importance: A Review. *PharmaTutor Mag.* **2014**, *2*, 109-113
- (20) Peng, J.; Ye, M.; Zong, C.; Hu, F.; Feng, L.; Wang, X.; Wang, Y.; Chen, C. Copper-Catalyzed Intramolecular C–N Bond Formation: A Straightforward Synthesis of Benzimidazole Derivatives in Water. *J. Org. Chem.* **2011**, *76*, 716–719.
- (21) Fletcher, S. R.; McIver, E.; Lewis, S.; Burkamp, F.; Leech, C.; Mason, G.; Boyce, S.; Morrison, D.; Richards, G.; Sutton, K.; Jones, A. B. The Search for Novel TRPV1-Antagonists: From Carboxamides to Benzimidazoles and Indazolones. *Bioorg. Med. Chem. Lett.* **2006**, *16*, 2872–2876.
- (22) Ma, D.; Cai, Q. Copper/Amino Acid Catalyzed Cross-Couplings of Aryl and Vinyl Halides with Nucleophiles. *Acc. Chem. Res.* **2008**, *41*, 1450–1460.
- (23) Adharvana Chari, M.; Shobha, D.; Sasaki, T. Room Temperature Synthesis of Benzimidazole Derivatives Using Reusable Cobalt Hydroxide (II) and Cobalt Oxide (II) as Efficient Solid Catalysts. *Tetrahedron Lett.* **2011**, *52*, 5575–5580.
- (24) Alinezhad, H.; Salehian, F.; Biparva, P. Synthesis of Benzimidazole Derivatives Using Heterogeneous ZnO Nanoparticles. *Synth. Commun.* **2012**, *42*, 102–108.

- (25) Biswas, G.; Ghorai, S.; Bhattacharjya, A. Mercuric Chloride and Iodide Mediated Cyclization of Tethered Alkynedithioacetals as a General Route to Five- and Six-Membered Rings: Tuning of Regioselectivity by Alkyne Substitution. *Org. Lett.* **2006**, *8*, 313–316.
- (26) Ghorai, S.; Bhattacharjya, A. Mercury(II) Chloride-Mediated Cyclization–Rearrangement of O-Propargylglycolaldehyde Dithioacetals to 3-Pyranone Dithioketals: An Expeditious Access to 3-Pyranones. *Org. Lett.* **2005**, *7*, 207–210.
- (27) Su, Y.-S.; Lin, M.-J.; Sun, M.-C. Mercury Chloride Assisted Cyclization toward Benzimidazoles by Focused Microwave Irradiation. *Tetrahedron Lett.* **2005**, *46*, 177–180.
- (28) Wang, J.; He, Z.; Chen, X.; Song, W.; Lu, P.; Wang, Y. Efficient Access to Polysubstituted Amidines, Benzimidazoles and Pyrimidines from Amides. *Tetrahedron* **2010**, *66*, 1208–1214.
- (29) Azumaya, I.; Okamoto, I.; Nakayama, S.; Tanatani, A.; Yamaguchi, K.; Shudo, K.; Kagechika, H. A Chiral N-Methylbenzamide: Spontaneous Generation of Optical Activity. *Tetrahedron* **1999**, *55*, 11237–11246.
- (30) Zhu, Y.; Chuanzhao, L.; Biying, A. O.; Sudarmadji, M.; Chen, A.; Tuan, D. T.; Seayad, A. M. Stabilized Well-Dispersed Pd(0) Nanoparticles for Aminocarbonylation of Aryl Halides. *Dalton Trans.* **2011**, *40*, 9320–9325.
- (31) Moghaddam, F. M.; Boeini, H. Z. Oxidative Cyclization of Thiobenzanilides to Benzothiazoles Using N-Benzyl-DABCO Tribromide under Mild Conditions. *Synlett* **2005**, *2005*, 1612–1614.
- (32) Pedersen, B. S.; Scheibye, S.; Nilsson, N. H.; Lawesson, S.O. Studies on Organophosphorus Compounds XX. Syntheses of Thioketones. *Bull. Sociétés Chim. Belg.* **1978**, *87*, 223–228.
- (33) Sheldrick, G. M. Crystal Structure Refinement with SHELXL. *Acta Crystallogr. Sect. C Struct. Chem.* **2015**, *71*, 3–8.
- (34) Dolomanov, O. V.; Bourhis, L. J.; Gildea, R. J.; Howard, J. a. K.; Puschmann, H. OLEX2: A Complete Structure Solution, Refinement and Analysis Program. *J. Appl. Crystallogr.* **2009**, *42*, 339–341.

CHAPTER V: Pyridine-thioamide Ligands as Extractants and Sensors for Hg^(II) in Alkaline Solutions

Adenike O. Fasiku, Indranil Chakraborty, and Konstantinos Kavallieratos*

5.1 Abstract

Mercury is known for its toxicity and threat to public health. Its high accumulation in different chemical forms at the Savannah River Site (SRS) high-level waste stream has prompted its removal from this waste site. A 2,6-diaminopyridine based thioamide ligand (**PDT**) has been synthesized for the selective removal and sensing of Hg^(II). This ligand has pyridine and thiocarbonyl moieties as potential soft-donor binding sites for Hg^(II) and long alkyl chains for compatibility with most processing solvents. A shorter alkyl chain derivative (**PDAT**) was also synthesized to enhance spectroscopic and structural studies with common laboratory solvents. We show that Hg^(II) was totally extracted by **PDT** at different pHs, ranging from 7.0 – 14.0. At pH 13.0, when the concentration of **PDT** was varied from 0.30 – 2.00 mM, the extraction was observed to be quantitative up to 1 equivalent of Hg^(II) concentration (1.0 mM) at a percentage as high as 99.7% before plateauing. Hg^(II) shows the most response with **PDT** or **PDAT** (**LH₂**) with a conspicuous decrease in the absorbance at 319 nm when compared to other metal ions such as Sr²⁺, Ca²⁺, K⁺, Na⁺, Cs⁺, Zn²⁺, Pb²⁺, Cd²⁺, and Co²⁺. UV-Vis titrations of **LH₂** and DIPEA with Hg^(II) carried out in the presence vs. absence of several SRS-prevalent metal salts (Sr²⁺, Ca²⁺, K⁺, Na⁺, Cs⁺) show identical responses. In the presence of other competitive metals (Zn^(II), Pb^(II), Cd^(II)), the response to Hg^(II) was affected, yet a linear slope was still observed for Hg^(II) addition, allowing mercury analysis in complicated

matrices. The binding constants (K_{11}) for 1:1 Hg^{II} complex formation with **PDAT** and **PDT** (K_{11}) are $2.9 (\pm 0.7) \times 10^7 \text{ M}^{-1}$ and $2.0 (\pm 1.3) \times 10^7 \text{ M}^{-1}$ respectively.

5.2 Introduction

Mercury is a toxic metal that is introduced into the environment by both natural and anthropogenic activities.^{1,2} Human exposure to elevated mercury levels may cause several acute and chronic harmful symptoms to the nervous system, liver, and the kidneys.^{3,4} A serious problem of mercury in the environment is the conversion of inorganic mercury to highly-toxic organic mercury forms, which pose life-threatening risks to humans and ecosystems.³ An example of particular interest is the presence of mercury at the Savannah River DOE Site (Aiken, SC) due to its use as catalyst for the dissolution of aluminum cladding in used nuclear fuel, which has generated an increasing amount of accumulated mercury in both the alkaline high-level waste (HLW) tanks, and also in saltstone where low activity waste is stored post-reprocessing.¹ Some of this mercury is accumulated in the very toxic organic forms.¹ Due to the dangers of Hg exposure, efficient methods for its selective removal from aqueous systems have attracted research interest, including adsorption,⁵ membrane separation,⁶ chemical precipitation,⁷ ion exchange,⁵ and solvent extraction.^{8,9} There has also been a substantial interest for sensing Hg^{II} , which is the most mobile form of mercury in the environment,¹⁰ by optical methods, such as UV-Vis¹¹ and fluorescence.¹² However, few of these methods are applicable for alkaline solutions that resemble the samples at the Savannah River Site, which also contain large quantities of other metals, such as Sr^{2+} , Ca^{2+} , K^+ , Na^+ , and Cs^+ .

Solvent extraction in a typical hydrometallurgical process involves complexation of the targeted species with an organic ligand, therefore forming organosoluble complexes that are transferred from the aqueous to the organic phase. The compatibility of the extractant with industrial processing solvents, such as dodecane and kerosene¹³ is very important in solvent extraction, as these solvents assure low ligand partition to the aqueous phase, and efficient solvent recycling and reuse.⁹ Practical extractants should show strong and reversible binding, good stability, and high selectivity for the metal of interest. Several complexants and extractants including EDTA derivatives,¹⁴ thiocrowns,^{15,16} Schiff bases,^{17,18} and calixarenes¹⁹ have been used for complexation and extraction of Hg^(II) from aqueous solutions, yet only few examples²⁰ have been reported that could be used in alkaline solutions.

Thioamide ligands have been reported to form stable complexes with Hg^(II).²¹⁻²⁴ Hg^(II)-mediated cyclization reaction of a di-thioamide ligand derived from *o*-phenylenediamine to a mono thioamide benzimidazole derivative has also been reported.²⁵ Thioamides are versatile compounds known for their affinity for soft acids, like heavy metals, as they contain soft base sulfur moieties. When deprotonated, there is delocalization of π -electrons due to resonance which increases the basicity and binding affinity of the S-donor sites.²⁶

In this work, we are presenting the thioamide ligand N,N'-(pyridine-2,6-diyl)didodecanethioamide, (**PDT**) with long alkyl chains for Hg^(II) extraction and sensing, which is compatible with industrial processing solvents, and the shorter alkyl chain derivative, N,N'-(pyridine-2,6-diyl)diacetylthioamide (**PDAT**), which is more applicable

for spectroscopic and structural studies in more common laboratory solvents. We are also reporting the pincer complexes of these ligands with Hg^(II), and a spectroscopic and extraction study of Hg^(II) extraction from alkaline aqueous phase into octanol:dodecane (10:90), which showed removal as high as 99.7% at pH 13.0 via formation of a 1:1 Hg-**PDT** complex. This ligand family was also shown to be a sensor for Hg^(II) as a linear response was observed in the UV-Vis titration spectra of **PDAT** with HgCl₂ even in the presence of competitive metals of interest (Sr²⁺, Ca²⁺, K⁺, Na⁺, Cs⁺, Zn²⁺, Pb²⁺, Cd²⁺, and Co²⁺).

5.3 Experimental section

5.3.1 Materials and methods

All chemicals and materials were purchased from Fisher Scientific or Sigma-Aldrich. All chemicals were standard reagent grade and were used without further purification. ¹H and ¹³C-¹H-NMR spectra were recorded on a 400-MHz Bruker Avance NMR spectrometer with chemical shifts, δ , reported in ppm. The UV-Visible spectra were recorded on a CARY 100 Bio UV-Visible spectrophotometer, and FT-IR spectra were recorded on a Cary 600 series FT-IR spectrometer. X-ray diffraction studies were carried out on a Bruker D8 Quest with PHOTON 100 detector. Elemental analysis was provided by Atlantic Microlab Inc. The amide precursors **PDAA** and **PDA** for the synthesis of newly reported thioamides, (**PDAT** and **PDT**, respectively) were synthesized as previously reported²⁷ and were found spectroscopically identical to reported compounds.²⁷

5.3.3 Synthesis of N,N'-(pyridine-2,6-diyl)dithioacetamide (PDAT)

N,N'-(pyridine-2,6-diyl)diacetamide (3.0 g, 15.5 mmol) was weighed into a 250 mL 3-neck round bottom flask. 150 mL of distilled dry toluene was added to the flask and was left to stir. To this solution, 15.7 g (38.8 mmol, 2.5 eq.) of 2,4-bis(4-methoxyphenyl)-1,3,2,4,-dithiadiphosphetane-2,4-disulfide (Lawesson's Reagent) was added. The reaction mixture was then heated to reflux under nitrogen with constant stirring. After 30 min, the solution turned yellow. The reaction was monitored with TLC until the disappearance of the amide spot on the TLC plate. After 4 h, the volatiles was evaporated to dryness. A small volume of dichloromethane was used to dissolve the residue, which was subjected to *silica gel* column chromatography with ethyl acetate/hexanes (7:3) as the eluent. The yellow-band eluted fraction was dried *in vacuo* and was dissolved in a small volume of dichloromethane. Dropwise addition of hexanes and cooling at 4 °C gave a crystalline yellow precipitate, which was filtered, washed with hexanes, and dried under vacuum. Yield: 1.14 g, 5.06 mmol (33 %). ¹H-NMR (400 MHz, CDCl₃) δ 9.59 (s, 2H), 8.83 (d, *J* = 7.9 Hz, 2H), 7.86 (t, *J* = 7.9 Hz, 1H), 2.79 (s, 6H). ¹³C-¹H-NMR (101 MHz, CDCl₃) δ 200.34 (s), 149.83 (s), 140.67 (s), 112.92 (s), 37.52 (s). FT-IR (cm⁻¹); ν = 1443 (C=S), 3341 (N-H), 1601 (C=N). Elemental analysis (%) calculated for C₉H₁₁N₃S₂: C 47.97, H 4.92, N 18.65; Found: C 48.18, H 4.91, N 18.65.

5.3.4 Synthesis of N,N'-(pyridine-2,6-diyl)didodecanethioamide (PDT)

The following reaction must be performed in dry conditions and all glassware should be oven-dried properly before use. Dry toluene (250 mL) was added to N,N'-

(pyridine-2,6-diyl)didodecanamide (6.95 g, 14.7 mmol). To this solution, 2.2 eq. of 2,4-bis(4-methoxyphenyl)-1,3,2,4,-dithiadiphosphetane-2,4-disulfide - Lawesson's Reagent (13.04 g, 32.2 mmol) was added. The reaction mixture was then heated to reflux under nitrogen with constant stirring. After this time, the solution turned reddish-orange. After 3 h and as TLC showed no spot for the amide starting material, the reaction was stopped, and all the volatiles were evaporated to dryness. A small volume of dichloromethane was then added to dissolve the residue, which was subjected to *silica gel* column chromatography with ethyl acetate/hexanes (2:8) as the eluent. The yellow-band eluted fraction was dried *in vacuo* and recrystallized from hot ethanol. The yellow solid obtained was then filtered and dried under vacuum. 4.28 g. 8.11 mmol, (56.5 % yield). ^1H NMR (400 MHz, CDCl_3) δ 9.20 (s, 2H), 8.90 (s, 2H), 7.90 – 7.76 (m, 1H), 2.84 (s, 4H), 1.97 – 1.71 (m, 4H), 1.47 – 1.14 (m, 32H), 0.88 (t, $J = 6.8$ Hz, 6H). ^{13}C NMR (101 MHz, CDCl_3) δ 205.71 (s), 149.17 (s), 141.01 (s), 112.65 (s), 50.38 (s), 31.90 (s), 29.60 – 28.8 (m), 22.67 (s), 14.09 (s). FT-IR (cm^{-1}); $\nu = 1440$ (C=S), 3320 (N-H), 1605 (C=N). Elemental analysis (%) calculated for $\text{C}_{29}\text{H}_{51}\text{N}_3\text{S}_2$: C 68.86, H 10.16, N 8.31; Found: C 68.70, H 10.20, N 8.14.

5.3.5 Synthesis of Hg^{II} complex of PDAT [$\text{HgCl}(\text{HPDAT})$]

170.4 μL of DIPEA (2.2 eq., 0.96 mmol) is added dropwise to a solution of **PDAT** (100.0 mg, 0.44 mmol) in MeOH (30 mL)/ CH_2Cl_2 (10 mL) at room temperature. After stirring for 10 min, HgCl_2 (120.6 mg, 0.44 mmol) dissolved in 5 mL of MeOH was added dropwise. The solution changed color from bright yellow to almost colorless with a white precipitate forming. The reaction was left stirring for 30 min. Filtration of the

solution resulted in a white precipitate and an orange filtrate. After evaporation of all volatiles in the filtrate, the residue was recrystallized from CH₂Cl₂/hexanes, giving an orange powder. (50.6 mg, 0.11 mmol, 23.9 % yield). ¹H-NMR (400 MHz, CDCl₃) δ 7.77 (t, *J* = 7.9 Hz, 1H), 6.66 (d, *J* = 7.9 Hz, 2H), 2.64 (s, 6H). FT-IR (cm⁻¹); ν = 1432 (C=S), 1630(C=N). ¹³C-NMR (101 MHz, CDCl₃) δ 161.27 (s), 142.04 (s), 111.52 (s), 109.36 (s), 33.95 (s). Elemental analysis (%) calculated for C₉H₁₀ClHgN₃S₂·CH₃OH: C 24.39, H 2.87, N 8.53; Found: C 24.74, H 2.60, N 9.14.

5.3.6 Synthesis of the Hg^(II) complex of PDT [HgCl(HPDT)]

155.2 μL of DIPEA (2.2 eq., 0.87 mmol) was added dropwise to a solution of PDT (200.0 mg, 0.39 mmol) in MeOH (40 mL)/CH₂Cl₂ (20 mL) at room temperature. After stirring for 20 min, HgCl₂ (107.3 mg, 0.40 mmol) dissolved in 5 mL of MeOH was added dropwise. The solution changed color from bright yellow to almost colorless. After 2h the volatiles were evaporated, 10 mL CH₂Cl₂ was added to the flask and the insoluble yellow precipitates gotten were filtered off using gravity filtration while the filtrate was dried *in-vacuo*. The product was then recrystallized from DCM/Hexanes, dried and weighed as 192.6 mg (0.26 mmol, 67.7 % yield). ¹H-NMR (400 MHz, CDCl₃) δ 7.74 (t, *J* = 7.9 Hz, 1H), 6.63 (d, *J* = 7.9 Hz, 2H), 2.89 – 2.72 (m, 4H), 1.89 – 1.74 (m, 4H), 1.49 – 1.14 (m, 32H), 0.88 (t, *J* = 6.8 Hz, 6H). FT-IR (cm⁻¹); ν = 1430 (C=S), 1644 (C=N). ¹³C-NMR (101 MHz, CDCl₃) δ 166.94 (s), 161.64 (s), 142.01 (s), 111.52 (s), 46.83 (s), 31.92 (s), 29.64 - 29.26 (m), 27.84 (s), 22.68 (s), 14.10 (s). Elemental analysis (%) calculated for C₂₉H₅₀ClHgN₃S₂: C 47.01, H 6.80, N 5.67; Found: C 46.98, H 6.70, N 5.75.

5.3.7 UV-Vis titration of PDAT or PDT with HgCl₂

Solutions of ligands **PDAT or PDT (LH₂)** and DIPEA in methanol were titrated with HgCl₂ at constant ligand concentration. In a typical experiment, a solution of **L** (2.0×10^{-5} M) in methanol and 2.2 eq. of DIPEA (solution A) was titrated with a solution of HgCl₂ (2.0×10^{-4} M) (solution B) prepared by the dissolution of 0.54 mg of HgCl₂ in solution A in a 10 mL volumetric flask, thus keeping a constant concentration of ligand upon titration of solution A with solution B. 2.300 mL of solution A were added to the UV-Visible cuvette and solution B was added in 5-50 μ L increments until a total of 550 μ L had been added. The absorbance changes were monitored, with the results plotted and fitted to the 1:1 binding isotherm using non-linear regression analysis. The UV-Vis titration of **PDAT** with HgCl₂ in the absence of an organic base was performed similarly, but without the addition of DIPEA.

5.3.8 Competitive UV-Vis titration of PDAT with HgCl₂ in the presence of other metals.

A solution of **PDAT** (2.0×10^{-5} M) and 2.2 eq. of DIPEA containing Sr²⁺ (1.0×10^{-3} M), Ca²⁺ (1.0×10^{-3} M), K⁺ (1.0×10^{-3} M), Na⁺ (1.0×10^{-2} M) as chloride salts and Cs⁺ (1.0×10^{-3} M) as fluoride salt was prepared in 50.0 mL methanol (solution A). Solution A was titrated with a solution of HgCl₂ (2.0×10^{-4} M) (solution B) prepared by the dissolution of 0.54 mg of HgCl₂ in solution A in a 10.0 mL volumetric flask, thus keeping a constant concentration of ligand and all metals, with the exception of Hg^(II) during the titration. Solution A (2.300 mL) was added to the UV-Visible cuvette, and solution B was added in 5-50 μ L increments until a total of 550 μ L had been added. The absorbance changes were monitored and compared with the titration when only Hg^(II) was

added, and no other metals were present. A similar titration experiment to the above was also performed by adding Pb^{2+} , Cd^{2+} and Zn^{2+} (1.0×10^{-4} M each, as chloride salts) to the ligand solution, in addition to the other metals (Sr^{2+} , Ca^{2+} , K^+ , Na^+ , and Cs^{2+}).

5.3.9 UV-Vis spectroscopic experiments ($\text{Hg}^{(II)}$ vs. other metals)

2.00 mL methanol solutions of the chloride salts of several metals (Ca^{2+} , K^+ , Cs^+ , Na^+ , Hg^{2+} , Ag^+ , Co^{2+} , Sr^{2+} , Pb^{2+} , Cd^{2+} and Zn^{2+} - 1×10^{-3} M) were added to 2.00 mL methanolic solutions of **PDT** (1.0×10^{-3} M) and DIPEA (2.5×10^{-3} M). The UV-Vis spectra were collected after equilibrium had been reached and the absorption at 319 nm was recorded.

5.3.10 Determination of complexation stoichiometry by the continuous variation method (Job Plot)

Information on the stoichiometry of the complex was obtained from the continuous variation method.²⁸ Solutions containing varying concentrations of $\text{Hg}^{(II)}$ and **PDT** were prepared in methanol. A stock solution of ligand (0.020 mM) and HgCl_2 (0.020 mM) was used. Both solutions were mixed from the molar fractions of 0.1 to 0.9 while maintaining a constant overall concentration of 0.020 mM. The absorbance of the solutions were measured. Afterward, the plot of the ΔA at 319 nm vs. mol ratio of the $[\text{PDT}]_t$ was obtained.

$$\text{Mol ratio of } \text{Hg}^{(II)} = \frac{[\text{Hg}^{(II)}]_t}{[\text{Hg}^{(II)}]_t + [\text{PDT}]_t} \quad (1)$$

5.3.11 Extraction studies

The $\text{Hg}^{(\text{II})}$ extraction at constant concentrations of **PDT** from aqueous phases of variable alkalinity was studied using aqueous solutions of HgCl_2 and NaOH . In a typical experiment, 5.00 mL of aqueous $\text{Hg}^{(\text{II})}$ solutions were prepared by adding various volumes of NaOH (10^{-6} – 1 M; pH 7, 8, 9, 10, 11, 12, 13, 14) to 0.5 mL of a 10.0 mM HgCl_2 solution and subsequently diluted up to 5.0 mL mark. The final $[\text{Hg}^{(\text{II})}]_t$ in aqueous solution was 9.8×10^{-4} M. The aqueous phases were then equilibrated with 5.00 mL solutions of 5 mM **PDT** in octanol:dodecane (1:9) by rotating on a wheel at 55 rpm. After contacting both phases for 24 h, the solutions were centrifuged for 5 min for proper separation of both layers. Slope analysis experiments were performed at both pH 13.0 and pH 7.0. Solutions of various concentrations of **PDT** in octanol:dodecane (1:9) were prepared and contacted with HgCl_2 solutions. The **PDT** dependence was determined by preparing 5.00 mL solutions of various concentrations of **PDT** (0.30 – 2.00 mM) in 1,2-dichloroethane (DCE) and contacting with 5.00 mL of aqueous solutions of HgCl_2 (1.0 mM) at pH 13.0 (NaOH ; 10^{-1} M).

The concentration of the residual unextracted $\text{Hg}^{(\text{II})}$ in the aqueous phase after extraction was determined using the dithizone method of mercury quantification.²⁹ The % extraction (% E) of $\text{Hg}^{(\text{II})}$ was calculated as follows:

$$\%E = \frac{C_0 - C}{C_0} \times 100 \quad (2)$$

C_0 is the initial concentration in the aqueous phase before extraction, and C denotes the concentration in the aqueous phase after extraction. The Distribution coefficient D , was calculated as

$$D = \frac{C_0 - C}{C} \quad (3)$$

5.3.12 X-ray crystallography

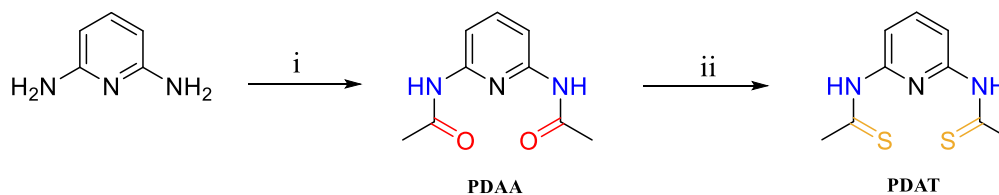
Dark yellow block-shaped crystals of **PDT** were obtained by slow diffusion of hexanes into a dichloromethane solution. Data collection and structure refinement details are summarized in Table 5.1. A suitable crystal was selected and mounted on a Bruker D8 Quest diffractometer equipped with PHOTON II detector operating at $T = 298$ K. The structure was solved in space group $P3_2$ (# 145) determined by the *ShelXS*³⁰ structure solution program using Direct Methods and refined by Least Squares using version 2018/3 of *ShelXL*.³¹ All non-hydrogen atoms were refined anisotropically. Calculations and molecular graphics were performed using *SHELXTL 2014* and *Olex2*³² programs.

5.4 Results and discussion

5.4.1 Synthesis

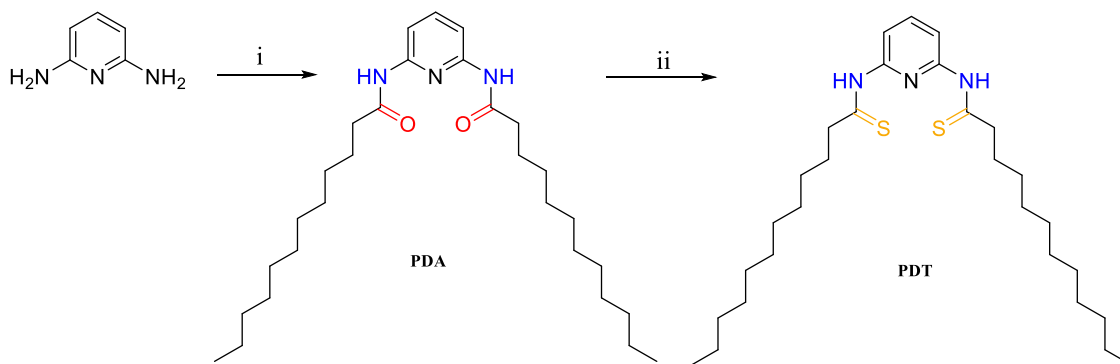
The thioamide ligands **PDAT** and **PDT (LH₂)** were synthesized from the corresponding amides PDAA and PDA²⁷ (Scheme 5.1) using Lawesson's reaction,³³ and were fully characterized by FT-IR, NMR, Elemental Analysis, and in the case of **PDAT** by X-ray Crystallography.

The Hg^(II) complexes of both ligands were isolated from the reaction of **L** with mercuric chloride. The complexes were characterized with ¹H-NMR, FT-IR and elemental analysis. The elemental analysis matches a complex formulation of the type [HgCl(LH)], where **LH₂** is either **PDAT** or **PDT**, indicating 1:1 complexation of the metal to the thioamide ligand with formulas for both complexes shown in Scheme 5.3.



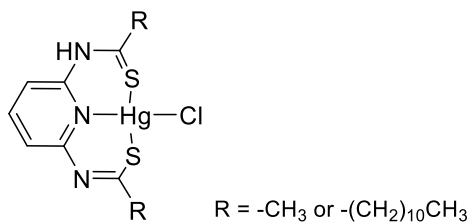
- i) 2.2 eq. acetic anhydride, Et₃N, CH₂Cl₂, 0 °C - rt, 24 hr
 ii) Lawesson's reagent, toluene, reflux, 4 hr

Scheme 5.1: Synthetic route to the short-chain thioamide ligand **PDAT**



- i) 2.2 eq. dodecanoyl chloride, THF, 0 °C - rt, 24 hr
 ii) Lawesson's reagent, toluene, reflux, 4 hr

Scheme 5.2: Synthetic route to the long-chain thioamide ligand **PDT**



Scheme 5.3: Proposed structure of Hg^(II) pincer complexes.

5.4.2 FT-IR studies

The infrared spectra of **PDT** and **PDAT** and their complexes are shown in Figure 5.1. For **PDAT** (Figure 5.1a), three distinct bands at 3341, 1443, and 1601 cm^{-1} are attributed to the stretching vibrations of N-H of the thioamide moiety, C=S of the thiocarbonyl group,³⁴ and C=N of the pyridine group³⁵, respectively. The N-H band disappeared in the IR spectrum of the complex, indicating the deprotonation of the amide N. The initial C=S stretch at 1443 cm^{-1} was observed at a lower frequency of 1432 cm^{-1} in the complex. Likewise, a large shift of the C=N band of the ligand from 1601 to 1630 cm^{-1} in the complex spectrum confirms the coordination of the pyridinyl N atom to the metal atom. Strong and medium intensity bands at 1600–1400 cm^{-1} correspond to the C=N and C=C stretching vibrations. Similar observations were recorded for the **PDT** ligand and its complex: The N-H band at 3320 cm^{-1} disappeared upon deprotonation. The C-N band increased in frequency from 1605 cm^{-1} from the ligand to 1664 cm^{-1} of the complex, as it would be expected by ligand deprotonation and Hg-S bond formation, which could increase the contribution of S-C=N resonance form to the structure. A shift to a lower frequency of the C=S band at 1440 cm^{-1} from the ligand to 1430 cm^{-1} of the complex was also observed, which may also be indicative of Hg-S bond formation.

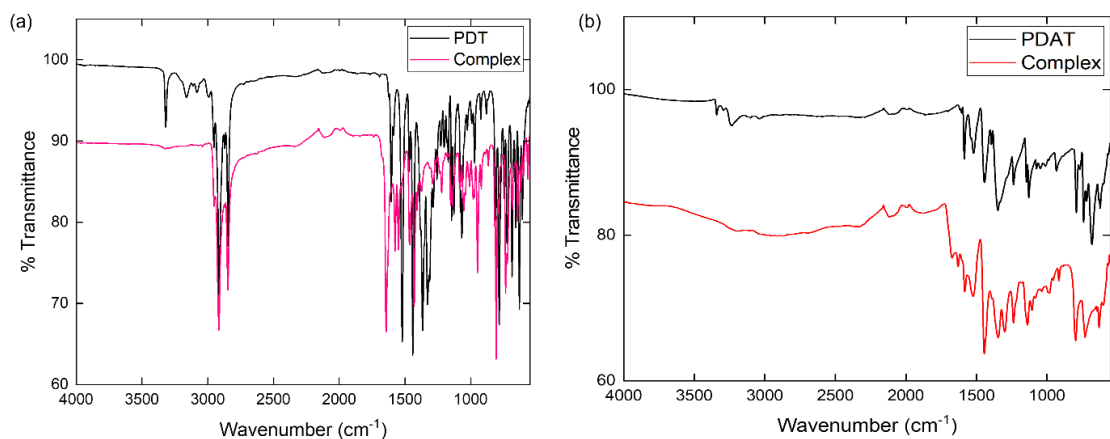


Figure 5.1: (a) FT-IR spectrum of **PDT** vs. the **PDT-Hg^(II)** complex (b) FT-IR spectrum of **PDAT** vs. the **PDAT-Hg^(II)** complex

5.4.3 NMR spectroscopy

The ¹H-NMR spectra of free **PDT**, **PDT** with DIPEA, and its isolated Hg^(II) complex in CDCl₃ are shown in Figure 5.2. The ligand and the complex spectra differ significantly. The signals appearing at δ 2.84 (triplet) ppm, 1.97 ppm (quartet), 1.47 - 1.14 ppm (multiplet), and 0.88 ppm (triplet) in the ligand spectra correspond respectively to the first four protons of (-CH₂-), labeled as 4 in Figure 5.2, second four protons of (-CH₂-), labeled as 5 in Figure 5.2, thirty-two protons of (-CH₂-), labeled as 6 in Figure 5.2, and last six protons of (-CH₃) alkyl chain labeled as 7 in Figure 5.2. The N-H resonance for **PDT** at δ 9.20 is no longer present at the spectrum of the Hg^(II) complex. The aromatic proton (H2) at δ 8.90 ppm assigned to the proton closest to the pyridine N shifted upfield to δ 6.63 ppm in the spectrum of the Hg^(II) complex. Slight chemical shift changes were observed for other protons.

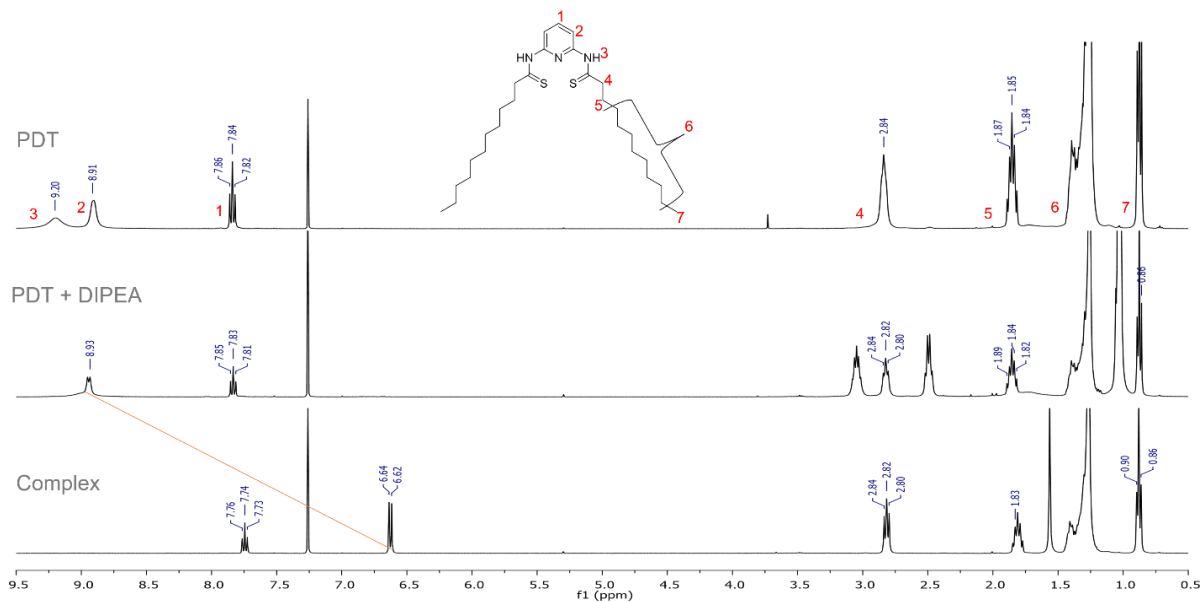


Figure 5.2: $^1\text{H-NMR}$ spectra of **PDT** vs. the **PDT-Hg^(II)** complex in CDCl_3 , 298K

$^1\text{H-NMR}$ titration of **PDAT** with HgCl_2 in MeOD was carried out at 298 K (Figure 5.3). Upon gradual addition of $\text{Hg}^{(\text{II})}$ (4.0×10^{-2} M) to the ligand solution (4.0×10^{-3} M), shift changes in the $^1\text{H-NMR}$ signals were observed until a 1:1 $\text{Hg}^{(\text{II})}$ -**PDAT** complex was completely formed. Just as observed for **PDT**, the gradual disappearance of the aromatic proton H_b at δ 8.83 ppm and its gradual appearance at δ 6.66 ppm indicates complex formation. Afterward, with excess $\text{Hg}^{(\text{II})}$ addition (2 equivalents of $\text{Hg}^{(\text{II})}$ or more), an insoluble complex was formed, and this precipitated out of the solution, thereby resulting in no $^1\text{H-NMR}$ signals.

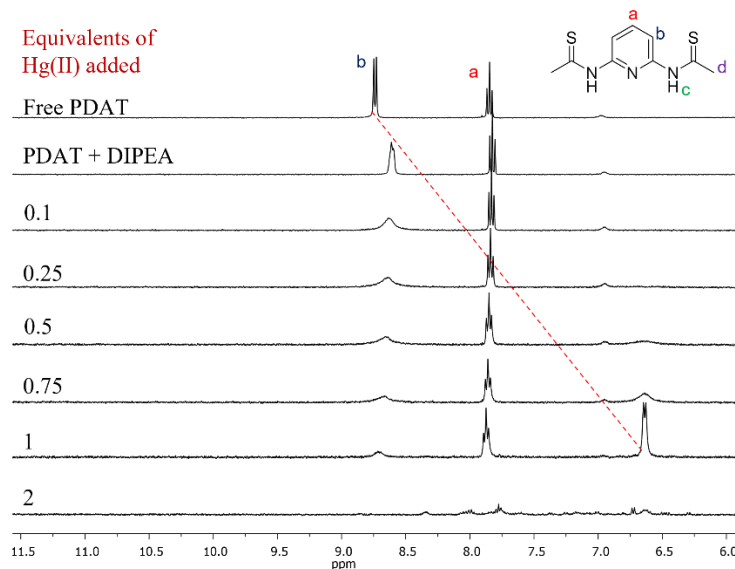


Fig. 5.3: Aromatic region of the $^1\text{H-NMR}$ titration spectra of **PDAT** with HgCl_2 . ($[\text{PDAT}]$: $4.0 \times 10^{-3} \text{ M}$, $[\text{Hg(II)}]$: $4.0 \times 10^{-2} \text{ M}$, **DIPEA**: 2.2 eq., Solvent: *MeOD*, temp: 298 K)

5.4.4 UV-Vis binding and sensing studies

5.4.4.1 UV-Vis titrations

The addition of HgCl_2 to solutions of **PDAT** or **PDT** and **DIPEA** in methanol gave a decrease in bands at 278 nm and 319 nm with a concurrent increase at 232 nm and two clear isosbestic points, which is indicative of the presence of a distinct $\text{Hg}^{\text{(II)}}$ complex in solution. Solutions of ligands (either **PDAT** or **PDT**, $2.0 \times 10^{-5} \text{ M}$) in methanol and 2.2 equivalents of **DIPEA** were titrated with HgCl_2 . The two thioamide ligands exhibit similar absorption spectra with two initial absorption bands at ca. 278 and 319 nm (Figures 5.4a and 5.5a). The two bands can be attributed respectively to the $\pi\text{-}\pi^*$ transitions of the pyridine ring and $\text{n-}\pi^*$ of the thiocarboxamide group, respectively. When the concentration of $\text{Hg}^{\text{(II)}}$ gradually increased, the absorption bands at these wavelengths

decreased with clear isosbestic points observed at 260 nm and 215 nm. After excess addition of $\text{Hg}^{(\text{II})}$, the isosbestic point at ca 215 nm gradually disappeared as a result of the absorption of uncomplexed excess HgCl_2 . The binding curves of the titration for both ligands (Figures 5.4b and 5.5b) taken at 319 nm show saturation at $2.0 \times 10^{-5} \text{ M}$ of $\text{Hg}^{(\text{II})}$, which corresponds to 1:1 binding. The binding constants for $\text{Hg}^{(\text{II})}$ complex formation were determined by non-linear regression analysis fitted to the 1:1 binding isotherm³⁶ from independent triplicate measurements and were found to be $K_{11} = 2.9 (\pm 0.7) \times 10^7 \text{ M}^{-1}$ for **PDAT** and $2.0 (\pm 1.3) \times 10^7 \text{ M}^{-1}$ for **PDT**.

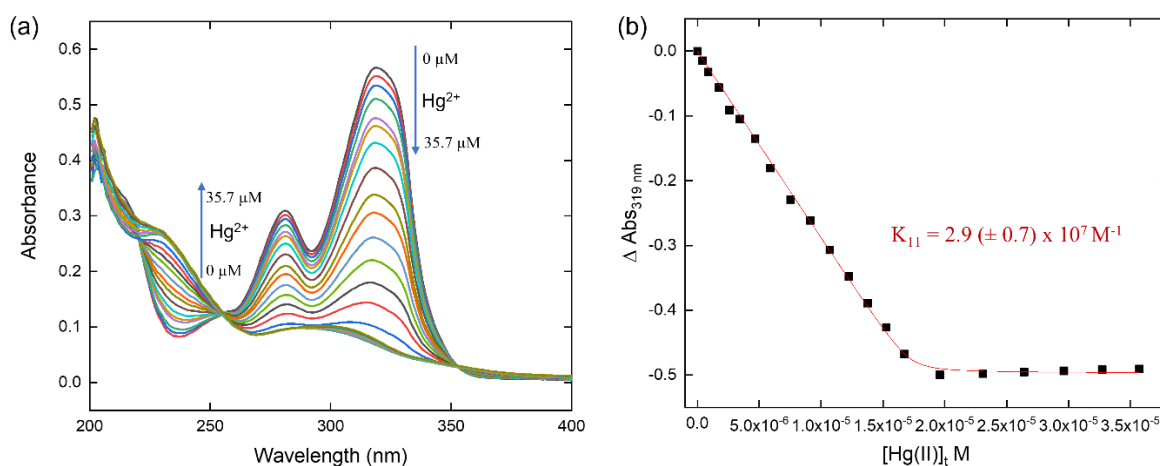


Figure 5.4: (a) UV-Vis titration spectra of **PDAT** ($2 \times 10^{-5} \text{ M}$) and **DIPEA** ($4.4 \times 10^{-4} \text{ M}$) with HgCl_2 ($2.0 \times 10^{-4} \text{ M}$) in methanol. (b) Absorption as a function of $\text{Hg}^{(\text{II})}$ concentration at 319 nm.

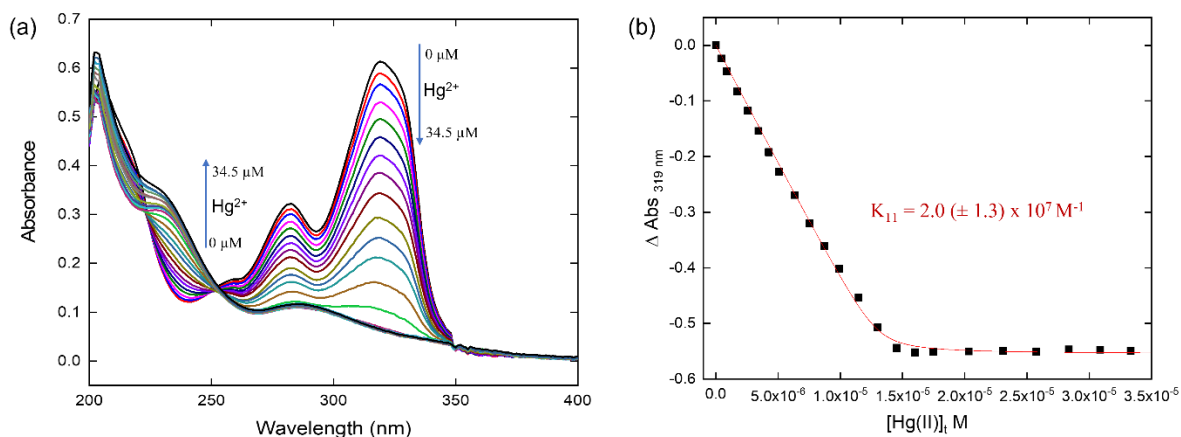


Figure 5.5: (a) UV-Vis titration spectra of **PDAT** ($2.0 \times 10^{-5} M$) and **DIPEA** ($4.4 \times 10^{-4} M$) with $HgCl_2$ ($2 \times 10^{-4} M$) in methanol. (b) Absorption as a function of $Hg^{(II)}$ concentration at 319 nm.

Similar titration experiments were performed with **PDAT** in the absence of an organic base in order to see if and how non-deprotonated **PDAT** can bind to $Hg^{(II)}$ (Figures 5.6(a) and (b)). This experiment shows different absorption spectra when $Hg^{(II)}$ was added in the absence of the base: Two new bands at 335 nm and 365 nm were observed. Until the amount of $Hg^{(II)}$ solution added reached 1.0 equivalent point, the absorption band at 319 nm reached the minimum value (thick blue line) and then gradually increased and red-shifted gradually to 365 nm (thick blue line) and finally blue-shifted to 335 nm (thick red line) until little or no further response was observed (Figure 5.6a). From the plot of ΔA at these four wavelengths (278, 319, 335, and 365 nm) as a function of $Hg^{(II)}$ -**PDAT** molar ratio (Figure 5.6b), we see that there was a quantitative response of our ligand to $Hg^{(II)}$ up until 1 equivalent of $Hg^{(II)}$ was added, followed by a different response up to the addition of 2 equivalents of $Hg^{(II)}$. This indicates the formation of two different mercury $Hg^{(II)}$ complexes with **PDAT**, when not deprotonated, in the

absence of an organic base. The spectroscopic changes are consistent with 1:1 Hg:PDAT complexation followed by 2:1 Hg:PDAT complexation in the presence of excess mercury.

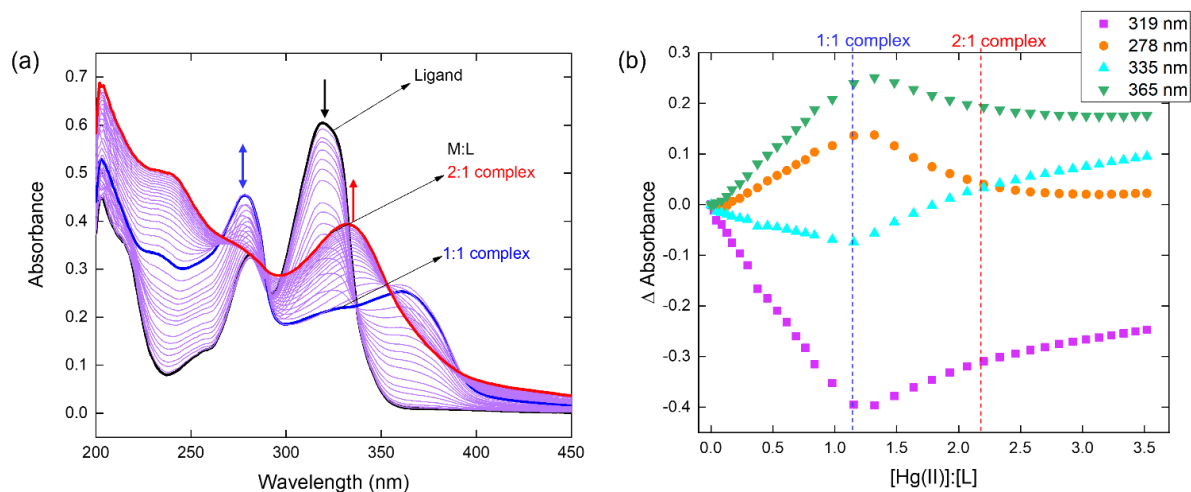


Figure 5.6: (a) UV-Vis titration spectra of **PDAT** with HgCl_2 in the absence of organic base ($[\text{PDAT}]$: $2.0 \times 10^{-5} \text{ M}$, $[\text{Hg}^{(\text{II})}]$: $2.0 \times 10^{-4} \text{ M}$, Solvent: Methanol) (b) absorption as a function of $\text{Hg}^{(\text{II})}$ -**PDAT** molar ratio at 278, 319, 335 and 365 nm. Dash lines indicate $\text{Hg}^{(\text{II})}$ -**PDAT** complex stoichiometries.

5.4.4.2 Determination of binding stoichiometry for $\text{Hg}^{(\text{II})}$ complexation (Job Plots)

The binding stoichiometry for complex formation of thioamide ligands **PDAT** and **PDT** with $\text{Hg}^{(\text{II})}$ was confirmed by the continuous variation method (Job Plots).²⁸ The Job plot obtained at 298 K in methanol ($1.0 \times 10^{-4} \text{ M}$) for binding of **PDAT** with $\text{Hg}^{(\text{II})}$ (monitored at 319 nm) is shown in Figure 5.7. It can be seen that the significant absorbance changes were observed when the molar ratio of the ligand to metal was 0.5, indicating the formation of a 1:1 $\text{Hg}^{(\text{II})}$:**L** complex. This is consistent with the proposed structure in Scheme 5.3.

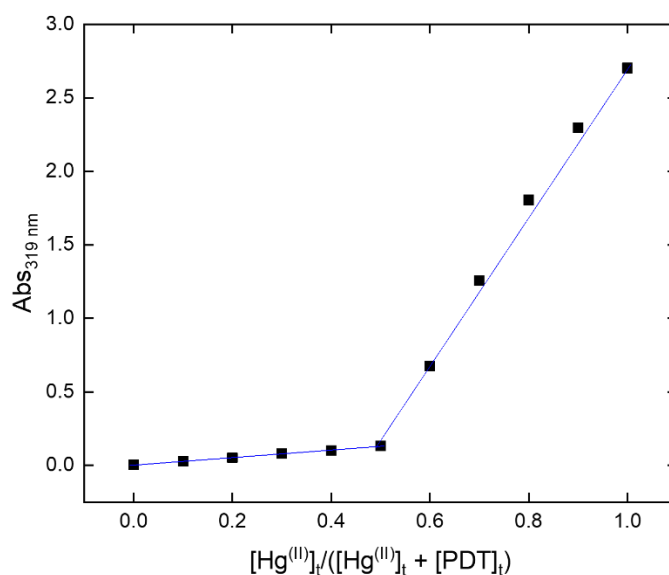


Figure 5.7: Job plot of **PDT** and $\text{Hg}^{(\text{II})}$ in methanol. ($[\text{PDT}]$: 1.0×10^{-4} M, $[\text{DIPEA}]$: 2.2×10^{-4} M, $[\text{Hg}^{(\text{II})}]$: 1.0×10^{-4} M)

5.4.4.3 Optical sensing of $\text{Hg}^{(\text{II})}$ with **PDT** and **PDAT**: comparison with other metals

The sensing response of **PDT** (1.0×10^{-4} M, in MeOH) for $\text{Hg}^{(\text{II})}$ in comparison with other metals such as $\text{Sr}^{(\text{II})}$, $\text{Ca}^{(\text{II})}$, $\text{K}^{(\text{I})}$, $\text{Na}^{(\text{I})}$, $\text{Cs}^{(\text{I})}$, $\text{Zn}^{(\text{II})}$, $\text{Pb}^{(\text{II})}$, $\text{Cd}^{(\text{II})}$, and $\text{Co}^{(\text{II})}$ in their chloride salts was monitored by the UV-Vis spectroscopic changes in solutions of the ligand after addition of the metal in methanol. One equivalent of these metals (1.0×10^{-4} M, in MeOH) was added separately to solutions of **PDT** and allowed to reach equilibrium. As shown in Figure 5.8, no changes were observed with $\text{Sr}^{(\text{II})}$, $\text{Ca}^{(\text{II})}$, $\text{K}^{(\text{I})}$, $\text{Na}^{(\text{I})}$, $\text{Cs}^{(\text{I})}$. Some changes were observed for $\text{Zn}^{(\text{II})}$, $\text{Pb}^{(\text{II})}$, $\text{Cd}^{(\text{II})}$, and $\text{Co}^{(\text{II})}$, while $\text{Hg}^{(\text{II})}$ gave the strongest response. In order to investigate the actual response of the **PDAT** to $\text{Hg}^{(\text{II})}$ in the presence of potentially competing metals, competitive experiments of **PDAT** with $\text{Hg}^{(\text{II})}$ in the presence of complex multi-cation matrices were carried out (Figure 5.9).

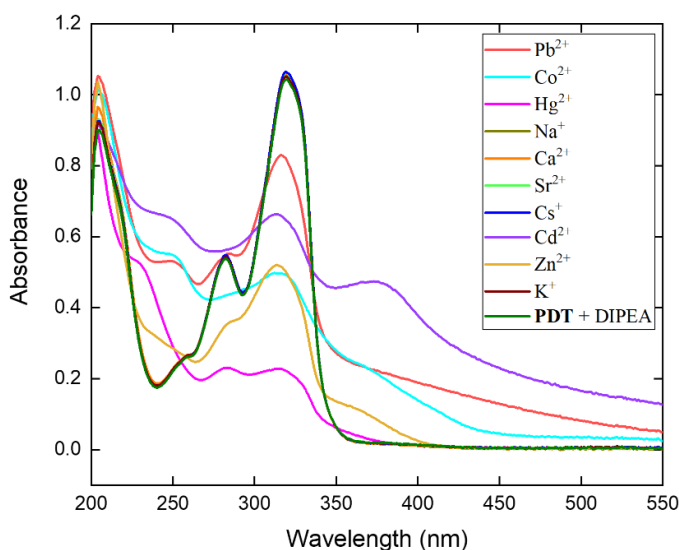


Figure 5.8: UV-Vis spectra of **PDT** and **PDT-metal** methanolic solutions ($[PDT]_i$: 1.0×10^{-4} M, DIPEA: 2.2 eq., $[M^{2+}]_i$ or $[M^+]_i$: 1.0×10^{-4} M (prepared as chloride or fluoride salts), solvent: methanol)

The titration of **PDAT** with $Hg^{(II)}$ in the presence of $Sr^{(II)}$, $Ca^{(II)}$, $K^{(I)}$, $Na^{(I)}$, $Cs^{(I)}$, which are abundant at HLW, was carried out in methanol. Figure 5.9a shows electronic spectra for the responses of **PDAT** to $Hg^{(II)}$ are completely unaffected even in the presence of higher concentrations of these metal ions, Na^+ (100 eq.) and $Sr^{(II)}$, $Ca^{(II)}$, $K^{(I)}$, $Cs^{(I)}$ (10 eq.) This result shows that these metals do not interfere with the $Hg^{(II)}$ complexation by **PDAT**, as the titration curves for $Hg^{(II)}$ addition in the presence vs absence of high constant concentration of competing metals is practically identical (Figure 5.9b).

To further ascertain the quantitative response of **PDAT** to the addition of $Hg^{(II)}$, competitive experiments of **PDAT** with $Hg^{(II)}$ in the presence of more competitive metals such as $Zn^{(II)}$, $Pb^{(II)}$, and $Cd^{(II)}$ (1.0×10^{-4} M) together with the prior alkaline/alkaline earth metal matrix were conducted (Figure 5.9c). Despite the presence of additional competing

metals, a linear quantitative response with addition of $\text{Hg}^{(\text{II})}$ was observed with saturation at exactly 1 equivalent of $\text{Hg}^{(\text{II})}$ to ligand (Figure 5.9d). These results indicate excellent selectivity toward $\text{Hg}^{(\text{II})}$ and point to potential applicability of this sensor in complicated matrices.

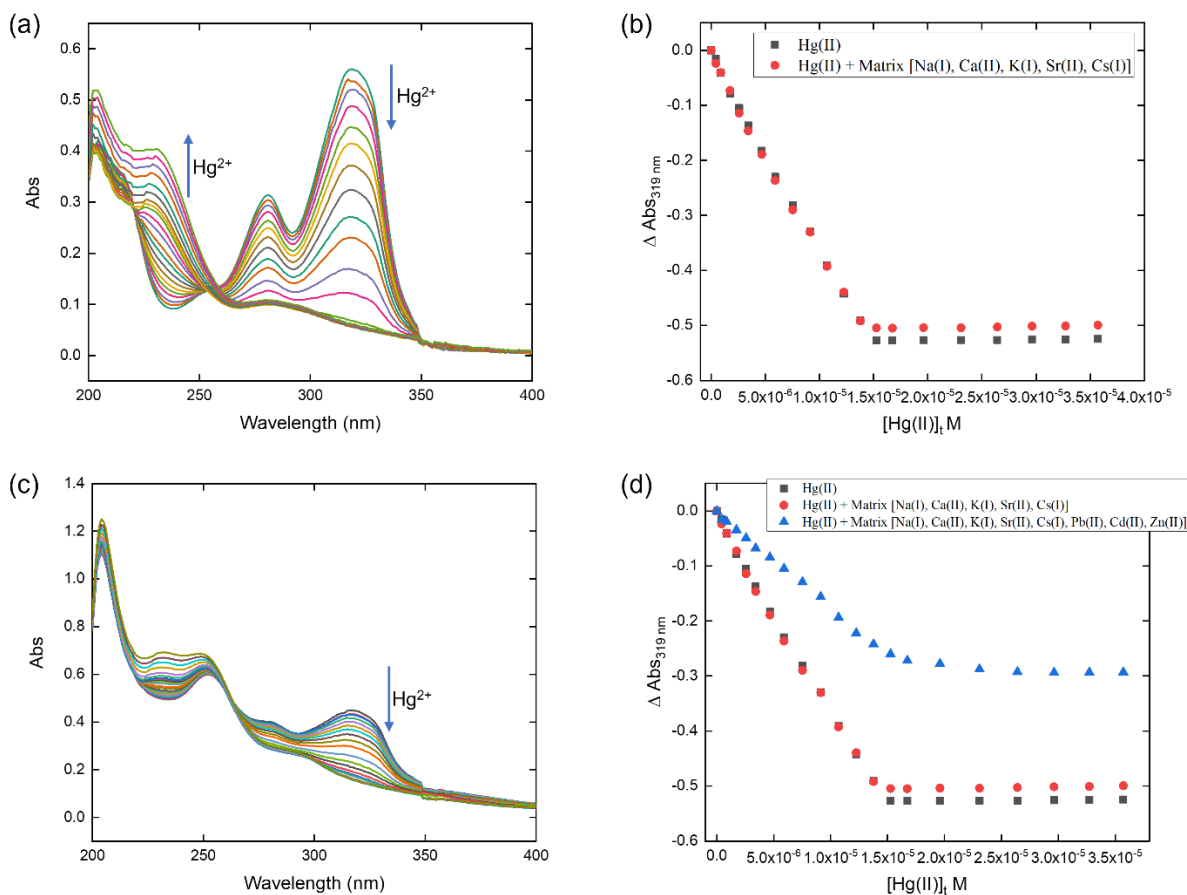


Figure 5.9: (a) UV-Vis titration spectra of **PDAT** with HgCl_2 in the presence of competitive cations ($[\text{PDAT}]$: $2.0 \times 10^{-5} \text{ M}$, DIPEA : 2.2 eq., $[\text{Hg}^{(\text{II})}]_i$: $2.0 \times 10^{-4} \text{ M}$, Solvent: Methanol, $[\text{Sr}^{(\text{II})}]_i$, $[\text{Ca}^{(\text{II})}]_i$, $[\text{K}^{(\text{I})}]_i$, $[\text{Cs}^{(\text{I})}]_i$: $1.0 \times 10^{-3} \text{ M}$, $[\text{Na}^{(\text{I})}]_i$: $1.0 \times 10^{-2} \text{ M}$) (b) absorption as a function of $\text{Hg}^{(\text{II})}$ concentrations at 319 nm comparing titration with $\text{Hg}^{(\text{II})}$ alone and titration with $\text{Hg}^{(\text{II})}$ in the presence of other cations. : (c) UV-Vis titration spectra of **PDAT** with HgCl_2 in the presence of competitive cations ($[\text{PDAT}]$: $2 \times 10^{-5} \text{ M}$, DIPEA : 2.2 eq., $[\text{Hg}^{(\text{II})}]$: $2.0 \times 10^{-4} \text{ M}$, Solvent: Methanol, $[\text{Sr}^{(\text{II})}]_i$, $[\text{Ca}^{(\text{II})}]_i$, $[\text{K}^{(\text{I})}]_i$, $[\text{Cs}^{(\text{I})}]_i$: $1.0 \times 10^{-3} \text{ M}$, $[\text{Zn}^{(\text{II})}]_i$, $[\text{Pb}^{(\text{II})}]_i$, $[\text{Cd}^{(\text{II})}]_i$: $1.0 \times 10^{-4} \text{ M}$, $[\text{Na}^+]_i$: $1.0 \times 10^{-2} \text{ M}$) (d) absorption as a function of $\text{Hg}^{(\text{II})}$ concentrations at 319 nm comparing titration with $\text{Hg}^{(\text{II})}$ alone and titration with $\text{Hg}^{(\text{II})}$ in the presence of other metals including Zn, Pb and Cd.

5.4.5 Extraction studies

5.4.5.1 pH dependent extraction of Hg^(II) by PDT

The extraction of Hg^(II) by PDT was studied at equilibrium conditions for pH range 7.0-14.0 by using equal volumes of aqueous (10^{-6} – 1 M; pH 7, 8, 9, 10, 11, 12, 13, 14 NaOH) and organic (10:90 octanol:dodecane) phases. 100 % extraction was recorded at all pHs indicating that the complexation of the PDT ligand to Hg^(II) can occur for both deprotonated and non-deprotonated forms of PDT. However, black precipitates were also observed for extraction solutions at pH 7.0-11.0. On the other hand, no precipitates were observed for solutions at pH 12.0-14.0. This shows that a stable complex that can be applied for practical extraction application is formed when the deprotonated PDT complexes mercury. Stripping and recovery of Hg^(II) from organic phases was, however, unsuccessful, as precipitates formed immediately when acidic aqueous solutions were contacted to the organic phase.

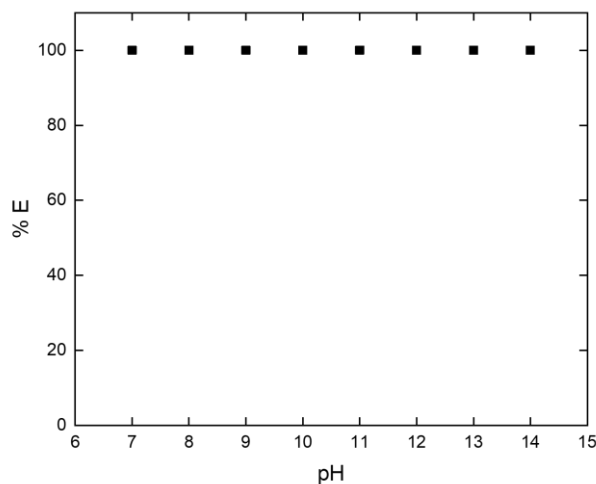


Figure 5.10: Effect of pH on the extraction of Hg^(II) by PDT. ($[PDT]_i$: 5.0×10^{-3} M, $[Hg^{(II)}]_i$: 1.0×10^{-3} M, Organic phase: 1:9 Octanol:Dodecane)

5.4.5.2 Effects of PDT concentration on the extraction of Hg^(II)

Further experiments carried out to determine the binding stoichiometry of **PDT** to Hg^(II) at pH 13.0 indicated 99.9 % extraction of Hg^(II) from the alkaline aqueous phase at exactly 1 equivalent of the ligand (Figure 5.11). The results show that as the ligand concentration increases from 0.3 to 1.0 mM, the % extraction (% E) of Hg^(II) increases and becomes essentially quantitative for 1 mM of ligand. This is consistent with the Job plot and UV-vis titration results.

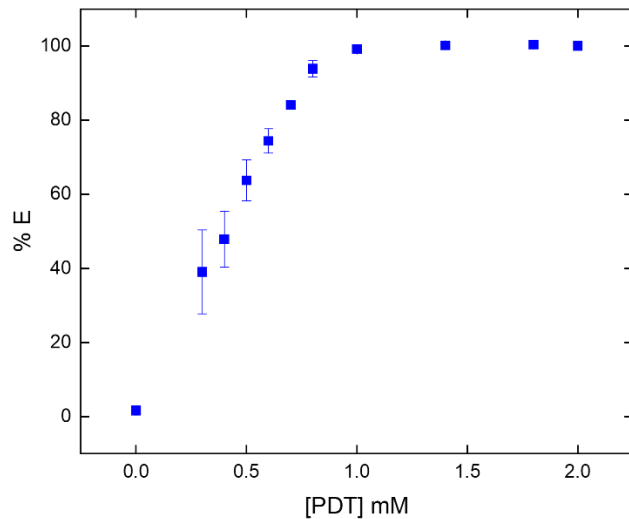


Figure 5.11: Extraction behavior of Hg²⁺ with **PDT** at pH 13.0. ($[Hg^{(II)}]_i$: 1.0×10^{-3} M, organic phase: 1:9 Octanol:Dodecane, pH: 13.0)

5.4.6 X-ray Crystallography

The identity of **PDAT** was clearly confirmed by X-ray diffraction analysis. Suitable single crystals were obtained by diffusion of hexanes into a concentrated solution of **PDAT** in CH₂Cl₂. The selected crystallographic data are represented in Table 4.1 and

the molecular structure is shown in Figure 5.12a. Figure 5.12b shows the ORTEP representation (50% probability ellipsoids) for the X-ray crystal structure of **PDAT**, with atom labeling scheme, showing three crystallographically independent molecules but molecularly/chemically the same within the asymmetric unit. The reason for the three molecules being within the asymmetric unit is most likely due to a significant intermolecular π - π stacking and a weak non-traditional H-bonding interaction. For the case of the Hg^(II) complexes with **PDAT** or **PDT**, analytically pure desired crystals suitable for X-ray diffraction have not been isolated despite several attempts.

Table 5.1: Crystal data of **PDAT**

Chemical formula	3(C ₉ H ₁₁ N ₃ S ₂)
M_r	675.98
Crystal system, space group	Monoclinic, $P2_1/c$
Temperature (K)	298
a, b, c (Å)	12.6548 (19), 12.5660 (18), 20.969 (3)
β (°)	96.558 (3)
V (Å ³)	3312.8 (8)
Z	4
Radiation type	Mo $K\alpha$
μ (mm ⁻¹)	0.45
Crystal size (mm)	0.25 × 0.20 × 0.17
Data collection	
Diffractionmeter	Bruker D8 Quest PHOTON II
Absorption correction	<i>SADABS2016/2</i> (Bruker,2016/2) was used for absorption correction. $wR2(int)$ was 0.074 before and 0.0587 after correction. The Ratio of minimum to maximum transmission is 0.7544. The $\lambda/2$ correction factor is not present.
T_{min}, T_{max}	0.562, 0.745
No. of measured, independent and observed [$I > 2\sigma(I)$] reflections	31096, 6065, 4888
R_{int}	0.043
($\sin \theta/\lambda$) _{max} (Å ⁻¹)	0.604
Refinement	
$R[F^2 > 2\sigma(F^2)], wR(F^2), S$	0.054, 0.134, 1.10
No. of reflections	6065

No. of parameters	385
H-atom treatment	H-atom parameters constrained
$\Delta\rho_{\max}$, $\Delta\rho_{\min}$ ($e \text{ \AA}^{-3}$)	0.32, -0.23

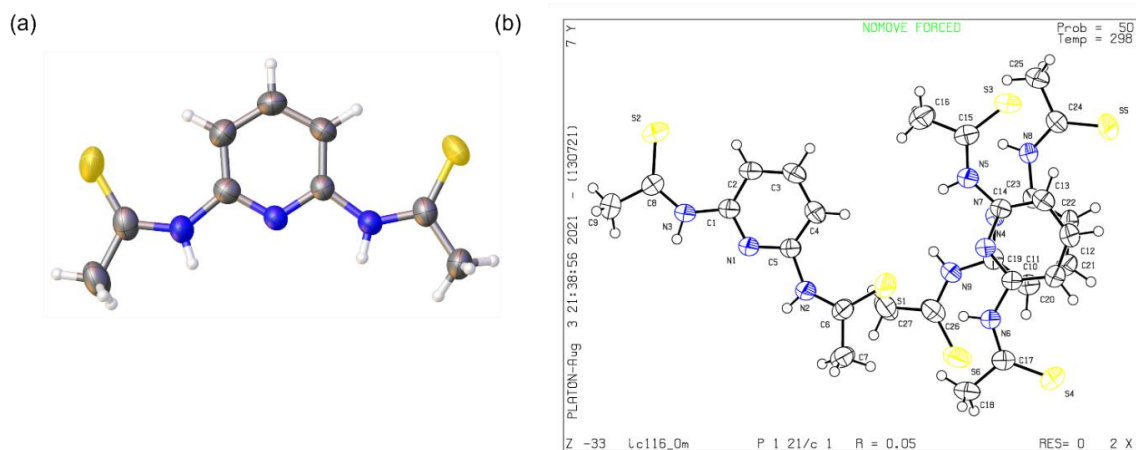


Figure 5.12: (a) X-ray crystal structure of **PDAT** (b) ORTEP representation (50% probability ellipsoids) for the X-ray crystal structure of **PDAT**, with atom labeling scheme, showing three 3 crystallographically independent molecules within the asymmetric unit

5.5 Conclusions

In summary, a new lipophilic thioamide ligand and its short-chain derivative have been synthesized and applied for complexation, extraction, and selective sensing of $\text{Hg}^{\text{(II)}}$. Selective response to $\text{Hg}^{\text{(II)}}$ in the presence of several metal salts indicates potential promise $\text{Hg}^{\text{(II)}}$ optical sensing in alkaline HLW and other applications. Likewise, promising results for $\text{Hg}^{\text{(II)}}$ extraction from highly alkaline aqueous solutions were obtained. The binding mode of **PDAT** and **PDT** to $\text{Hg}^{\text{(II)}}$ is consistent with a 1:1 metal-ligand complex stoichiometry as confirmed by elemental analysis and the NMR and UV-Vis spectroscopic studies.

5.6 Acknowledgments

This research project was supported by the US Department of Energy Minority Serving Institution Partnership Program (MSIPP) managed by the Savannah River National Laboratory under SRNS contract BOA No: 541, TOA No. 0000332972 and 0000403067 to FIU. We also acknowledge the financial support of the Florida International University Dissertation Year Fellowship for Adenike Fasiku (DYF Spring/Summer 2021 Fellow).

5.7 References

- (1) Brosset, C. The Behavior of Mercury in the Physical Environment. *Water. Air. Soil Pollut.* **1987**, *34*, 145–166.
- (2) Ebinghaus, R.; Tripathi, R. M.; Wallschläger, D.; Lindberg, S. E. Natural and Anthropogenic Mercury Sources and Their Impact on the Air-Surface Exchange of Mercury on Regional and Global Scales. In *Mercury Contaminated Sites*; Ebinghaus, R., Turner, R. R., Lacerda, L. D., Vasiliev, O., Salomons, W., Eds.; Springer Berlin Heidelberg: Berlin, Heidelberg, **1999**, 3–50.
- (3) Bernhoft, R. A. Mercury Toxicity and Treatment: A Review of the Literature. *J. Environ. Public Health* **2012**, *2012*.
- (4) Olson, A. O. Mercury Toxicity: Background, Etiology, Epidemiology. **2019**.
- (5) Chiarle, S.; Ratto, M.; Rovatti, M. Mercury Removal from Water by Ion Exchange Resins Adsorption. *Water Res.* **2000**, *34*, 2971–2978.
- (6) Zunita, M. Graphene Oxide-Based Nanofiltration for Hg Removal from Wastewater: A Mini Review. *Membranes* **2021**, *11*, 269.
- (7) Li, Q.; Liu, T.; Deng, P. Recovery of Mercury and Lead from Wastewater by Sulfide Precipitation-Flotation. In *Characterization of Minerals, Metals, and Materials 2015*; Carpenter, J. S., Bai, C., Escobedo, J. P., Hwang, J.-Y., Ikhmayies, S., Li, B., Li, J., Monteiro, S. N., Peng, Z., Zhang, M., Eds.; Springer International Publishing: Cham, **2016**, 667–674.
- (8) Hua, K.; Xu, X.; Luo, Z.; Fang, D.; Yi, J.; Bao, R. Effective Removal of Mercury Ions in Aqueous Solutions: A Review. *Current Nanoscience*; **2020**, *16*, 363-375.

- (9) Fábrega, F. M.; Guimarães, A. S.; Resende, G. P. S.; Mansur, M. B. Solvent Extraction of Mercury(II) from Aqueous Chloride Solutions Using Cyanex 302. *Miner. Process. Extr. Metall.* **2017**, *126*, 193–198.
- (10) Chen, B.; Wu, Y.; Guo, X.; He, M.; Hu, B. Speciation of Mercury in Various Samples from the Micro-Ecosystem of East Lake by Hollow Fiber-Liquid–Liquid–Liquid Microextraction-HPLC-ICP-MS. *J. Anal. At. Spectrom.* **2015**, *30*, 875–881.
- (11) Yin, C.; Iqbal, J.; Hu, H.; Liu, B.; Zhang, L.; Zhu, B.; Du, Y. Sensitive Determination of Trace Mercury by UV–Visible Diffuse Reflectance Spectroscopy after Complexation and Membrane Filtration-Enrichment. *J. Hazard. Mater.* **2012**, *233–234*, 207–212.
- (12) Aliberti, A.; Vaiano, P.; Caporale, A.; Consales, M.; Ruvo, M.; Cusano, A. Fluorescent Chemosensors for Hg²⁺ Detection in Aqueous Environment. *Sens. Actuators B Chem.* **2017**, *247*, 727–735.
- (13) Cheremisinoff, N. P. *Industrial Solvents Handbook, Revised and Expanded*; CRC press, 2003.
- (14) Sorvari, J.; Sillanpää, M. Influence of Metal Complex Formation on Heavy Metal and Free EDTA and DTPA Acute Toxicity Determined by *Daphnia Magna*. *Chemosphere* **1996**, *33*, 1119–1127.
- (15) Grant, G. J. Mercury(II) Complexes with Thiocrowns and Related Macrocyclic Ligands. In *Recent Developments in Mercury Science*; Atwood, D. A., Ed.; Structure and Bonding; Springer: Berlin, Heidelberg, **2006**, 107–141.
- (16) Baumann, T. F.; Reynolds, J. G.; Fox, G. A. Polymer Pendant Crown Thioethers: Synthesis, Characterization and Hg²⁺ Extraction Studies of Polymer-Supported Thiocrowns ([14] AneS4 and [17] AneS5). *React. Funct. Polym.* **2000**, *44*, 111–120.
- (17) Mahmoudi, G.; Gargari, M. S.; Afkhami, F. A.; Lampropoulos, C.; Abedi, M.; Corrales, S. A.; Khandar, A. A.; Mague, J.; Van Derveer, D.; Ghosh, B. K.; Masummi, A. Mercury (II) Coordination Complexes Bearing Schiff Base Ligands: What Affects Their Nuclearity and/or Dimensionality. *Polyhedron* **2015**, *93*, 46–54.
- (18) Synthesis, physico-chemical and spectral studies of Hg(II) and Cu(II) complexes with sulfamethoxazole schiff base. *Der Chemica Sinica*, **2013**, *4*, 40-45
- (19) Reddy, M. L. P.; Francis, T. Recent Advances in the Solvent Extraction of Mercury(Ii) with Calixarenes and Crown Ethers. *Solvent Extr. Ion Exch.* **2001**, *19*, 839–863.

- (20) Jalilvand, F.; Leung, B. O.; Izadifard, M.; Damian, E. Mercury(II) Cysteine Complexes in Alkaline Aqueous Solution. *Inorg. Chem.* **2006**, *45*, 66–73.
- (21) Habibi, M. H.; Tangestaninejad, S.; Fallah-Shojaie, A.; Mohammadpoor-Baltork, I.; Tayyari, S. F.; Emtiazi, G.; Hamidimotlagh, R. Preparation and Spectral Investigation of Bis[*N*- (Substituted-Phenyl)Thiobenzamidato]Mercury(II) Complexes. *J. Coord. Chem.* **2005**, *58*, 955–962.
- (22) Stålhandske, C. M. V.; Stålhandske, C. I.; Sandström, M.; Persson, I. Crystal Structure of *N,N*-Dimethylthioformamide Solvates of the Divalent Group 12 Ions with Linear Coordination Geometry for Mercury(II), Tetrahedral for Zinc(II), and Octahedral for Cadmium(II). *Inorg. Chem.* **1997**, *36*, 3167–3173.
- (23) Kagaya, S.; Miyazaki, H.; Ito, M.; Tohda, K.; Kanbara, T. Selective Removal of Mercury(II) from Wastewater Using Polythioamides. *J. Hazard. Mater.* **2010**, *175*, 1113–1115.
- (24) Okamoto, K.; Kuwabara, J.; Kanbara, T. Secondary Thioamides as Multidentate Ligands for Functional Metal Complexes. *Chem. Lett.* **2014**, *44*, 102–110.
- (25) Fasiku, A. O.; Fortunato, M. T.; Chakraborty, I.; Kavallieratos, K. Mercury (II) Sensing via Cyclization of a Dithioamide into a Benzimidazole Derivative: A Structural and Spectroscopic Study. *Inorganica Chim. Acta* **2020**, *510*, 119680.
- (26) Suzuki, T.; Kajita, Y.; Masuda, H. Deprotonation/Protonation-Driven Change of the σ -Donor Ability of a Sulfur Atom in Iron(II) Complexes with a Thioamide SNS Pincer Type Ligand. *Dalton Trans.* **2014**, *43*, 9732–9739.
- (27) Tamura, N.; Mitsui, K.; Nabeshima, T.; Yano, Y. Synthesis of 2,6-Diamidopyridine Derivatives and Their Functions as Flavin Receptors in Chloroform. *J. Chem. Soc. Perkin Trans. 2* **1994**, *10*, 2229–2237.
- (28) Job, P. Formation and stability of inorganic complexes in solution. *Ann Chim* **1928**, *9*, 113–134.
- (29) Khan, H.; Ahmed, M. J.; Bhangar, M. I. A Simple Spectrophotometric Determination of Trace Level Mercury Using 1,5-Diphenylthiocarbazone Solubilized in Micelle. *Anal. Sci.* **2005**, *21*, 507–512.
- (30) Sheldrick, G. M. A Short History of SHELX. *Acta Crystallogr.* **2008**, *64*, 112–122.
- (31) Sheldrick, G. M. Crystal Structure Refinement with SHELXL. *Acta Crystallogr. Sect. C Struct. Chem.* **2015**, *71*, 3–8.

- (32) Dolomanov, O. V.; Bourhis, L. J.; Gildea, R. J.; Howard, J. a. K.; Puschmann, H. OLEX2: A Complete Structure Solution, Refinement and Analysis Program. *J. Appl. Crystallogr.* **2009**, *42*, 339–341.
- (33) Pedersen, B. S.; Scheibye, S.; Nilsson, N. H.; Lawesson, S.-O. Studies on Organophosphorus Compounds XX. Syntheses of Thioketones. *Bull. Sociétés Chim. Belg.* **1978**, *87*, 223–228.
- (34) Rao, C. N. R.; Venkataraghavan, R. The C=S Stretching Frequency and the “-N-C=S Bands” in the Infrared. *Spectrochim. Acta* **1962**, *18*, 541–547.
- (35) Zaki, M. I.; Hasan, M. A.; Al-Sagheer, F. A.; Pasupulety, L. In Situ FTIR Spectra of Pyridine Adsorbed on SiO₂-Al₂O₃, TiO₂, ZrO₂, and CeO₂: General Considerations for the Identification of Acid Sites on Surfaces of Finely Divided Metal Oxides. *Colloids Surf. Physicochem. Eng. Asp.* **2001**, *190*, 261–274.
- (36) Ackermann, T. K. A. Connors: Binding Constants — the Measurement of Molecular Complex Stability, John Wiley & Sons, New York, Chichester, Brisbane, Toronto, Singapore. *Für Phys. Chem.* **1987**, *91*, 1398–1398.

CHAPTER VI: Summary and General Conclusions

The use of mercury in the acidic dissolution of aluminum cladding at the Savannah River Site (SRS) has led to its accumulation over the years in highly-alkaline high-level waste tanks post-processing. Its existence in different forms (both organic and inorganic) poses many threats to the workers and the surrounding ecosystem. Several methods, such as steam stripping and adsorption using thio-functionalized resins, have been used for mercury removal. However, these methods are either not efficient or require some form of secondary waste disposal. The main objective of this project is to provide a means of mercury removal from these highly alkaline aqueous high-level waste solutions in a more efficient, safe, and clean way with little or no secondary waste accumulation or disposal. For this purpose, I synthesized and tested thioamide and sulfonamide ligands for the complexation, sensing, and extraction of $\text{Hg}^{\text{(II)}}$ from alkaline solutions for potential applications to the SRS alkaline tank waste processing.

The present dissertation describes how this goal can be achieved. It comprises six chapters and two appendices. An introduction chapter (Chapter I) reviews past studies on closely-related topics, identifies research gaps, and introduces necessary background knowledge for following the latter chapters. The main part of the dissertation (Chapters II – V) consists of four manuscripts that have already been published (Chapter IV) or are in the final stages of preparation for publication in peer-reviewed journals (Chapters II, III, and V). Chapter VI gives a general conclusion on the whole research project. Appendices A and B comprise research projects with

significant preliminary results directly related to our main aims that are yet to be completed.

In Chapter II, the complexation patterns of bis-arylsulfonamide ligand derivatives with $\text{Hg}^{(\text{II})}$ using several spectroscopic methods was shown. The crystal structure of the L-Hg complex confirms the complexation of $\text{Hg}^{(\text{II})}$ with the ligand with two triethylammonium counteranions, which was corroborated by the $^1\text{H-NMR}$ titration obtained after the addition of various equivalents of $\text{Hg}^{(\text{II})}$ with 4 mM ligand in MeOD. An advantage of these ligands is the low ligand concentration required for quantitative extraction from alkaline conditions and that the recovery of extracted metal is straightforward. Likewise, the high extraction efficiencies obtained for $\text{Hg}^{(\text{II})}$ in alkaline conditions point to potential application for $\text{Hg}^{(\text{II})}$ removal from the alkaline high-level waste streams at the SRS.

In Chapter III, a bis-dansyl-sulfonamide ligand was shown to be a potential chemosensor for $\text{Hg}^{(\text{II})}$ due to its fluorescent quenching upon gradual addition of HgCl_2 in methanol. The detection limit for $\text{Hg}^{(\text{II})}$ was recorded as $0.78 \mu\text{M}$, satisfying the detection limit recommended by EPA and WHO organizations.

Chapter IV describes a novel method for sensing $\text{Hg}^{(\text{II})}$ via mercury-mediated cyclization of a bis-thioamide ligand to a novel benzimidazole derivative, which was confirmed by several spectroscopic methods. This study has been published in the peer-reviewed journal *Inorganica Chimica Acta*. The selectivity for $\text{Hg}^{(\text{II})}$ compared to other metal salts and the color change observed after reaction with $\text{Hg}^{(\text{II})}$ can be utilized towards optical sensing of $\text{Hg}^{(\text{II})}$.

Chapter V concludes our main study with two new thioamide ligands derived from 2,6-diaminopyridine that show extraction efficiencies as high as 99.7% for Hg^(II) removal and, perhaps more importantly, are applicable for extraction from highly alkaline aqueous phases to 90/10 v/v dodecane/octanol, which is a solvent that is fully compatible with industrial processing.

In conclusion, I have shown that thioamide and sulfonamide ligands studied and presented over the five chapters of this dissertation can be used as potential Hg^(II) complexants and extractants from high-level tank waste and other applications which involve highly-alkaline aqueous media. The versatility of these ligands, high extraction efficiency, and efficient recovery after stripping (after only a single cycle) point to direct application for mercury removal and sensing. The PDT ligand, in particular, is especially promising for direct application, as its long lipophilic chain makes it compatible with most industrial processing solvents. A pincer complex of this ligand with Hg^(II) was formed at exceptionally high binding strength, extracted Hg^(II) at pH 13, and also discriminated the presence of Hg^(II) over a wide range of SRS prevalent metal ions, making it a premier candidate for mercury removal applications at SRS. Although other extractants, such as calixarenes, crown thioethers, and some high molecular weight amines (alamine, primene, aliquat) have been reported to extract Hg^(II) in acidic and neutral media at high extraction efficiency, our sulfonamide and thioamide ligands can complex and extract mercury from highly alkaline aqueous media into organic media with extraction efficiency as high as 99.7%, which is unprecedented. Overall, the results from this work pave the way for potential applications of these thioamide and sulfonamide ligands to high-level waste processing at SRS for mercury removal because

of their versatility, strong binding strength, and compatibility with industrial processing solvents. Other environmental remediation and sensing applications for $\text{Hg}^{(\text{II})}$ with these frameworks are also possible.

APPENDICES

Appendix A: A Nitro Sulfonamide Ligand and Its Hg^(II) Complexation Properties

Adenike O. Fasiku, Carlos Aguilera, and Konstantinos Kavallieratos*

A.1. Abstract

Due to mercury toxicity and threat to the environment and public health, it is necessary to develop methods for its sensing and removal. We have therefore synthesized a nitro-sulfonamide ligand for the purpose of recovering mercury from aqueous solutions. The ligand, N,N'-(4-nitro-1,2-phenylene)bis(4-(tert-butyl)benzenesulfonamide), **L**, is a sulfonamide derivative with a nitro substituent on the *o*-phenylenediamine ring. Complexation reactions of **L** with either HgCl₂ or Hg(OAc)₂ were carried out, and the resulting complexes **C**₁ and **C**₂ were studied spectroscopically. There were significant differences between the two Hg^(II) salts, as HgCl₂ addition showed decreased absorption at the 400 nm region in the UV-Vis spectrum while Hg(OAc)₂ addition enhanced it. ¹H-NMR spectroscopy was also performed. Our work showed that this nitro-sulfonamide ligand has potential for Hg^(II) sensing, complexation, and removal.

A.2 Introduction

Due to its prominent role as an environmental pollutant, mercury has been extensively studied in various toxic metal storage sites across the world. Due to concerns regarding mercuric pollution, efforts have been undertaken to discover compounds that can safely and efficiently remove it from the environment. With this goal in mind, we have synthesized a nitro-sulfonamide chelating ligand, **L** (Scheme 1). Sulfonamide-based

compounds were considered as candidates because previous studies showed successful complexation with softer metals in conditions in which amine deprotonation allows metal binding and complex formation.¹⁻⁴ Deprotonation occurs due to the addition of a base, which leaves the N group as a potential electron donor in the coordinate covalent interaction with metal Lewis acids. Evidence of complex formation was observed through the characterization of the complexes by ¹H-NMR and UV-Vis spectroscopy. Results from UV-Vis spectroscopy allowed us to compare how a difference in the nature of counteranions affects mercury complexation, as specificity varies in accordance with the nature of the mercuric salt. Herein, we present the synthesis of this nitro-sulfonamide ligand, as well as a comparison of its complexation thermodynamics with two different mercuric salts.

A.3 Experimental Section

A.3.1 Materials and methods

All chemicals, materials, and solvents were obtained from Aldrich Chemical Company and Fischer Scientific. ¹H-NMR spectroscopy was performed in a 400 MHz Bruker NMR spectrometer, and UV-Vis spectroscopy was performed on a Varian Cary 300 Bio UV-Vis spectrophotometer.

A.3.2 Synthesis of N,N'-(4-nitro-1,2-phenylene)bis(4-(tert-butyl)benzenesulfonamide), L

A solution of 4-nitro-*o*-phenylenediamine (1.08 g, 7.05 mmol) and pyridine (1.3 mL, 16.25 mmol) in 50 mL of 1,2-dichloroethane was added dropwise to a solution of 4-*tert*-butylbenzenesulfonyl chloride (3.6 g, 15.51 mmol) dissolved in 25 mL of 1,2-dichloroethane. The reaction mixture was refluxed under nitrogen for 24 h and was

monitored by TLC (60:40, hexanes/EtOAc). The crude product was washed sequentially with 1 M HCl, 0.2 M NaHCO₃, and finally, deionized H₂O. The resulting organic phase was then separated and dried with granular Na₂SO₄, then volatiles were evaporated, and the solid was recrystallized from dichloromethane/hexanes. (590 mg, 15.34 % yield) (C₂₆H₃₁N₃O₆S₂). ¹H-NMR (400 MHz, CDCl₃) δ 8.03 (s, 1H), 7.98 (dd, J = 9.1, 2.5 Hz, 1H), 7.84 (d, J = 8.7 Hz, 2H), 7.58 (d, J = 8.7 Hz, 2H), 7.51 (m, 5H), 7.30 (d, J = 2.5 Hz, 1H), 6.49 (s, 1H), 1.33 (d, J = 5.9 Hz, 18H).

A.3.3 Synthesis of L-Hg complex from HgCl₂ (C₁)

A solution of HgCl₂ (149.8 mg, 0.55 mmol) in 10 mL of EtOH was added dropwise to a solution of (99.3 mg, 0.18 mmol) of **L** and Et₃N (218.9 mg, 2.16 mmol) in 20 mL of EtOH. After stirring for 72 h, the excess solvent was removed, and hexanes was added, giving a rusty-brown product (269 mg, 51 % yield). The reaction mixture was evaporated until 5 mL remained and an equal volume of H₂O was added. ¹H-NMR (400 MHz, CDCl₃) δ 8.17 (s, 1H), 7.97 (d, J = 6.9 Hz, 1H), 7.84 (d, J = 6.7 Hz, 2H), 7.64 – 7.57 (m, 2H), 7.53 – 7.42 (m, 5H), 7.36 (s, 1H), 1.32 (d, J = 2.0 Hz, 18H).

A.3.4 Synthesis of L-Hg complex from Hg(OAc)₂ (C₂)

A solution of Hg(OAc)₂ (149.1 mg, 0.47 mmol) in 10 mL of EtOH was added dropwise to a solution of (130.0 mg, 0.24 mmol) of **L**. The solution mixture was then allowed to reflux for 24 h. The excess solvent was rotovaped, and hexane was added. The orange product was filtered and dried (161 mg, 84.8 % yield). ¹H NMR (400 MHz, CDCl₃) δ 7.80 (s, 5H), 7.54 (s, 1H), 7.43 (d, J = 22.6 Hz, 4H), 7.08 (s, 1H), 1.29 (d, J = 8.6 Hz, 18H).

A.3.5 UV-Vis titration of L with HgCl₂

Solutions of ligand **L** in CH₃CN and 2.2 equiv. of Et₃N were titrated with HgCl₂ at constant ligand concentration. In a typical experiment, a solution of **L** (2.0×10^{-5} M) and Et₃N (0.55 μ L) in CH₃CN (solution A) was titrated with a solution of HgCl₂ (2.0×10^{-4} M) (solution B) prepared by the dissolution of 0.66 mg HgCl₂ in solution A in a 10 mL volumetric flask, thus keeping a constant concentration of ligand upon titration of solution A with solution B. 2.300 mL of solution A were added to the UV-Vis cuvette and solution B was added in 2-100 μ L increments until a total of 1000 μ L had been added. The absorbance changes were monitored, with the results plotted and fitted to the 1:1 binding isotherm using non-linear regression analysis.

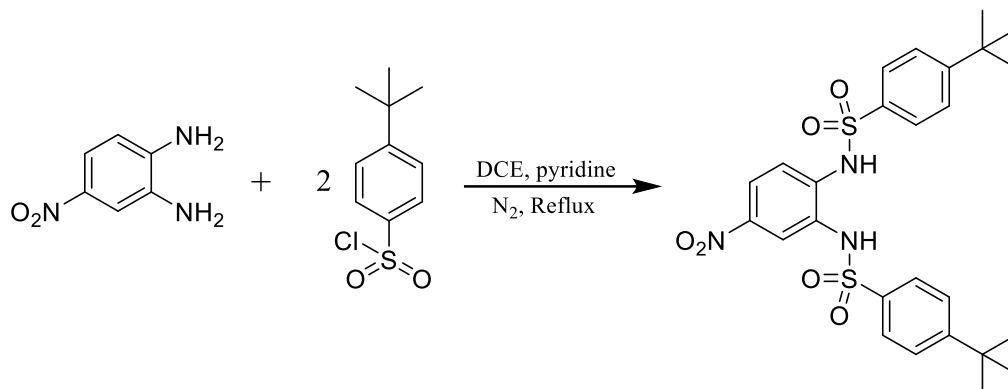
A.3.6 UV-Vis titration of L with Hg(OAc)₂

Solutions of ligand **L** in CH₃CN were titrated with Hg(OAc)₂ at constant ligand concentration. In a typical experiment, a solution of **L** (2.0×10^{-5} M) in CH₃CN (solution A) was titrated with a solution of Hg(OAc)₂ (2.0×10^{-4} M) (solution B) prepared by the dissolution of 0.64 mg HgCl₂ in solution A in a 10.0 mL volumetric flask, thus keeping a constant concentration of ligand upon titration of solution A with solution B. 2.300 mL of solution A were added to the UV-visible cuvette and solution B was added in 2-100 μ L increments until a total of 1000 μ L had been added. The absorbance changes were monitored, with the results plotted and fitted to the 1:1 binding isotherm using non-linear regression analysis.

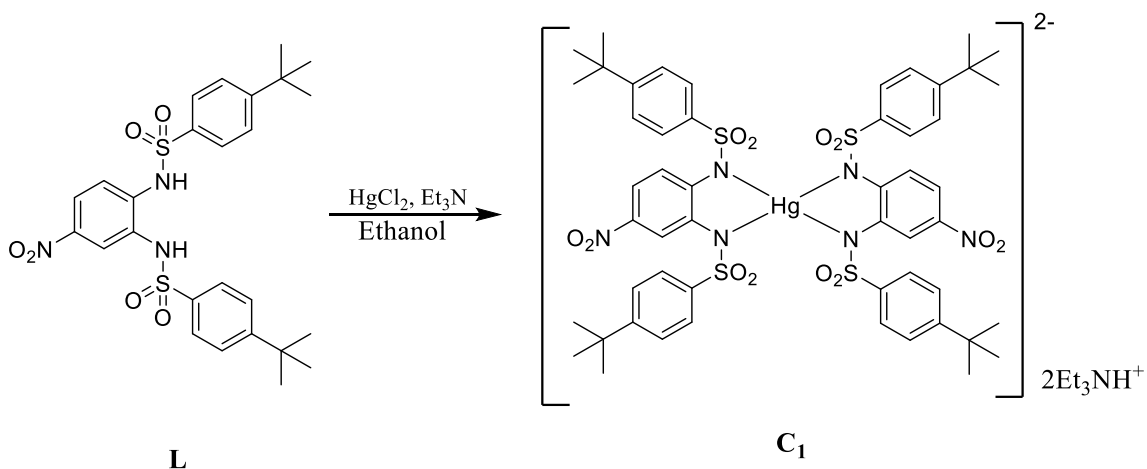
A.4.0 Results and Discussion

A.4.1. Synthesis

L was synthesized by reacting 4-nitro-*o*-phenylenediamine, pyridine, and 4-*tert*-butylbenzenesulfonyl chloride in 1,2 dichloroethane (DCE). The synthesis is straightforward in one step from readily available starting materials. The product was characterized by ¹H-NMR. (Scheme A.1).



Scheme A.1: Synthesis of *N,N'*-(4-nitro-1,2-phenylene)bis(4-(*tert*-butyl)benzenesulfonamide), **L**



Scheme A.2: Possible structure of isolated mercury complex

As seen in scheme A.2, **L** can complex Hg^(II) irrespective of the type of mercury salt used (HgCl₂ vs. Hg(OAc)₂). The chloride salt required an organic base in order for ligand deprotonation to occur, whereas the acetate leaving group functioned as its own weak base. Complexation with both salts led to 1:1 binding of **L** to Hg^(II).

A.4.2. NMR Studies

In order to compare differences in the complexation of both mercury salts with **L**, the ¹H-NMR spectra for both complexes were collected. As seen in Figure A.1, each proton in **L** was labeled in alphabetical order, which allowed easy visualization and recognition of each spectral reading. As seen in Figure A.2, comparison of **L** and **C**₁ complex spectra allude to the loss of protons labeled 4 and 8, which correspond to the amine hydrogens. The loss of these resonances at 6.5 and 7.5 ppm provides evidence for the deprotonation of **L** by triethylamine and the possible binding of mercury to the electron-rich nitrogen group (11). The same result can be observed in Figure A.2, when comparing **L** and the **C**₂ complex. The loss of resonances at 6.5 and 7.5 ppm indicates possible complex formation via coordinate covalent interactions between mercury and nitrogen. Although, one must also account for the possibility that loss of hydrogen resonances in the spectra only indicates successful deprotonation by the acetate group of the mercuric acetate salt and not subsequent binding by mercury.

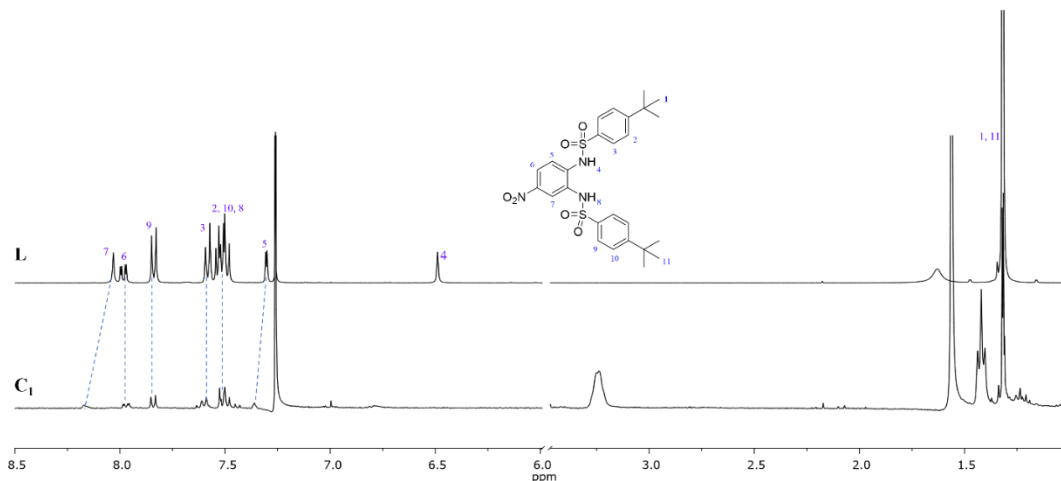


Figure A.1. $^1\text{H-NMR}$ spectra comparison of **L** and isolated **C₁**

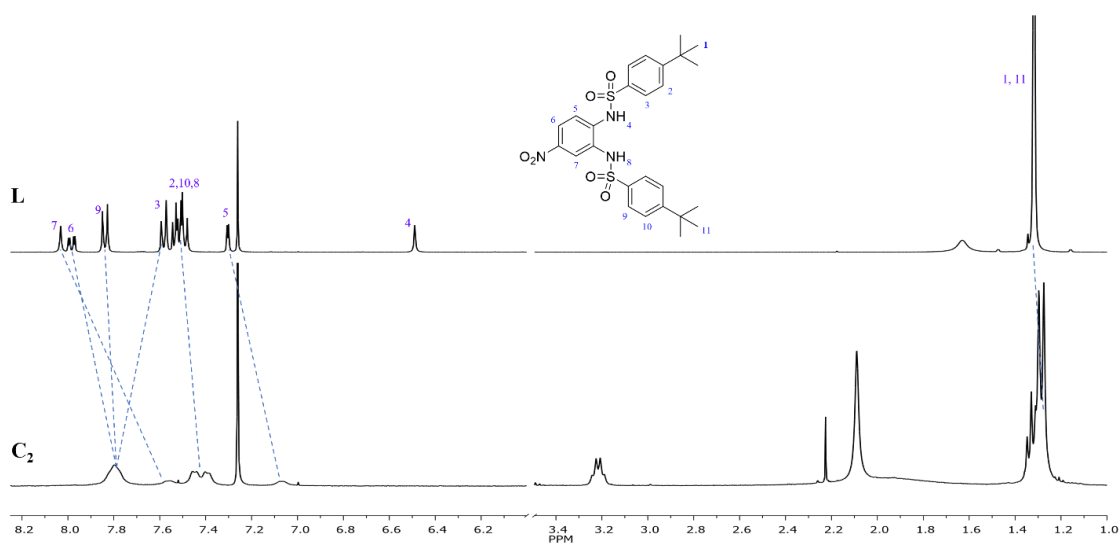


Figure A.2. $^1\text{H-NMR}$ spectra comparison of **L** and isolated **C₂**

A.4.3. UV-Vis studies

To further assess the possibility of complex formation and ligand binding strength, UV-Vis spectroscopy was performed with each salt. As seen in Figure A.3a, the

UV-Vis spectra show complex formation with the chloride salt due to isosbestic points at the 350 nm and 450 nm regions.

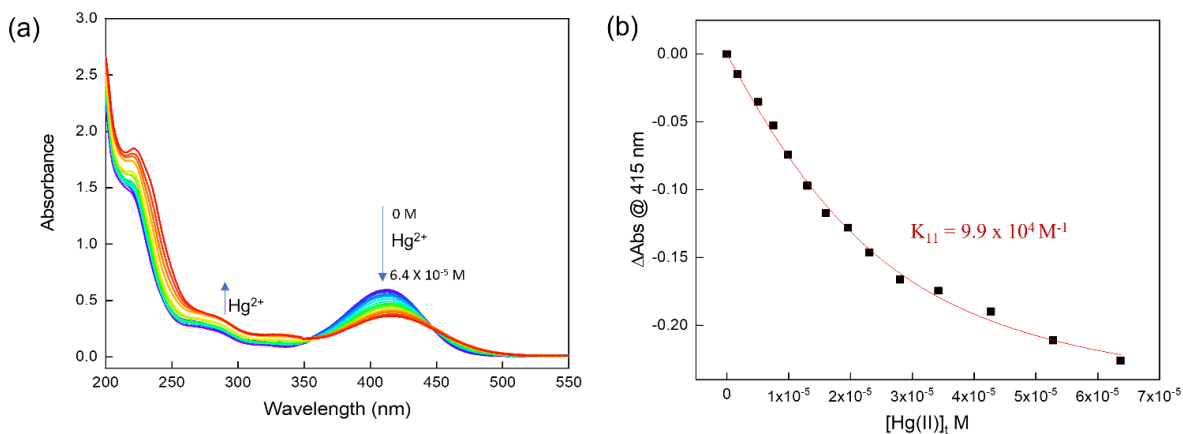


Figure A.3. (a) UV/Visible spectra for the titration of **L** ($2.0 \times 10^{-5} \text{ M}$) and 2.2 eq. of triethylamine with HgCl_2 ($2.0 \times 10^{-4} \text{ M}$) in acetonitrile. (b) absorption as a function of $\text{Hg}^{\text{(II)}}$ concentrations at 415 nm.

A control titration of HgCl_2 solution into methanol and Et_3N in the absence of the ligand (under the same experimental conditions as Figure A.3a) gives further evidence of complex formation with the ligand, as the lack of any absorbance in the UV-Vis spectrum at ca 350 – 500 ppm indicates no coordination of $\text{Hg}^{\text{(II)}}$ to either the solvent or the organic base, as the control experiment shows no absorbance in this region, and the UV-Vis titration with ligand shows a prominent absorption at that range. The presence of an isosbestic point at 450 nm in the ligand-only titration provides further evidence for complex formation as such a UV-Vis absorption pattern is not found in the control.

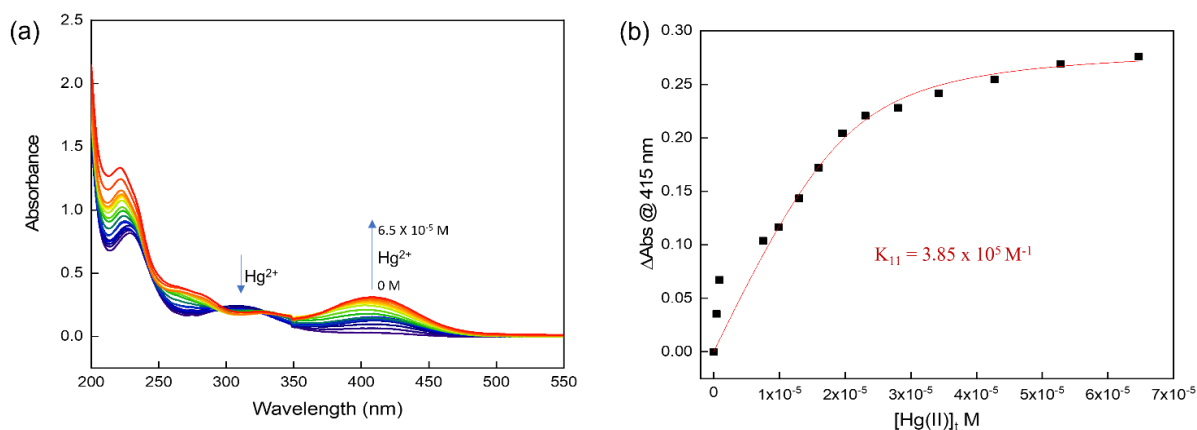


Figure A.4. (a) UV-Visible spectra for the titration of **L** ($2.0 \times 10^{-5} \text{ M}$) with $\text{Hg}(\text{OAc})_2$ ($2.0 \times 10^{-4} \text{ M}$) in acetonitrile. (b) absorption as a function of $\text{Hg}^{(\text{II})}$ concentrations at 415 nm.

The UV-Vis titration of **L** with the $\text{Hg}(\text{OAc})_2$ salt (Figure A.4a) also provides two isosbestic points at 325 and 290 nm, which can once again be taken as evidence of complex formation. Nevertheless, a stark difference can be observed when comparing the UV-Vis titration spectra with HgCl_2 vs. $\text{Hg}(\text{OAc})_2$ (Figure A.3a and A.4a). By focusing on the 400 nm region, one notices a decrease of the absorption at 415 nm when HgCl_2 is added, whereas the addition of $\text{Hg}(\text{OAc})_2$ displays enhanced absorption in the same region. This difference can be attributed to the effects of variable deprotonation by the base on the complexation of the ligand with these mercuric salts, as in the acetate experiment, no organic base has been added. It is notable that the ligand does not have absorption at the 400 nm, unless it is deprotonated. For titration with HgCl_2 , the base facilitates deprotonation of the ligand, which leads to stabilized anionic species through resonance as the NO_2^- is electron-withdrawing, therefore leading to a strong absorption at this region. As HgCl_2 is being added, the absorption is decreasing by the loss of resonance and complex formation. However, when the acetate salt acts as a base, and no

additional organic base is used, we observe an enhancement of this absorption for OAc^- addition because complexation only gradually deprotonates the ligand and therefore, the complexation occurs directly from the neutral ligand to the complex and does not involve a stabilized anionic species, only a transient one. A comparison of best-fit lines of each UV-Vis spectrum for the two complexes, as seen in Figure A.3b and A.4b, yields a binding constant of $9.9 \times 10^4 \text{ M}^{-1}$ for HgCl_2 and a binding constant of $3.85 \times 10^5 \text{ M}^{-1}$ for $\text{Hg}(\text{OAc})_2$. Thus, it can be confidently stated that complexation with $\text{Hg}(\text{OAc})_2$ is stronger than with HgCl_2 , possibly because the organic base may be interfering with binding resulting to a weaker complexation.

A.5. Conclusion

This research project was undertaken in order to investigate sulfonamide ligands for the complexation of $\text{Hg}^{\text{(II)}}$, as well as to determine how the nature of counteranion affects ligand mercury complexation. $^1\text{H-NMR}$ showed evidence for deprotonation and binding of a mononitrosulfonamide ligand, **L**, with two $\text{Hg}^{\text{(II)}}$ salts (HgCl_2 and $\text{Hg}(\text{OAc})_2$). This was a result of the loss of amine hydrogens, which leave electron-rich nitrogen as a likely candidate for coordinate covalent bonding to $\text{Hg}^{\text{(II)}}$. Comparison of the UV-Vis spectra of the two complexes, **C**₁ and **C**₂, showed different effects from mercury complexation. In the 350 – 450 nm region of the UV spectra with λ_{max} at 415 nm, chloride salt addition showed loss of absorbance, while acetate salt addition showed enhancement of absorbance. Nevertheless, both UV-Vis spectra demonstrated complex formation as seen by the presence of multiple isosbestic points in each. Spectral changes

also allowed fitting of the curves to obtain K_{11} values of $9.85 \times 10^4 \text{ M}^{-1}$ and $3.85 \times 10^5 \text{ M}^{-1}$ for the chloride and acetate salts, respectively.

These sulfonamide derivatives are important due to their potential application in mercury removal from lakes, rivers, and the Savannah River Site. Future work will focus on obtaining a crystal structure for **L** and its isolated mercury complexes. Furthermore, future efforts will also focus on the synthesis of fluorescent ligands and the determination of their sensing properties.

A.6 References

- (1) Diaz, J. R. A.; Baldo, M. F.; Echeverría, G.; Baldoni, H.; Vullo, D.; Soria, D. B.; Supuran, C. T.; Camí, G. E. A Substituted Sulfonamide and Its Co (II), Cu (II), and Zn (II) Complexes as Potential Antifungal Agents. *J. Enzyme Inhib. Med. Chem.* **2016**, *31*, 51–62.
- (2) Alvarado, R. J.; Rosenberg, J. M.; Andreu, A.; Bryan, J. C.; Chen, W.-Z.; Ren, T.; Kavallieratos, K. Structural Insights into the Coordination and Extraction of Pb(II) by Disulfonamide Ligands Derived from o-Phenylenediamine. *Inorg. Chem.* **2005**, *44*, 7951–7959.
- (3) Diaconu, D.; Mangalagiu, V.; Amariuca-Mantu, D.; Antoci, V.; Giuroiu, C.; Mangalagiu, I. Hybrid Quinoline-Sulfonamide Complexes (M^{2+}) Derivatives with Antimicrobial Activity. *Molecules* **2020**, *25*, 2946.
- (4) Katakya, R.; Knell, M. A. Complexation Studies of Pyridyl Sulfonamide Ligands for Sensing Zinc and Copper Ions. *J. Solut. Chem.* **2009**, *38*, 1483.

Appendix B: A Novel Tripodal Thioamide as Soft-Donor Site Ligand for Mercury(II) Complexation

Adenike O. Fasiku, Indranil Chakraborty, Raphael G. Raptis and Konstantinos

Kavallieratos*

B.1 Abstract

A novel tripodal thioamide ligand (**L_{4a}**) based on the 1,3,5-tris(2-aminomethyl)-2,4,6-triethylbenzene framework was synthesized and characterized by spectroscopic methods, X-ray crystallography, and elemental analysis. Hg^(II) complexes with this ligand are formed instantaneously and precipitate out of the reacting solution making it a potential mercury precipitant at tank 50 at the Savannah River Site (SRS). The UV-Vis spectra obtained from the addition of several metal salts (Cd^(II), Pb^(II), Zn^(II), Ca^(II), Ag^(I), Cu^(II), Co^(II), Cr^(III), and Hg^(II)) to the ligand solution show changes only for Hg^(II) addition while other metal salts show little to no changes in the spectra when compared with the spectrum of the ligand. The rigidity and the soft S-donor site of thiocarboxamide with the favorable binding characteristics of the preorganized tripodal ring enhance this ligand's ability to complex Hg^(II).

B.2 Introduction

Previous studies in the coordination chemistry of Hg^(II) have reported various heteroatom-containing ligands, such as nitrogen-, phosphorous-, and sulfur-based ligands but thiocarbonyl ligands have not received as much attention, partly due to their limited commercial availability and their difficult synthesis, which makes use of fetid reagents such as phosphorus pentasulfide, Lawesson's reagent, and alkyl- and aryl- thiols.

However, thioamides possess higher stability than other thiocarbonyls such as thionoesters, thioketones, and thioaldehydes.¹ Thus, we are exploring thioamides in the coordination chemistry of mercury as few studies of this ligand family have been completed with Hg^(II).²⁻⁵

Recently Lehman-Andino et al., synthesized⁶ the soft-donor ligand, *N*²,*N*⁶-diphenylpyridine-2,6-bis(carbothioamide) by conversion of the amide derived from the reaction of pyridine carboxylic acid chloride with aniline to give the thioamide using Lawesson's reagent. The resulting dithiopicolinamide ligand was shown to complex Hg^(II) in a dinuclear complex pattern (Figure 4.1).

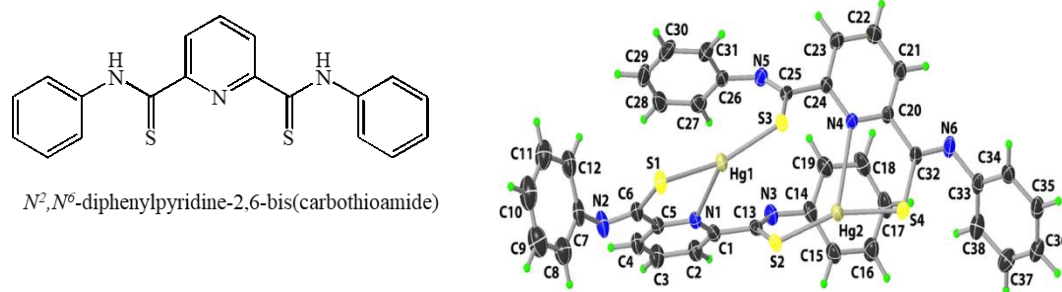


Figure B.1: X-ray structure of dinuclear mercury complex formed from the complexation of *N*²,*N*⁶-diphenylpyridine-2,6-bis(carbothioamide) with Hg^(II)

In this work we are combining the rigidity and the soft S-donor site of thiocarboxamide group with the favorable binding characteristics of the preorganized tripodal 1,3,5-tris(2-aminomethyl)-2,4,6-triethylbenzene framework. *N,N',N''*-((2,4,6-triethylbenzene-1,3,5-triyl)tris(methylene))tribenzothioamide (**L**_{4a}) was synthesized from inexpensive starting materials in few steps. This ligand, when deprotonated, can coordinate through both the nitrogen and the thiocarbonyl groups and has shown

favorable binding properties towards $\text{Hg}^{(\text{II})}$ with complete and selective precipitation of $\text{Hg}^{(\text{II})}$ from solutions, which can be applied for a $\text{Hg}^{(\text{II})}$ separation process in the tank 50 of the SRS site.

B.3 Experimental Section

B.3.1 Materials and method

All chemicals and materials were purchased from Fisher Scientific or Sigma Aldrich. All chemicals were standard reagent grade and were used without further purification except for toluene. $^1\text{H-NMR}$ spectra were recorded on a 600-MHz Bruker Avance NMR spectrometer. The UV-Visible spectra were recorded on a CARY 100 Bio UV-Visible spectrophotometer.

B.3.2 Synthesis of tris-carboxamide ligand

1,3,5-Tris(2-aminomethyl)-2,4,6 triethylbenzene (1.0037 g - 9.281 mmol) was dissolved in 10 mL of DMF in a round-bottom flask, and 2.2 equiv. of Et_3N were added. Under stirring, benzoyl chloride (2.37 mL -2.2 equiv., 20.42 mmol) was added dropwise to this mixture. This resulted in a smoky reaction with formation of precipitate and the reaction mixture was allowed to stir for 1 h for complete reaction. 50 mL of DI water was added, and the product was then filtered under vacuum, followed by washing with DI water. The residue was then placed under a vacuum to remove the volatiles. After 12 h, the product was weighed at 1.489 g. Recrystallization from hot/cold ethanol gave 0.8438 g of the pure solid (50.1% yield). $^1\text{H-NMR}$ (600 MHz, DMSO) δ 10.07 (s, 2H), 7.95 (d, J

= 7.4 Hz, 4H), 7.67 (dd, $J = 5.9, 3.6$ Hz, 2H), 7.59 (t, $J = 7.4$ Hz, 2H), 7.53 (t, $J = 7.6$ Hz, 4H), 7.32 – 7.28 (m, 2H).

B.3.3 Synthesis of tris-thiocarboxamide ligand (**L_{4a}**)

The following reaction must be performed in dry conditions and all glassware should be oven dried properly before use. In dry toluene (100 mL), 0.500 g (0.89 mmol) of the tris-carboxamide ligand was added. To this solution, 1.44 g (2.94 mmol, 3.3 equiv. of Lawesson's reagent was added. This reaction mixture was then heated to reflux under nitrogen with constant stirring for 12 h. After this time, the solution turned yellow. The solvent was reduced with the aid of the rotary evaporator to dryness. The solid thus obtained was washed with ether, filtered, and finally recrystallized from DCM/hexanes. The solid formed was then vacuum filtered and dried under vacuum. 0.331 g (53 % yield). ¹H NMR (600 MHz, CDCl₃) δ 7.71 (d, $J = 7.3$ Hz, 2H), 7.48 – 7.42 (m, 1H), 7.36 (t, $J = 7.7$ Hz, 2H), 7.27 (d, $J = 7.5$ Hz, 1H), 5.01 (d, $J = 4.2$ Hz, 2H), 2.84 – 2.70 (m, 2H), 1.32 – 1.21 (m, 3H). FT-IR (cm⁻¹); $\nu = 1373$ (C=S), 3262 (N-H), 1446 (C-N). Elemental analysis for C₃₆H₃₉N₃S₃·CH₂Cl₂ (% C, H, N calculated/found): 63.96/64.39, 5.95/6.09, 6.05/6.08.

B.3.4. Synthesis of Hg-L_{4a} complex

A solution of HgCl₂ (10.5 mg, 0.039 mmol) in 10 mL of acetonitrile was added dropwise to a 20 mL acetonitrile/chloroform (50:50) solution of **L_{4a}** (20.3 mg, 0.033 mmol) and DIPEA (14.2 μ L, 0.078 mmol). Instantaneous precipitation was observed. The precipitate was filtered under vacuum and washed with acetonitrile and then

chloroform. A light yellow product was obtained after drying (8.9 mg). FT-IR (cm^{-1}); ν = 1319 (C=S), 1484 (C-N).

B.3.5. UV-Vis studies

Solutions of **L4a** in MeOH were titrated with HgCl_2 at constant ligand concentration. In a typical experiment, a solution of **L4a** (2.0×10^{-5} M) and 2.2 eq. of DIPEA in CH_3CN was titrated with a solution of HgCl_2 (1.0×10^{-4} M) prepared by dilution with the **L4a**/DIPEA solution to maintain constant ligand/DIPEA concentration. For spectra collection, 2.300 mL of ligand solution was added to the cuvette, and the HgCl_2 solution was added in 5-200 μL increments until a total of 1200 μL had been added.

Selectivity test of **L4a** with various metal salts (Cd^{II} , Pb^{II} , Zn^{II} , Ca^{II} , Ag^{I} , Cu^{II} , Co^{II} , Cr^{III} , and Hg^{II}) was performed by adding 1 equivalent of these salts to solutions of **L4a** (0.1 mM in MeOH) and allowing the solutions to stand for 24 h. UV-Vis spectra for each solution were recorded.

B.3.6. X-ray crystallography for **L4a**

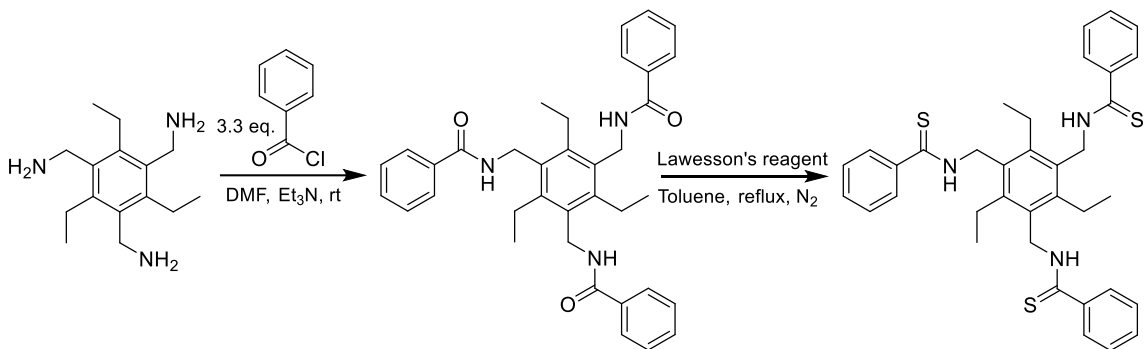
Yellow block-shaped crystals of the ligand were obtained by slow diffusion of hexanes into its dichloromethane solution. Data collection and structure refinement details are summarized in Table B.1. A suitable crystal was selected and mounted on a Bruker D8 Quest diffractometer equipped with PHOTON II detector operating at $T = 298$ K. The structure was solved in space group $P3_2$ (# 145) determined by the *ShelXS*⁷ structure solution program using Direct Methods and refined by Least Squares using

version 2018/3 of *ShelXL*.⁸ All non-hydrogen atoms were refined anisotropically. Calculations and molecular graphics were performed using *SHELXTL 2014* and *Olex2*⁹ programs.

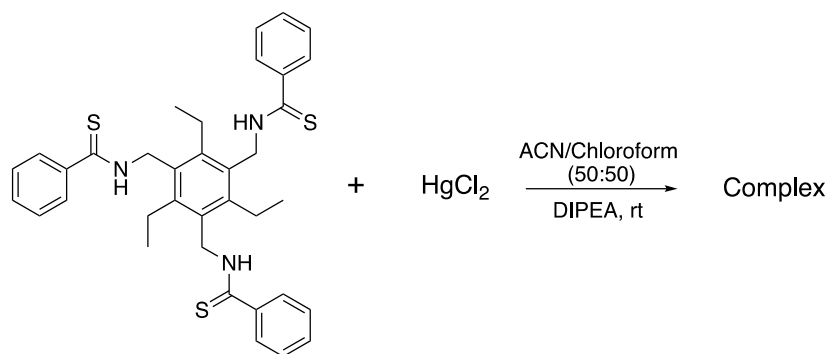
B.4 Results and Discussion

B.4.1 Synthesis

The synthesis of this tripodal thioamide can be accomplished in a few steps from inexpensive and readily available starting materials. The starting material, 1,3,5-tris(2-aminomethyl)-2,4,6-triethylbenzene was synthesized following the procedure from Wallace et al.¹⁰. The reaction pathway of this new ligand is described in the experimental section. The complexation of this ligand with mercury was studied (Scheme B.2.). The spontaneity of the reaction is indicated by the precipitates observed upon dropwise addition of Hg^(II). However, the major challenge in this work is that the precipitate is insoluble in all solvents, making it difficult to characterize it. This may be a very advantageous feature towards application to tank 50 at SRS, yet, understanding the system by full characterization is also necessary.



Scheme B.1: Synthesis of trithioamide ligand **L_{4a}**



Scheme B.2: Synthesis of the $\text{Hg}^{(\text{II})}$ complex of trithioamide ligand L_{4a}

B.4.2 FT-IR Spectroscopy

Spectra of L_{4a} vs. its $\text{Hg}^{(\text{II})}$ complex is seen in Figure B.2. The disappearance of the N-H peak at 3263 cm^{-1} shows the deprotonation of the ligand. C=S stretching band at 1373 cm^{-1} is shifted to 1319 cm^{-1} , this significant shift to lower frequency indicates a new bond formation with the thiocarbonyl S. The $\nu(\text{C-N})$ also shifted to a higher frequency with about 38 cm^{-1} difference, presumably due to resonance between the deprotonated nitrogen and the thiocarbonyl sulfur.

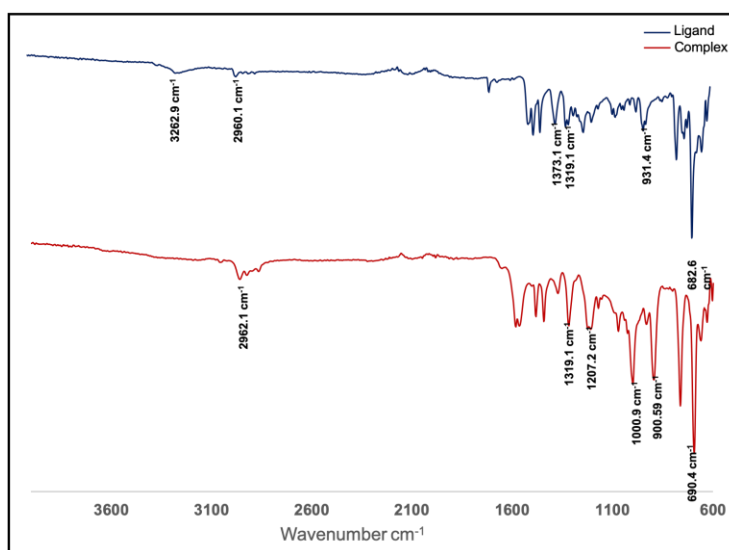


Figure B.2. FT-IR spectra of ligand L_{4a} vs. its $\text{Hg}^{(\text{II})}$ complex.

B.4.3 ^1H and ^{13}C -NMR spectroscopy

NMR spectra of the ligand were collected in CDCl_3 . All ^1H -NMR resonances are duly assigned to their corresponding protons with appropriate integrations (Figure B.3a). Aromatic protons are observed between 7.3-7.8 ppm and alkyl protons between 1.2 - 5.1 ppm. The broad resonance at 7.3 ppm is assigned to the amine proton. Carbon resonances are also appropriately assigned (Figure B.3b). The resonance at 200 ppm is assigned to the thiocarbonyl carbon, and all aromatic carbons are observed between 125 - 150 ppm. All alkyl carbon resonances are observed between 17 - 47 ppm. Resonances at 15.2 and 65.83 ppm (not identified on the spectrum) are attributed to the presence of residual ethyl ether.

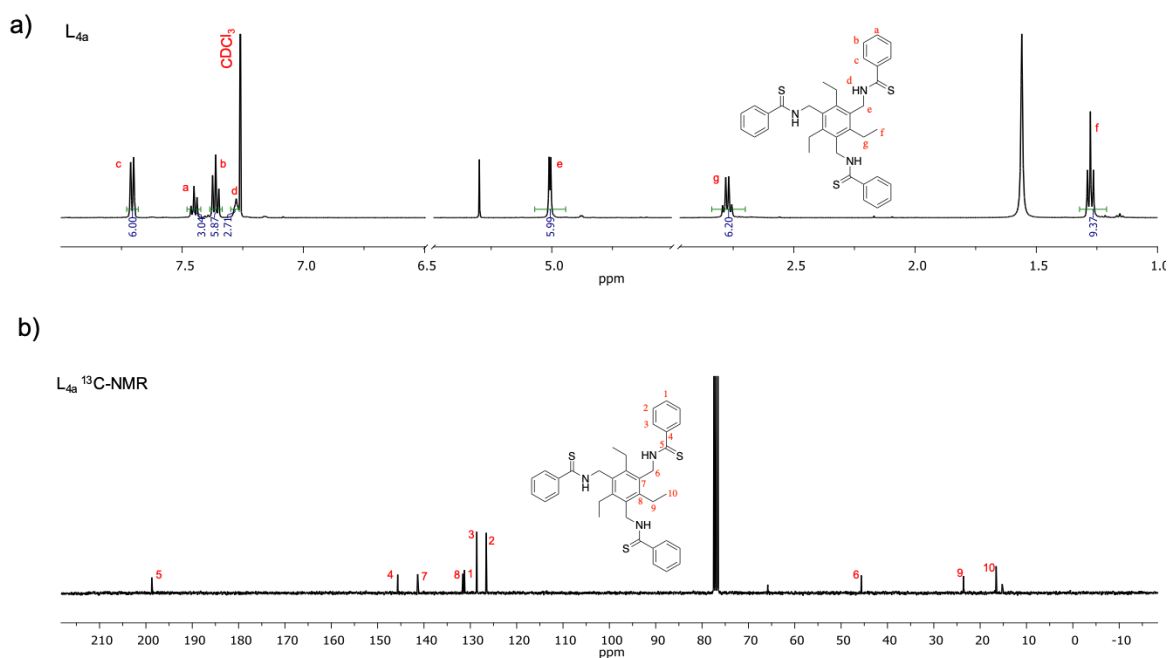


Figure B.3. (a) ^1H -NMR and (b) ^{13}C -NMR of new tripodal thioamide ligand, L_{4a}

B.4.4 UV-Vis Spectroscopy

As seen in Figure B.4a, the maximum absorbance for **L4a** was observed around 240 nm. Titration of this ligand with $\text{Hg}^{(\text{II})}$ in acetonitrile solution in the presence of DIPEA leads to an enhancement and red-shifting of this band. An isosbestic point observed at 275 nm indicates an equilibrium in the system with two species present (ligand and one formed complex). The binding curve at 282 nm shows a downward trend which ends at 0.02 mM of $\text{Hg}^{(\text{II})}$ corresponding to 1:1 ligand:metal ratio, as the ligand concentration in the solution, is 0.02 mM. With additional $\text{Hg}^{(\text{II})}$, a new upward trend in absorbance was observed. This indicates that more than one complexation pattern is possible for higher $\text{Hg}^{(\text{II})}$ concentrations. Selectivity of this tris-thioamide ligand, **L4a** for $\text{Hg}^{(\text{II})}$ vs. various other metal salts ($\text{Cd}^{(\text{II})}$, $\text{Pb}^{(\text{II})}$, $\text{Zn}^{(\text{II})}$, $\text{Ca}^{(\text{II})}$, $\text{Ag}^{(\text{I})}$, $\text{Cu}^{(\text{II})}$, $\text{Co}^{(\text{II})}$, $\text{Cr}^{(\text{III})}$) was tested by adding 1.0 equivalent of these metals (as chloride salts) to solutions of **L4a** (0.1 mM in MeOH) and allowing the solutions to sit for 24 h. UV-Vis spectra for each solution were collected as shown in Figure B.4b. The spectra after mercury addition show the disappearance of the ligand absorbance while no significant changes were observed for any of the other metal salts. In addition, there was an isosbestic point only for $\text{Hg}^{(\text{II})}$ addition, indicating selectivity of this ligand to mercury vs. other metals.

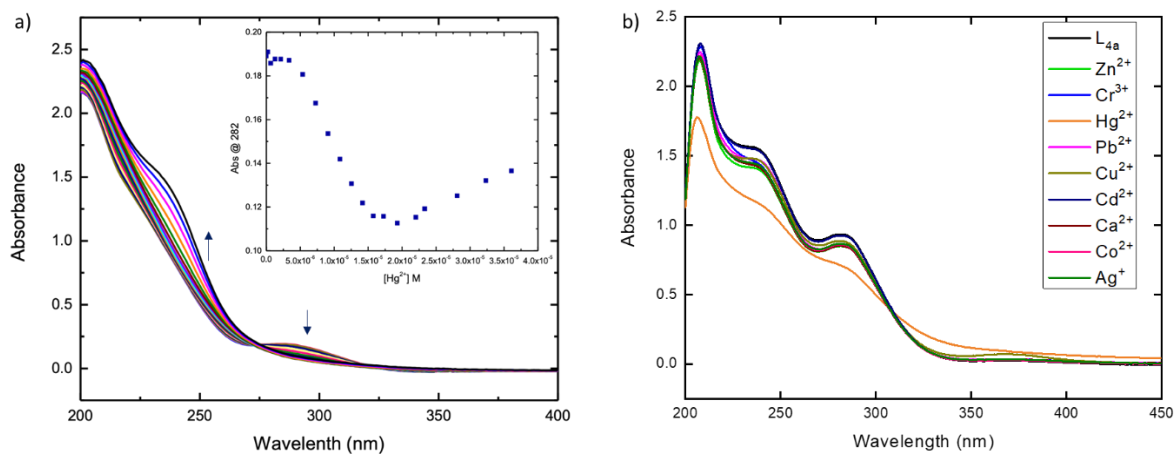


Figure B.4. UV-Vis study of ligand L_{4a} (a) Titration spectra taken after gradual addition of $HgCl_2$ to ligand and DIPEA (3.3 equiv.) in CH_3CN solution (0.020 mM). (b) UV-Vis responses of L_{4a} (0.10 mM, 3.3 Et_3N) to the addition of various metals added as chloride salts (1 equiv.) in $MeOH$ after standing for 24 h.

B.4.4. X-ray Crystallography

The X-ray crystal structure of ligand L_{4a} , including a molecule of chloroform, is shown in Figure B.5. The crystal data are also provided in Table B.1.

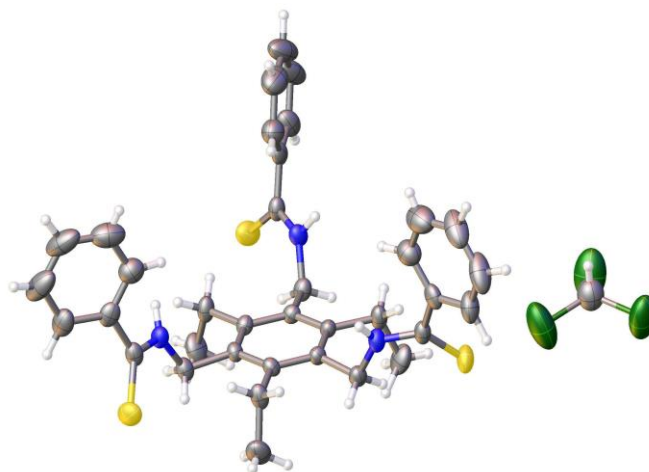


Figure B.5. X-ray crystal structure of tris-thioacarboxamide ligand, L_{4a}

Table B.1: Crystal data of tris-thiocarboxamide ligand, L_{4a}

Chemical formula	$C_{36}H_{39}N_3S_3 \cdot CHCl_3$
M_r	729.25
Crystal system, space group	Trigonal, $P3$
Temperature (K)	298
a, c (Å)	15.681 (8), 8.905 (5)
V (Å ³)	1896 (2)
Z	2
Radiation type	
Mo $K\alpha$ μ (mm ⁻¹)	0.44
Crystal size (mm)	0.20 × 0.17 × 0.12
Data collection	
Diffractometer	Bruker D8 Quest PHOTON 100
Absorption correction	Multi-scan <i>SADABS</i> 2016/2: Krause, L., Herbst-Irmer, R., Sheldrick G.M. & Stalke D., <i>J. Appl. Cryst.</i> 48 (2015) 3-10
T_{min}, T_{max}	0.511, 0.745
No. of measured, independent and observed [$I > 2\sigma(I)$] reflections	12852, 2172, 1541
R_{int}	0.077
$(\sin \theta/\lambda)_{max}$ (Å ⁻¹)	0.589
Refinement	
$R[F^2 > 2\sigma(F^2)], wR(F^2), S$	0.082, 0.248, 1.06
No. of reflections	2172
No. of parameters	193
H-atom treatment	All H-atom parameters refined
$\Delta\rho_{max}, \Delta\rho_{min}$ (e Å ⁻³)	1.41, -0.84

B5. Conclusions

A new tripodal thioamide ligand was synthesized and characterized. It shows interesting reactivity and selectivity towards $Hg^{(II)}$. The observed selectivity of this ligand towards $Hg^{(II)}$ and the instantaneous complex precipitation observed during reaction with $Hg^{(II)}$ can be utilized towards the separation of $Hg^{(II)}$ in tank 50 at the SRS.

B.6 References

- (1) Okamoto, K.; Kuwabara, J.; Kanbara, T. Secondary Thioamides as Multidentate Ligands for Functional Metal Complexes. *Chem. Lett.* **2014**, *44*, 102–110.
- (2) Begum, R. A.; Powell, D.; Bowman-James, K. Thioamide Pincer Ligands with Charge Versatility. *Inorg. Chem.* **2006**, *45*, 964–966.
- (3) Gurrieri, S.; Seminara, A.; Siracusa, G.; Cucinotta, V. Complexes of Pyridinthioamides. *J. Inorg. Nucl. Chem.* **1976**, *38*, 239–242.
- (4) Bingham, A. G. C. Studies on the Synthesis and Reactivity of Copper Thiolate and Thioamide Complexes. A thesis presented in partial fulfillment of the requirements for the degree of Doctor of Philosophy at Massey University." PhD diss., *Massey University*, **1984**.
- (5) Kagaya, S.; Miyazaki, H.; Ito, M.; Tohda, K.; Kanbara, T. Selective Removal of Mercury(II) from Wastewater Using Polythioamides. *J. Hazard. Mater.* **2010**, *175*, 1113–1115.
- (6) Lehman-Andino, I.; Chakraborty, I.; Fortunato, M.; Raptis, R.; Kavallieratos, K. A Distinctive Dinuclear Mercury(II) Complex Derived from N,N'-Bis(Phenyl)Pyridine-2,6-Dicarbothioamide: Potential Extractant for Hg(II) from Mixed Alkaline Wastes. In Preparation.
- (7) Sheldrick, G. M. A Short History of SHELX. *Acta Crystallogr. A* **2008**, *64*, 112–122.
- (8) Sheldrick, G. M. Crystal Structure Refinement with SHELXL. *Acta Crystallogr. Sect. C Struct. Chem.* **2015**, *71*, 3–8.
- (9) Dolomanov, O. V.; Bourhis, L. J.; Gildea, R. J.; Howard, J. a. K.; Puschmann, H. OLEX2: A Complete Structure Solution, Refinement and Analysis Program. *J. Appl. Crystallogr.* **2009**, *42*, 339–341.
- (10) Wallace, K. J.; Hanes, R.; Anslyn, E. V.; Morey, J.; Kilway, K. V.; Siegel, J. Preparation of 1,3,5-Tris(Aminomethyl)-2,4,6-Triethylbenzene from Two Versatile 1,3,5-Tri(Halosubstituted) 2,4,6-Triethylbenzene Derivatives. *Synthesis* **2005**, *12*, 2080–2083.

VITA

ADENIKE O. FASIKU

Born: Akure, Ondo State, Nigeria

- 2005 – 2010 B.Tech - Industrial Chemistry
Federal University of Technology,
Akure, Nigeria
- 2015 – 2016 MSc. - Environmental Chemistry and Pollution Control
University of Ibadan,
Ibadan, Nigeria
- 2017 – 2021 Doctoral Candidate – Chemistry with Environmental Track
Florida International University,
Miami FL
Advisor: Dr. Konstantinos Kavallieratos
- 2021 Dissertation Year Fellowship (DYF) Award,
FIU University Graduate School

PUBLICATIONS AND PRESENTATIONS

A. O. Fasiku, M. T. Fortunato, I. Chakraborty, and K. Kavallieratos. (2020) Mercury (II) Sensing via Cyclization of a Dithioamide into a Benzimidazole Derivative: A Structural and Spectroscopic Study. *Inorganica Chim. Acta.*, 2020, 510, 119680.

A. R. Ipeaiyeda and A. O. Fasiku. (2017). Sorption of Cypermethrin from Alfol and Inceptisol using acidified simulated rainwater in a soil column set-up. *Afr. J. Pure Appl. Chem.* 2017, 11, 30-36.

A. O. Fasiku, I. Chakraborty, R. Panzer, R. G. Raptis, and K. Kavallieratos. Complexation and Efficient Extraction of Mercury(II) in Alkaline Conditions by a family of Bis-Arylsulfonamide Ligands (*In preparation*)

A. O. Fasiku, I. Chakraborty, L. M. Garcia, and K. Kavallieratos. A bis-Dansylamide Derivative of *o*-Phenylenediamine as a Fluorescent Chemosensor for the Detection, Complexation, and Extraction of Mercury from Alkaline High-Level Waste (*In preparation*)

A. O. Fasiku, I. Chakraborty, and K. Kavallieratos. A Novel Pyridine-didodecanethioamide Ligand as a Potential Complexant and Extractant of Hg(II) from Alkaline High-Level Waste Tanks. (*In preparation*)

A. O. Fasiku, I. Chakraborty, R. Panzer, R. G. Raptis, & K. Kavallieratos. Complexation, Extraction, and Sensing of Hg(II) by Sulfonamide Ligands Derived from *o*-Phenylenediamine (oral presentation). ACS National Meeting & Exposition, virtual conference, April 2021.

A. O. Fasiku, S. K. Wheeler, G. A. Flores, I. Chakraborty, R. G. Raptis, & K. Kavallieratos. Benzenesulfonamide Derivatives as Complexants and Extractants for Addressing the Mercury Problem at the Savannah River Site (poster presentation). Waste Management Symposia (*WM2020*), Phoenix, Arizona. March 08-13, 2020

A. O. Fasiku, I. Chakraborty, R. G. Raptis, & K. Kavallieratos. Sulfonamides and thioamides for mercury complexation and extraction from alkaline high-level waste at the Savannah River Site (poster presentation). Florida Inorganic and Materials Symposium (*FIMS*), Gainesville, Florida, October 2019

A. O. Fasiku, I. Chakraborty, T. M. Jonah, G. A. Flores, R. G. Raptis, & K. Kavallieratos. Sulfonamide and thioamide chelators as mercury extractants and sensors for potential application to high-level waste processing at the Savannah River Site (poster presentation). 257th ACS National Meeting & Exposition, Orlando, Florida, March 2019.